SPECTRAL ANALYSIS

OF

EARLY F-TYPE SUPERGIANTS

by

J.C. Castley, B.Sc.(Hons.)

submitted in fulfilment of the

requirements for the degree of

Doctor of Philosophy

UNIVERSITY OF TASMANIA

HOBART

February, 1974

This thesis contains no material which has been accepted for the award of any other degree or diploma in any University.

To the best of my knowledge and belief, the thesis contains no material previously published or written by another person except where due reference is made in the text.

J C Castley

J.C. Castley

TABLE OF CONTENTS

	ABSTRACT	
	ACKNOWLEDGEMENTS	
	PREFACE	
Chapter 1	LUMINOUS EARLY F-TYPE STARS	
1.1	Introduction	1
1.2	Observational Information	4
	(a) Microturbulent Velocities	
	(b) Abundances	
Chapter 2	OBSERVATIONAL MATERIAL AND MEASUREMENTS	
2.1	Introduction	15
2.2	Spectroscopic Observations	15
2.3	Program Stars	16
2.4	Spectrograms	18
2.5	Spectroscopic Reductions	22
2.6	Hydrogen and Calcium H and K Lines	26
2.7	Line Blocking Measurements	29
2.8	Line Identifications	32
2.9	Selection and Measurement of the Metal Lines	32
2.10	Line Intensities	34
Chapter 3	ATMOSPHERIC TEMPERATURES AND GRAVITIES	
3.1	Introduction	37
Part A	EFFECTIVE TEMPERATURE AND GRAVITY	
	DETERMINATIONS FOR α CAR	
3.2	Model Atmospheres	38
3.3	Comparison of Observational Data with Models	43

Part B (T_{eff}, log g) DETERMINATION FOR THE OTHER PROGRAM STARS

3.4 Use of *ubvy* Photometry 52

(a) The Technique

(b) Reddening

(c) Use of $(b-y)_o$

(d) Results

3.5 Other Factors Affecting (T_{eff}, log g) Estimates 67

(a) Rotational Velocities

(b) Non-Local Thermodynamic Equilibrium

(c) Turbulent Motions and Mass Loss

(d) Radial Velocity Variations

(e) Convection

(f) Line Blanketing

(g) Abundance Effects

Part C THE RESULTS

3.6 Absolute Values of (T_{eff}, log g) for the F-Type Supergiants 87

Chapter 4 CURVE OF GROWTH ANALYSIS OF THE PROGRAM STARS

4.1 Introduction 93

4.2 Theoretical Curve of Growth 94

(a) Selection of Theoretical Model

(b) The Reduction Program

4.3 Microturbulent Velocities 98

(a) Introduction

(b) Determination of Excitation Temperatures

(c) Microturbulence Results

(d) Interpretation of Observed Trends in Microturbulence

(e) Comments on the Determination of Microturbulent Velocities and Abundances using Model Atmospheres

4.4 The Abundances of the Elements 111

(a) Atmospheric Parameters of the 'Reversing Layer'

(b) The Results

(c) Discussion of Individual Elements

(d) Discussion of Observed Stellar Abundances

4.5 Abundance Comparisons with Other Interesting Supergiant Stars 148

(a) Introduction

(b) HD 33579

(c) 89 Her and HD 161796

(d) R Coronae Borealis

4.6 Summary 159

CONCLUSION 162

BIBLIOGRAPHY 166

APPENDICES

I INSTRUMENTATION OF THE 40CM TELESCOPE

AI.1 Introduction AI

AI.2 Some Statistics about the Observing Site A2

AI.3 The Spectrograph A3

AI.4 Wavelength Calibration A8

AI.5	Photometric Calibration	A8
AI.6	Rocking Quartz Block for Widening Spectra	AII
AI.7	The Slit-Viewing Optics and Autoguider	AI3
AI.8	The Exposure Meter	AI6
AI.9	The Pre-Flashing Unit	AI7
AI.10	Photographic Plate Processing Facilities	AI9
AI.II	The Low-Resolution Scanner	A20
II	PHOTOMETRY DATA	A23
III	HYDROGEN BALMER AND CALCIUM K LINE DATA	A26
IV	METAL LINE STRENGTHS	A30
V	CENTRAL DEPTHS AND EQUIVALENT WIDTHS OF SELECTED LINES IN α CAR	A55

ABSTRACT

High or moderately-high dispersion spectra covering the wavelength interval 3800Å to 5000Å were obtained for ten luminous early F-type stars and an F8Ia supergiant south of declination -15°. These spectroscopic plates have been used to measure line blocking, the profiles of the strongest lines (hydrogen and calcium K), and to determine the equivalent widths of as many metal lines as possible in this wavelength range.

The line blocking measurements, hydrogen-line profiles and scanner or *ubvy* photometry data have been used with model atmosphere predictions to determine effective temperatures and gravities. A discrepancy between the gravity indicated by the Balmer jump and the H_γ line profiles has been found in the most luminous stars. The gravities determined from the H_γ profiles have been compared with the gravities derived from cluster members and there is found to be a small discrepancy, the gravities from the profiles being lower. Some evidence for the presence of macroscopic turbulent motions in the more luminous early F Ia stars and A Ia stars is presented, and it is shown that the inclusion of a turbulent pressure term in the equation of hydrostatic equilibrium largely removes the discrepancy between the gravity indicated by the H_γ profiles and that indicated by the cluster members.

A study of the rotational velocities of the program stars show that the early F Iab and Ib stars exhibit very little or no macroturbulence. The observed rotational velocity of θ Sco (a Ib supergiant) shows that this star must have lost very little of its angular momentum during its evolution off the main sequence and must

have rotated as a rigid body for some, if not all, of this phase of its evolution.

Using the Wruble curve of growth for the Milne-Eddington model, the microturbulent velocity in the program stars was determined, indicating that the F0Ia supergiants exhibit very high microturbulent velocities of up to 20 km sec^{-1}. The abundances of the program stars, using the same curve of growth, have also been determined; except for δ CMa and θ Sco, all stars have essentially solar abundances. δ CMa shows a ten-times overabundance in carbon, and significant overabundances in barium, cerium and lanthanum, with respect to the solar abundances. The abundance anomalies in δ CMa show similar trends to those observed in the R Coronae Borealis stars R CrB and RY Sag. The previously-suggested abundances for R CrB need significant corrections because of the abundance anomalies found in δ CMa. A comparison between the abundances found for the 'normal' program stars and those of HD 33579, 89 Her and HD 161796 has been made, suggesting that these stars have essentially the same abundances as the program stars.

The curve of growth analysis of the stars studied at high dispersion show that the equivalent width data presented here is sufficiently accurate to warrant a detailed abundance analysis based on the model atmosphere approach.

ACKNOWLEDGEMENTS

Firstly, I would like to thank my supervisor, Dr. M.D. Waterworth, without whose support and financial backing the 40cm telescope-spectrograph system would not be what it is today. The helpful criticism by Dr. Waterworth, Dr. R.D. Watson, Mr. I.R. Beresford and Mr. P.T. Rayner during the preparation of this thesis is appreciated.

I am deeply indepted to Dr. R.D. Watson, Mr. D. King, Mr. D. Pythian and Mr. P.T. Rayner, who spent many cold nights as assistants at the telescope.

Thanks also go to the technical staff associated with the Observatory for their skilful construction, and in some cases design, of the many pieces of equipment associated with a telescope and Coudé spectrograph. The assistance of Mr. N. Schapira in the electronic design of the various components and initial alignment of the telescope and spectrograph was greatly appreciated. The efficiency and helpfulness of Larraine Brown, who typed the thesis, is also appreciated.

I must make special mention of my wife Diane, who spent many days and nights at the telescope assisting in various ways. She also assisted in many of the tedious jobs associated with the production of this thesis, and typed the first draft.

Finally, I acknowledge with gratitude the financial support of a Commonwealth Post-graduate Scholarship throughout this study.

PREFACE

Because of the size of the telescope available, only the brightest stars in the sky can be observed at high dispersion. The early F-type supergiants were chosen for three reasons. Firstly, this particular group of stars had not been studied in a systematic manner previously. Secondly, there are a sufficient number of bright stars of this type to allow a survey of their abundances to be undertaken. Thirdly, interest had been generated in α Car by a partial analysis of two high-dispersion plates of this star during my honours year.

When this project was commenced in 1970, the University of Tasmania's Observatory was equipped with a partially-complete 40cm telescope. The initial two years of the work, and some of the third, were taken up in my design and construction of the spectrograph and associated equipment for which I had responsibility. Because the spectrograph construction was an essential part of the thesis project, and in order to provide relevant information for the benefit of future users, I include a detailed account of its specifications as Appendix I. The spectra were obtained and analysed during the last two years of the project.

Chapter I

LUMINOUS EARLY F-TYPE STARS

I.1 Introduction

Supergiants, because of their fast evolution, are relatively rare. However, due to their intrinsic brightness, in some cases in excess of $10^5 L_\odot$, they can be seen at large distances and make up a large proportion of the brighter stars in the sky.

The early F I stars can be analysed satisfactorily using moderately high dispersion (4 to 9 $\mathring{A}\ mm^{-1}$), whereas the G I stars, which are slightly more luminous, require higher dispersion (1 to 2 $\mathring{A}\ mm^{-1}$) because of severe line crowding. These properties, and the moderate effective temperatures (about $6700^\circ K$) of the F I stars, make them important in astronomical research for at least three reasons.

Firstly, they imply that the stars are young, rapidly evolving and have not had time to move far from the interstellar clouds in which they originated. Accordingly, because they can be analysed in detail, even though they are at large distances, they are useful tracers of recent star formation in galaxies. In the same vein, they are useful probes to study composition differences, both between galaxies, and as a function of radius in our own galaxy.

Secondly, since their intrinsic luminosity apparently can be easily determined to a reasonable degree of certainty (± 0.5 mag, Osmer 1972), they provide a distance indicator that is substantially brighter than the cepheid variables.

Thirdly, the stars have radii of the order of 200 $R_\odot$ and quite low

surface gravities, so they are useful for the study of low pressure phenomena in stellar atmospheres.

From the work of many investigators it is known that the F I stars have the following basic characteristics:

(1) their range of absolute magnitudes is roughly $-9 < M_V < -4$ (Osmer, 1970 and references cited therein),

(2) some are cepheids, and most of those that are not show semi-regular variations in light, radial velocity (Abt, 1957 a,b) and, on the basis of recently published work by Rosendhal and Wegner (1970) on the A I stars, possibly microturbulence. Recent investigations by Parsons (1970) and Osmer (1972), based on the model atmosphere approach, have shown that the F Ib stars can be successfully analysed using LTE blanketed models in which turbulent pressure has been included. However, Osmer (1970) has shown that these models are not sufficiently realistic to be able to adequately describe the atmospheres of the most luminous early F Ia stars.

F-type supergiants are distinguished from lower luminosity stars on classification spectra because they have stronger lines of ionized metals. The hydrogen lines are principally dependent on temperature, except for the most luminous early F stars, and are not as useful luminosity indicators as in the A stars. It is difficult to pick out F I stars on blue sensitive objective prism plates. Merrill (1934) found, in his studies of infrared spectra, that the oxygen triplet at 7774Å was stronger in the early type supergiants than in dwarfs. Keenan and Hynek (1950) showed in an extensive study that it was an excellent luminosity criterion for B, A and F stars; Parsons (1964)

demonstrated that it could be used to pick out supergiants, even at objective prism dispersions. Albers (1969) has since carried out an objective prism survey of the southern Milky Way and has presented a list of seventy six stars which show the high-luminosity O I triplet.

More recently, Osmer (1970, 1972) has reported narrow-band photoelectric measurements of the O I λ7774 line strengths for 59 stars, having spectral types from A0 to G0 and luminosity class I-V, as well as 21 supergiants for which absolute magnitudes have been previously determined. He has shown that the O I line is apparently insensitive to temperature within the spectral ranges A0 to A5 and F0 to G0, and can be used as a measure of absolute magnitude for stars with $-4 > M_V > -9$ to an accuracy of 0.5 magnitudes. There is a discontinuity in the calibration between these two spectral ranges, the A-type supergiants showing the larger line strengths, which may reflect a temperature dependence or simply a change in the bolometric correction required.

Osmer made up to 23 observations on any one star and no variations with time were apparent in any of the program stars, but, as the error associated with each measurement was quite significant (typically 20% of the equivalent width), the possibility of small variations in the strength of the O I line has not been precluded. A significant advantage of the O I line strength as a luminosity indicator is that its measurement is reddening independent.

Model atmosphere calculations by Osmer show that the increase in the O I line strength with luminosity is due to both the decrease in the continuous opacity and the observed increase in the microturbulence. Although non-LTE effects may be present in the oxygen line, Osmer has concluded that they do not change significantly with luminosity and do

not contribute to the observed increase in strength.

The Balmer jump is also a useful gravity indicator for the less luminous F-type supergiants, as it is almost temperature independent. However, it suffers the disadvantage that any measurement of it is reddening and metal-line blocking dependent. The use of the Balmer jump as a gravity indicator leads to erroneous results for stars with $\log g < 1.0$ and $T_{eff} > 6500^{\circ}K$. These points are discussed more fully in Chapter 3.

1.2 Observational Information

(a) Microturbulent Velocity

Struve and Elvey (1934) were the first to show that the unusually large strengths of the saturated lines in the spectra of A and F high-luminosity stars could be attributed to microturbulent motions, i.e. motion which occurs on a scale smaller than the one over which the lines are formed. There are several methods by which the microturbulent velocity can be determined. The two most commonly used methods are the curve of growth and the curve of line-width correlation.

The Doppler broadening term in the line absorption coefficient is assumed to have the form

$$\Delta\nu_0 = \frac{\nu}{c} V_0 \quad , \text{ where } V_0^2 = \frac{2kT}{M} + \xi_s^2 \quad .$$

ξ_s is the microturbulent velocity and M is the mass of the absorbing atom. $\Delta\nu_0$ is directly proportional to the vertical shift required to make the flat section of the observed and the theoretical curves match. The absolute scale of the microturbulences derived in this manner depends, in some cases, on the model chosen, but the relative trends

observed when the same model is used should be reliable.

Huang and Struve (1955) have shown that the slope of the curve of central depth versus equivalent width at its origin, and its overall form are related to the microturbulent and macroturbulent (rotational) velocities. If a measure of the macroturbulent velocity is known, the microturbulent velocity can be derived from the curve in a straightforward manner. These two techniques are considered more fully in Sections 4.3 and 3.5(a) respectively.

In the past four or five years there has been an upsurge in interest in the microturbulence of both the main-sequence and supergiant stars. The dependence of the microturbulence on the spectral type, luminosity class and depth in the atmosphere have been investigated. Microturbulent velocities of up to 20 km sec^{-1} have been observed in some stars, but these are associated with circumstellar gas streams, and therefore do not imply that the atmospheric turbulence is that high. Abt (1960) and Osmer (1972) have observed microturbulent velocities in excess of 15 km sec^{-1} in the most luminous stars between F0 and G0.

The investigations of Abt (1957, 1958), Bonsack and Calver (1966), Rosendhal (1970b), Rosendhal and Wegner (1970) and Osmer (1972) show that:

(1) The Fe I microturbulent velocities in the Ia supergiants increase from 8 km sec^{-1} for the early-A stars to 10 km sec^{-1} at F0 to F2, decrease to 6 km sec^{-1} at F5, increase to 12 km sec^{-1} at G0, then decrease rapidly to about 3 km sec^{-1} at K0.

(2) The Fe II microturbulence apparently increases from 11 km sec^{-1} at A0 to 16 km sec^{-1} at G0.

(3) In the Ib supergiants and type II giants the microturbulence increases from A0 to F0, remains constant to G0, and then decreases to K0. Chaffee (1970) found that for main-sequence stars the velocity range is 2 to 4 km sec^{-1}. The microturbulence apparently increases from 2 km sec^{-1} at A2 to 4 km sec^{-1} at F0, then decreases to 2 km sec^{-1} at F5 and increases to 4 km sec^{-1} at G0.

Unno (1959 a,b) has used the Golberg (1958) method, which is insensitive to line transfer problems, to investigate the depth dependence of the turbulence in the photosphere and lower atmosphere of the sun. Unno found that the velocity decreased from 1.5 km sec^{-1} at τ_{5000} = 0.6 to 0.7 km sec^{-1} at τ_{5000} = 0.2, and then increased outward in the chromosphere, reaching 6 km sec^{-1} at a height of 3000km. Furthermore, the velocity was density dependent ($\rho^{-1/4}$) in the atmosphere.

His interpretation of these results gives a good idea of the current understanding of turbulence in stellar atmospheres. He attributes the velocity decrease with increasing height in the photosphere to the decay of convective motions above the region of instability. The chromospheric velocities, on the other hand, are caused by progressive waves travelling outward; they are proportional to $\rho^{-1/4}$, not $\rho^{-1/2}$, as they would be if they were acoustic waves, because the waves lose energy in being scattered by inhomogeneities in the gas.

To explain the depth dependence of the microturbulence along the main sequence, Chaffee has suggested that the depth dependence of the microturbulence in all the main-sequence stars is the same as that in the sun, i.e. initially decreasing with depth, reaching a minimum, and finally increasing. He proposed that the depth at which the minimum occurs depends on the depth of the convective zone, and thus the minimum moves down in the atmosphere with decreasing temperature.

Figure I.I shows this schematically; the vertical line represents the depth (τ = 0.3) at which the microturbulent velocities have been measured. Rosendhal (1970b) has demonstrated that this model is consistent with his results on the depth dependence of the microturbulence in the A-type supergiants. Chaffee's model is also consistent with the depth dependence of the microturbulence in α Per (F5Ib) observed by Parsons (1967). The depth dependence of the microturbulence in the supergiants will be considered in more detail in Section 4.3.

Rosendhal (1970b) and Rosendhal and Wegner (1970) found from their detailed investigations of A-type supergiants, that some of these stars show variations in microturbulence. These variations appear to be correlated with radial velocity variations, indicating a strong coupling between large-scale and small-scale mass motions. There also appears to be a correlation between absolute magnitude, mean value of the microturbulence, and amplitude of variability of both microturbulence and radial velocity. Rosendhal and Wegner have suggested that the mechanism which gives rise to the observed high microturbulent velocities in F and G supergiants may also be the cause of the variability.

It should be pointed out that the majority of the above-mentioned investigations have been carried out using the theoretical curve of growth calculated by Wrubel (1949), for the Milne-Eddington approximation. Because this is such a simplified model of the stellar atmosphere, the absolute scale of the microturbulent velocities is uncertain, but the variations along the spectral sequence and with luminosity are considered to be real.

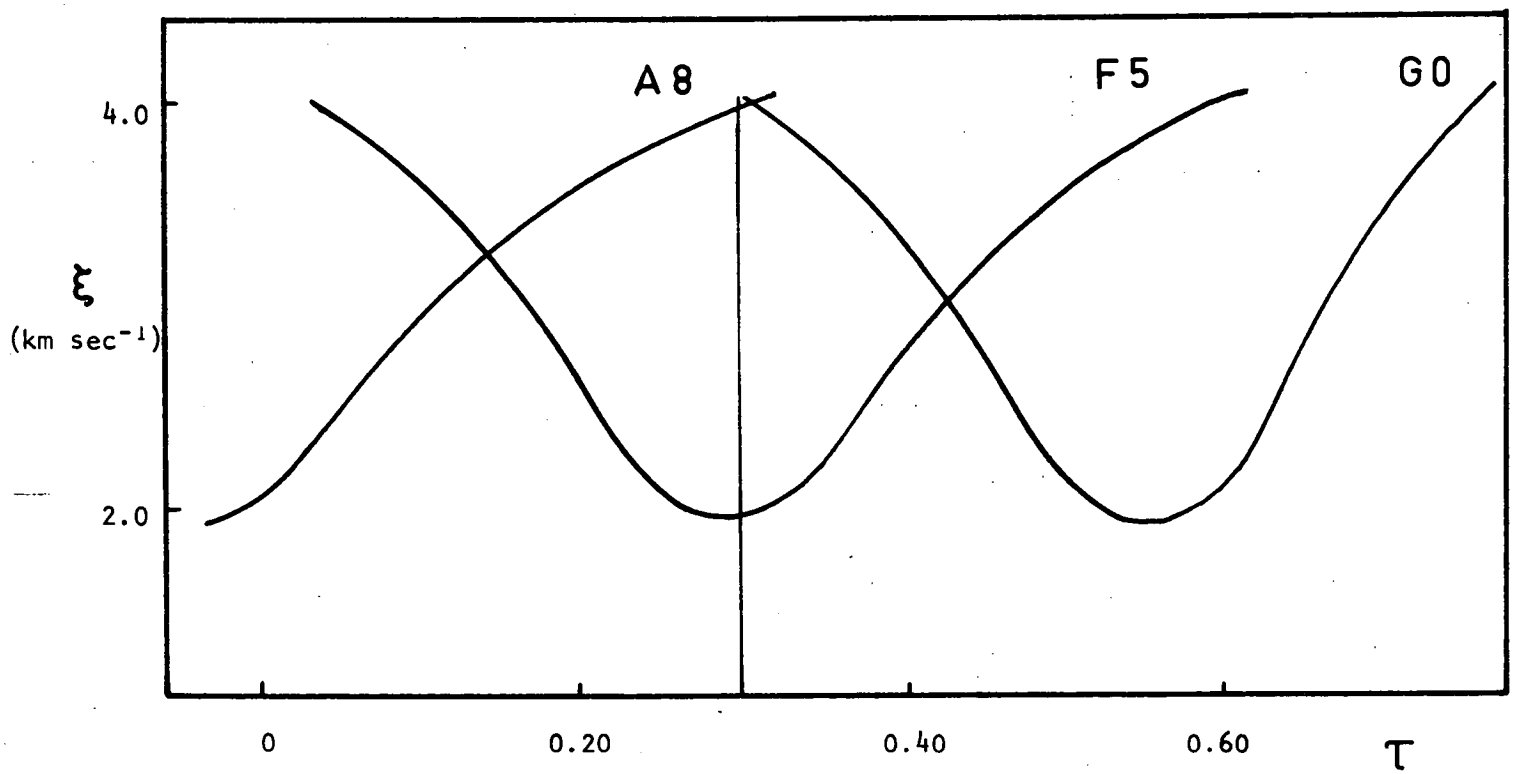

Figure 1.1 Inferred relation between the microturbulent velocity (ξ) and optical depth (τ) for various spectral types along the main sequence, (after Chaffee 1970).

The scale of the microturbulence is important for a number of reasons. First, one hopes to learn more about the hydrodynamical nature of the microturbulence itself, assuming that this represents a real velocity field in the atmospheres of stars (an assumption open to question). Second, the true Doppler profile must be accurately established as a fundamental parameter in the emerging generation of spectral synthesis computations. Third, the use of an incorrect microturbulence scale, even in a relative analysis, will lead to second order abundance errors, particularly for elements exhibiting only very weak or very strong lines.

Smith (1973) has attempted to fix the scale of the microturbulent velocity in the main-sequence A stars by using model atmosphere techniques to examine the profiles of weak and saturated lines in six sharp-lined Am stars. Smith found that the scale of the microturbulence was dependent upon the line blocking corrections, the model atmosphere adopted, dispersion-dependent equivalent width errors and errors in oscillator strength scales and damping constants. His results show that in these stars $2 \leq \xi_s \leq 4$ km sec^{-1}, where the curve of growth results indicate $\xi_s = 7$ km sec^{-1} but, as Smith points out, most, if not all, of the discrepancy can be attributed to differences in the numerical data used. Smith's and other investigations indicate that the microturbulent velocities derived from simple curve of growth techniques are systematically slightly larger than those derived from model atmosphere calculations.

It has been suggested by Underhill (1949) and Mihalas (1969) that the unstable pressure inversion zone just below the line-forming regions in the FIa supergiants may be the driving mechanism for the

large microturbulent motions observed in these stars. As pointed out by Underhill, if the mechanical force exerted by the photons exceeds the surface gravity, one obtains a negative gas pressure gradient inward. When we recall that the requirements of radiative equilibrium imply a positive temperature gradient inward, it is evident that a very strong density inversion occurs, so that the star becomes susceptible to a Rayleigh-Taylor instability (Chandrasekhar 1961). This instability should lead to violent, turbulent convection, with tongues of dense material falling into the less dense fluid. This mechanism thus provides a means of feeding energy from the luminous flux directly into mass motions. Underhill derives an estimate of the surface gravity (g_{min}) as a function of T_{eff} at which this instability must occur. This estimate is based upon the assumptions that the material is strongly ionized, so that electron scattering alone contributes to the opacity (σ) and only the continuum flux contributes to the radiative acceleration, leading to

$$g_{min} = \sigma_e \left(\frac{\sigma_k \, T_{eff}^{\,4}}{c} \right) \quad .$$

Böhm-Vitense (1973) found that for stars with $T_{eff} < 8000^{\circ}K$ and $\log g > 0.0$ the radiative acceleration at the surface of a star is increased by at least a factor of 6, and possibly even 60, by the inclusion of the line, as well as the continuum radiation pressure. This indicates that the pressure inversion zone is going to be significantly stronger than present models (Carbon and Gingerich 1969, Osmer 1970), which are calculated with the inclusion of continuum radiation pressure only, would suggest. This will increase the lower limit of the gravitational acceleration of stable stars and indicates that mass

loss is possible, due to radiation pressure, in stars with $M_v < -7$ and $T_{eff} > 8000^{o}K$. If large velocity gradients can be obtained in supergiants, for instance by pulsational instability, then the radiative acceleration may lead to mass loss in supergiant stars with T_{eff} as low as $5000^{o}K$.

Mass loss has been observed in two F I stars, ρ Cas and 89 Her. ρ Cas, normally a F8Ia star, occasionally throws out enough cool material to make it look like a K or M star (Payne-Gaposchkin and Mayall 1946 as quoted by Osmer 1970). Bidelman and McKeller (1957) report that after one large outburst in 1946, it gradually reverted to its normal spectral type, although many strong metallic lines in its spectrum had developed components, which were shifted to the blue by 40 km sec^{-1}. Its spectrum also showed unusual metallic emission lines which were blue shifted by 25 km sec^{-1} (Sargent 1961). Sargent and Osmer (1968) have shown that the outflowing material in 89 Her has velocities up to 150 km sec^{-1} with respect to the photosphere, but its nature is different to that in ρ Cas, for the absorption components are seen in the Balmer and Na D lines, not the metallic lines. Gillett, Hyland and Stein (1970) have found evidence for a circumstellar dust cloud surrounding 89 Her, which may reduce the observed visual flux by as much as 0.5 mag in this star. Humphreys, Strecker and Ney (1971) have observed a similar cloud surrounding the G8Ia^{+} supergiant HR 5171, and less optically-thick clouds surrounding other G-type supergiants. ρ Cas and 89 Her have been mentioned for the following two reasons: firstly, to show that large instabilities can occur in the F I stars, and secondly, to point out that the line spectra of other stars could be contaminated by unresolved circumstellar material.

(b) Abundances

A survey of the literature shows that the abundances (relative or absolute) of very few luminous F-type stars have been determined; Table I.I lists some of these investigations.

Table I.I

Previous Analyses of Luminous F-type stars

Star	Sp. Type	Reference
α Car	F0Iab	Greenstein (1942)
α Per	F5Ib	Greenstein (1948), Parsons (1967)
i Sco	F2Ia	Abt (1960)
35 Cyg	F5Ib	Preston (1961)
γ Cyg	F8Ib	"
φ Cas	F0Ia	Searle, Sargent and Jugaku (1963)
89 Her	F2Ia	"
HD 161796	F3Ib	"
41 Cyg	F2 - 4Ib	Kipper (1967)
ν Her	F2II - III	"

Those stars which have been studied, have been analysed using different theoretical models, different atomic constants, and by different workers. The resulting abundances of these apparently normal stars show a considerable spread, typically 0.6 dex, and the 'normal' abundances of these stars are extremely difficult, if not

impossible, to determine from these results. There is little point in discussing the published abundances any further here, except to say that firstly, the abundances observed in these stars are nearly all within the usual factor of two or three of the solar abundances, and secondly, they demonstrate that extreme care is needed when a comparison is being made between abundances derived in different investigations.

It is well recognized that different methods of analysis give rise to different abundances, from ± 0.2 to ± 0.4 dex (e.g. Cayrel and Cayrel de Strobel 1966, Aller 1963). There is also an apparent dependence of abundance on the spectral type and class of the star which is being analysed. Thus it is of little use to compare the abundances derived using the same techniques and atomic constants for the sun and, say, a luminous F-type star, except to check for large abundance discrepancies, i.e. > 0.5 dex.

The F I stars are amongst the most luminous stars and can be analysed in other galaxies, or at the extremes of our own galaxy. To enable a comparison to be drawn between these distant objects and the stars in closer proximity to the sun, it is necessary to know the average, and the standard deviation of the observed abundances for 'normal' stars in the vicinity of the sun, as derived using a particular technique of analysis and a particular set of numerical constants. Also, there are several F I stars, such as 89 Her and HD 161796, for which it would be of interest to determine any abnormalities in observed abundances.

Apparently the reason why a detailed study of a significant number of F I stars has not been carried out is that the majority of the

F-type supergiants in the northern sky have $m_v > 5.0$ magnitudes and a high resolution spectroscopic analysis of a number of these stars requires a considerable amount of telescope time. In the southern sky there are 10 F I stars with $m_v < 4.8$, currently the limiting magnitude for the 40cm telescope-spectrograph system at a dispersion of 9 $\mathring{A}\ mm^{-1}$, so a survey of these stars was possible, and was commenced in January 1972, when the telescope-spectrograph system became operational for the first time.

Despite the brightness of some of the program stars (Chapter 2), only α Car and i Sco have been the subjects of detailed analyses. α Car (Canopus) is representative of supergiants of intermediate luminosity, with spectral type near F0. Its spectrum is relatively simple because the lines of neutral metals are weak, and the star shows no appreciable rotational broadening. Greenstein (1942) analysed α Car using high resolution plates (2.4 to 4.0 $\mathring{A}\ mm^{-1}$) over the wavelength range 3800$\mathring{A}$ to 6700$\mathring{A}$. Assuming solar abundances, he investigated the continuous opacity and ionization equilibra and found log Pe = 1.0 and $\theta_{ion} = 0.69$. He also showed that the hydrogen lines indicated a gravity of log g = 1.5, and he concluded that

> "the abundances of the metals are all probably close to their solar values, since the discussion of the ionization equilibra and opacity left no large discrepancies between the predicted and observed intensities of the metallic lines".

i Sco was analysed by Abt (1960). However, as pointed out by Searle, Sargent and Jugaku (1963), both the excitation and mean atmospheric temperatures used by Abt were too low, which lead to an incorrect estimate of the microturbulent velocities and abundances.

It is known that different telescope, spectrograph and observer systems give different equivalent width scales of up to about ± 0.15 dex, e.g., Preston (1961), Bell and Rogers (1965), Chaffee (1970). As a check on our equivalent width scale, the F8Ia supergiant δ CMa, which has been the subject of many detailed analyses, was included in the program. In passing it should be noted that only the iron abundance, microturbulent and macroturbulent velocities have been studied (see Bell and Rogers 1965). δ CMa is cooler than the rest of the program stars, and therefore should indicate the spectral range over which the observed abundances are independent of spectral type, when the same analysis techniques are used.

Chapter 2

OBSERVATIONAL MATERIAL AND MEASUREMENTS

2.1 Introduction

The observational material obtained in this work takes the form of high and medium dispersion spectroscopic plates of all the early F I stars in the southern sky brighter than fifth magnitude. These plates have been taken to obtain information on hydrogen-line profiles, blanketing measures, and metal-line strengths. The highest dispersion plates are suitable for metal-line profile measurements, but this has not been undertaken in this investigation, except for the determination of rotational velocities. The hydrogen-line profiles, blanketing measures and the narrow-band *ubvy* photometry data can be combined to enable detailed comparisons with model atmospheres.

In this chapter we discuss how this set of spectroscopic plates was obtained, the procedures involved in the basic reduction of the observational data, and the reliability of the basic data thus obtained.

2.2 Spectroscopic Observations

All the high dispersion spectral observations used for this project were obtained with the Coudé spectrograph of the 40cm telescope at the University of Tasmania's Astronomical Observatory. This instrument, and associated equipment, is described in detail in Appendix I; only a very brief description is given here.

The collimator mirror (focal length 365cm) accepts the f/31 beam from the slit; the dispersing media are gratings, 15cm x 11cm in ruled area. Cameras with 120cm and 180cm focal lengths are

available; all observations for the present investigation were made with the 180cm off-axis camera.

Two gratings were available: the A grating, 600 lines mm^{-1}, is blazed near 5500Å in the first order. With the 180cm camera, this grating gives a linear dispersion of 9 Å mm^{-1}. The B grating, 1200 lines mm^{-1}, is blazed at 5000Å in the second order; with the 180cm camera it gives a linear dispersion of 2.1 Å mm^{-1} in the blue (2nd order), and 1.4 Å mm^{-1} in the ultraviolet-violet region of the spectrum (3rd order).

Widening of the spectra was accomplished by means of a rocking plane-parallel quartz plate in the front of the slit. After installation of the exposure meter, which measured both instantaneous and total flux entering the slit, observational efficiency with the spectrograph was high. All plates exposed, except those stopped by cloud, were usable, partly because guiding was better and partly because the required exposure could be accurately estimated. In the latter part of the observing program guiding was performed automatically for stars brighter than fourth magnitude.

2.3 Program Stars

The program stars are listed in Table 2.1, along with some basic information about each of them. This list contains all the stars of spectral class I, with spectral type in the range A5 to F5, brighter than $m_v = 4.7$ and south of declination -15° that are included in the *Bright Star Catalogue*. $m_v = 4.7$ is the limiting magnitude of the 40cm telescope-spectrograph system at a dispersion of 9 Å mm^{-1}, using pre-flashed 103a-O plates. ν Car, 196 Car and π Sag

Table 2.1

Program Stars

Star	HR Number	HD Number	R.A.	Dec.	l	b	m_v	Sp
α Lep	1865	36673	5^h 28.2	-17° 54'	220° 57'	-25° 9'	2.56	F0Ib
α Car	2326	45348	6^h 21.4	-52° 38'	261° 12'	-25° 18'	-0.73	F0Ib, Iab
δ CMa	2693	54605	7^h 4.2	-26° 14'	238° 25'	-8° 16'	1.84	F8Ia
b Vel	3445	74180	8^h 37.2	-46° 18'	265° 17'	-2° 57'	3.89	F2Ia
i Car	3699	80404	9^h 14.2	-58° 51'	278° 27'	-7° 0'	2.24	F0Iab
ν Car	3890	85123	9^h 44.4	-64° 36'	285° 2'	-8° 49'	3.15	A9II
195 Car	4110	90772	10^h 23.4	-57° 8'	284° 35'	0° 2'	4.66	F0Ia*
196 Car	4114	90853	10^h 24.1	-58° 14'	285° 13'	0° 54'	3.82	F0II
	4352	97534	11^h 8.2	-54° 46'	290° 59'	0° 15'	4.59	F0Ia
θ Sco	6553	159532	17^h 30.1	-42° 56'	347° 8'	-5° 58'	1.88	F0Ib
i Sco	6615	161471	17^h 40.3	-40° 5'	350° 37'	-6° 7'	2.98	F2Ia
π Sag	7264	178524	19^h 3.5	-21° 11'	15° 53'	-13° 17'	2.90	F2II-III

* 195 Car has been re-classified by Lloyd Evans (1969) as A7Ia.

(all luminosity class II) were included in the program to investigate possible luminosity-dependent abundance variations. No sufficiently bright class III star was available to further increase the luminosity range observed. δ CMA (F8Ia) was included to check the equivalent width scale and investigate possible temperature-dependent abundance variations.

2.4 Spectrograms

Details of the spectrographic plates analysed in this investigation are given in Table 2.2. For the violet and blue regions, IIa-0 plates were preferred for their smaller grain and were used wherever possible; in the cases where plates of higher speed were necessary, 103a-0 or Ia-0 plates were used. In some cases (Table 2.2), the plate speed was increased by pre-flashing to a background density of approximately 0.3 (Section A1.9).

Spectra of the program stars were widened to 1 mm and a Coudé slit width, corresponding to 70μ when projected on the plate, was used. The only exceptions were the high dispersion IIa-0 plates of α Car, which were widened to 1.5 mm and a slit width corresponding to 40μ used. Comparison spectra from a neon lamp were exposed on one side of the stellar spectra, and the spectra calibrated using a triangular wedge.

All plates were developed in D19 developer for six minutes at 20°C, using mechanical agitation (Section A1.10). Exposures were judged so that the section of the plates used had densities lying in the top section of the near-linear part of the calibration curve.

Table 2.2

Spectrograms Analysed in this Investigation

Date	emulsion type	dispersion ($\AA\ mm^{-1}$)	centre wavelength	resolution[1] ($\AA$)	exposure time (min)	Pre-flash
			α Lep			
Jan '73	103a-0	1.4	3720	0.11	150	yes
Jan '73	103a-0	1.4	3950	0.11	130	yes
Dec '72	103a-0	2.1	3800	0.18	190	yes
Dec '72	103a-0	2.1	4200	0.18	135	yes
Dec '72	103a-0	2.1	4200	0.18	145	yes
Jan '73	103a-0	2.1	4500	0.18	140	yes
Jan '73	103a-0	2.1	4800	0.18	170	yes
			α Car			
Jan '73	IIa-0	1.4	3720	0.10	25	yes
Jan '73	IIa-0	1.4	3950	0.10	15	no
Jan '72	103a-0	2.1	3800	0.18	35	no
Feb '72	IIa-0	2.1	4200	0.17	26	no
Feb '72	IIa-0	2.1	4500	0.17	30	no
Feb '72	IIa-0	2.1	4800	0.17	40	no
Feb '72	103a-D	2.1	5100	0.20		no
Feb '72	103a-D	2.1	5400	0.20		no
Feb '73	103a-0	2.1	4200	0.18	8	no
Feb '73	103a-0	2.1	4500	0.18	8	no
Feb '73	Ia-0	2.1	4200	0.20	5	no
Feb '73	IIa-0	9	4300	0.35	4.5	no
Feb '73	103a-0	9	4300	0.4	3	yes

Date	emulsion type	dispersion (Å mm^{-1})	centre wavelength	resolution[1] (Å)	exposure time (min)	Pre-flash
			δ CMa			
Feb '73	103a-0	1.4	3720	0.13	105	yes
Jan '73	IIa-0	1.4	3950	0.11	200	yes
Jan '73	103a-0	2.1	4200	0.18	120	no
Jan '73	103a-0	2.1	4500	0.18	120	no
Feb '73	103a-0	2.1	4800	0.19	140	no
March '73	103a-0	9	4300	0.4	33	no
			b Vel			
March '73	103a-0	9	4300	0.4	135	no
			i Car			
Feb '73	103a-0	1.4	3720	0.11	150	yes
March '73	103a-0	1.4	3950	0.11	90	no
Jan '73	103a-0	2.1	4000	0.18	140	no
Feb '73	103a-0	2.1	4200	0.18	150	no
Feb '73	103a-0	2.1	4500	0.18	135	no
Feb '73	103a-0	2.1	4700	0.18	105	yes
			ν Car			
March '73	IIa-0	9	4300	0.35	180	yes
			195 Car, HD 97534			
March '73	103a-0	9	4300	0.4	200	yes
			196 Car			
March '73	103a-0	9	4300	0.4	150	yes

Date	emulsion type	dispersion (Å mm^{-1})	centre wavelength	resolution[1] (Å)	exposure time (min.)	Pre-flash
			θ Sco			
Aug '72	Ia-0	2.1	3800	0.20	120	yes
Aug '72	Ia-0	2.1	4200	0.20	85	no
Aug '72	Ia-0	2.1	4500	0.20	85	no
Aug '72	Ia-0	2.1	4800	0.21	180	no
Sept '72	103a-D	9	5200	0.4	105	yes
Sept '72	IIa-0	9	4300	0.30	90	yes
			i Sco			
Aug '72	Ia-0	2.1	3800	0.20	180	yes
Aug '72	Ia-0	2.1	4200	0.20	105	yes
Aug '72	Ia-0	2.1	4200	0.20	140	no
Aug '72	Ia-0	2.1	4500	0.20	110	yes
Aug '72	Ia-0	2.1	4500	0.20	105	yes
Aug '72	Ia-0	2.1	4800	0.20	180	yes
Sept '72	Ia-0	2.1	4900	0.20	200	yes
			π Sag			
Aug '72	Ia-0	2.1	3800	0.20	150	yes
Aug '72	Ia-0	2.1	4100	0.20	120	yes
Aug '72	Ia-0	2.1	4500	0.20	120	yes
Sept '72	Ia-0	2.1	4800	0.20	140	yes

Notes to Table 2.2

1 The resolution has been determined from the comparison lines that have an intrinsic width at half-height of approximately 0.08Å, so the values quoted are only upper limits, although close upper limits for all plates other than the extra high resoltion plates of α Lep, α Car and i Car.

Inspection of the plate of 196 Car showed that it was later (F8III) than the listed spectral type (F0II), and the spectrum of this star was not analysed further. 196 Car was also excluded from the determination of atmospheric parameters (Chapter 3).

2.5 Spectroscopic Reductions

All plates were traced on the Observatory's Hilger microphotometer, at a linear magnification of approximately 45 for the 1.4 and 2.1 $\mathring{A}\ mm^{-1}$ plates, and 70 for the 9 $\mathring{A}\ mm^{-1}$ plates, using a projected slit width of approximately 35μ on the plate. The reference zero level for each plate was taken as the mean of clear plate tracings on either side of the stellar spectrum.

It should be noted that the zero level on all plates, whether pre-flashed or not, showed very little variation along the length of the plate, except for the last 12mm, where the background decreased slowly towards the edge of the plate.

Calibration curves for a plate at a particular wavelength were obtained by driving the plate perpendicular to the dispersion with a suitable linear magnification. The co-ordinates of the resultant curve are plate transmission versus intensity of incident light. The density-intensity conversion was carried out with a Moseley curve follower, using the appropriate calibration curve.

To determine the variation in shape of the calibration curve with wavelength, the calibration spectrum was run on the microphotometer at a number of wavelengths with the curve follower, using a calibration curve derived at a different wavelength. If there is no change of calibration curve with wavelength, a straight line should

be traced, the slope of which depends on the density of the exposure at that particular part of the calibration spectrum. This was, in fact, found to be the case over a range of 3640Å to 4300Å and 4300Å to 5000Å for IIa-O, 103a-O and Ia-O emulsions, 5000Å to 6000Å for 103a-D emulsion and 5700Å to 6700Å for 103a-F emulsion. When a number of calibration curves had been constructed, it was found that one could often be selected to satisfy the above straight line condition for a new plate.

For the less luminous program stars, which are relatively free from crowding of strong absorption lines, establishment of the continuum level on the tracings was not difficult, and was subject to a small uncertainty, except in the region surrounding the calcium H and K lines. For the stars of higher luminosity and those studied at low dispersion, the placement of the continuum is more difficult and, in some cases, is subject to a rather large uncertainty. A brief description of the techniques used to find the continuum level follows.

Tracings of the calibration spectra at the same mean intensity as the stellar continuum were made to determine the noise level on the plates, and indicate the wavelength dependence of the plate sensitivity. The plates of O-sensitizing showed a smooth, slowly varying dependence of sensitivity on wavelength, but the plates with D- and F-sensitizing showed significant wave-like variations, which complicated the task of determining the continuum. In the line-free regions of the stellar spectrum, a mean value was sketched through the noise on the trace and, with the aid of a length of thread, a smooth envelope was drawn through the upper values of this mean.

In the most luminous stars studied at high dispersion, δ CMa and i Sco, there were very few regions that were line free, particularly for wavelengths less than 4200Å in the case of δ CMa, and 4080Å in the case of i Sco.

For δ CMa, from the appearance of the tracings for λ less than 4070Å, it is dubious whether the true continuum was ever represented because of the crowding of the metal lines. Equivalent widths reported for lines in this region may be subject to a large systematic error. θ Sco, because of its high rotational velocity, poses a special problem. To reduce the effects of plate noise, the high-dispersion plates of θ Sco were traced, using a projected slit width of 100μ and a linear magnification of 30. It is considered doubtful whether the true continuum is reached at wavelengths less than 4250Å. In fact, the placement of the continuum is doubtful for wavelengths less than 4500Å. Because of this, and the small number of usable lines due to blending, plates of θ Sco were taken at 9 Å mm^{-1} dispersion to cover the wavelength range 4950Å to 5900Å. Similar comments as those made for θ Sco apply to the two F0Ia stars studied at 9 Å mm^{-1}, 195 Car and HD 97534. Although their rotational broadening was less than that in θ Sco, the intrinsic strengths of the metal lines, particularly those due to singly-ionized atoms, were much larger. Due to the faintness of these two stars, plates at longer wavelengths could not be taken. Table 2.3 gives the estimated uncertainty in the placement of the continuum for the various star, plate, and dispersion combinations.

Table 2.3

Estimated Uncertainty in Placing the Continuum

Star	Dispersion	Plate type	Uncertainty (%)	Comments
α Car	1.4, 2.1	IIa-0	0.70	extra high resolution plates
α Lep α Car i Car	1.4, 2.1	103a-0 103a-D Ia-0	1.2	
δ CMa	2.1	103a-0	1.6	$\lambda > 4300\text{Å}$
δ CMa	2.1	103a-0	2.0	$4180\text{Å} < \lambda < 4300\text{Å}$
δ CMa	1.4	103a-0 IIa-0	unknown	$\lambda < 4080\text{Å}$
i Sco	2.1	Ia-0	1.5	$\lambda > 4080\text{Å}$
i Sco	2.1	Ia-0	2.0	$\lambda < 4080\text{Å}$
π Sag	2.1	Ia-0	1.5	
θ Sco	2.1	Ia-0	2.0	$\lambda > 4250\text{Å}$
θ Sco	2.1	Ia-0	unknown	$\lambda < 4250\text{Å}$
θ Sco	9	IIa-0	2.5	$\lambda > 4300\text{Å}$
θ Sco	9	IIa-0	unknown	$\lambda < 4300\text{Å}$
θ Sco	9	103a-D	3	
b Vel	9	103a-0	2	
ν Car	9	IIa-0	1.7	
195 Car HD 97534	9	103a-0	2.5	$\lambda > 4250\text{Å}$
195 Car HD 97534	9	103a-0	3.5	$\lambda < 4250\text{Å}$

Confidence in the stability of the observing system is important for later rotational velocity determinations. To this end, a trace of a few selected comparison spectrum lines was made on each plate, with a projected slit width of 30μ and a linear magnification of 200. Their widths at half-height were then measured. The average values of each plate (Table 2.2) showed remarkably small variations from plate to plate (e.g. 0.007Å for the 103a-0 plates), and no systematic trend was evident from the August-September 1972 plates to the plates taken in the 1972-1973 summer observing period.

2.6 Hydrogen and Calcium H and K Lines

Profiles of the hydrogen and calcium K lines were sketched through the plate noise of each tracing, and residual intensities were measured at fixed wavelengths from each line centre, using the envelope fitted to the plate continuum to define the continuum level above the line. Mean profiles over all the plates for a given star, weighted for plate quality, were then obtained. The variation from plate to plate indicates that the mean internal standard deviations of these measurements are 0.01 at line centre, 0.025 at $R_c = 0.50$ and 0.015 at $R_c = 0.95$, for the 1.4 Å mm^{-1} and 2.1 Å mm^{-1} plates. For the 9 Å mm^{-1} plates, the internal deviations are typically 0.010 larger.

The hydrogen-line profile measurements (H_γ, H_δ and H_8) for stars observed are given in Appendix III; the measured equivalent widths of H_β to H_{15} are also given. These tables list the mean residual intensities for each star as a function of distance, $\Delta\lambda$(Å), from the line centre. The number of plates used to form the mean value is

also indicated. The profiles listed are the means of both the blue and red wings. Specific remarks are given as footnotes to the tables. The H_γ profiles of 19 Cam and HD 97534 are not given because their measurements were very doubtful due to large metal lines in the wings. The profiles of H_ε and the calcium H line could not be measured because of their severe blending with each other.

Measurement of the calcium K line profile poses special problems in the stars for which the calcium or hydrogen line wings extend beyond about 15Å from the line centre, because in this case the true continuum is not reached over a 60 to 70Å section of the tracing, from approximately 3918Å to 3985Å. A further complication is introduced when tracings of 9 Å mm^{-1} or 2.1 Å mm^{-1} dispersion plates are being used because the continuum is not of uniform density over this wavelength range. The density decreases towards the violet. The 1.4 Å mm^{-1} dispersion plates have an almost constant continuum density over the range 4070Å to 3850Å; the decrease in energy per unit wavelength is apparently compensated for by the increase in efficiency of the spectrograph towards the ultraviolet.

Tracings of the 1.4 Å mm^{-1} dispersion plates can be used to resolve the problem of where to draw the continuum envelope, because they make it possible to find the stars in which the true continuum is reached between the calcium H and K lines. In α Lep and i Car the true continuum is apparently only reached in a 0.7Å interval at 3946.5Å. Knowing this, the continuum can be drawn in on the tracings of the 2.1 Å mm^{-1} dispersion plates for these stars. The resultant continuum shape was then transferred to the tracings of the 2.1 Å mm^{-1} plates covering this region for the other stars. Tracings of the

1.4 Å mm^{-1} plates of α Car showed that at 3946.5Å, the apparent continuum came to within 2% of the true continuum envelope. This measurement enables the continuum to be drawn in on the tracings of the 9 Å mm^{-1} plates of α Car. However, due to the presence of several very small lines in the 0.7Å interval about 3946.5Å, which will not be resolved on the 9 Å mm^{-1} tracings, but will depress the apparent continuum, the true continuum envelope was drawn 3% above the apparent continuum. This continuum shape was then transferred to the tracings of the other 9 Å mm^{-1} plates, with the exception of 195 Car and HD 97534, where the smallness of the hydrogen and calcium lines made it possible to draw the continuum directly, but with quite a large uncertainty because of the strength of the metal lines. The tracings along the photometric calibration spectra were of little use in this wavelength region since they showed that the density of the calibration spectra decreased considerably more rapidly than the stellar continuum.

Equivalent widths of the hydrogen and calcium K lines were measured in two different ways, depending on the size of the line. For the smaller lines (< 35cm in length on the tracings), the planimeter was used. The planimeter could not be used for the larger lines unless they were broken up into smaller sections, or the plates retraced. As the profiles had already been measured, the equivalent widths were determined using the trapezoidal rule. Checks showed that the differences between the two methods were less than 1.5%. Means for each star were formed, and the internal standard deviation of the measured equivalent widths for one star, from 1.4 or 2.1 Å mm^{-1} plates, averaged ± 4.5%. The 9 Å mm^{-1} and high-dispersion plates of α Car

gave the same equivalent widths to within ± 4%, so it is anticipated that the errors in the hydrogen and calcium line equivalent widths derived from 9 Å mm^{-1} plates should not exceed 5%. It should be noted that the observed equivalent widths, particularly for the hydrogen lines, depend strongly on the position of the continuum. A 1% change in continuum level corresponds approximately to a 4% change in the observed equivalent width.

It is unfortunate that the only means of making an external check for systematic errors in the observed hydrogen-line profiles is a comparison between the H_δ profile of α Car observed here, and that reported by Greenstein (1942). The comparison with Greenstein's H_δ profile is shown in Figure 2.1. Examination of this figure shows that there are significant differences between the two profiles, particularly in the core region and about 7Å from line centre, the reasons for which are unknown.

2.7 Line Blocking Measurements

Line blocking* measurements for three different scanner or photometry systems have been made. Firstly, the blanketing for α Car in 9Å wide rectangular band-pass intervals about set wavelengths was needed so that the scanner observations of Aller, Faulkner and Norton (1966) could be used (Section 3.3). The results of these measurements are given in Table 3.2. Secondly, the line blocking under the *u*, *b* and *v* filters of the Strömgren four-colour photometry system was measured

---

* Throughout this dissertation we distinguish between the term 'line blocking' and 'line blanketing'. The former refers to the fraction of energy covered by absorption lines, where the lines are removed by correcting the continuum of the emergent flux, whereas the latter term is used only when the effect of line absorption on the atmospheric structure is being considered.

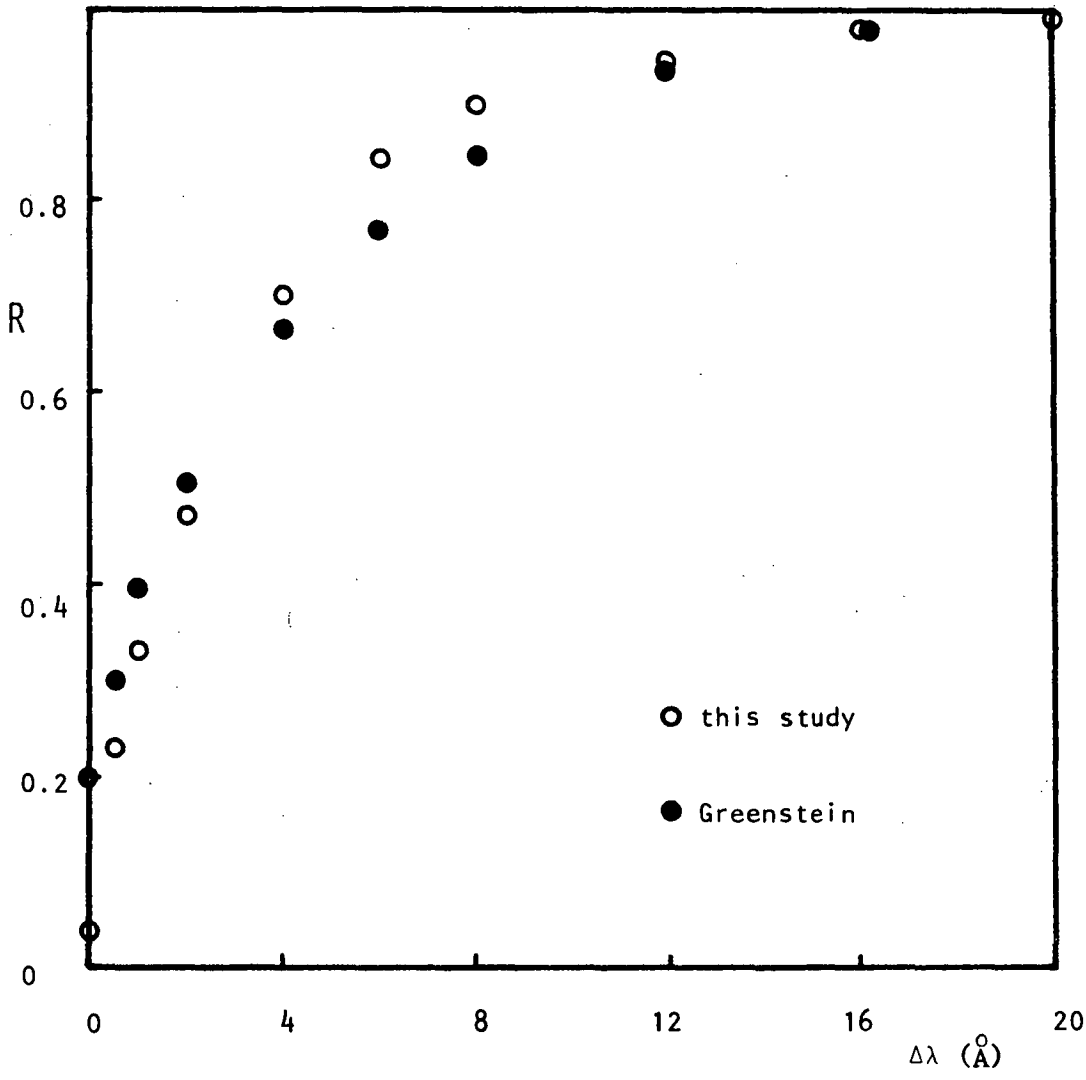

Figure 2.1 An intercomparison of H_δ line profiles observed for α Car. The ●'s represent points taken from Greenstein (1942) and the o's represent the observations made here.

for the program stars. Since the spectroscopic plates for the majority of the program stars only went out to 5000Å, the blocking under the *y* filter could only be measured in α Car and θ Sco. The methods used, and the results of these measurements, are given in Section 3.4. Finally, the line blocking in the standard 50Å Oke passbands, in the wavelength range studied in each star, were measured; the results of these measurements are given in Table 2.4. This data will enable approximate blanketing corrections to be made in stars of similar spectral type, for which high-dispersion spectroscopic data is not available.

The line blocking measurements for the 9Å and 50Å rectangular bandpasses were made by breaking the appropriate wavelength interval up into a suitable number of equal sections, about 25cm of tracing, measuring the fraction, Fb, of the continuum removed by the lines using the planimeter, and calculating the average, $(Fb)_{av}$. The average, in magnitudes, $\Delta b = -2.5 \log_{10} (Fb)_{av}$, can then be added directly to the flux observed with the scanner.

The line blocking measurements for each star were made from as many plates as possible. The observed plate to plate variations indicate an internal mean standard deviation of 0.02 magnitudes for the 1.4 Å mm^{-1} and 2.1 Å mm^{-1} dispersion plates.

The largest values of line blocking encountered in the early F I stars are about 0.24 magnitudes, so errors in the microphotometry will have a significant effect on the derived temperatures and gravities. The uncertainty in the continua (Table 2.3) can be used to estimate the uncertainty in the microphotometry results by noting that ± 1% in the continuous level corresponds to ~ ± 0.01 magnitudes in the measured line blocking.

Table 2.4

Line Blocking Measurements for the Program Stars

Star	Central Wavelengths (Å)											
	3636	3704	4032	4167	4255	4464	4566	4785	5000	5263	5556	5840
α Lep		0.36	0.22	0.23	0.19	0.17	0.13	0.09				
α Car	0.06	0.38	0.12	0.13	0.10	0.10	0.09	0.04	0.04	0.05	0.04	
δ CMa			0.42	0.63	0.44	0.42	0.35	0.11				
b Vel			0.20	0.20	0.15	0.13	0.14	0.06				
i Car		0.33	0.11	0.12	0.11	0.09	0.08	0.03	0.04			
ν Car			0.11	0.12	0.09	0.08	0.08	0.04				
195 Car[1]			0.23	0.20	0.22	0.22	0.17	0.12	0.			
HD 97534[1]			0.23	0.19	0.23	0.22	0.18	0.11				
θ Sco[1]			0.21	0.22	0.18	0.23	0.18	0.11	0.10	0.14	0.08	0.06
i Sco[1]			0.30	0.26	0.27	0.22	0.25	0.09				
π Sag			0.20	0.20	0.16	0.14	0.10	0.06				

Note

1 There is a possibility of large systematic errors in the results of these stars, particularly for $\lambda < 4255$Å, because of the difficulty in placing the continuum.

2.8 Line Identifications

Line identifications in α Car were carried out using the line lists for this star by Greenstein (1942) (3900Å to 4490Å) and Castley (1969) (3830Å to 4450Å), and the solar identifications of Moore, Minnaert and Houtgast (1966). The relative strengths of the components in the suggested blends were determined by comparison with other lines of the same multiplets in the sun and α Car. There are only a few lines in α Car which remain unidentified.

Having identified the lines in α Car, these identifications could be transferred to the other program stars, providing the differences in line strengths due to differences in excitation temperature and electron pressure were taken into account. Reference was made to the lists of Abt (1960) and Bell and Rogers (1965) for i Sco and δ CMa respectively. It was noted that some of the lines used by Abt (1960) for his analysis show up as two resolved lines, or an obvious blend, in the tracings of α Car. These lines were not used unless it was obvious that one component would be less than 10% of the other, due to the differences in electron pressure and excitation temperature between α Car and the other star.

2.9 Selection and Measurement of the Metal Lines

Selection of a line for measurement was based on the estimation of possible blending from neighbouring lines, the possibility of establishing the effective continuum, and the existence of reliable oscillator strengths for that line. All the lines chosen were estimated to contribute 80% or more to the blend. Errors in positioning the continuum affect the weak lines much more strongly

than the strong lines, and can therefore lead to errors in the observed excitation temperature and microturbulence.

There are three commonly used methods of determining the equivalent width of a line. They are :-

(1) planimetry of the line profile,

(2) use the central depth of the line as a measure of the equivalent width,

(3) approximation of the lines by triangles.

The first two of these methods will be described in turn, since they were both considered in this study.

(1) Planimetry.

By observing the way in which line profiles vary with strength of the line, complete "Gaussian" profiles were drawn for all the measurable lines. If the central intensity of the line was lowered by blending with a neighbouring line, both profiles were drawn in according to the combination graphs of Moore, Minnaert and Hautgast (1966) (eye estimates only). It was hoped in this way to avoid the possibility that a weaker blended line would have the same strength as a stronger unblended line because the central intensities were the same. This method requires an empirical judgement concerning the relative strengths of the two lines. In all cases the enclosed area was measured using a planimeter. Measures were considered acceptable when two successive measures were within 1% for the strong lines (> 150mÅ), increasing to 5% for the smallest lines (< 20mÅ). To obtain the 5% accuracy for the smallest lines, it was found necessary to planimeter around the line a number of times and average the results.

(2) Central depths of the Lines

If we assume that all lines of the same strength formed in a stellar atmosphere have the same shape, then it is possible to establish a unique relationship between the equivalent width, W, of a line and its central depth R'(0). From the tracings of α Car and i Sco, selections were made of a number of unblended lines covering the widest possible range in strength. Figure 3.8 shows a plot of equivalent width against line depth for α Car. For α Car, there was very little deviation from the mean curve, but for i Sco (F2Ia) there was a large scatter, which was in excess of that expected from the anticipated errors in the measurements. A similarly large scatter was observed by Bell and Rogers (1965) for the F8Ia supergiant δ CMa. Because of the high quality of the plate material, and to avoid any unnecessary uncertainty in the equivalent widths, this method was not employed to determine the equivalent widths.

2.10 Line Intensities.

The table containing the relevant material concerning individual lines has been included as Appendix IV. This data represents some 4,000 values, averaged from 9,000 measurements, taken from the tracings of over 50 plates. The data constitutes an essentially complete sample of the lines in the wavelength ranges studied, with strengths down to about 12mÅ for the sharpest-lined stars. The mean error of an equivalent width ranges from ± 4mÅ to ± 15mÅ for the fine-line stars studied at high dispersion. The weakest lines measured, with W of the order of 12mÅ, have an error as large as 40 percent; the

strongest lines (omitting hydrogen and the calcium H and K lines) have W in the order of 300mÅ, and the error is about 4 percent. The internal error in the equivalent widths measured for the stars studied at low dispersion could possibly reach twice the above values. The equivalent width data has been screened using internal standard deviations of individual lines from the curves of growth and many errors were found in this manner. This was an attempt to remove any large mistakes in measurement or reduction, but it is inevitable that such a large body of data will contain some errors of lower significance.

δ CMa was included in the program so that an external check could be made on our equivalent width scale. Bell and Rogers (1965) observed δ CMa at 2.7 Å mm^{-1} with an instrumental half-width of 0.08Å. Comparison of their equivalent widths with the results of two previous investigations showed only minor differences. A comparison of the equivalent widths in δ CMa found in this investigation with those of Bell and Rogers is given in Figure 2.2. Inspection of Figure 2.2 shows that there are no systematic differences between the two equivalent width scales, and the scatter is small.

A further, but less reliable check, can be made by comparing the equivalent widths found here for i Sco and those of Abt (1960). Abt measured his equivalent widths from 9 Å mm^{-1} plates. Figure 2.3 shows this comparison, and it is evident that our measures of log W/λ differ from those of Abt, in the sense that he measures lines to be weaker than we do. The differences in the two equivalent width scales are equivalent width dependent; for the large lines, log $W/\lambda \simeq 3.8$, the average difference is 0.09, whereas for the small lines the average difference approaches 0.18. This trend suggests that the

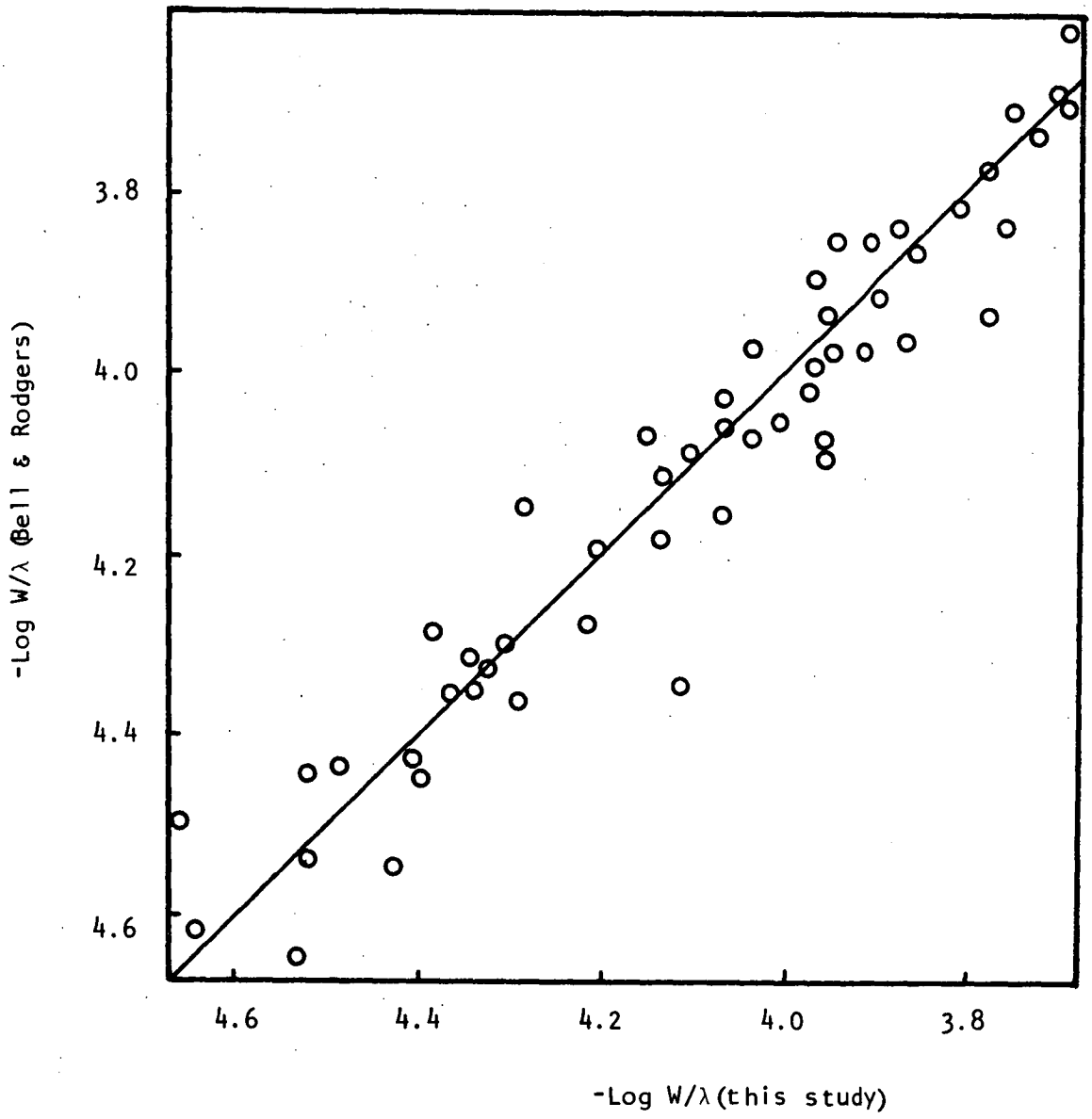

Figure 2.2 Comparison of the iron equivalent widths for δ CMa measured in this investigation plotted as abscissa and the equivalent widths of Bell & Rogers (1965) plotted as ordinate.

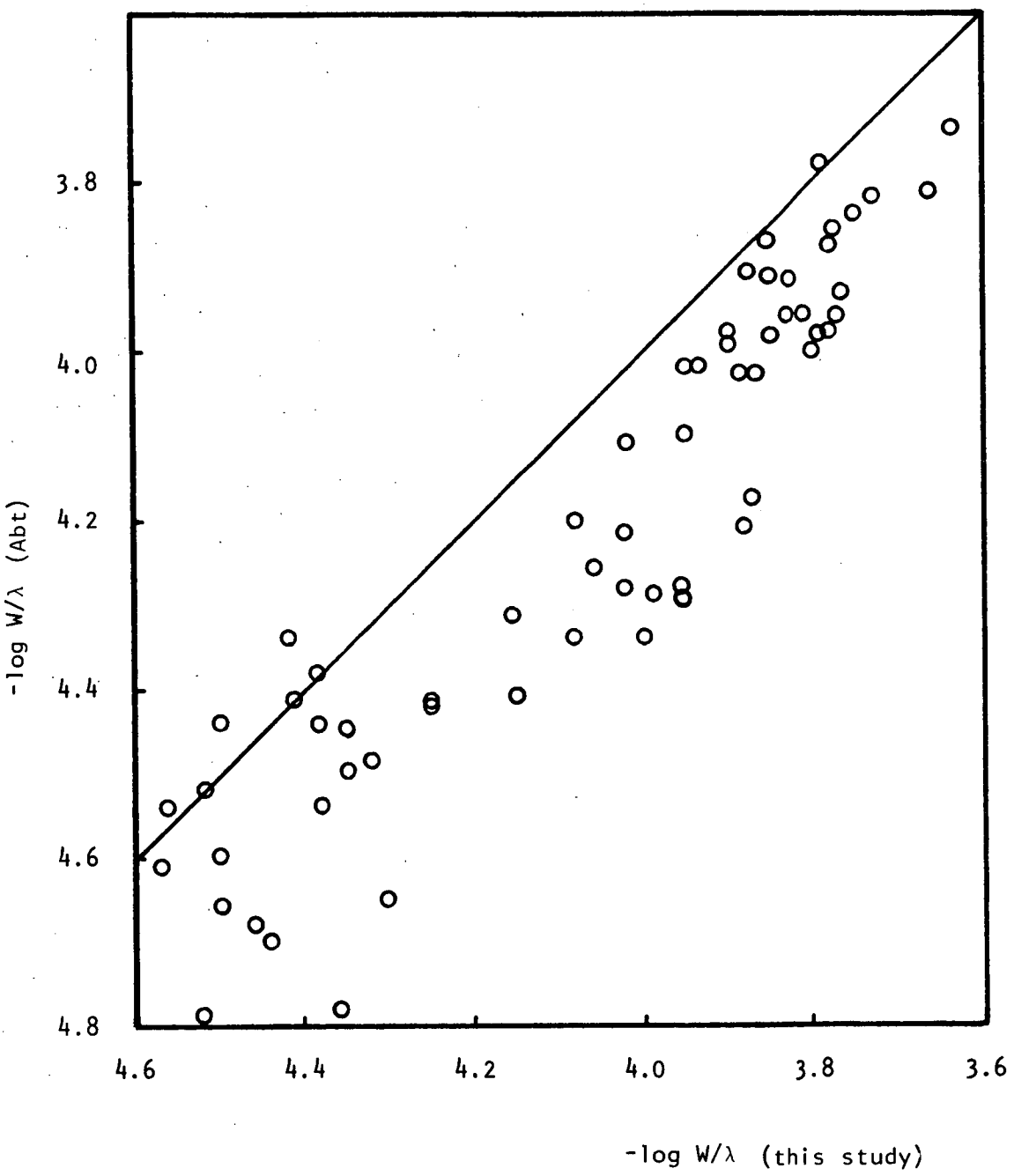

Figure 2.3 Comparison of iron equivalent widths for iSco measured in this investigation plotted as abscissa and the equivalent widths of Abt (1960) plotted as ordinate.

discrepancies are possibly due to the differences in the positioning of the continuum in the two investigations, Abt's continuum being lower than ours. This is understandable because of the line crowding in i Sco and the lower dispersion used by Abt.

Chapter 3

ATMOSPHERIC TEMPERATURES AND GRAVITIES

3.1 Introduction

In this chapter we discuss the techniques used to obtain the atmospheric parameters, T_{eff} and log g, of the program stars. These parameters specify the stellar effective temperature and the surface gravity respectively. The factors which influence the correctness of the (T_{eff}, log g) values derived are also considered. In particular, the effects of stellar rotation, line blocking, NLTE and turbulent motions are considered.

The chapter falls naturally into three distinct sections. Part A (Sections 3.2 to 3.3) contains details of the determination of T_{eff} and log g for α Car (Canopus), the only star for which there is scanner data available. Part B (Sections 3.4 to 3.5) contains details of the procedures used to determine the T_{eff} and log g values for the remaining stars, using less exact methods and data from other sources. As some of the methods are non-standard, checks have been included, making use of the few F-type giant and supergiant stars for which reliable T_{eff} and log g measurements are available. The results themselves are given in Part C of the chapter (Section 3.6).

The significant facts which emerge from these results are:-

(1) The existence of a discrepancy between the gravities indicated by the Balmer jump and the H_γ profiles for the extremely luminous supergiants earlier than F3.

(2) A discrepancy between the gravity determined from the H_γ profiles and that indicated by the cluster members for the most

luminous stars.

(3) The observed rotational velocity of θ Sco implies that the early FIb supergiants rotate as rigid bodies for at least some, if not all, of their evolution off the main sequence.

Part A

Effective Temperature and Gravity Determinations for α Car

3.2 Model Atmospheres

Our knowledge of the physical conditions in the atmospheres of giant and supergiant stars is deficient, especially when it is compared with our knowledge of the conditions in the more numerous, and more predictable main-sequence stars. For example, in the outer atmospheres of some medium-temperature supergiants, there is evidence for the existence of very high microturbulent velocities (e.g. Abt 1960, Osmer 1972).

To be realistic about the physics of these stars, one must include effects such as turbulent pressure and line blanketing, which are usually ignored in model atmosphere construction. Therefore, the determination of T_{eff} and log g for stars such as α Car and the rest of the program stars involves the use of the most realistic models possible. Ideally, models computed without the assumption of local thermodynamic equilibrium (LTE) would be preferable because, at the low pressures and densities that prevail in these atmospheres, large deviations from the LTE populations of H^- and the lower levels of hydrogen occur. However, very few non-local thermodynamic equilibrium (NLTE) model atmospheres have been calculated because of the large amount of machine time required, and a grid of LTE model atmospheres

must be used. The effects of NLTE, and corrections for these to the derived (T_{eff}, log g) values, will be considered in Section 3.5(d).

There is not a single grid of published model atmospheres which cover the entire region of the (T_{eff}, log g) plane of interest ($6500 < T_{eff} < 7600^{\circ}K$ and $0.5 < \log g < 3$). However, there are three grids of sophisticated model atmospheres which partly cover the region:

(1) Those published by Parsons (1969), which cover the region $5700^{\circ}K \leq T_{eff} \leq 6600^{\circ}K$ and $1.2 \leq \log g \leq 2.4$; the effects of convection, radiation pressure (continuous absorption alone), line blanketing and microturbulent pressure are included. The models were iterated to a flux constancy of two to three percent.

(2) Parsons grid has been extended by Osmer (1972), who computed a grid of unblanketed, radiative models in LTE with the computer program ATLAS, which is described by Kurucz (1969). The models cover the temperature and gravity ranges $6000^{\circ}K \leq T_{eff} \leq 7500^{\circ}K$ and $0.1 \leq \log g \leq 1.8$. Parsons (1969) indicates convection plays a significant part in energy transport in the convective zone of stars in the low-temperature, high log g section of this region, hence these non-convective models are not very realistic for stars in this section. Osmer has shown that a comparison of his grid with that of Parsons indicates that the effective temperature scale defined by his models should be reduced by $200^{\circ}K$ to bring his temperatures onto the same scale as those of Parsons. Osmer, who has not published his actual models, published graphs showing how the half-width of the hydrogen gamma line at 80% residual intensity, $W_{\gamma}(0.8)$, the Balmer jump index $[m_{\nu}(3500\text{Å}-m_{\nu}(4110\text{Å})]$, and the Paschen slope index $[m_{\nu}(4110\text{Å}-m_{\nu}(7550\text{Å})]$ vary over the (T_{eff}, log g) plane.

(3) The very extensive grid published by Carbon and Gingerich (1969), computed using the program SOURCE, covers the region $4000^{\circ}K < T_{eff} < 10{,}000^{\circ}K$ and $2.0 \leq \log g \leq 4.0$. While these models include the effect of convection, continuum radiation pressure blanketing, and are iterated to a flux constancy of 1% or better, they do not include turbulent pressure, which is significant in the low gravity models of interest in this grid, as noted in Section 3.5(c).

The model atmospheres calculated by Parsons and those calculated by Carbon and Gingerich have essentially the same temperature structure, and predict the same energy distributions, since the method for incorporating the effects of line blanketing was very similar in both cases.

Porteus (1973) has extended and filled in these grids to cover the remaining section of the (T_{eff}, log g) plane using interpolated $T(\tau)$ relations. It has been shown by Carbon and Gingerich that scaling an empirical solar $T(\tau)$ relation by the ratio $T_{eff}^{star}/T_{eff}^{\odot}$ leads to reliable $T(\tau)$ relations for models with temperatures up to $2000^{\circ}K$ different from that of the sun. Thus one would expect that linear interpolation over small temperature ($\leq 500^{\circ}K$) and gravity (≤ 0.5 in the log) intervals would lead to accurate $T(\tau)$ relations. This hypothesis has been tested using four of Parsons' calculated $T(\tau)$ relations (i.e., those for the models (6000, 2.4), (6000, 1.2), (6600, 2.4) and (6600, 1.2)) to predict the $T(\tau)$ relation for the model (6300, 1.8). The calculated and predicted $T(\tau)$ relation for this model agreed to within 0.5% for optical depths less than 6, and 2.5% for the larger optical depths. Therefore, it would appear that this method of determining intermediate $T(\tau)$ relations is quite satisfactory. Porteus has adopted the same elemental abundances

as Carbon and Gingerich in integrating the hydrostatic equilibrium equation to obtain the pressure characteristics of the model atmospheres.

Profiles of the hydrogen lines appear to be best represented by using the semi-empirical quasi-static broadening theory of Edmonds, Schlüter, and Wells (1967), (ESW). Olson (1968), and Strom and Peterson (1968) have noted that this theory reproduces the gravities found from binary systems and stellar interior calculations for early type stars more realistically than the theory of Griem (1967). Careful study of double-star systems in which mass and luminosity are known could lead to a test of both the model atmospheres and hydrogen line-broadening theories for the F-type stars, but at present there is no observational data available. Porteus' (1973) calculations employed the ESW theory to calculate the H_β, H_γ, and H_δ line profiles for the grid of models. The H_γ profiles will be used for the initial fitting, and the other profiles used as a check on the resulting (T_{eff}, log g) for each star.

In order to choose models which were most likely to fit the observational data for any star, a standard method was followed. This involves the choosing of temperature- and gravity-dependent 'observables' such that their loci in the (T_{eff}, log g) plane intersect at large angles. For the section of the (T_{eff}, log g) plane of interest, there are two such pairs of 'observables':

(1) the half-width of the H_γ line at 80% residual intensity, $W_\gamma(0.8)$, and the Paschen slope index $[m_v(4670\text{Å})-m_v(5470\text{Å})]$*;

---

* The reason for choosing a Paschen slope index that only covers the small wavelength range 4670Å - 5470Å is that these two wavelengths are the centre wavelengths of the *b* and *y* filters in the Strömgren *ubvy* photometric system. In Section 3.4, the *b-y* index is used to calculate this Paschen slope index.

(2) the Paschen slope index and the Balmer jump index $[m_\nu(3500\text{Å})-m_\nu(4110\text{Å})]$, where $m_\nu(i)$ is the flux per unit frequency interval expressed in magnitudes at wavelength i. The dependence of $W_\gamma(0.8)$ and the Paschen slope index on T_{eff} and log g is shown in Figure 3.1. The curves intersect at large angles and are useful for obtaining temperatures and gravities for all but the cooler, less luminous giants. The situation is not as favourable for the Balmer jump index and $W_\gamma(0.8)$, whose loci only intersect at large angles for $T_{eff} < 7000^\circ K$ and log g > 1.5 (Figure 3.2). Outside this range each one is sensitive primarily to gravity. It is useful to note that the only 'observable' that gives an indication of temperature in the region $T_{eff} > 7200^\circ K$, log g < 1.5 is the Paschen slope index, which is affected by interstellar reddening, line blocking, and convection. Thus temperatures determined in this section of the plane are suspect. More useful temperature indicators are red colours analogous to V-R or V-I, however, measurements in these colours are not available for the program stars which lie in this region, namely 195 Car and HD 97534.

The variation in the relative importance of different opacity sources explains the behaviour of the Balmer jump and the H_γ width. As long as neutral hydrogen is the dominant opacity source, the Balmer jump increases with decreasing temperature because of the increasing ratio of hydrogen atoms in the second level to the third. However, at sufficiently low temperatures H^- becomes important and causes the Balmer jump to decrease. Because the H^- opacity is also proportional to the electron pressure, the Balmer jump maximum occurs at lower temperatures in supergiants than in main-sequence stars.

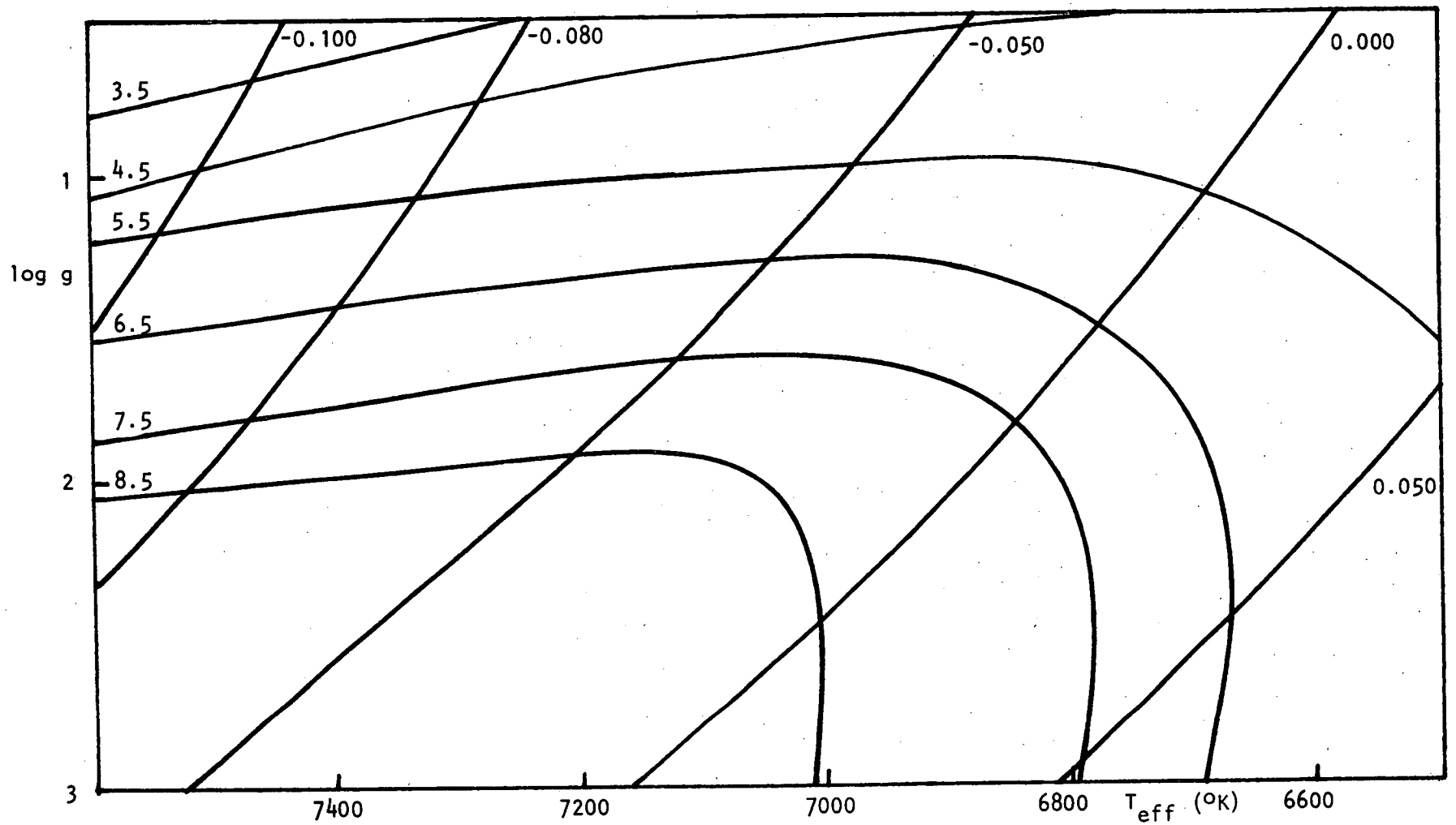

Figure 3.1 Computed curves for the H_γ width ($W_\gamma(0.8)$, curves with numbers ranging from 3.5 to 8.5) and the Paschen slope index ($[m_\upsilon(4670Å) - m_\upsilon(5470Å)]$, numbers ranging from -0.100 to 0.050).

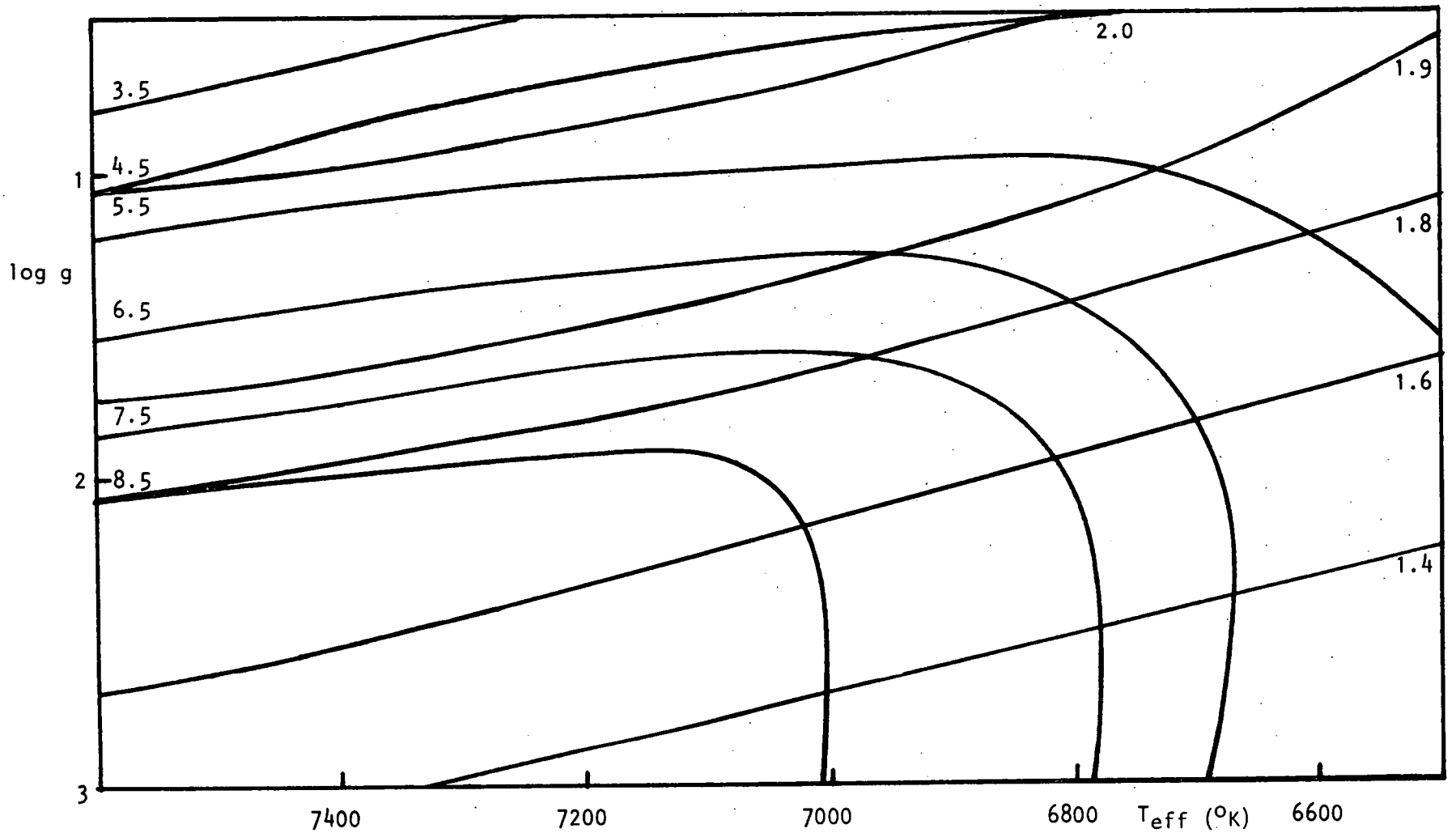

Figure 3.2 Computed curves for the H_γ width (see Figure 3.1) and the Balmer jump index ($[m_v(3500\text{Å}) - m_v(4110\text{Å})]$, horizontal lines with numbers ranging from 1.4 to 2.0).

The hydrogen-line widths are insensitive to gravity for $T_{eff} < 7000^{\circ}K$ because the line and continuous opacities have nearly the same dependence on electron pressure. At higher temperatures, where neutral hydrogen dominates, the ratio of line to continuous opacity is very sensitive to electron pressure, and the widths of the Balmer lines begin to exhibit a gravity dependence analogous to that of the A stars.

3.3 Comparison of Observational Data with Models

α Car was the only star in the program for which continuum energy scan data was available. Aller, Faulkner and Norton (1966) measured the continuum flux in α Car from 3392Å to 5868Å, using a Cassegrain Scanner with a 9Å nearly-rectangular band-pass. The fluxes given by Aller et al. have been corrected onto the scale defined by the Oke and Schild (1970) recalibration of α Lyrae, which has the same Paschen slope as the Hayes (1970) calibration, but indicates a 0.04 magnitude smaller Balmer jump. Note that this corresponds to 0.2 change in log g for the program stars, indicating the need for accurate absolute calibration for fixing absolute T_{eff} and log g values. Because line blocking is significant in α Car, it has been determined in 9Å intervals about the given wavelengths from intensity tracings of the 1.4 Å mm^{-1} and 2.1 Å mm^{-1} dispersion Coudé spectrograms. The observed line blocking (in magnitudes) is given in Table 3.2.

The observed fluxes for α Car are not expected to be strongly affected by interstellar extinction, but it still may have a significant effect. This star is not a member of a cluster, so an independent measure of the reddening cannot be made. However, the

amount of reddening can be estimated by noting that the stars α Lep, α Car, ν Car and i Car have similar spectral characteristics, in that they have similar metal line strengths, hydrogen-line profiles and photometric indices in both *ubvy* and UBV systems. The only differences indicate that ν Car and i Car are more luminous than α Lep and α Car (≃ 1.0 magnitude). The reddening-independent indices from four-colour and Hβ photometry are given in Table 3.1. They show little scatter, whereas $b-y$, which is reddening-dependent, shows a considerable spread, which is clearly related to the visual magnitude (m_v) of the star. In order to correct the $b-y$ indices for the differences between the stars, the calibration of the intrinsic $b-y$, $(b-y)_o$, by Crawford (1970) has been used. If we define $\Delta(b-y)$ and $(b-y)_{cr}$ for each star such that

$$\Delta(b-y) = (b-y)_o^{\alpha\ \mathrm{Car}} - (b-y)_o$$

and $$(b-y)_{cr} = (b-y) + \Delta(b-y) \ ,$$

then the differences in the $(b-y)_{cr}$ values are now due to the reddening differences between the stars. If it is assumed that the interstellar reddening is uniform throughout the region of interest, then an estimate of the reddening for each star can be made if the relative distance to each of the stars is known. The relative distances were estimated using their apparent magnitudes, and tentative temperatures and gravities derived using the indices approximately corrected for reddening. The results of these calculations are given in Table 3.1.

Johnson (1966) has published the experimentally determined intrinsic colours of the supergiant stars for the UBVRI system. The reddening for any supergiant may be estimated from these, assuming a

Table 3.1

Data[1] for the Calculation of Interstellar Reddening for α Car

Star	HR no.	$[c1]^2$	$[m1]^2$	β	$(b-y)_o$[3]	$(b-y)$	m_v	$\Delta(b-y)$	$(b-y)_{cr}$	$E_{(b-y)}$
α Lep	1865	1.476	0.173	2.730	0.296	0.139	2.56	-0.003	0.136	0.05 ± 0.02
α Car	2326	1.490	0.148	2.732	0.293	0.110	-0.80	0.00	0.110	0.012 ± 0.004
i Car	3699	1.517	0.152	2.755	0.268	0.123	2.2	0.025	0.148	0.04 ± 0.01
ν Car	3890	1.361	0.151	2.724	0.300	0.193	3.2	-0.007	0.186	0.09 ± 0.03

Notes

1 The four colour and Hβ photometry values used are taken from the lists of Crawford, Barnes and Golson (1970).

2 The reddening-independent indices $[c1] = c1 - 0.20(b-y)$, $[m1] = m1 + 0.18(b-y)$ are taken from Strömgren (1966) and are based on the normal law of interstellar extinction.

3 The $(b-y)_o$ used here is the calibration given for the A stars (β between 2.880 and 2.700) by Crawford (1970), $(b-y)_o = 2.943 - 1.0\beta - 0.1\Delta c1 - 0.1\Delta m1$.

particular wavelength dependence for the interstellar extinction. Using Whiteoak's (1966) average wavelength dependence for the interstellar extinction and the UBVRI data for α Car (Appendix II), a value of $E_{(B-V)} \simeq 0.02$ is found. This corresponds to $E_{(b-y)} = 0.013$, which is in close agreement with the value previously determined ($E_{(b-y)} = 0.012$). The continuous energy distribution of α Car as measured by Aller et al., corrected for line blocking, reddening and recalibration of α Lyrae, is given in Table 3.2.

Kondo, Henize and Kotila (1970), hereafter referred to as KHK, have also measured the Balmer jump in α Car by direct spectrophotometry. They report a value of 1.32 for the Balmer jump index, $[m_v(3640\text{Å}) - m_v(4000\text{Å})]$, which is in disagreement with the value of 1.51 derived for this index from the photometry of Aller et al. Both values are uncorrected for line blocking and interstellar extinction, but the value of Aller et al. has been corrected for the Oke-Schild (1970) recalibration of α Lyrae.

Figure 2 of KHK indicates that their continuum was fitted above the Balmer jump to the lowest point on the continuum, between the hydrogen lines H_8 and H_9 (3860Å). My direct intensity tracings of the 1.4 Å mm^{-1} Coudé spectrograms indicate that the overlapping wings of the two hydrogen lines depress the continuum by a further 0.10 magnitudes in going from a 9Å rectangular bandpass (Aller et al.) to a 15Å halfwidth Gaussian bandpass (KHK). The results of Aller et al. indicate that the flux per unit wavelength interval at 3860Å is 0.05 magnitudes more than the flux at 4000Å. These corrections (+0.15 mag.) bring the result of KHK (now 1.47) into reasonable agreement with the value obtained by Aller et al. (1.51) for this Balmer jump index.

Table 3.2

Data on the Continuous Energy Distribution for α Car

λ(Å)	$\frac{1}{\lambda}$ (μ^{-1})	Observed Energy Distribution, Aller et al.	Line Blocking	Oke-Schild Recalibration of α Lyrae	Reddening Correction ($E_{(b-y)}$=0.012)	Corrected Energy Distribution
3392	2.948	+1.858	-(0.06)	-(0.10)	-(0.035)	+1.76
3441	2.906	+1.811	-(0.06)	-(0.07)	-0.035	+1.75
3504	2.854	+1.755	-(0.06)	-0.03	-0.035	+1.73
3567	2.803	+1.698	-(0.06)	-0.02	-0.034	+1.69
3634	2.752	+1.608	-0.06	-0.02	-0.032	+1.61
3703	2.701	+1.178	-0.385	-0.00	-0.031	+0.86
4032	2.480	+0.009	-0.164	-0.083	-0.024	-0.162
4082	2.450	+0.007	-0.134	-(0.083)	-0.023	-0.134
4167	2.400	+0.004	-0.142	-0.083	-0.022	-0.144
4255	2.350	+0.000	-0.100	-0.085	-0.019	-0.105
4367	2.290	-0.004	-0.084	-(0.075)	-0.018	-0.082

Table 3.2 (cont.)

λ(Å)	$\frac{1}{\lambda}$ (μ^{-1})	Observed Energy Distribution, Aller et al.	Line Blocking	Oke-Schild Recalibration of α Lyrae	Reddening Correction ($E_{(b-y)}$=0.012)	Corrected Energy Distribution
4464	2.240	-0.011	-0.118	-0.066	-0.017	-0.113
4566	2.190	-0.014	-0.095	-0.060	-0.014	-0.084
4673	2.140	-0.021	-0.095	-(0.055)	-0.012	-0.084
5000	2.000	-0.039	-0.080	-0.036	-0.008	-0.064
5127	1.950	-0.043	-0.078	-(0.027)	-0.005	-0.064
5261	1.901	-0.047	-0.085	-0.019	-0.003	-0.055
5556	1.800	-0.054	-0.045	-0.000	-0.000	-0.000
5868	1.704	-0.059	-0.045	+(0.022)	+0.005	+0.022

Note -

Brackets indicate interpolated values obtained with reference to the line blocking measurements for α Per (Parsons 1970), or interpolation between the Oke-Schild data points.

Stecher (1969) reports a value of 1.65 ± 0.05 for the index $[m_\nu(3000\text{Å})-m_\nu(5475\text{Å})]$ for α Car, measured by direct spectrophotometry. So that this result may be compared with the photometry of Aller et al., we note that the model atmosphere calculations (Parsons and Peytremann 1973, their Figure 1) indicate that, in the region 3000Å-3600Å, the flux per unit wavelength varies linearly with wavelength. Linear extrapolation of the results of Aller et al. to 3000Å gives a value of 1.63 ± 0.07 for the index $[m_\nu(3000\text{Å})-m_\nu(5475\text{Å})]$, which is in very good agreement with the value reported by Stecher. It is interesting to note that both sets of measurements are completely independent of each other in that the techniques used are radically different and both measurements started with different standards.

Stecher and KHK have both measured the ultraviolet fluxes for α Car, Stecher in the region 1700Å to 3000Å and KHK from 2300Å to 4000Å; the KHK data from 3300Å to 4000Å has been discussed previously. These two sets of data agree very well for wavelengths less than 3000Å, if they are fitted to each other at 3000Å. The effects of interstellar reddening have been removed by the respective authors; the effects of line blocking cannot be completely removed because they are unknown, only the large absorption features can be smoothed over (KHK, Figure 2).

To fit a theoretical model atmosphere to the observed continuous energy distribution, use is made of Figures 3.1, 3.2, the observed values of $W_\gamma(0.8)$, the Balmer jump index, the Paschen slope index, and the Balmer slope index, $[m_\nu(1988\text{Å})-m_\nu(3172\text{Å})]$. The values of these parameters for α Car are given in Table 3.3.

Table 3.3

Data for the Determination of T_{eff} and log g for α Car

Parameter	Value	± σ
BJ index $[m_v(3500\text{Å})-m_v(4110\text{Å})]$	1.85	0.07
PS index $[m_v(4670\text{Å})-m_v(5470\text{Å})]$	-0.060	0.012
$W_\gamma(0.8)$ half width of the H_γ line 80% residual intensity	8.03	0.11
BS index $[m_v(1800\text{Å})-m_v(3000\text{Å})]$	-1.30	0.10

Table 3.4

(T_{eff}, log g) Pairs Derived for α Car

Source	T_{eff}	± σ	log g	± σ
$W_\gamma(0.8)$, PS	7250	150°K	1.81	0.04
BJ, PS	7250	150°K	1.70	0.12
BS	7450	200°K	——	
Hanbury-Brown et al. (1967)	7350	200°K	1.77 (used)	
Weighted average	7350	100°K	1.77	0.04

The quoted errors in the photometry have been estimated from the errors suggested by Aller et al., the uncertainty in the calibration of α Lyrae, the uncertainty in the reddening and the uncertainty in the line blocking corrections. The error quoted for $W_\gamma(0.8)$ is the standard deviation between the measured values of $W_\gamma(0.8)$ from three Coudé spectrograms, two at 2.1 $\mathring{A}\ mm^{-1}$ and one at 9 $\mathring{A}\ mm^{-1}$. The (T_{eff}, log g) pairs resulting from this fitting are given in Table 3.4. The Balmer slope index, which is largely independent of gravity, has been used independently to give a third estimate of the temperature of α Car, the first two being wholly controlled by the Paschen slope index.

Hanbury-Brown, Davis, Allen and Rome (1967) have determined the effective temperature of α Car by interferometrically measuring the angular diameter of the star. The absolute monochromatic flux at 4425$\mathring{A}$ is then determined and compared with model atmosphere data, assuming a particular log g for the star. For α Car, a log g value of 2.5 was used, giving T_{eff} = 7510 ± 200°K, whereas the Balmer jump and $W_\gamma(0.8)$ data indicate a log g of 1.77 ± 0.04 would be more appropriate. If a value of log g = 1.77 is used, the observed flux indicates a T_{eff} of 7350 ± 200°K. The three measurements of T_{eff} for α Car agree to within 200°K, and the adopted value of T_{eff} is 7350°K. Superficially log g appears to be well determined, but it will be shown (Section 3.5) how effects such as NLTE and turbulent pressure, which are not included in the models, can affect these parameters and lead to an erroneous estimate of log g.

The continuous energy distribution for an interpolated model (Section 3.2) with parameters T_{eff} = 7350°K and log g = 1.77 has been calculated by Porteus (1973); the results are shown in Figure 3.3. The fit is very good, except in the far-UV region, where the model

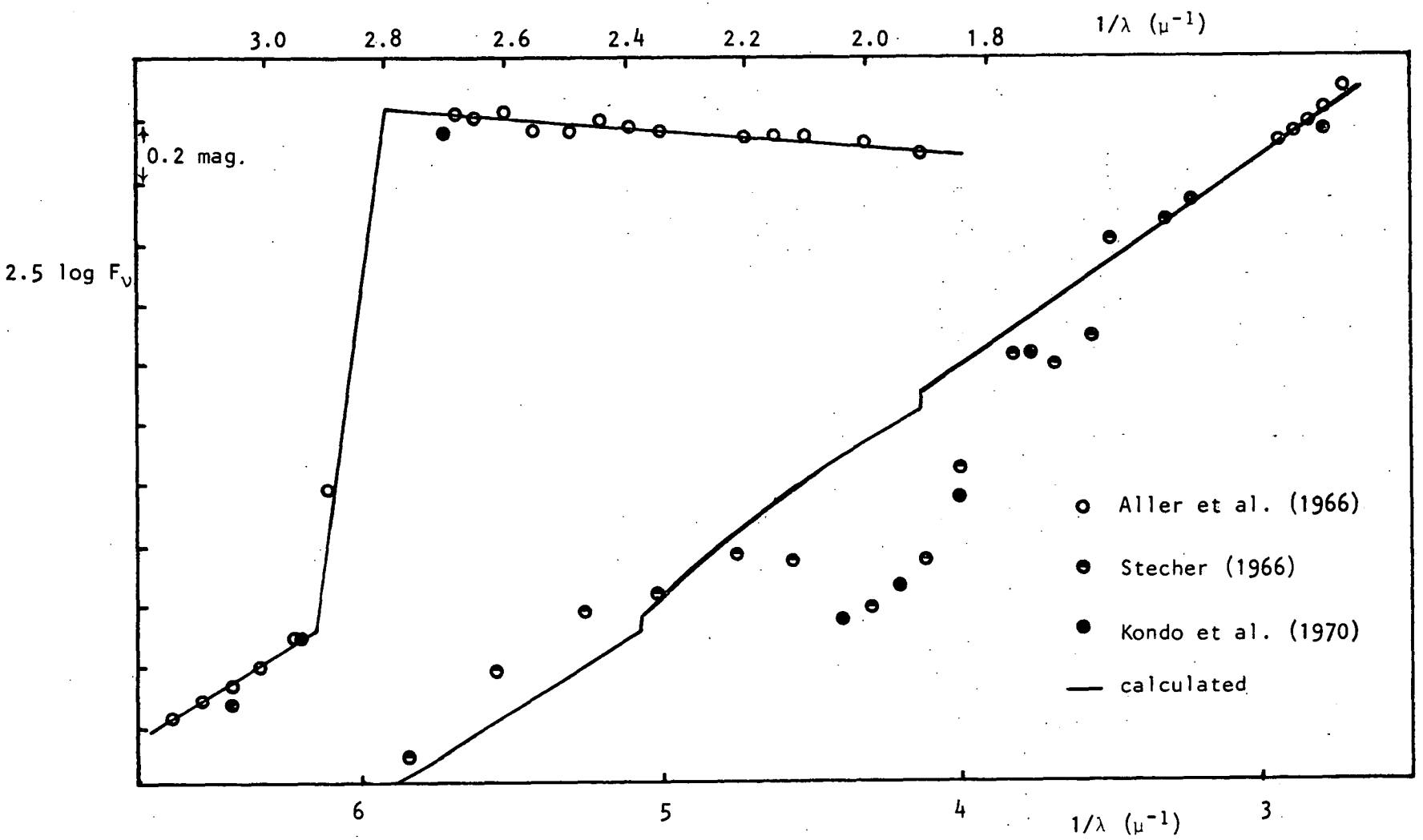

Figure 3.3 Observed continuous energy distribution for α Car and predicted energy distribution (T_{eff} = 7350°K, log g = 1.77).

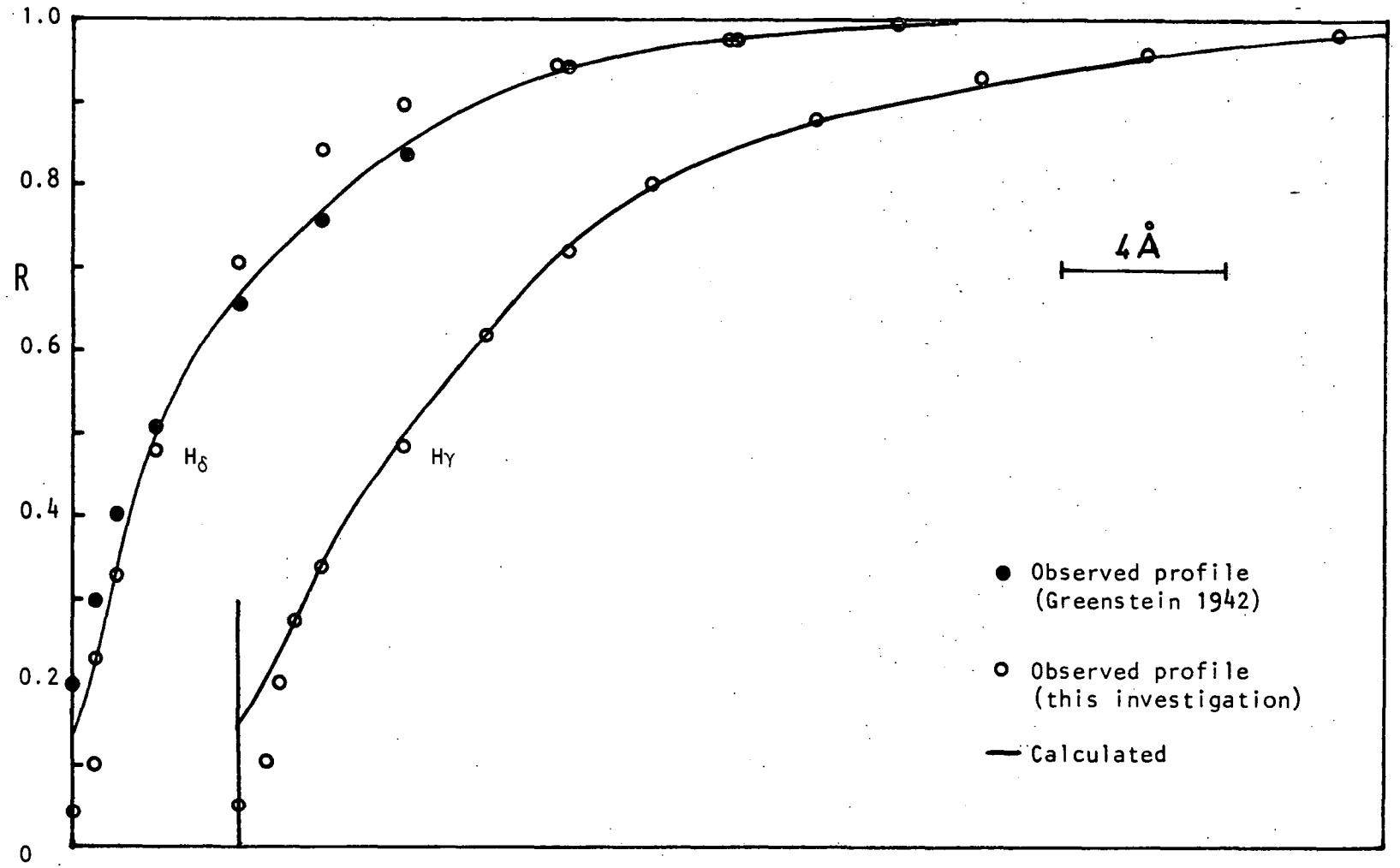

Figure 3.4 Observed H_γ and H_δ line profiles in α Car and those calculated from the model atmosphere T_{eff} = 7350°K, log g = 1.77.

atmosphere flux is slightly less than the observed flux. Hydrogen-line profiles have also been calculated for this model, and the resulting fits are shown for H_γ and H_δ in Figure 3.4. The fit to H_γ is very good. The profiles of H_δ reported by Greenstein (1942) and that reported here are both shown. The fit to either profile is not good, Greenstein's profile giving the best fit in the wing region and the profile reported here fitting more closely in the region $\Delta\lambda < 3\mathring{A}$.

Part B

(T_{eff}, log g) Determination for the other Program Stars

3.4 Use of *ubvy* photometry

(a) The Technique

Narrow-band *ubvy* and broad-band UBVRI photometry are both suitable for the determination of T_{eff} and log g for any star. Data in the UBVRI system is not available for all the program stars, whereas the *ubvy* data is. Thus the latter system of photometry has been used in the following section, and the UBVRI photometry has been used where available in order to obtain an independent measure of the reddening.

The *ubvy* photometry data can be used to calculate a Balmer jump index, $[c1] = c1 - 0.20(b-y)$, (Strömgren 1966), which is reddening independent if the normal law of interstellar extinction is applicable, and a Paschen slope index, $b-y$, which is affected by interstellar reddening. The conversion from the theoretical flux to the observed colour indices is considerably easier in the *ubvy* system than the UBVRI, since the former system depends less on the earth's atmosphere or on the photocell than does the latter.

The sensitivity of the i^{th} filter, $S_i(\lambda)$, is a uniquely defined function of λ and we need only determine the normalization constant in each colour. Thus we may relate an observed colour index $(i-j)_c$, computed from the monochromatic fluxes, by an additive constant k_{ij} such that

$$i-j = (i-j)_c + k_{ij}$$

where

$$(i-j)_c = 2.5 \log \left[\int_0^\infty F_\lambda S_j(\lambda) d\lambda \Big/ \int_0^\infty F_\lambda S_i(\lambda) d\lambda \right],$$

in which F_λ is the flux per unit wavelength, given either by photoelectric scanner observations or from model atmosphere predictions.

The normalization constants for the various indices have been determined by Matsushima (1969) by fitting the natural colour index, $(i-j)_c$ with the observed value for a number of stars for which both monochromatic scanner observations and four-colour photometry data are available. Matsushima found that

$$b-y = (b-y)_c + (0.118 \pm 0.004),$$

$$c1 = (c1)_c - (0.061 \pm 0.014)$$

and thus $$[c1] = [c1]_c - (0.085 \pm 0.014),$$

when the effects of line blocking were not taken into account. The normalization constants, derived when line blocking was included, were not used because the calibrating stars were main-sequence stars in which the line blocking is not as strong as that in the giant and supergiant stars being considered here.

Line blocking corrections have been made for each star individually. The line blocking for the i filter has been determined in the usual way by determining the line blocking in 25Å intervals under

the i filter response curve. If we denote the fraction of emergent energy removed by the metal lines at λ by $(1-\eta_\lambda)$, the metal-line blocking expressed in magnitude units is given by

$$\Delta i = -2.5 \log \left[\int_i F_\lambda \eta_\lambda S_i(\lambda) d\lambda \Big/ \int_i F_\lambda S_i(\lambda) d\lambda \right],$$

where F_λ refers to the line-removed continuum or the theoretical flux as given by the models. For the v filter, Δv includes the line blocking due to Hδ, as well as that due to the metal lines.

The calibrations of Matsushima are based on the Hayes (1970) calibration of α Lyrae. The Oke-Schild (1970) calibration, upon which the (T_{eff}, log g) pair determinations are to be based, gives essentially the same Paschen slope in the region of interest (4500Å to 5500Å). However, the Balmer jump index $[m_v(3500Å)-m_v(4110Å)]$ is reduced by 0.04 magnitudes in the Oke-Schild calibration compared with that of Hayes.

Therefore, the transformation equations become

$$b-y = (b-y)_c + (0.118 \pm 0.004),$$

$$c1 = (c1)_c - (0.02 \pm 0.02)$$

$$\text{and} \quad [c1] = [c1]_c - (0.045 \pm 0.02),$$

when based on the Oke-Schild calibration of α Lyrae.

Using the $S_i(\lambda)$ functions as given by Matsushima (1969), it can be shown that

$$([c1])_c = m_v(3500Å) - 2m_v(4110Å) + 0.8m_v(4670Å) + 0.20m_v(5470Å) - 0.150,$$

$$([c1])^*_c = [c1] + 0.045 + \Delta u + 0.80\Delta b + 0.20\Delta y - 2.0\Delta v,$$

$$(b-y)_c = m_v(4670\text{Å}) - m_v(5470\text{Å}) + 0.037,$$
$$(b-y)_c^* = (b-y)_o - 0.118 - (\Delta b - \Delta y),$$

where $([c1])_c$ is the natural $[c1]$ index calculated from monochromatic fluxes, and $([c1])_c^*$ is the observed $[c1]$ index corrected for line blocking and transformed onto the natural system. Similarly, for the Paschen slope indices $(b-y)_c$ and $(b-y)_c^*$, $(b-y)_o$ is $b-y$ corrected for interstellar reddening. Figure 3.5 shows how the pair of indices $(([c1])_c^*, [m_v(4670\text{Å}) - m_v(5470\text{Å})])$, calculated from the grid of model atmospheres, vary with temperature and gravity.

There are three stars, ϕ Cas, α Per and α Car, whose spectral types are in the range under consideration, for which *ubvy* photometry data is available and (T_{eff}, log g) have been determined by scanner observations of their continuous energy distributions and measurement of $W_\gamma(0.8)$. Table 3.5 gives the *ubvy* data, the results derived from it and the previously-determined (T_{eff}, log g) pairs for each star. The agreement between the (T_{eff}, log g) pairs for α Car and α Per is very good, but that for ϕ Cas is poor. However, Osmer (1972) points out that the gravity derived from the Balmer jump index and the Balmer lines ($W_\gamma(0.8)$) do not agree for ϕ Cas. The result obtained from his measurements of the Balmer jump and the Paschen slope indices is $T_{eff} = 6200^\circ$K and log g = 0.7, which Osmer had to disregard because they are unreasonable for a F0Ia star. $W_\gamma(0.8)$ and the Paschen slope index from *ubvy* photometry give $T_{eff} = 7150^\circ$K and log g = 0.4, which is in good agreement with Osmer's result ($T_{eff} = 7100^\circ$K and log g = 0.4) derived from $W_\gamma(0.8)$ and his Paschen slope index. Thus, the results of the *ubvy* photometry confirm the discordance noted by Osmer between the gravities obtained from $W_\gamma(0.8)$ and the Balmer jump index for ϕ Cas.

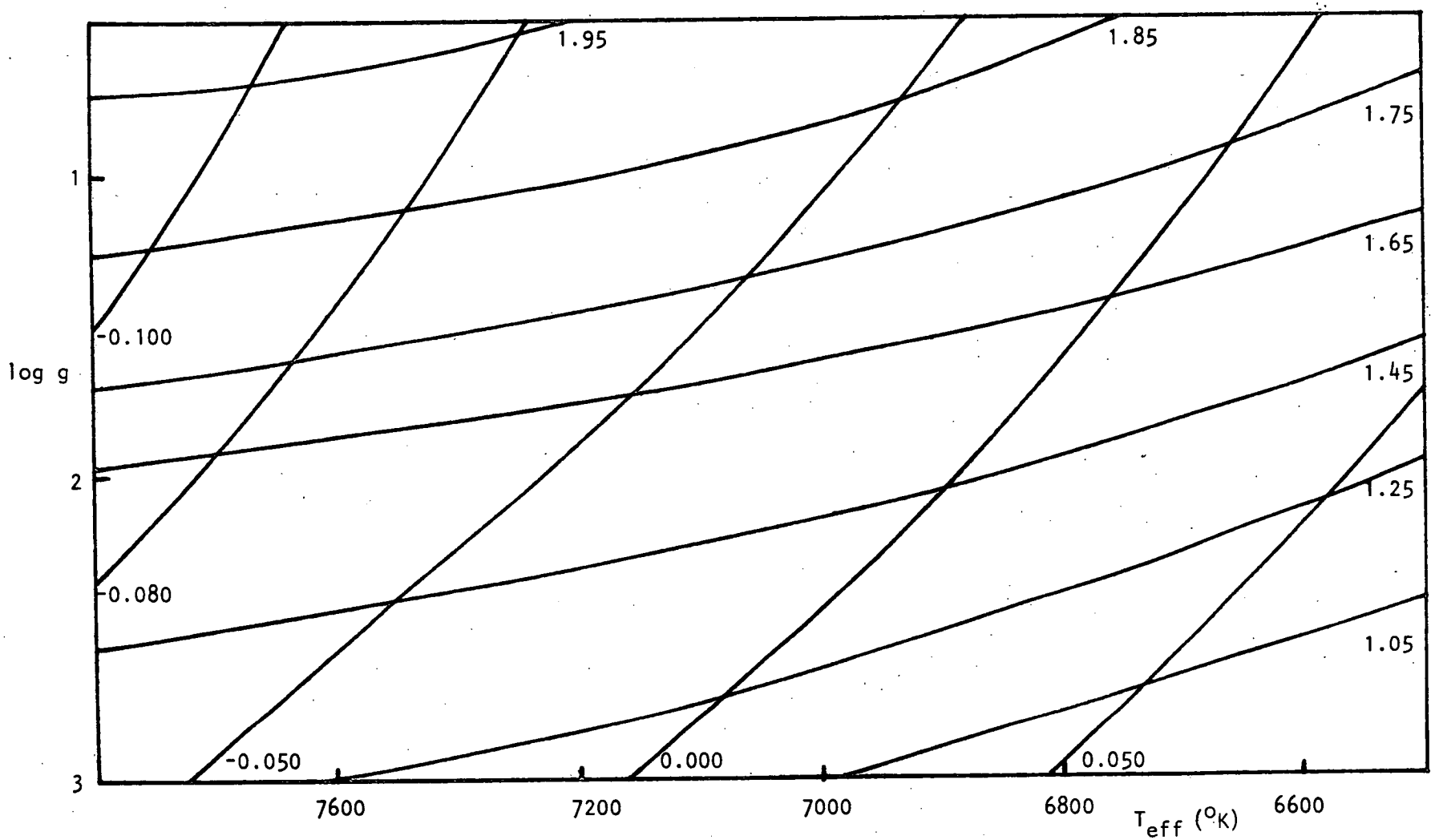

Figure 3.5 Computed curves for the Paschen slope index ([m_v(4670Å) - m_v(5470Å)], curves with numbers varying from -0.100 to 0.050) and the index $([c1])^{*}_{c}$ (curves with numbers ranging from 1.05 to 1.95).

Table 3.5

Data for Checking (T_{eff}, log g) Determinations using *ubvy* Photometry

Star	*b-y*	*[c1]*	Line Blocking (mag)[1]				$([c1])^*_c$	$\pm\sigma^4$	$W_\gamma(0.8)$[2]	$E_{(b-y)}$[3]
			$-\Delta u$	$-\Delta v$	$-\Delta b$	$-\Delta y$				
ϕ Cas	0.492	1.375	0.18	0.27	0.12	0.09	1.75	0.03	3.55	0.37
α Per	0.304	1.013	0.36	0.40	0.12	0.08	1.37	0.03	5.25	0.005
α Car	0.110	1.490	0.09	0.18	0.08	0.07	1.71	0.03	8.00	0.012

Star	$[m_\nu(4670\text{Å}) - m_\nu(5470\text{Å})]$	$\pm\sigma^4$	$([c1])^*_c$, $[m_\nu(4670\text{Å}) - m_\nu(5470\text{Å})]$				Previous determinations				Reference
			T_{eff}	$\pm\sigma^4$	log g	$\pm\sigma^4$	T_{eff}	$\pm\sigma$	log g	$\pm\sigma$	
ϕ Cas	-0.070	0.02	7300	200	1.6	0.1	7100	200	0.4	0.2	Osmer (1972)
α Per	0.060	0.01	6350	100	1.4	0.1	6400	200	1.5	0.2	Parsons (1970)
							6350	150	1.5	0.2	Osmer (1972)
α Car	-0.067	0.01	7300	100	1.7	0.1	7350	100	1.77	0.05	Section 3.3

Notes to Table 3.5

1 Line blocking for α Per and φ Cas taken from Osmer (1972).

2 $W_Y(0.8)$ for α Per and φ Cas taken from Osmer (1972).

3 The $E_{(B-V)}$ values were taken from Parsons (1972) for α Per and Pesch (1959) for φ Cas and converted to $E_{(b-y)}$ using the relationship $E_{(b-y)} = 0.72\ E_{(B-V)}$.

4 The σ's represent the estimated errors due to the uncertainties in the data alone.

It would appear that the above method for deriving T_{eff} and log g for stars in the spectral range of interest gives reliable results.

(b) Reddening

As mentioned previously, the only index strongly dependent on temperature in the region $T_{eff} > 6800^{o}K$ and log g < 2.0 is the Paschen slope index, which is also affected by interstellar reddening. The accuracy to which the interstellar reddening can be measured imposes the limit on the accuracy to which the temperature of a star in this region can be determined. The reddening may be estimated for the stars that are very similar to α Car by the same method as used for α Car. The results are shown in Table 3.1, but the larger the reddening, the lower the accuracy of its determination. The star 195 Car is a well recognized member of the cluster IC 2581, whose reddening has been determined by Fernie (1963) to be $E_{(b-v)} = 0.37$ and redetermined by Lloyd Evans (1969), using more cluster members, to be 0.43 ± 0.04; this amended value has been adopted.

It is obvious from the photometry data and metal line equivalent widths (Table 3.6) that HD 97534 is almost identical to 195 Car in distance and atmospheric parameters. Thus HD 97534 has been assigned the same reddening as found for 195 Car. Alternatively, the (T_{eff}, log g) values found for 195 Car could be said to apply to HD 97534. The two approaches give essentially the same values of T_{eff} and log g for HD 97534.

Kron (1958) and Parsons (1970) have shown how the UBVGRI photometry of Stebbins and Kron (1964) can be used to estimate the colour excesses, T_{eff} and log g for any star. α Lep and δ CMa are

Table 3.6

Comparison Between 195 Car and HD 97534

(a) Photometry and Balmer Line Profiles

Star	m_v	Sp. Type	*b-y*	[*c1*]	[*m1*]	β	B-V	U-B	$W_\gamma(0.8)$
195 Car	4.66	FOIa	0.402	1.105	0.051	2.567	0.50	-0.01	3.1
HD 97534	4.59	FOIa	0.420	1.104	0.062	2.572	0.53	0.03	3.0

(b) Equivalent Widths of Metal Lines (mÅ)

Species	Ca II	Fe II	Fe II	Fe II	Fe I	Fe I	Fe I
λ(Å)	3933	3938	4369	4629	4144	4376	4384
195 Car	4300	482	230	646	130	60	239
HD 97534	4300	465	190	774	120	55	245

the only two stars in the program for which data is available in this photometry system (Appendix II). Kron (1958) found the colour excesses, $E_{(B-V)}$, of δ CMa and α Lep to be 0.055 and 0.011 respectively. The value of 0.011 for δ CMa would seem too small when one considers that it has a distance modulus approximately 0.5 magnitudes smaller than α Lep. From the reddening of the stars in Table 3.1 and that observed for α Lep by Kron, it would appear that a reddening of $E_{(B-V)} = 0.04$ would be more appropriate for δ CMa.

The five colour system formed by combining the UBV colours of Johnson and Morgan (1953) with the RI system of Kron, White and Gascoigne (1953) can be used in the same manner as the UBVGRI colours to determine colour excesses. The intrinsic colours as published by Johnson (1966) for the Ia supergiant stars in the UBVRI system and the UBVRI data from Johnson, Mitchell, Iriarte and Wiśniewski (1966) (Appendix II) were used. There are only five of the program stars, α Lep, α Car, b Vel, θ Sco and π Sag for which photometry data in this system is available. θ Sco and π Sag are not suitable because their Balmer jump and $W_\gamma(0.8)$ values indicate that they are giants, and intrinsic colours are not available for giants of their spectral type (F0). The reddening for α Lep and α Car is obviously small and within the accuracy to which it can be determined by this method. Thus b Vel is the only star for which this method is useful. The best fit between the observed colours and intrinsic colours occurs at about F2, with $E_{(B-V)} = 0.45 \pm 0.05$. Parsons and Peytremann (1973) have suggested a value of $E_{(B-V)} = 0.21$ for b Vel. However, there is no indication of the reliability of this value, or its source. A value of $E_{(B-V)} = 0.45 \pm 0.05$ has been adopted for b Vel because $E_{(B-V)} = 0.21$ indicates a temperature corresponding to $\simeq$ F8 and will not give a fit to

the five-colour photometry.

Data is not available to enable an accurate determination of the reddening for the three remaining stars, θ Sco, i Sco and π Sag. The reddening has been estimated for these stars by estimating their distances relative to the stars with known reddening, using the absolute magnitudes of Blaauw (1963). Luminosity classes have been assigned using the gravity indicated by $W_\gamma(0.8)$ and the Balmer jump index, assuming log g values ~ 1.0, 1.9 and 2.5 for luminosity classes Ia, Ib, and II respectively around spectral class F0 (Parsons and Peytremann 1973, and this investigation). The estimated values for the colour excess ($E_{(b-y)}$) are 0.01 and 0.02 for θ Sco and π Sag respectively. These estimates are based upon the assumption that the reddening is the same per unit distance to all the program stars. However, since the reddening for these two stars is small, any errors in the reddening will show up as negligible errors in the derived temperatures. The reddening for i Sco is larger, $E_{(b-y)} \simeq 0.14$, and the uncertainty in this value makes a temperature determination using this value very dubious.

(c) Use of $(b-y)_o$

For the stars of similar spectral type and luminosity to α Car, an independent measure of the Paschen slope index $[m_\nu(4670\text{Å})-m_\nu(5470\text{Å})]$ can be made, making use of the calibration for the intrinsic colour, $(b-y)_o$, for the A stars†. Crawford (1970) has

† Crawford (1970) indicates that the F stars follow a similar relationship to the A stars (with slightly different coefficients). At this time the calibration for the F stars has not been published, so the calibration for the A stars must be used. Actually, the stars of interest satisfy the requirements on $\Delta c1$ and satisfy, or almost satisfy, the requirements on β placed on the equation.

found that for stars with β between 2.880 magnitudes and 2.700 magnitudes and *c1* less than 0.280 magnitudes, $(b-y)_o = 2.943 - 1.0\beta + 0.1\Delta c1 - 0.1\Delta m1$. $\Delta c1$ and $\Delta m1$ are defined as the differences between the observed values and the values of *c1* and *m1* derived from the standard relations for the stellar value of β. The correction required to convert the intrinsic colour to the Paschen slope index $[m_v(4670\text{Å})-m_v(5470\text{Å})]$ was determined using the observed Paschen slope index and the computed $(b-y)_o$ for α Car. The agreement between the two methods for the determination of the Paschen slope index is good, and the results are given in Table 3.7.

(d) Results

Here the results of the (T_{eff}, log g) determinations are presented, and a discussion of the uncertainty in the results due to the observational uncertainties is given. Table 3.7 gives (T_{eff}, log g) derived using the two pairs of indices ($W_\gamma(0.8)$, $[m_v(4670\text{Å})-m_v(5470\text{Å})]$) and ($([c1])^*_c$, $[m_v(4670\text{Å})-m_v(5470\text{Å})]$) in conjunction with Figures 3.1 and 3.5. δ CMa, which lies outside the range of my graphs, was assigned the parameters $T_{eff} = 6000^\circ$K and log g = 0.1, using the graphs published by Osmer (1972). A value of the Balmer jump index, $[m_v(3500\text{Å})-m_v(4110\text{Å})] = 1.86$, was calculated for this star using the *ubvy* photometry results, and assuming a reddening of $E_{(B-V)} = 0.04$.

The two pairs of (T_{eff}, log g) values for each star agree very well for the lower luminosity stars, but for the three stars with log g < 1.0, $W_\gamma(0.8)$ indicates a significantly lower gravity than $([c1])^*_c$. ν Car ($T_{eff} = 7150^\circ$K, log g = 1.2) hereafter written as

Table 3.7

Data for the Determination of T_{eff} and log g from the *ubvy* Photometry of the Program Stars

Star	*b-y*	[*c1*]	Line Blocking (mag)[1]				$([c1])^{*}_{c}$	$\pm \sigma^{3}$	$W_{Y}(0.8)$	$E_{(b-y)}$	$[m_{\nu}(4670\text{Å}) - m_{\nu}(5470\text{Å})]$	$\pm \sigma^{3}$
			$-\Delta u$	$-\Delta v$	$-\Delta b$	$-\Delta y$						
α Lep	0.139	1.476	(0.20)	0.25	0.12	(0.09)	1.70	0.04	8.45	0.05	-0.08	0.02
α Car	0.110	1.490	0.09	0.18	0.08	0.07	1.71	0.03	8.00	0.012	-0.067	0.010
δ CMa	0.375	0.854	(0.24)	0.55	0.18	(0.13)	1.58	0.04	3.00	(0.03)	+0.14	0.03
b Vel	0.512	1.297	(0.08)	0.24	0.08	(0.07)	1.66	0.03	3.50	0.34	+0.01	0.05
i Car	0.123	1.517	(0.08)	0.20	0.08	(0.07)	1.80	0.03	7.21	0.04	-0.08	0.02
ν Car	0.193	1.361	(0.08)	0.23	0.08	(0.07)	1.71	0.03	5.7	0.09	-0.06	0.03
195 Car	0.402	1.105	(0.10)	0.22	0.12	(0.10)	1.37	0.04	3.1	0.33	-0.10	0.06
HD 97534	0.420	1.104	(0.10)	0.22	0.12	(0.10)	1.37	0.04	3.0	(0.33)	-0.08	0.06
θ Sco	0.234	0.963	(0.14)	0.28	0.14	0.10	1.29	0.04	6.02	0.01	+0.04	0.02
i Sco	0.337	1.395	(0.20)	0.30	0.14	(0.12)	1.66	0.03	5.39	(0.14)	+0.01	0.04
π Sag	0.227	1.037	(0.10)	0.24	0.10	(0.07)	1.36	0.03	6.23	0.02	+0.03	0.02

Table 3.7 (cont.)

Star	$(b-y)_c$	$[m_v(4670Å) - m_v(5470Å)]$	$(W_\gamma(0.8), [m_v(4670Å)-m_v(5470Å)])$				$(([c1])_c, [m_v(4670Å)-m_v(5470Å)])$			
			T_{eff}	$\pm \sigma^3$	log g	$\pm \sigma^3$	T_{eff}	$\pm \sigma^3$	log g	$\pm \sigma^3$
α Lep	0.296	-0.06	7400	200	2.00	0.10	7400	200	1.8	0.1
α Car	0.293	-0.067	7300	100	1.83	0.05	7300	100	1.7	0.1
b Vel			6500	300	0.2	0.10	6750	200	1.3	0.1
i Car	0.268	-0.09	7450	200	1.74	0.10	7450	200	1.4	0.1
β Car	0.300	-0.06	7100	200	1.08	0.10	7200	200	1.6	0.02
195 Car			7450	400	0.5	0.4	7700	400	2.8	0.2
HD 97534			7250	400	0.2	0.4	7600	400	2.8	0.2
θ Sco			6600	150	1.8	0.1	6650	150	2.1	0.2
i Sco	0.359	0.00	6600	300	1.1	0.2	6700	300	1.3	0.2
π Sag			6650	150	1.8	0.1	6650	150	2.0	0.1

Notes

1 Brackets indicate estimates made with reference to the measured line blocking in α Per, Parsons (1970), φ Cas, HD 10494 and 60° 2532, Osmer (1972), and my measurements for α Car.

2 Brackets indicate estimates made with reference to the stars of known reddening.

3 The σ's represent the estimated errors due to the uncertainties in the data alone.

ν Car (7150, 1.2), also shows this effect, but it is less pronounced than in the other three stars. Osmer (1972) observed the same effect in ϕ Cas (7150, 0.3).

The lower-temperature supergiants, δ CMa (6000, 0.1) (this investigation), HD 10494 (6200, 0.2) (Osmer 1972) and i Sco (6700, 1.2) (this investigation), do not show this discrepancy, indicating this effect is restricted to the top left-hand section of the (T_{eff}, log g) plane (Figure 3.5). This discrepancy and its significance will be considered further in Sections 3.5(b) and 3.5(c).

The (T_{eff}, log g) pairs for the stars for which model atmospheres were available (Section 3.2) were then checked by comparing the theoretical H_γ and H_δ hydrogen-line profiles with those observed. Most weight was given to the wing region stretching from ~ 1.5Å from the line centre out to a residual depth of 0.90. This avoids the uncertainty in the theoretical profiles near the core and the uncertainty of the observations in the shallow-wing regions. In general, the profiles predicted by the models had deeper cores and their wings extended further than the observed profiles, even though due care had been taken to avoid placing the continuum too low. The hydrogen-line profile measurements for the program stars are given in Appendix III.

The final fits to the observed H_γ and H_δ profiles for i Sco and π Sag are shown in Figures 3.6 and 3.7 as examples. The fit to H_γ in both stars is very good and the fit to H_δ in π Sag is good; the fit to H_δ in i Sco is poor, the observed profile being much smaller than the theoretical profile. This effect is evident in a number of the more luminous program stars and, in the cases where an approximate H_β profile is available, the opposite effect is observed (i.e. the

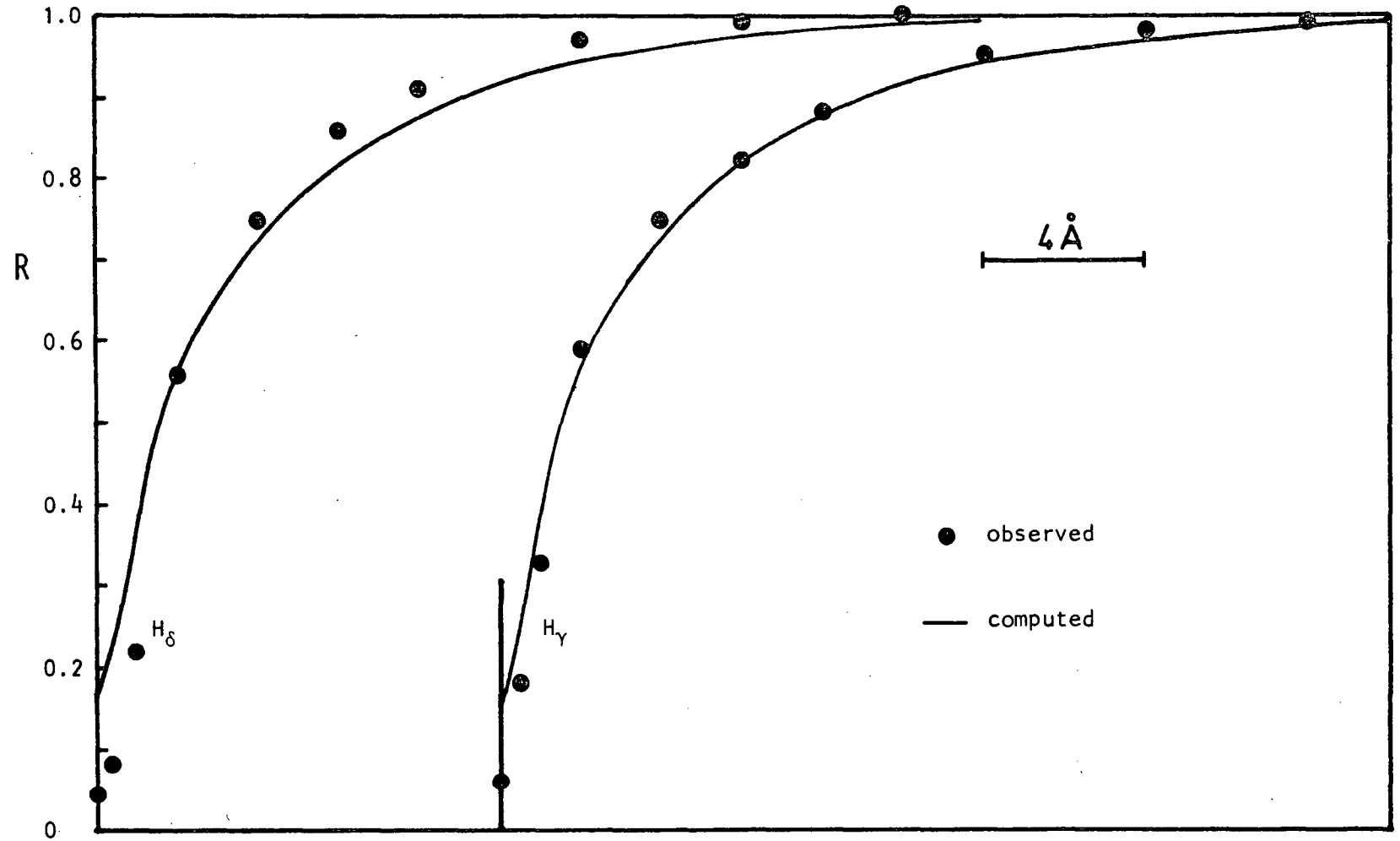

Figure 3.6 Observed H_δ and H_γ line profiles for i Sco and those calculated based on the model atmosphere T_{eff} = 6600°K, log g = 1.2.

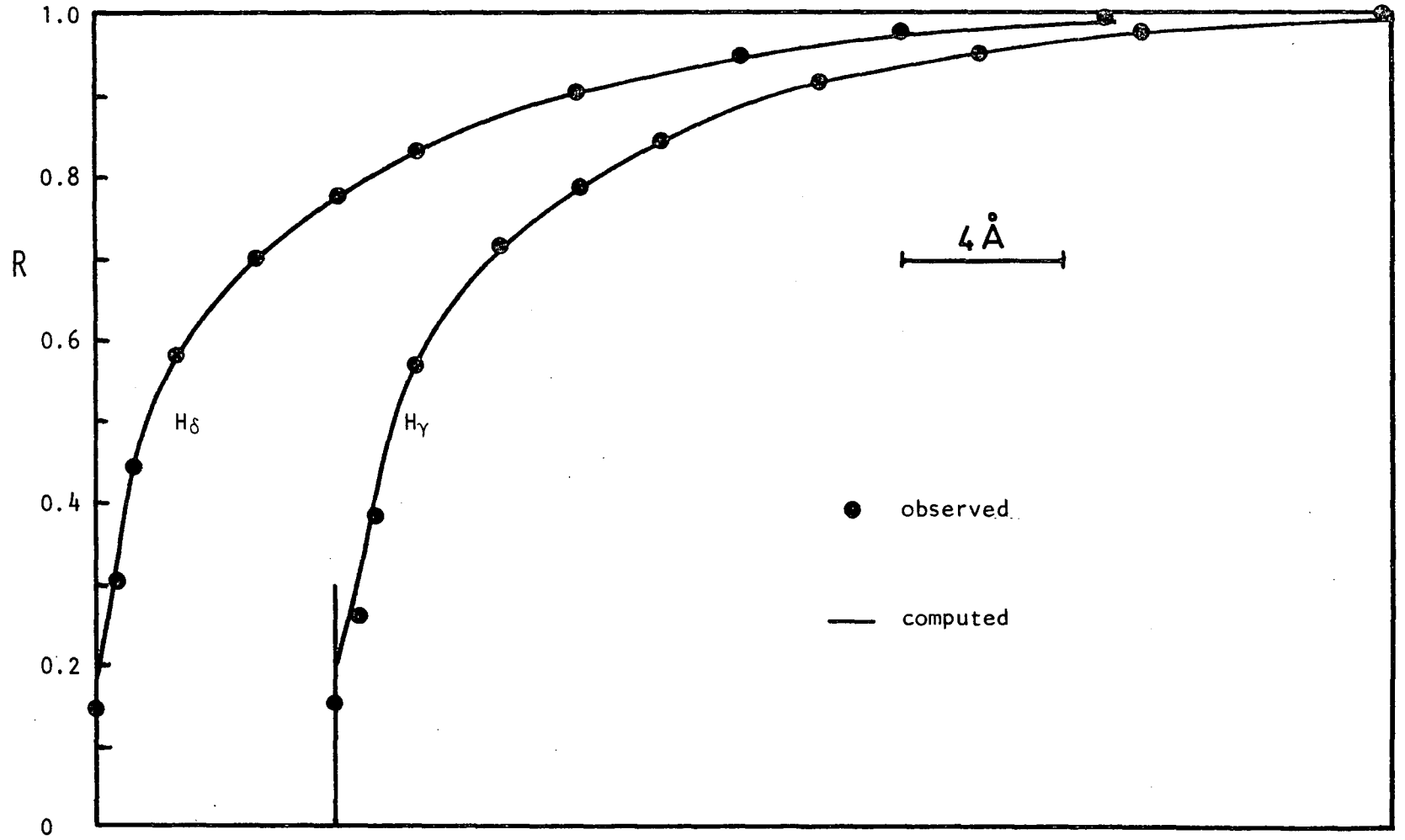

Figure 3.7 Observed H_δ and H_γ line profiles for π Sag and those calculated based on the model atmosphere $T_{eff} = 6650^{o}K$, log g = 1.9.

H_β observed profile is larger than the theoretical profile). The significance of these discrepancies is not clear at this time.

We now consider the effect of observational errors on the accuracy of the (T_{eff}, log g) values found by the technique described. The three plates taken for α Car covering the H_γ region indicate a standard deviation of 0.11Å in $W_\gamma(0.8)$. The plates of α Lep and δ CMa gave results that agreed to within this value for H_γ and H_δ. An error of 0.11Å in $W_\gamma(0.8)$ is insignificant compared with the error due to the inadequacy of the model atmospheres. Errors quoted for $([c1])^*_c$ (Table 3.7) are due mainly to the expected errors in the estimated blanketing shortward of the Balmer jump, and the error in the transformation to the natural *ubvy* system. This uncertainty, $\simeq 0.04$ magnitudes, corresponds to about 0.3 in log g. Errors in the colour excess, $E_{(b-y)}$ are the major source of error for the Paschen slope index. The Paschen slope index will also be affected by errors in the blanketing measurements. The estimated standard deviations in T_{eff} and log g due to the possible observational errors are given in Table 3.7.

The (T_{eff}, log g) pairs derived represent the models which best fit the observations and would possibly be most suitable for use in abundance analyses. So far, we have only considered the effects of interstellar reddening and line blanketing in comparing the observations with the models. In the subsequent section, other assumptions made in constructing the model atmospheres will be considered in relation to 'real stars'.

3.5 Other Factors Affecting (T_{eff}, log g) Estimates

(a) Rotational Velocities

The model atmospheres used in this investigation do not take into account the effects of stellar rotation. The projected equatorial velocities, $V_e \sin i$, of the F-type supergiant stars are, in general, quite small (Aller 1963, page 412). However, there are several exceptions where the rotational velocity is possibly large enough to affect the measured values of $W_\gamma(0.8)$ and $[c1]$. Also the mean effective temperatures and gravities are lower in rapidly rotating stars.

There are no detailed calculations on the effects of rotation available for the stars in the spectral range of interest. Several investigations of rotation effects in main-sequence stars in this spectral region have found that rapid rotation seen edge-on causes an apparent reduction in $[c1]$. Thus the only correction that can be made to T_{eff} and log g values are those due to the increase in $W_\gamma(0.8)$ because of the stellar rotation. Rotational velocity estimates have been made for all the stars studied in this program.

Rotational velocities have been calculated using a first-order limb-darkening approximation, the formula for which is given by Unsöld (1955) as

$$R_r(\lambda) = \int_{-1}^{+1} R_o(\lambda')\, M(x)\, dx \ ,$$

where

$$x = \left(1 - \frac{\lambda'}{\lambda}\right) = \frac{v}{c}\ m$$

$$M(x) = \left[\frac{2}{\pi}\sqrt{1-y^2} + \frac{\beta}{2}\,(1-y^2) \right] \Big/ \left[1 + \frac{2\beta}{3} \right]$$

$$y = \frac{\Delta\lambda}{\lambda} \frac{c}{V_e \sin i} ,$$

and

β = limb-darkening coefficient.

Here $R_r(\lambda)$ is the rotated profile of a line, the intrinsic profile of which is given by $R_o(\lambda)$, in a star of axial aspect i. The calculations were carried out using a computer program, loaned by Dr. R.D. Watson, for the Elliot 503 computer. Computations were carried out with a value of $\beta = 0.67$ (Parsons 1971). It should be noted that variations of β within the range 0.70 to 0.50 makes an insignificant difference to the resulting profile.

For small rotational velocities, the small metal lines are the most sensitive criteria of rotation. The standard procedure of selecting a sharp line star of similar spectral type to the program stars and taking its profiles to represent $V_e \sin i = 0$, was adopted. Of the program stars which were observed at high dispersion, there are two (α Car and i Car) which have equally narrow metal lines, half width at half-height values of 0.06 to 0.10Å.

To measure the macroscopic motions, if any, in α Car a curve of central depth, R'(0), versus equivalent width was constructed (Figure 3.8). Huang and Struve (1955) have shown that the slope of this graph at the origin, $dR'(0)/d(W/\lambda)_o$, is related to the microturbulent velocity ξ_s by

$$\left[\frac{dR'(0)}{d(W/\lambda)}\right]_o = \frac{c}{\sqrt{\pi}} \frac{1}{\xi_s} ,$$

when the ratio of the microturbulence to rotation, or macroturbulence, is large. Using this relation, and the observed slope at the origin, we find $\xi_s = 5.5$ km sec^{-1}. This is the same as the microturbulence

observed for the neutral species from the curve of growth (Section 4.3(c)). The theoretical curves shown in Figure 3.8 were calculated for ξ_s = 6 and 12 km sec^{-1}, ξ_ℓ = 0 km sec^{-1}, ε = 0, log a = -3.0 and B_0/B_1 = 2/3. Figure 3.8 shows there is no apparent separation of the curves defined by the points for the lines of neutral and singly-ionized species, and the stronger lines show a slightly higher velocity (6.5 km sec^{-1}) than the weak lines (5.5 km sec^{-1}). It is evident from this investigation that the macroturbulent motions and rotation are very small (< 1 km sec^{-1}), and thus α Car was used as the rotational velocity standard.

Rotational velocity calibration plates of α Car were taken for each of the spectrograph-photographic plate combinations used for the program stars. To reduce the problems of plate noise and line to line variations, graphs relating W/λ to the $\Delta\lambda/\lambda$, where $\Delta\lambda$ is the width of the line at half-height, were constructed for each star, using the unblended lines in the wavelength range 4130$\mathring{A}$ < λ < 4850$\mathring{A}$. A line of best fit was calculated for these points. The profiles of four metal lines in α Car, whose points were on the line of best fit or close to it, were measured. These profiles were then rotated to give a calibration of half-width against $V_e \sin i$ for a range of equivalent widths.

Calibrations were made for each of the spectrograph-photographic plate combinations used. The reduced resolution of the 9 $\mathring{A}$ mm^{-1} plates is closely equivalent to a rotational broadening effect of 15 km sec^{-1}. The half-width at half-height of the comparison lines (Section 3.5) indicates the stability of the observing system is within the line to line variations on each plate.

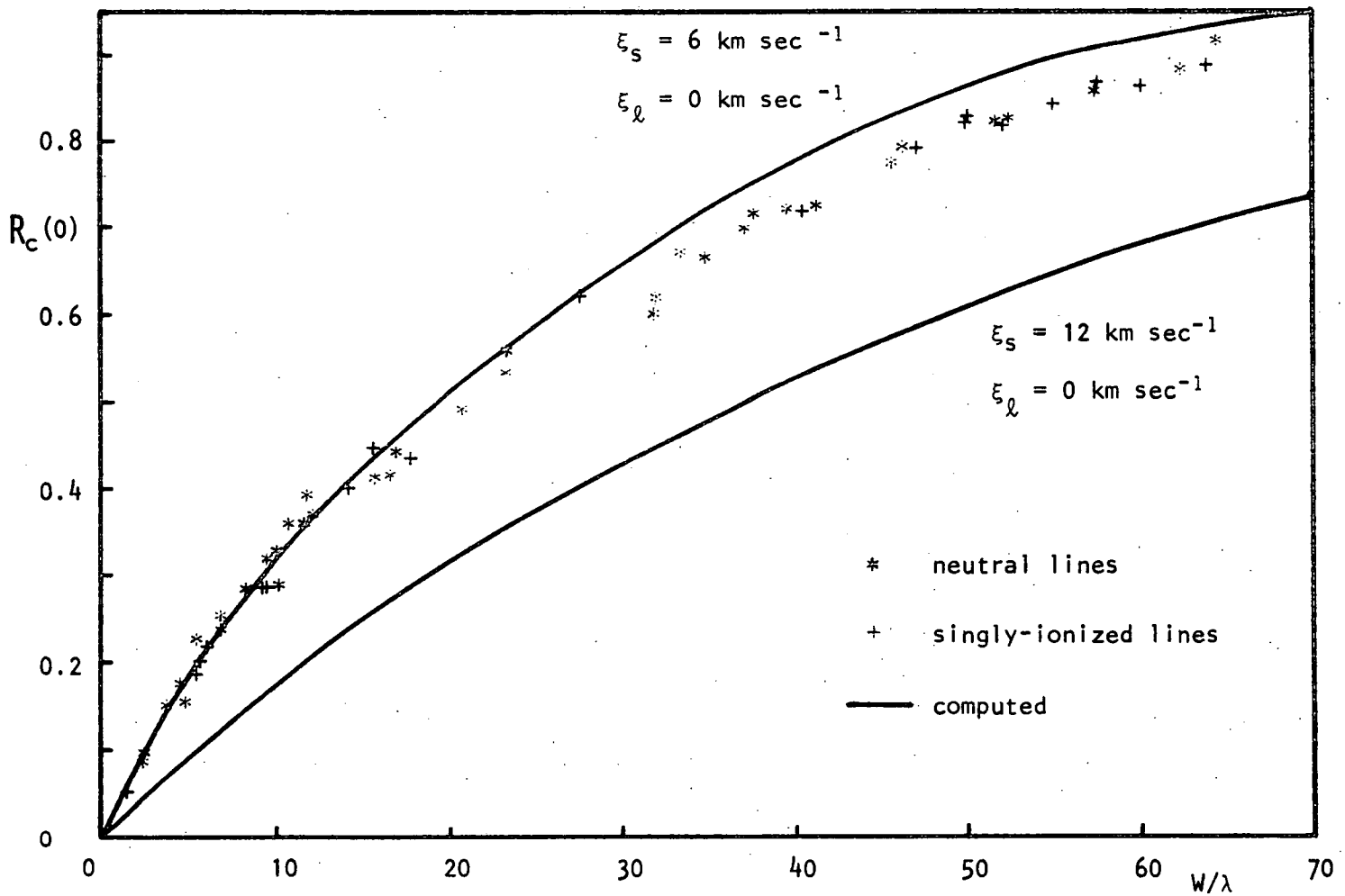

Figure 3.8 Residual intensity plotted against equivalent width in Fraunhofers. The *'s and +'s represent the lines of neutral and singly-ionized species respectively. The continuous line represents theoretical contours based on the Milne-Eddington model.

The observed profiles of the four lines in α Car used to form the calibration curves for the (2.1 $\mathring{A}$ mm^{-1}, 103a-0) spectrograph-photographic plate combination are given in Table 3.8. Figure 3.9 shows the calibration curves calculated using these four lines. As an example, the graph relating W/λ to $\Delta\lambda/\lambda$ for α Lep is shown in Figure 3.10. The scatter in the points is a little more extreme in this star than the other low dispersion stars. This scatter in the points exemplifies the danger involved in using only one line for rotational velocity measurements. It appears as though the scatter of the points about the line of best fit is random from star to star (i.e., any particular line is not too broad or too narrow in all stars). There is no significant separation between points from neutral and singly-ionized lines for any of the stars observed, indicating there are no large differences in the macroturbulent velocities associated with the neutral and singly-ionized atoms. It has been assumed that the intrinsic profiles of the metal lines in each star would be the same if they all had the same microturbulent velocity. This is not strictly true because the apparent macroturbulent velocities associated with each line in the stars are different, and increase with increasing equivalent width. To reduce, and possibly eliminate this effect, most weight has been given to lines of small equivalent width.

Using the line of best fit through the points, the half-width appropriate to the equivalent widths of the calibration lines can be found, and these used in conjunction with the calibration curves to determine the rotational velocity. The standard deviation of the points from the line of best fit was used as a measure of the uncertainty associated with the rotational velocity determination. The results are given in Table 3.9, along with the results of previous determinations and their sources.

Table 3.8

Selected Metal Line Profiles in α Car (2.1 Å mm^{-1}, 103a-0)

Δλ(Å)	Residual intensity			
	Fe I λ4143.9	Fe I λ4148.9	Mg I λ4167.3	Fe I λ4250.1
0.000	0.160	0.535	0.420	0.295
0.025	0.185	0.580	0.465	0.330
0.050	0.280	0.705	0.595	0.475
0.075	0.400	0.785	0.710	0.625
0.100	0.520	0.885	0.785	0.725
0.125	0.635	0.915	0.850	0.800
0.150	0.695	0.950	0.900	0.865
0.175	0.740	0.965	0.940	0.905
0.200	0.820	0.975	0.965	0.930
0.225	0.865	0.990	0.980	0.945
0.250	0.910		0.990	0.965
0.275	0.930			0.980
0.300	0.965			0.990
0.325	0.980			
0.350	0.990			
E.W.(mÅ)	224	74	110	140

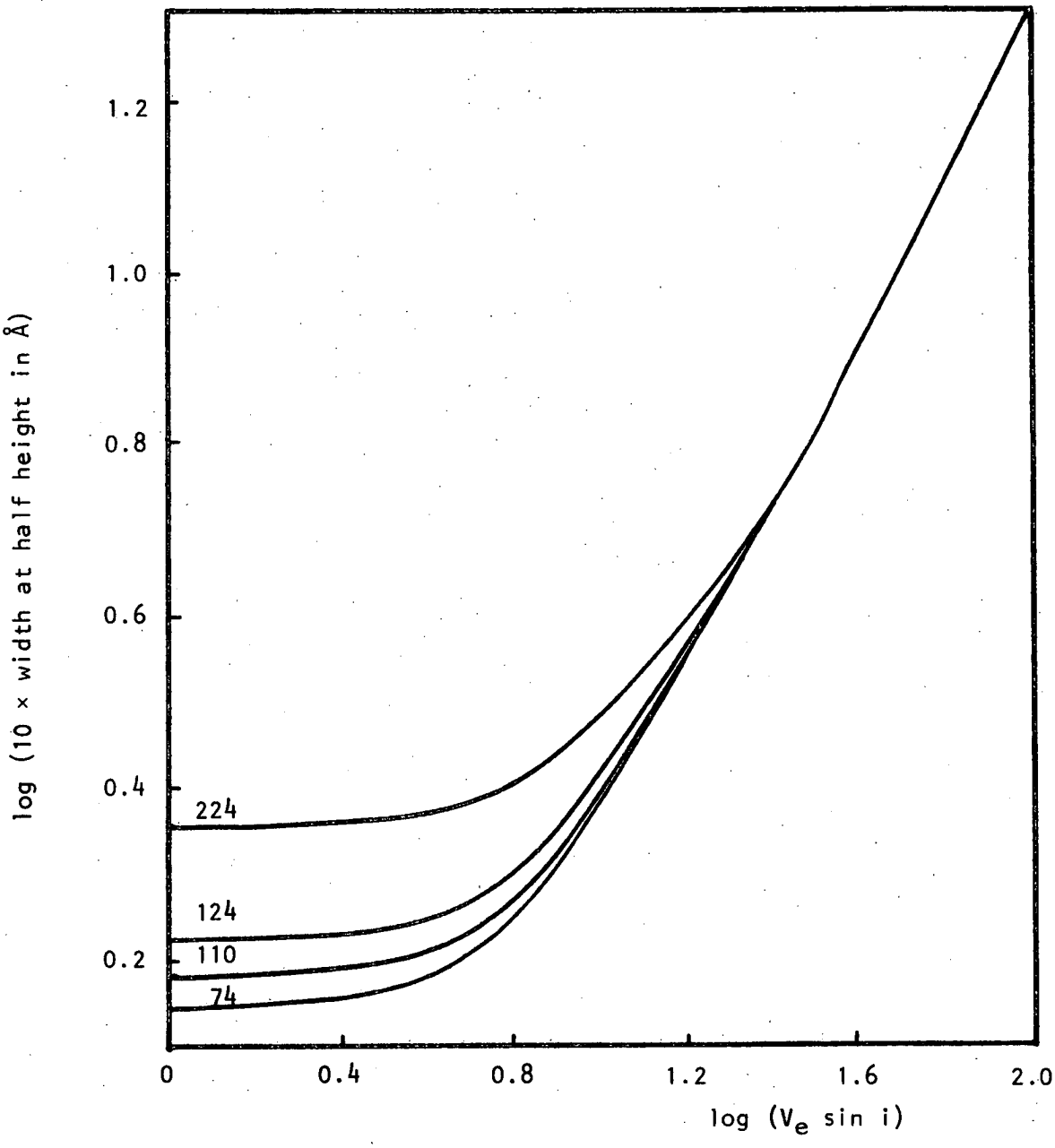

Figure 3.9 Rotational velocity calibration curves for the 2.1 Å mm^{-1}, 103a-0 system. The numbers on the curves refer to the equivalent widths (in mÅ) of the lines used to calculate them.

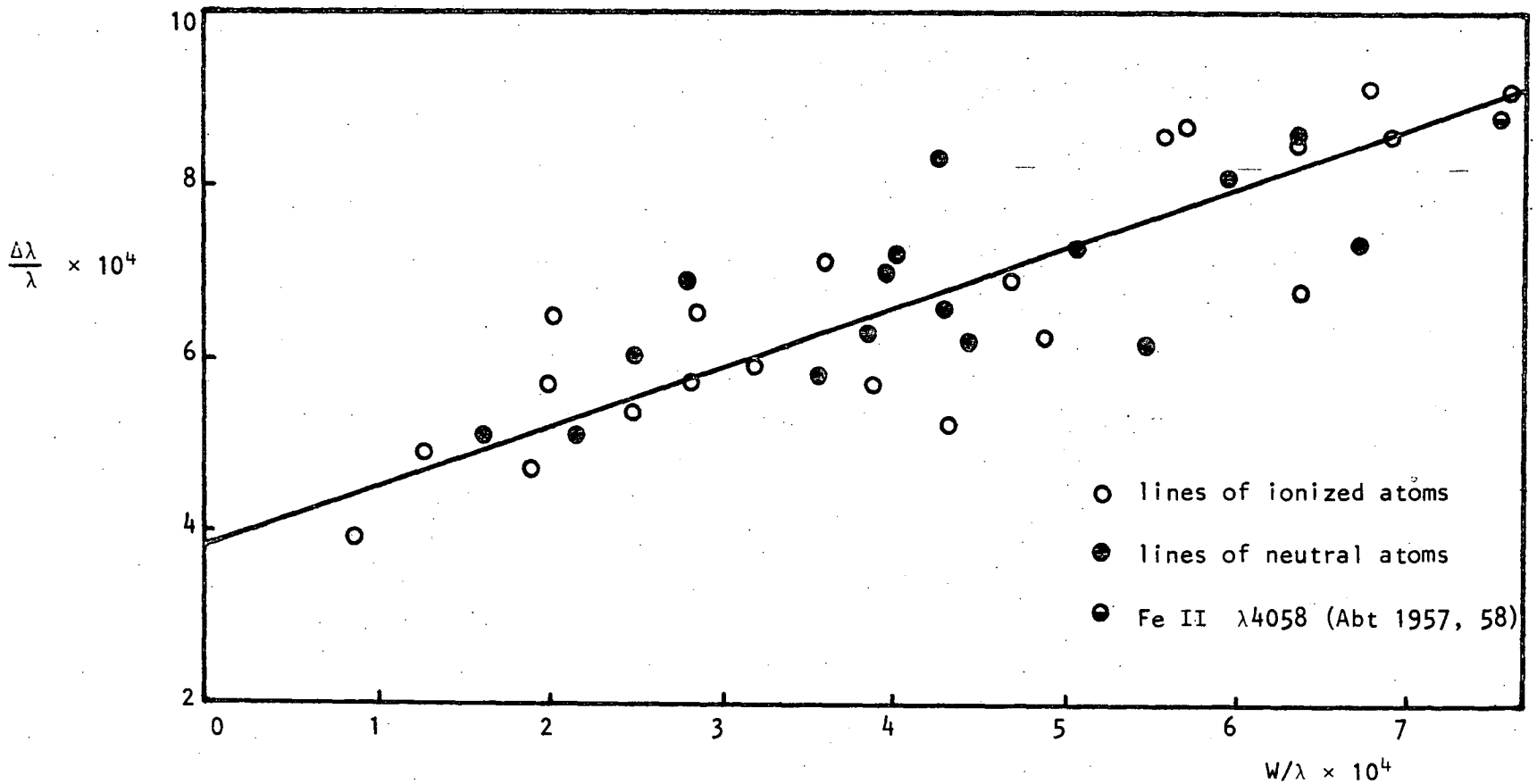

Figure 3.10 Observed relationship between $\Delta\lambda/\lambda$ and W/λ for α Lep. The solid line is the line of best fit. The ○'s and the ●'s represent lines of singly-ionized and neutral atoms respectively. ⊖ shows the Fe II λ4058 line which was used by Abt (1957,58) for his rotational velocity measurements.

Table 3.9

The Rotational Velocities of the Program Stars

Name	Rotational Velocity (km sec^{-1})		Reference
	This Determination	Previous	
α Lep	9 ± 2	15	Abt (1958)
α Car	0 (by definition)	0	Huang (1953)
δ CMa	3 ± 2	0	Bell and Rogers (1965)
b Vel	50 ± 6	38	Huang (1953)
i Car	0 + 2	0	"
ν Car	0 + 5	0	"
195 Car	40 ± 5	42	"
HD 97534	38 ± 5	34	"
θ Sco	90 ± 10	105	"
i Sco	19 ± 4	36	"
π Sag	34 ± 4	28	Abt (1957b)

The results have been corrected for the effects of variation of microturbulence from star to star (Section 4.3(c)). Because the metal-line strengths are not particularly large, the accuracy of the rotational velocity determinations degenerates above 60 km sec^{-1}. There does not appear to have been any information lost by just using the width at half-height rather than the full profile, since the full profiles of the program stars fit the theoretically-rotated profiles adequately. This is shown in Figure 3.11 for θ Sco (Cr I λ4242.4, Fe I λ4404.8) and i Sco (Ca I λ4425.4, Ti I λ4493.5). The rotational velocities measured in this study agree well with those of previous investigations (Table 3.9).

A test to determine the effect of the observed rotational velocities on $W_\gamma(0.8)$ was made on θ Sco, the most rapid rotator observed. Theoretical rotation of the observed H_γ line profile for θ Sco by a further 100 km sec^{-1} caused an insignificant increase in $W_\gamma(0.8)$. Therefore, the $W_\gamma(0.8)$ values observed are not affected directly by rotation effects and no correction need be made.

In conclusion, it should be noted that the rotational velocities in the majority of the stars are small enough not to have significant effects on (T_{eff}, log g). The effect on the rapid rotator (θ Sco) is a possible overestimation of log g, entering through the reduction in [*c1*], and an underestimation of the temperature. The magnitude of these effects is unknown at this present time.

There have been several investigations into the nature of the distribution of angular momentum within the luminous giant and supergiant stars (such as those by Abt 1957, 1958 and Rosendhal 1970a). Rosendhal (1970a) has shown that the observed rotational velocities

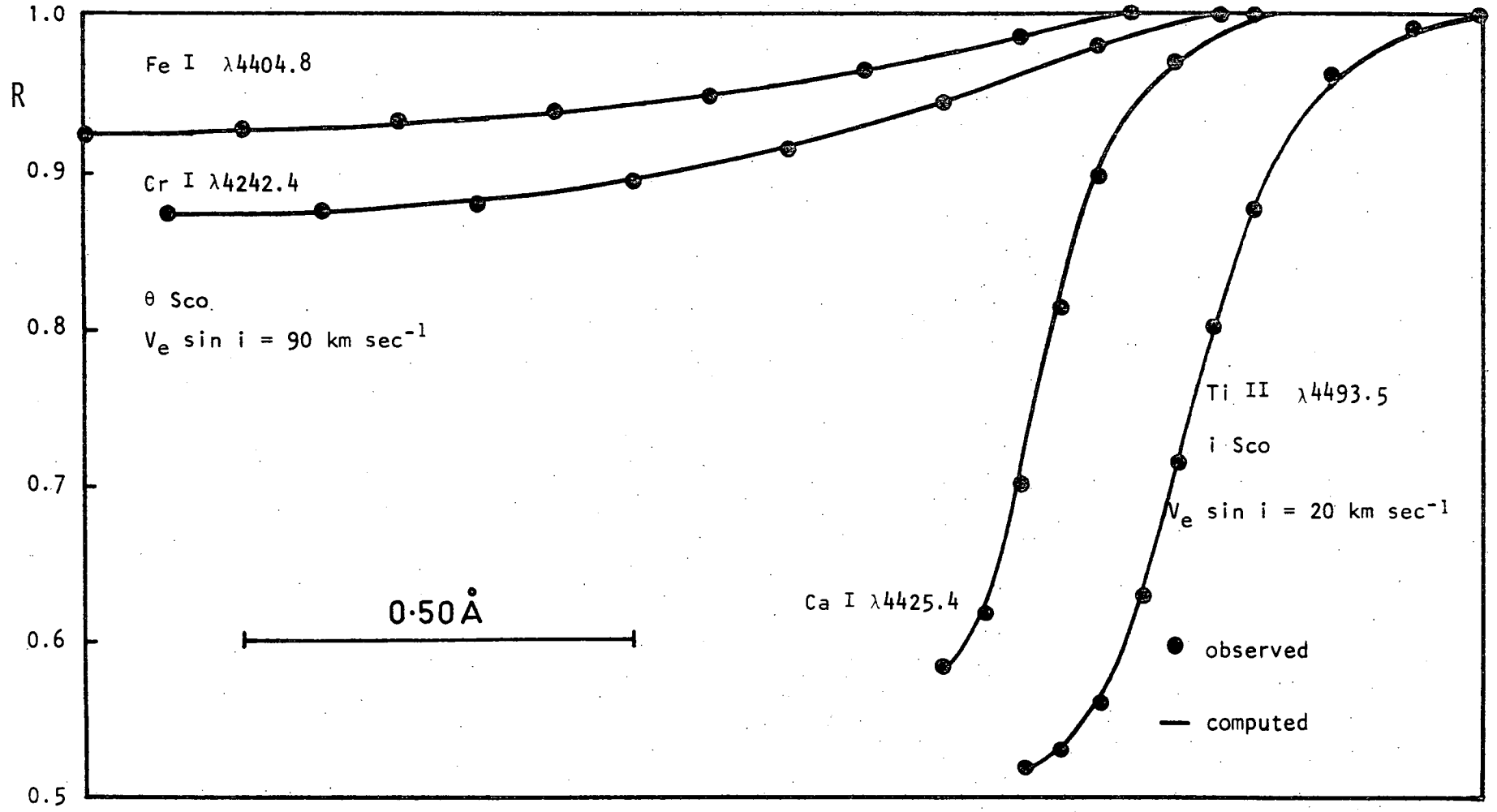

Figure 3.11 The measured metal line profiles (filled circles) for θ Sco and i Sco and the theoretically rotated α Car profiles (full lines).

of the giant and supergiant stars are too large for there to have been a large loss of angular momentum in their evolution from the main sequence. The two extreme cases in the application of conservation of angular momentum are:

(1) a free radial transfer of angular momentum within the stars (rigid-body rotation), and

(2) no such transfer (i.e. differential rotation in which each thin shell retains its own angular momentum).

To determine which of these two cases apply, the average observed rotational velocities of luminous giants and supergiants are converted back to the average rotational velocities their main-sequence predecessors would have required, assuming (1) or (2) to hold. These rotational velocities are compared with the present average rotational velocities observed for the main-sequence predecessors.

The results as given by Abt are shown in Table 3.10a and indicate that it is most likely that, in the A and F-type luminous giants and Ib supergiants, the angular momentum is conserved in discrete shells.

Another alternative explanation is that the stars rotate as rigid bodies and a large proportion of the stars' initial angular momentum has been lost to the surrounding medium via mass loss. Schatzman (1962) has shown that an outflow of ionized matter in the presence of a magnetic field exerts appreciable torques on a star, and that a large loss of angular momentum can result from a rather small loss of mass.

Rosendhal has compared the observed rotational velocities

(corrected for macroturbulence) of the O, B and A Ia and Iab supergiants with those expected from the average observed rotational velocities of their main sequence predecessors, assuming (1) or (2) to hold. His results, Table 3.10b, indicated that the early B supergiants may be rotating as rigid bodies, and in the later spectral types, the angular momentum may be conserved in spherical shells.

Rosendhal has used the fact that there are no supergiants with zero rotational velocities in the spectral range his investigations have covered to indicate that some of the line broadening is due to macroturbulence. He has used a statistical approach to remove the effects of macroturbulence, which he found to be very large ($\simeq$ 22 km sec^{-1}). It is interesting to note that F0 Iab supergiants with very small (< 1 km sec^{-1}) apparent rotational velocities do exist, indicating macroturbulence is not significant in these stars. The jump in macroturbulent velocities from < 1 km sec^{-1} at F0 to 22 km sec^{-1} at A5 and above seems to be a little extreme, and possibly the effect of macroturbulence has been overestimated by Rosendhal in these stars. Abt has noted that in the 25 stars he observed, there were no stars with velocities less than 10 km sec^{-1}. It has been observed that the apparent macroturbulent velocities in solar-like supergiants of class Ib vary with line intensity, increasing with increasing line strength (e.g. Bell and Rogers 1965). The spectral line used by Abt (Fe II λ4508) for his rotational velocity measurements is moderately strong (~ 350m$\mathring{A}$ in α Lep, F0Ib), and may therefore show some macroturbulence.

Comparison between the Fe II λ4508 line in α Lep and a theoretically-rotated (9 km sec^{-1}) line profile, calculated from the profile of a line with the same equivalent width in α Car, showed

Table 3.10a

Rotational Velocity Data (Abt 1957, 1958)

Spectral Class	$V_e \sin i$ (km sec^{-1})				Main Sequence Predecessor
	Observed Average	Initial (1)	Initial (2)	Predecessor Observed Average	
A0-F8 Ib	77	77	177	158	B2-5V
A5-F8 II	26	76	162	152	B8V

Table 3.10b

Rotational Velocity Data (Rosendhal 1970a)

Spectral Class (Ia and Ib)	$V_e \sin i$ (km sec^{-1})			
	Recovered Rotation	Predicted Rotation		Apparent Rotation
		(1)	(2)	
A0-A5	13 ± 6	20 ± 4	8 ± 4	≃ 40
B3-B6	14 ± 9	40 ± 8	18 ± 8	≃ 60
09.5-B1	40 ± 20	50 ± 10	26 ± 10	≃ 90

Table 3.11

Rotational Velocities of θ Sco

Assumed Spectral Type	$V_e \sin i$ (km sec^{-1})				Predecessor Spectral Type
	Observed	Initial (1)	Initial (2)	Predecessor Maximum	
FoIb	95	380	850	420	B3V
F2II	95	258	530	400	B8V

excellent agreement. This indicates that there are no, or very small, differences between the macroturbulent velocities of weak and strong lines in α Lep, and thus probably the macroturbulent motions in stars of this type are very small. This is the same conclusion as reached by Abt for the bright giants (i.e., the observed line broadening in these stars is due to rotation and microturbulence alone).

Now consider the star θ Sco, classified as FOIb, but from its apparent (T_{eff}, log g) (Section 3.4), it would appear to be F2II. Note that [*c1*] is affected by rotation and log g may have been overestimated. Table 3.II gives the initial rotational velocities required to produce the observed rotational velocity for both cases of angular momentum conservation, and the two limiting spectral types. The largest observed rotational velocity for a star similar in spectral type to θ Sco when it was a main-sequence star is 450 km sec^{-1} in HD 35407 (B5V) (Uesugi and Fukuda 1970). Hence, it is unlikely that the angular momentum could have been conserved in spherical shells in θ Sco because the required initial rotational velocity is too large. Abt has suggested that during the initial expansion (to a factor of about 4) a star rotates as a rigid body, but that subsequently it commences to rotate differentially. This could have been the case for θ Sco if it is F2II, where the expansion factor is about 6. An initial rotational velocity of 350 km sec^{-1} would be sufficient to have produced the observed rotational velocity of 90 km sec^{-1}.*

If θ Sco is FOIb, it must have rotated as a rigid body throughout

---

* Stars of similar spectral type to θ Sco have been observed with rotational velocities less than 20 km sec^{-1}, indicating that the macroturbulence in θ Sco is probably $\leq$ 20 km sec^{-1}, and will thus have an insignificant effect on the observed profiles.

its evolution off the main sequence. The curve of growth results for this star (Chapter 4) show that it does not have normal abundances and it is probably a F0Ib supergiant rather than a F2II giant. The data for θ Sco suggests that the F0Ib supergiants rotate as rigid bodies for at least some of, if not all, of their evolution off the main sequence, and lose very little of their angular momentum to the surrounding medium. This is similar to the conclusion reached by Rosendhal for the early B stars, and could apply to the A0-A5 supergiants if the macroturbulence has been overestimated, which seems likely. A reduction of the mean macroturbulence from 22 km sec^{-1} to 15 km sec^{-1} would be sufficient.

3.5 (b) Non-Local Thermodynamic Equilibrium (NLTE)

In this section we will consider the effects of NLTE on the values of T_{eff} and log g previously determined. For the purposes of this discussion, it is convenient to divide the program stars into two groups: the lower temperature less luminous stars, $T_{eff} < 7000^{o}K$, log g > 2.0, in which the negative hydrogen ion (H^-) is the dominant opacity source, and the higher temperature more luminous stars $T_{eff} > 7000^{o}K$, log g < 2.0, where H^- is not the dominant opacity source.

In the stars where H^- is the dominant source of opacity, we need to consider the effects of departures from LTE in H^-. Qualitatively, we expect from the work of Kalkofen (1968) and others that:

(1) The departure coefficient, b^-, expressing the ratio of the true H^- number density to the LTE value, will be greater than unity (i.e., there will be more H^- than we expect on the basis of LTE calculations).

(2) The boundary temperature will be greater than that computed from LTE models.

For neutral hydrogen, because of the rapid increase in flux in the Balmer continuum with increasing depth, the second level will be underpopulated. With $b_2 < 1$ the Balmer discontinuity is small, and hence gravities will be overestimated. Moreover, the hydrogen lines are weakened since $b_n/b_2 > 1$, for $n \geq 3$. Therefore the effective temperature is chosen too small from the equivalent widths of the Balmer lines.

For the stars in which H^- is not the major source of opacity, departures from LTE result in $b_2 < 1$ and $b^- > 1$. Hence the Balmer discontinuity is again smaller than the LTE value and the gravities will be overestimated. In these stars the hydrogen line formation is analogous to that in B stars, where the equivalent width of H_γ essentially measures the surface gravity, rather than the temperature. The NLTE effects cause a decrease in H_γ and therefore the gravities chosen will be too low.

Calculations reported by Osmer (1972) indicate that at temperatures near 6750°K and log g ≃ 0.3, the differences between the LTE and non-LTE models were negligible. At $\tau_{5000} = 0.1$ the populations of all levels of H and H^- were within 4% of their equilibrium values and at $\tau_{5000} = 1$ the deviations were less than 1%. Osmer's calculations (his Table 15) show that the H_γ equivalent width and the Paschen slope index $[m_v(4110\text{Å}) - m_v(7550\text{Å})]$ are unaffected by the deviations from LTE in the very low gravity stars. No indication of the effects of NLTE on the Balmer jump index $[m_v(3500\text{Å}) - m_v(4110\text{Å})]$ was given.

Calculations by Parsons (1970) indicate that for supergiants with parameters within the range $6600 > T_{eff} > 6000$°K, $1.2 < \log g < 2.4$, departures from LTE cause an insignificant (< 10°K) departure from the

LTE temperature structure. However, there is a 0.05 magnitude reduction in the Balmer discontinuity. The Paschen slope is unaffected by the deviations from LTE. This Balmer jump reduction corresponds to an overestimate of 0.2 to 0.3 in log g values derived using LTE model atmospheres. A similar effect has been noted by Strom (1969) for the high-luminosity A stars ($2 < \log g < 4$). Thus, it appears reasonable to assume that the effect of NLTE is to cause an overestimate of 0.2 to 0.3 in log g, determined from the Balmer jump using LTE models for all the program stars with $\log g \geq 1$. For stars with $\log g < 1$, the effect is smaller, $\Delta \log g \simeq 0.1$.

NLTE models show a small decrease in H_γ, but Osmer's calculations indicate that it is insignificant for stars with $\log g \simeq 0.3$, but it may be significant for stars of higher gravity. There is currently a program under way at the University of Tasmania to develop the routines for the calculation of NLTE continuum fluxes and hydrogen-line profiles using the method of Parsons (1970). At the present time, only the tentative corrections mentioned above can be made to take into account the effects of departures from LTE. The corrected (T_{eff}, log g) values are given in Table 3.12.

(c) Turbulent Motions and Mass loss

In this section we will consider the effects of turbulent motion on the electron and gas pressures in the atmospheres, and how changes in these affect the observed hydrogen-line profiles. The evidence for macroscopic motions in the A and early F-type supergiants is then presented and the macroturbulent velocities considered appropriate for the program stars given. We will then consider the effect of radiative acceleration and how this makes mass loss possible

in the more luminous stars.

Calculations by Osmer (1972) indicate that the inclusion of a 7 km sec^{-1} (constant with depth) microturbulent velocity term in the equation of hydrostatic equilibrium reduces the gas and electron pressures enough to narrow the Balmer lines by 10%. He then used the relations

$$Pe \propto \sqrt{g/(1 + \text{const } V^2)}$$

and

$$\frac{1_\nu}{k_\nu} \propto Pe\, W_\gamma(0.8)^{-5/2}$$ (if hydrogen is the dominant continuous opacity source),

where Pe is the electron pressure, V is the velocity (micro or macroturbulent) and $1_\nu/k_\nu$ is the ratio of line to continuous absorption, to show that a turbulent velocity of 16 km sec^{-1} was sufficient to reduce the observed value of $W_\gamma(0.8)$ by 1Å in low-gravity supergiants with log g ≃ 0.3.

The F0Ia supergiants exhibit the largest observed microturbulent velocities of any stars (Section 4.3(a)), but these are observed for the stronger lines, which are not formed in the region of the atmosphere where the hydrogen-line wings are formed. In fact, the microturbulent velocities are expected to be very small in the region of hydrogen-line wing formation because in these stars they decrease with increasing density (Section 4.3(a), Parsons 1967 and Osmer 1972).

Rosendhal (1970a) has presented some statistical evidence indicating the A0 - A5 Ia and Iab supergiants exhibit appreciable macroturbulent velocities (15 - 25 km sec^{-1}). Abt (1958), who studied the rotational velocities of 13 Ib supergiants between A0 and F8, did not find any stars with a rotational velocity less than 10 km sec^{-1},

which suggests that some of the observed line broadening may be due to macroturbulence. It has been observed that the macroturbulent velocities in α Car and i Car (F0Iab) are very small (Section 3.5(a)), and Bell and Rogers (1965) have found macroturbulent velocities in δ CMa (F8Ia) that increase from 0 km sec^{-1} for the weak lines to 30 km sec^{-1} for the strong lines. Sargent (1961) analysed the profiles of the weak lines, which are formed at the same depth as the hydrogen-line wings, in ρ Cas (F8Ia) and found macroturbulent velocities of 19 km sec^{-1} for the ionized atoms and 15 km sec^{-1} for the neutral atoms.

All the high-luminosity stars (log g < 1.2) in the program, with the exception of δ CMa, exhibit discrepancies between the log g values indicated by the Balmer jump and the Balmer line profiles, even after the log g values have been corrected for NLTE effects. The *ubvy* photometry data (Appendix II) and the observed value of $W_\gamma(0.8) \simeq 3.5\text{Å}$ (Searle, Sargent and Jugaku 1963) for 89 Her (F2Ia) indicate gravities of log g ≃ 1.5 and 0.3 respectively, using $T_{eff} = 6800^\circ K$ (Searle et al.) and the blanketing observed for i Sco (F2Ia)(Table 4.7). Thus the discrepancy is apparent in 89 Her. It has also been noted in φ Cas (F2Ia) by Osmer (1972) and in this investigation. δ CMa, in which the turbulent velocity observed for the small lines is zero, and HD 10494 (F5Ia) (studied by Osmer 1972) do not show this difference in log g values. The values determined for these two stars apparently indicate that this discrepancy in log g values is restricted to the early F-type supergiants of high luminosity.

Thus, there is some evidence that large scale motions with the appropriate velocities could exist in the region of hydrogen-line wing

formation in the most luminous and early F-type supergiants. The following macroscopic motions will be assumed for the program stars, with the exception of δ CMa:

(1) 16 km sec^{-1} for stars with values of log g derived from Balmer line profiles less than 1.0 (i.e., the observed value of $W_\gamma(0.8)$ is too small by $1\mathring{A}$),

(2) 8 km sec^{-1} for the stars with log g in the range $1 < \log g < 1.4$ (i.e., $0.4\mathring{A}$ reduction in $W_\gamma(0.8)$),

(3) 0 km sec^{-1} for the stars with log g in the range $1.4 < \log g < 2.0$.

The (T_{eff}, log g) pairs corrected according to the above scale are given in Table 3.12.

We have considered the observational evidence for the existence of turbulence in the atmospheres of the luminous early F stars. Now we will show that the pressure inversion zone, which is unstable, could be the driving mechanism for these motions. The effects of radiation pressure are then considered, with particular attention to the possibility of mass loss.

Model atmosphere calculations by Osmer (1972) have shown that there is a region in the atmospheres of F stars with $\log g \leq 1.8$ where the acceleration due to radiation pressure, g_{rad}, exceeds the surface gravity, causing a pressure inversion. The temperature and gravity dependence of some characteristics of the zone are shown in Figure 3.12, which has been taken from Osmer. The maximum value of g_{rad}/g in a model and the density ratio, $\rho(\tau = 2.15)/\rho(\tau = 21.5)$, increase with decreasing gravity and with decreasing temperature, while the upper boundary, at the region where $g_{rad} > g$, moves outward with decreasing gravity and increasing temperature.

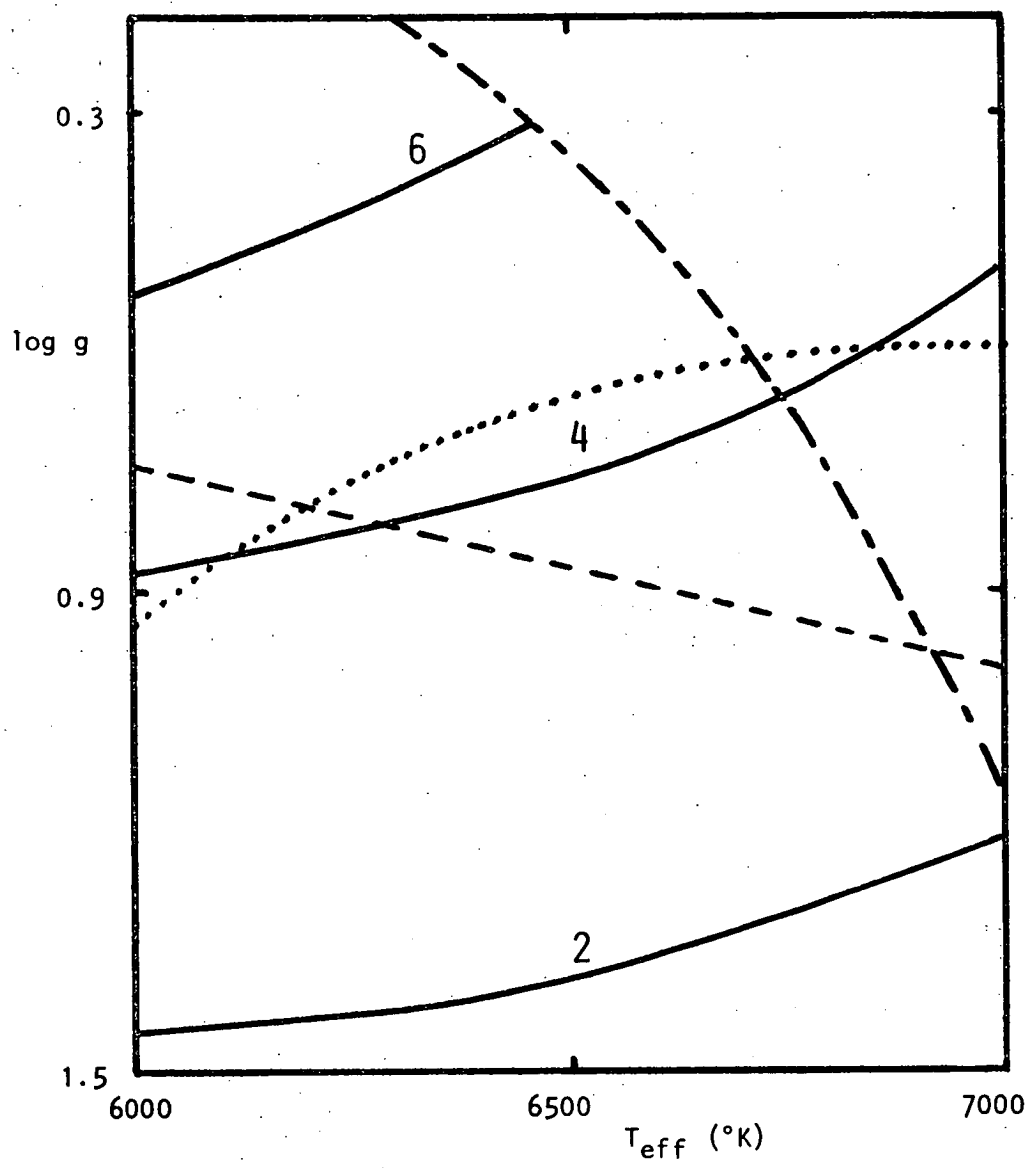

Figure 3.12 Characteristics of the gas pressure inversion zone as a function of temperature and gravity. The solid lines denote the maximum value of g_{rad}/g in a given model. The dotted line is for the density ratio $\rho(\tau = 2.15)/\rho(\tau = 21.5) = 3$ and the dot-dashed line indicates where the upper boundary of the zone occurs at $\tau = 2$. The dashed line indicates the locus of constant luminosity. (This diagram is taken from Osmer 1970.)

Böhm-Vitense (1973) has noted that the expression for g_{rad} used by Osmer

$$g_{rad} = \frac{\sigma}{c} T_{eff}^4 \bar{K}$$

only gives a lower limit to g_{rad} and the actual value is likely to be at least a factor of 6, and possibly 60, times greater in the region of line formation. This is because the expression used by Osmer does not include the effects of line absorption. The line absorption coefficient may be 10^6 times as large as the continuous absorption coefficient, while at the surface the flux in the lines remains of the order

$$F(\text{line}) \simeq 0.01\ F(\text{continuum}) .$$

This increase in g_{rad} at the surface means the zone of pressure inversion extends further out in the atmosphere than indicated by Figure 3.12, and the zone may exist in stars with gravities higher than log g = 1.8.

Note that the inversion zone approaches the region of hydrogen wing formation in the F0Ia stars, but is deeper in the F8Ia stars. Also, the inversion zone becomes more extreme and closer to the surface in the hotter Ia supergiants; this may be the reason for the increase in the turbulent motions observed by Rosendhal (1970a) in going from the A5 to the B6 (Ia and Iab) supergiants.

Böhm-Vitense indicates that the radiative acceleration is possibly large enough to cause mass loss in supergiants with $M_v < -7$ and $T_{eff} > 8000^{\circ}K$. If large velocity gradients exist in the atmospheres of supergiants, then the radiative acceleration may lead to mass loss for stars with $T_{eff} > 5000^{\circ}K$. Mass loss has been observed in 89 Her ($T_{eff} = 6800$, $M_v = -7.1$) (Sargent and Osmer 1968) and is possibly

taking place in ρ Cas (Sargent 1961). The short time scale over which the circumstellar features change, and the fact that high velocities of expansion (up to 150 km sec^{-1}) are observed in the spectrum of 89 Her, imply that very energetic phenomena are occurring in its atmosphere.

Two of the program stars, 195 Car and HD 97534 ($T_{eff} \simeq 7400^{o}K$, $M_v \simeq -8.0$) are both very good candidates for mass loss. Crawford, Barnes and Golson (1970) have indicated that 195 Car was variable in H_β from February 1967 to February 1968, and discordant in *b-y*, *ml* and *cl* between March 1963 and January 1965. HD 97534 has been included in the catalogue of early-type stars whose spectra have shown emission lines (Wackerling 1970), indicating this star possibly has a circumstellar envelope and is probably losing mass. However, none of the usual spectral features associated with a circumstellar envelope, two weak emission lines at λ4727.9 and λ4732.0 and absorption in the Balmer lines, were observed in the spectral range analyzed (3670Å-4800Å). This is inconclusive, because the plates were of low resolution (0.4Å) and the strong features characteristic of a circumstellar envelope, such as H_α emission and absorption features and splitting of the sodium D lines, occur at longer wavelengths. Red plates to investigate this point further are unfortunately outside the range of the 40cm telescope with the lowest dispersion (14 Å mm^{-1}) currently available.

3.5 (d) Radial Velocity Variations

Abt (1957) has observed that the F-type supergiants exhibit semi-periodic radial velocity variations, the maximum amplitude, A, of which is about 10 km sec^{-1}. Böhm-Vitense (1956) found a period, P, of 70 days for 89 Her. Following Osmer (1970) and assuming that the

semi-regular velocity variations of supergiants can be characterised by the formula

$$V_{radial} = A\cos(2\pi T/P) \text{ km sec}^{-1} ,$$

then the acceleration which produces them is

$$g_{puls} \leq A2\pi/P .$$

Using this formula and the above observed amplitude and period we find that

$$g_{puls} < 1 \text{ cm/sec}^2 ,$$

which is approximately 10% of the expected gravity in an FIa star. Since the electron pressure varies as the square root of gravity, it would be changed by 5% or less because of the pulsations and will have a minimal effect on the observed hydrogen-line profiles ($W_\gamma(0.8) \propto P_e^{2/5}$). Thus the pulsations associated with the radial velocity variation will not significantly affect the atmospheric parameters derived from $W_\gamma(0.8)$ in the FIa stars.

(e) Convection

Calculations by Parsons (1969) and Carbon and Gingerich (1969) show that convective energy transport is unimportant in supergiants with the parameters $T_{eff} = 6600^{\circ}K$, log g = 1.8 and $T_{eff} = 7000^{\circ}K$, log g = 2.0 respectively. Since the differences between the adiabatic and radiative temperature gradients decrease with increasing temperature while the convective flux decreases with decreasing density, convective energy transport is unimportant in the spectral range of interest.

(f) Line Blanketing

The model atmospheres of Parsons (1969) and Carbon and Gingerich (1969) include the effects of line blanketing, while those of Osmer (1972) do not. The temperature scale of Osmer's models has been reduced by the 200°K suggested by Osmer to compensate for the non-inclusion of line blanketing effects.

(g) Abundance Effects

In Chapter 4 we find that the program stars have either normal abundances or are slightly underabundant. Strom (1969) notes that for metal-to-hydrogen ratios less than the solar value, the slope of the Paschen continuum, the equivalent width of H_γ, and the Balmer discontinuity are unaffected by metal content, except through the influence of the metal-line blocking. Thus, there are no corrections to be made to the (T_{eff}, log g) values of the program stars because of abundance effects.

Part C

The Results

3.6 Absolute Values of (T_{eff}, log g) for the F-type Supergiants

In this section the absolute values of (T_{eff}, log g) for the program stars are presented. The gravities determined from observations are then compared with those calculated for stars that are cluster members using evolutionary models.

Table 3.12 gives (T_{eff}, log g) for the program stars, ϕ Cas and 89 Her, derived from $W_\gamma(0.8)$ corrected for turbulent motions, the

Table 3.12

Absolute (T_{eff}, log g) Values

Star	$W_Y(0.8)$ corrected, $[m_v(4670Å)-m_v(5470Å)]$		$([c1])$ corrected, $[m_v(4670Å)-m_v(5470Å)]$		Weighted Mean Values			
	T_{eff}	log g	T_{eff}	log g	T_{eff}	± σ	log g	± σ
φ Cas	7300	0.9	7300	1.4	7300	200	1.1	0.3
α Lep	7400	2.0	7400	1.7	7400	100	1.8	0.2
α Car	7300	1.8	7300	1.6	7300	100	1.7	0.2
δ CMa	6000	0.2	6000	0.0	6000	200	0.1	0.3
b Vel	6500	0.9	6600	1.2	6550	150	1.0	0.2
i Car	7450	1.7	7350	1.3	7400	100	1.5	0.3
ν Car	7150	1.4	7200	1.4	7150	100	1.4	0.2
195 Car	7500	0.8	7600	2.6	7550	400	0.8	0.4
HD 97534	7300	0.6	7500	2.6	7400	400	0.6	0.4
θ Sco	6600	1.8	6600	1.9	6600	100	1.8	0.2
i Sco	6700	1.3	6650	1.1	6700	200	1.2	0.2
89 Her	6800	0.6	6800	1.3	6800	200	0.9	0.4
π Sag	6650	1.8	6600	1.8	6650	100	1.8	0.2

Balmer jump index corrected for NLTE effects, and the Paschen slope index. The weighted average value of T_{eff} and log g are also given, along with the estimated errors. The gravities indicated by the Balmer jump for the most luminous stars do not agree with the gravities indicated by the H_γ line profile; for 195 Car and HD 97534 they are excessively large, considering their spectral type, and must be discounted.

The F stars that are cluster members offer a check on the log g values determined from the observations. Since the luminosity, L, stellar radius, R, and the effective temperature are related by

$$L = 4\pi R^2 \sigma T_{eff}^4 ,$$

R can be found from the L and T_{eff} values given in Table 3.13. Thus the expected gravity, g, can be computed from

$$g = GM/R^2$$

and compared with the gravity derived using the model atmospheres, if the mass is known. Following Osmer, the mass can be estimated using the equation

$$\log M/M_\odot = 0.25 - 0.132 M_{bol} ,$$

which is based on the evolutionary models of Iben (1966) for a $9M_\odot$ star, and Stothers (1966) for a $30M_\odot$ star.

The gravities determined in this manner are given in Table 3.13, along with the gravities determined from $W_\gamma(0.8)$ corrected for macroscopic motions. The data for ϕ Cas, α Per, HD 10494 and $+60^\circ 2532$, except the observed log g values, is taken from Osmer (1972). Lloyd Evans (1969) indicated an absolute magnitude of -8.0 for 195 Car and

Table 3.13

Observed and Calculated Gravities for the F-type Supergiants

Star	Observed log g[1]	Calculated log g	M_V	$M/M_\odot$
θ Cas	(1) 0.9	0.8	-8.8	27
	(2) 0.9	1.1	-7.8	19
α Per	1.6	1.8	-4.6	7
HD 10494	0.5	1.0	-7.5	17
$+60^\circ$ 2532	1.3	1.6	-4.8	8
195 Car	0.8	1.2	-8.0	18

Notes

1 The values of log g shown are those derived from $W_\gamma(0.8)$ corrected for macroscopic turbulent motions (Section 3.5(c)).

2 Searle, Sargent and Jugaku (1963) have noted that the radial velocity of φ Cas suggests that it may be closer than the cluster NGC 457, and an absolute magnitude of -7.8 may be more appropriate. Lloyd Evans (1969) has since suggested that φ Cas is a member of the cluster NGC 457.

the calculations of Parsons (1970) indicate a bolometric correction of approximately 0.1 magnitudes is appropriate for F0 to A7 Ia supergiants.

Examination of Table 3.13 shows that the observed gravities are less than the predicted ones, the discrepancy apparently increasing with decreasing gravity. This discrepancy may be due to:

(1) the inability of the theory on which the models are based to deal with the zone of pressure inversion, which is entering the region of continuum and line formation in the more luminous stars,

(2) the underestimation of the macroturbulent velocities,

(3) errors in the evolutionary tracks of Iben (1966) and Stothers (1966), which assume no mass loss, upon which the calculations of the gravities are based.

However, Sargent and Osmer (1968) suggest that the rate of mass loss from 89 Her is probably quite small ($10^{-8} M_{\odot}$/year). These stars are approximately 10^{7} years old and probably lose mass at a slower rate than 89 Her, indicating only a very small percentage of their mass will be lost during their evolution off the main sequence. Thus mass loss should not significantly affect the gravities determined from calculations based on these evolutionary models.

Another possibility is the existence of a dust cloud about some of the more luminous supergiants. According to Gillet, Hyland and Stein (1970), the shell about 89 Her may reduce the visual flux by as much as 0.5 magnitudes in this star. Assuming the existence of a similar cloud about 19 5 Car, which reduces the visual flux by 0.5 magnitudes, the calculated gravity is reduced by $\Delta \log g \simeq 0.1$, which is not sufficient to remove the discrepancy.

The above results indicate that neither the Balmer jump nor the profiles of the Balmer lines give a reliable measure of the gravity for the most luminous ($\log g \leq 1.0$) early F-type supergiants, but the observed Balmer line profiles can be reproduced by a reduction in the gravity of the model.

Chapter 4

CURVE OF GROWTH ANALYSIS OF THE PROGRAM STARS.

4.1 Introduction

In this chapter we discuss the determination of the microturbulent velocities and elemental abundances in the program stars. A fine analysis based on model atmospheres was not undertaken because the currently available programs (e.g. *Width* program of R.L. Kurucz) are not compatible with our computing facilities, and there was not sufficient time after the construction of the spectrograph and associated equipment to allow the writing of our own model atmosphere based analysis program.

Section 4.2 is concerned with a discussion of the possible theoretical models that are available for use in a coarse analysis. A brief description of the reduction program, which is based on the Wruble (1949) curve of growth, is also given.

In Section 4.3 we deal with the determination of the microturbulent velocities and the factors affecting the accuracy of these determinations. The variation of microturbulent velocity with stage of ionization and spectral type and luminosity class is considered, with special reference to the form of the depth dependence of this parameter.

The observed abundances of between 18 and 32 different species in each star are presented in Section 4.4. The Wruble curve of growth enables the determination of accurate relative abundances within a group of similar stars, and eight of the program stars are shown to have essentially the same abundances. 195 Car and HD 97534 are found to have almost identical abundances, which are possibly slightly different from the normal program stars. θ Sco and δ CMa also show

definite abundance differences with respect to the eight 'normal' stars; the most significant deviation is the apparent 1.2 dex overabundance of carbon in δ CMa relative to the sun.

Section 4.5 deals with comparisons between the apparent abundances in the Large Magellanic Cloud supergiant HD 33579, the two high latitude supergiants (89 Her and HD 161796), the variable R Coronae Borealis, and the 'normal' program stars.

4.2 Theoretical Curve of Growth

(a) Selection of Theoretical Model

In this section we discuss the selection of a theoretical curve of growth, and show that the relative turbulent velocities and abundances are largely insensitive to the choice of model. Previously, there has been no observational evidence for a choice in favour of either the Milne-Eddington (M-E) or the Schuster-Schwartzschild (S-S) approximation to the atmosphere. Observations have shown that the derived parameters differ slightly when different models are used. Wruble (1954) has noted that these differences are approximately 0.07 for log V/c (V is the most probable velocity of the atoms) and 0.25 for log $N/\rho K$, if a M-E curve is fitted to data from a S-S atmosphere. The M-E curve indicates a larger velocity and a higher abundance.

Most recent investigations of microturbulence (e.g. Abt 1957a,b, 1958, Searle, Sargent and Jugaku 1963, Bell and Rogers 1965, Bonsack and Culver 1966, Rosendhal 1970b, Rosendhal and Wegner 1970 and Osmer 1972) have used the curves of growth calculated by Wrubel (1949) for a M-E atmosphere and pure scattering. These curves are the ones that were used in this investigation, both for the estimation of microturbulence

and the abundance determinations. The Wrubel curve of growth has the ordinate and abcissa as follows:

$$\log \frac{Wc}{\lambda V} = \log W/b \quad ,$$

$$\log \eta_o = \log N_{r,s} + \log \alpha_o - \log k_\lambda \quad ,$$

where (1) W = equivalent width in $\mathring{A}$ units.

(2) V = most probable velocity of the absorbing atoms and $V^2 = \frac{2kT}{M} + \xi^2$, where ξ = microturbulent velocity in km sec^{-1}, M = atomic mass of the species.

(3) $\log N_{r,s} = \log N_r + \log g_{r,s} - \log U(T) - \theta_{exc} \chi_{r,s}$,

where N_r = number density of atoms in the r^{th} stage of ionization,

$U(T)$ = partition function (temperature dependent),

θ_{exc} = excitation temperature,

$\chi_{r,s}$ = excitation potential of the transition being studied,

and $g_{r,s}$ = statistical weight of the transition being studied.

(4) $\alpha_o = 0.015\ f\lambda/V$,

where f = Landenburg f-value or oscillator strength.

(5) k_λ = continuum absorption coefficient at wavelength $\lambda(\mathring{A})$.

An advantage of the M-E curves is that a relationship between the continuous opacity and number density of the atoms, rather than the number of atoms above the photosphere, is derived. The opacity can be more easily related to physical parameters in the star's atmosphere. Another reason for using the M-E scattering approximation to the atmosphere is that this seems more compatible with the deep lines

observed in the stars studied here.

Because the derived parameters from a curve of growth analysis such as this are dependent on the scale of absolute oscillator strengths used, and a comparison between the solar and program star abundances is to be made, the absolute oscillator strengths used in the most recent solar abundance determinations were used where possible. A list of the sources of absolute oscillator strength data is given at the end of Appendix IV. The solar abundances presented by Aller (1968) were adopted in this investigation. The values of the partition functions, atomic weights, and ionization potentials were taken from the lists of Aller (1963) and Allen (1963).

(b) The Reduction Program

A reduction program was written for the Elliot 503 computer in the Hydro-University Computing Centre. The value of B_0/B_1 for each line was calculated using the following expression (Aller 1963):

$$\frac{B_0}{B_1} = \frac{8}{3}\,\frac{k_\lambda}{\bar{k}}\,\frac{(1 - \exp(-h\nu/kT_0))}{h\nu/kT_0} \quad ,$$

where T_0 is the boundary temperature and assumed to follow the relationship $\theta_0 = \theta_{eff} + 0.14$, where $\theta_0 = 5040/T_0$; $\bar{k}$ is the mean absorption coefficient (assumed to be k at $\lambda 4500$), and k_λ is the absorption coefficient in the neighbourhood of the line. Contributions to the opacity due to H^-, H and electron scattering were included in the opacity calculations. Plots of the wavelength dependence of all possible opacity sources using the temperature, T_{rev}, and electron pressure, Pe, for the "reversing layer" showed that, in the wavelength range of interest ($3750\text{A}^{\circ} < \lambda < 5500\text{A}^{\circ}$), H^- was the dominant opacity

source in the higher-gravity stars, and H and electron scattering became dominant in the most luminous stars. The inclusion of all the other opacity sources in the program would lead to an insignificant increase (0.02 dex) in the derived abundances. Since lines covering a considerable wavelength range were used, a single value of B_0/B_1 was not valid and small corrections were made, depending on the value of B_0/B_1 at the wavelength of the line in question. The data for all stars, with the exception of π Sag, was transformed to the curve $B_0/B_1 = 2/3$ and log a = -3.0. For π Sag, a value of log a = -2.2 was found to give the best fit.

The reduction program was arranged so that, initially, a graph of the points (log W/λ, log $gf\lambda$ + C (line)) could be made, with different symbols being used for each small range of excitation potential. C (line) is a constant depending on the line, the atmospheric parameters and theoretical curve being used. The graph for each range of excitation potential was then compared with the theoretical curve, and the vertical shift required to bring them into coincidence gave a measure of log V/c.

Following Rosendhal (1970b), the thermal contribution to V was removed by using the excitation temperature as a measure of the kinetic temperature. Since the kinetic motions were less than 2 km sec^{-1} in all cases, errors in the kinetic temperature will have an insignificant effect on the derived microturbulent velocities.

The excitation temperature, θ_{exc}, can be derived from the same graphs by plotting the shift in abscissae required to make the points for each range of excitation temperature coincide against excitational potential. Using the derived values of V and θ_{exc}, the program then plotted the

composite curve of growth. The horizontal shift required to bring this curve into coincidence with the theoretical curve gives the ratio of the continuum opacity to the apparent abundance, $\bar{k}/N$.

If there are insufficient lines to derive both V and θ_{exc}, there is the facility to enable an estimated value of θ_{exc} (see Section 4.3) to be used to construct the composite curve of growth. The vertical and horizontal shifts required to bring this curve into coincidence with the theoretical curve give measures of V and the ratio k/N respectively. In cases where there were very few lines available, both V and θ_{exc} must be assumed and the ratio k/N once again derived from the horizontal shift required to make the two curves coincide. Note that in this manner the *relative* abundances can be derived without the need to know T_{rev} and Pe. Only the wavelength dependence of the continuous opacity is important in this application and this is relatively insensitive to temperature and electron pressure.

4.3 Microturbulent Velocities

(a) Introduction

The microturbulent velocities in supergiant stars of all spectral types have been the subject of many detailed studies in recent years (e.g. references given in Section 4.2(a)). The results of these investigations are:

(1) From detailed model atmosphere calculations of the mean depth of formation of the lines, it has been shown tentatively that for the F-type supergiants, the microturbulent velocity increases outwards in the region where the lines are formed.

(2) The microturbulence in the more extreme supergiants is variable over a time scale of a few days, and may be related to variations in radial velocity and hydrogen-line emission.

(3) The Fe I microturbulence in the Ia supergiants appears to increase from early to late A, reach a maximum somewhere in the range F0 to F2, then decrease to F6, increase to another maximum at G0 and then decrease rapidly to K5. The Fe II microturbulence in the Ia supergiants apparently increases from A0 to G0.

(b) Determination of Excitation Temperatures

In order to fit the observations together to form an empirical curve of growth, the excitation temperature (hereafter written as θ_{exc}I and θ_{exc}II for the neutral and ionized species respectively) must be known. For the Fe I lines, there was enough spread in the excitation potentials represented, and adequate unblended lines, to enable θ_{exc}I to be determined directly by the normal procedure. The points from the zero volt lines were found to lie above the line defined by the points from the other lines, and because of this, the zero volt lines in all species were given low weight. A similar result has been found by Searle et al (1963) in the stars they studied. We may interpret this as either an increase in microturbulence, an increase in the number density of absorbing atoms or a decrease in excitation temperature in the region where these lines are formed. The effect appears to increase with luminosity. Alternatively, it may be a spurious effect due to the inadequacy of the model used.

Fe I was the only neutral species for which θ_{exc}I could be determined in all stars, so the observed θ_{exc}I for Fe I was assumed to

apply to all the neutral species. There is some evidence to suggest that this is reasonable. In the narrow-lined stars α Car and i Car, there were sufficient suitable lines to enable the determination of θ_{exc}I for Ca I, Cr I, Mn I and Ni I; the observed θ_{exc}I for these species were in close agreement with the θ_{exc}I observed for Fe I in both stars. The adopted θ_{exc}I values are given in Table 4.1.

θ_{exc}II is sometimes assumed to be the same as that for the neutral species (e.g. Searle et al. 1963 and Rosendhal 1970b). Analysis of the Fe II and Ti II lines in α Car and i Car indicate that θ_{exc}II is less than θ_{exc}I by about 0.15 in both cases. From the relative depths of formation of the lines of neutral and ionized atoms (τ = 0.20 and τ = 0.05 respectively), one might expect from the temperature distribution in the models that θ_{exc}II is greater than θ_{exc}I by approximately 0.07. This discrepancy has been noted previously (e.g. Griffin and Griffin 1967), but the significance and reason for the observed θ_{exc}I and θ_{exc}II values is not understood.

Further trial reductions showed that by using the excitation temperature observed for the neutral species for the singly-ionized species, their microturbulent velocity would be underestimated by about 20%. There was a significant improvement in the fit to the theoretical curve when θ_{exc}II, rather than θ_{exc}I, and the 'best fit' microturbulent velocities were used. For the following stars α Lep, α Car, δ CMa, i Car, i Sco and π Sag, values of θ_{exc}II were determined from analyses of the Fe II, Ti II and V II lines. Agreement between the three results was satisfactory, although the θ_{exc}II observed for Ti II was slightly larger (0.03) than that derived from the Fe II and V II lines (Figure 4.5(b)). The same observation has been made by Rosendhal (1970b) in A-type supergiants, and attributed to differences in the

depth of formation of the lines.

For the remainder of the program stars, there were not sufficient lines of any ionized species available to enable the direct determination of θ_{exc}II, and hence an estimate of θ_{exc}II must be made. The observed data for stars of similar spectral type was used to derive a mean difference between θ_{exc}I and θ_{exc}II; the observed θ_{exc}I for the star and the mean difference was then used to estimate θ_{exc}II. The adopted values of θ_{exc}II are given in Table 4.1.

(c) Microturbulence Results

Having derived values for θ_{exc}I and θ_{exc}II, the microturbulent velocities could then be determined by the procedure outlined in Section 4.2. Only for four atomic species, Ti II, Cr II, Fe II and Fe I, were the curves of growth sufficiently well defined in all stars to permit the determination of the microturbulent velocity. As Fe I was the only neutral species for which a microturbulent velocity could be determined in all stars, the Fe I value (V_n) was assumed to apply to all the neutral species. There is some evidence to suggest that this is a reasonable assumption. For example, in the stars studied at high dispersion, with the exception of θ Sco, there were sufficient suitable lines for the determination of the microturbulent velocity for Ca I, Cr I, Ni I and, in the fine-lined stars, Ti I. These species all indicated essentially the same microturbulent velocity as the Fe lines. For the singly-ionized species, the velocity determined for Ti II was consistently slightly lower than that for Cr II and Fe II. Rosendhal (1970b) observed a similar result in the A-type Ia and Iab supergiants. The derived values of V_n and the average velocity for the singly-ionized species V_{ion} are listed in Table 4.1.

Table 4.1

Observed Curve of Growth Data for the Program Stars

Parameter \ Star	α Lep	α Car	δ CMa	b Vel	i Car	ν Car	195 Car	HD 97534	θ Sco	i Sco	π Sag†
Spectral Type	F0Ib	F0Iab	F8Ia	F2Ia	F0Iab	A9II	F0Ia	F0Ia	F0Ib	F2Ia	F2II
θ_{exc} I	0.87	0.85	0.99	0.91	0.86	0.84	0.83	0.84	0.87	0.89	0.91
θ_{exc} II	0.72	0.71	0.83	0.75	0.72	(0.73)	(0.71)	(0.72)	(0.73)	0.75	0.75
V_n (km sec^{-1})	6.5	5	11	8	4	5	9	8	8	12	5
V_{ion} (km sec^{-1})	9	6.5	14	16	7	8	17	20	10	18	7
θ_{ion} (= θ_{rev})	0.76	0.75	0.91	0.80	0.75	0.76	0.74	0.75	0.76	0.80	0.81
T_{ion} (^{o}K)	6630	6700	5440	6300	6700	6630	6800	6700	6630	6300	6220
log Pe	1.0	0.9	0.2	0.5	0.8	1.0	0.4	0.4	1.0	0.6	1.3

Notes Brackets indicate an estimated value (see Section 4.3(b))

† All the program stars were fitted to a theoretical curve with log a = -3.0, with the exception of π Sag, where a value of log a = -2.2 was found to give the best fit.

The stars for which two spectra are available indicate that the internal errors of the microturbulent velocities for the stars taken at high dispersion are about 10%. For stars taken at low dispersion, it is estimated from the scatter of the points that the internal errors could be as large as 25%. Since the microturbulent velocities observed for stars of similar spectral type studied at high and low dispersion are similar, it appears as though the observed microturbulences are dispersion independent. A comparison with published values (Table 4.2) shows that the average scatter is 15%, but there is no significant systematic difference between the present results and those of other workers.

To investigate the dependence of the observed microturbulences on spectral type and spectral class, the results of the present study have been combined with those of Bonsak (1959), Bonsak and Culver (1966), Chaffee (1970), Rosendhal (1970b) and Osmer (1972). Two criteria have been used in selecting results from the literature. We have required that the data consist of equivalent widths obtained from high-dispersion (< 10 Å mm^{-1}) spectrograms, and that the analyses must have been performed by using the same curves of growth that we have employed, so that a differential comparison is meaningful.

It should be noted that the use of different sets of lines of the same species often give rise to differences in the observed microturbulence. Osmer (1970) has suggested that this may be due to differences in the mean depth of formation of the lines. Osmer (1972) used lines in the higher wavelength range ($5000\text{Å} < \lambda < 6000\text{Å}$) for his measurements of the microturbulent velocities. However, we do not feel that this will significantly alter the qualitative trends in the microturbulence, but may cause a discontinuity in the

Table 4.2

Comparison of the Microturbulent Velocities Observed for for Neutral Atoms with the Published Values

Star	V_n (km sec^{-1})		Reference
	Present	Other	
α Lep	6.5	6.9	Abt (1958)
α Car	5	3	Greenstein (1942)
δ CMa	11	12	Bell and Rogers (1965)
		9.8	Osmer (1972)
i Sco	12	8	Abt (1960)
89 Her[1]	10	9.1	Searle, Sargent and Jugaku (1963)
HD 161796[1]	10.7	11	"

Note

1 Details of the analysis of these two stars are given in Section 4.5(c).

observed microturbulent velocities in the spectral range F2 to F4, where the change from lines in the wavelength range $3800\text{Å} < \lambda < 4900\text{Å}$ to lines in the range $5000\text{Å} < \lambda < 6000\text{Å}$ was made. This is because the blue lines are generally stronger than the lines at higher wavelengths, and are therefore formed closer to the surface. Thus the microturbulent velocities derived from blue lines are expected to be larger than those derived from lines of longer wavelengths because of the apparent increase in microturbulence towards the surface in stars of this spectral type. Chaffee (1970), in his study of microturbulence along the main sequence, changed from Fe I lines in the wavelength range $4000\text{Å} < \lambda < 4750\text{Å}$ for stars earlier than F0 to Fe I lines in the range $5000\text{Å} < \lambda < 6250\text{Å}$ for stars later than F0, so the above discussion also applies to his results.

Because the lines of V I were used in the analysis of the K and M stars, there is the same question as to whether the results for these stars should be compared with those for earlier spectral types. Analysis of several neutral species in α Car gave the same microturbulence. We were unable to include V I in this sample because of the lack of suitable lines, but the above evidence suggests that the V I microturbulence should not differ significantly from that observed for Fe I.

Because of stratification effects, the dependence of microturbulence on spectral type and class must be independently investigated for both neutral and ionized species. Figures 4.1 and 4.2 show the variation observed for the Fe I and Fe II microturbulences respectively. Both V_n and V_{ion} in the Ia supergiants increase from A2 to a maximum somewhere in the range A7 to F2, then decrease to F5, increase to G0; V_n then falls away rapidly to K5.

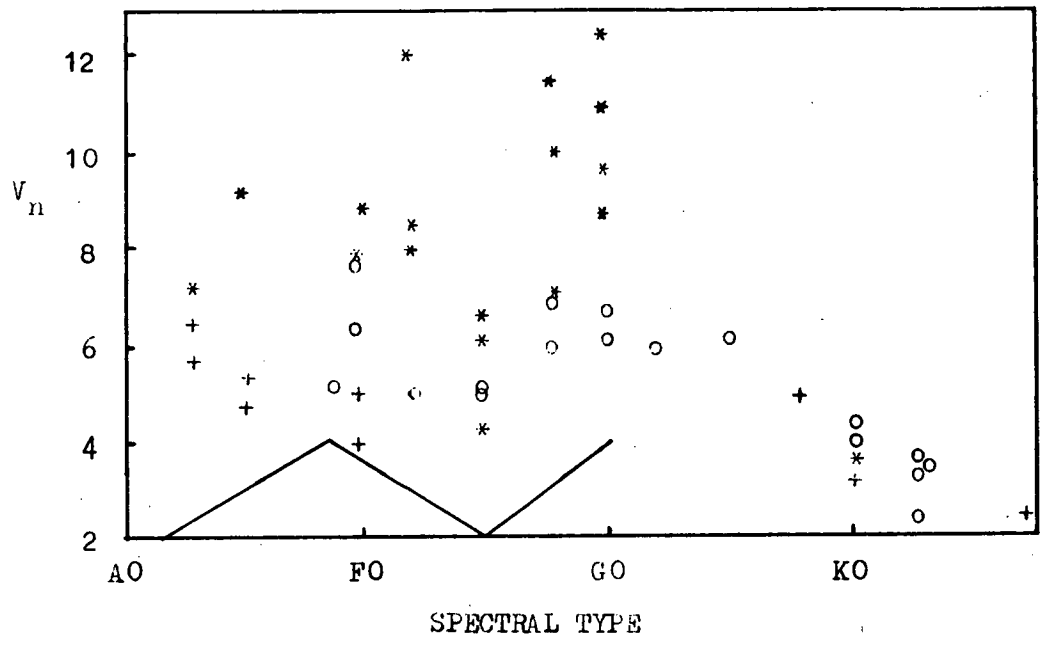

Figure 4.1 The microturbulent velocity of the neutral atoms as a function of spectral type and luminosity class.
* = Ia, + = Iab, o = Ib and II, —— main sequence.

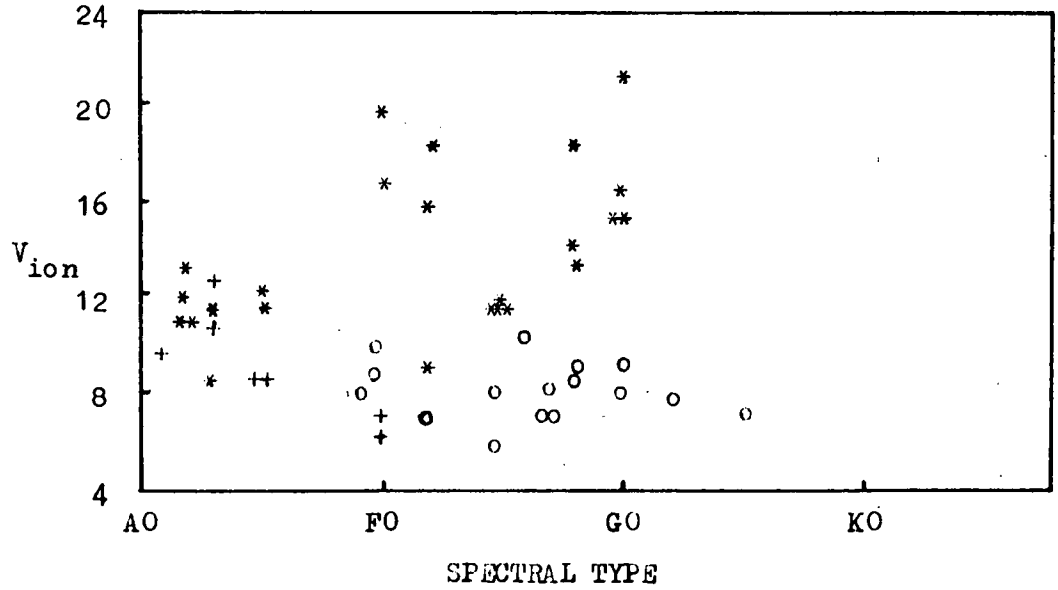

Figure 4.2 The microturbulent velocity of the ionized atoms as a function of spectral type and luminosity class.
* = Ia, + = Iab, o = Ib and II.

The peak in the Fe I microturbulence in the range A7 to F2 has not been previously observed. The observed trends in both V_n and V_{ion} are much larger than the accidental errors. A similar, but less prominent trend is observed in the Ib and type II stars. Chaffee (1970) has also observed the same variation in V_n with spectral type in the main-sequence stars (solid line, Figure 4.1). The few Iab stars studied indicate there is a rapid increase in both V_n and V_{ion} in these stars over the spectral range F0 to A0.

The Ia supergiants exhibit by far the largest microturbulent velocities for both neutral and ionized atoms. There does not appear to be any distinct separation in the mean magnitude of the microturbulent velocities for the stars in the other three spectral classes studied (Iab, Ib and II). However, the main-sequence stars show a significantly lower Fe I microturbulence than these stars.

Rosendhal and Wegner (1970) have observed variations in the microturbulence exhibited by two early A-type Ia supergiants, 6 Cas and 9 Per. They also speculated that the agent which is responsible for the microturbulence reaching a peak value in the F stars is also responsible for the variability. If this is the case, we expect large variations in the observed microturbulence in the program stars. This point has not been investigated in this study. However, this variability may account for the discrepancy in the observed microturbulence for Fe I in i Sco (Table 4.2). Abt (1957a) has suggested that all supergiants are semi-regular variables in luminosity and radial velocity. According to Rosendhal and Wegner (1970), it appears that the radial velocity variations in 6 Cas and 9 Per are correlated with variations in the microturbulence. This point deserves further investigation, particularly in the most luminous F0 supergiants

195 Car and HD 97534.

Osmer (1972) has shown that the strength of the O I λ7774 line is correlated with luminosity in the range $-4.0 > M_V > -9.0$ and the correlation appears insensitive to spectral type in the ranges A0 to A5 and F0 to G0. Osmer has also shown by model atmosphere calculations that the increase in the O I line strength with luminosity is partly due to an increase in microturbulence. The O I line is formed in the same region as the Fe II lines, thus, with the pronounced drop in the observed Fe II microturbulence at F5 in the Ia supergiants, one would expect the O I line strength to show a similar reduction at F5. Osmer's results do not preclude this because only 3 Ia stars in the range A5 to F2 were analysed and one of these was 89 Her, which, due to peculiar mass loss effects as noted in Section 4.5(c), is not a typical F2Ia star. This evidence suggests that the O I line strength may be temperature dependent within the range F0 to G0 for the most luminous stars, and will therefore have to be used cautiously as a luminosity indicator until this point is resolved.

(d) Interpretation of the Observed Trends in Microturbulence

We will now discuss the possible theoretical reasons for the observed dependence of microturbulence on spectral type and spectral class. It is shown that an extension of Chaffee's model for the depth dependence of the microturbulence in the main-sequence stars explains some, but not all, of the observed trends in the microturbulence.

Consideration of the degree of ionization of Fe in the supergiants indicates that the relative depth of formation of Fe I and Fe II lines changes with gravity. The depth of formation of a line is proportional to k_ν/ℓ_ν, the ratio of the continuous to line absorption coefficients.

In the supergiants virtually all the iron is in the form of Fe II. The number density of Fe I is proportional to the electron pressure, which varies as $g^{1/3}$ when H^- is the dominant opacity source and $g^{1/2}$ when H is the dominant opacity source. Consequently, as shown by Osmer (1972) for the supergiants in the spectral range A0 to G0,

$$\tau(\text{Fe I})/\ (\text{Fe II}) \quad \propto \quad N(\text{Fe II})/N(\text{Fe I}) \quad \propto \quad 1/g^{x},$$

where

$$1/3 \leq x \leq 1/2 \ .$$

τ(Fe I) and τ(Fe II) are the mean optical depths of formation of the Fe I and Fe II lines. N(Fe I) and N(Fe II) are the number densities of Fe I and Fe II respectively.

This implies that the Fe I lines move inward with respect to the Fe II lines as the gravity is decreased, and therefore the relative behaviour of Fe I and Fe II should change with gravity if a depth-dependent turbulence exists in the F-type supergiants. Figure 4.3 shows the variation of the ratio of the observed microturbulence for Fe II and Fe I atoms, V_{ion}/V_n. Inspection of Figure 4.3 shows that, in the spectral range F0 to G0, the ratio decreases with increasing gravity, which is consistent with a model in which the microturbulent velocity increases outwards. Figure 4.3 also shows there is an apparent inversion of the ratio exhibited by the four early A-type supergiants (i.e., V_{ion}/V_n for the Iab stars is greater than that for the Ia stars).

Chaffee (1970) has proposed a stratification model in which the microturbulence initially decreases with increasing height in the atmosphere, reaches a minimum, and then increases again, to explain the behaviour of microturbulence along the main sequence. Following

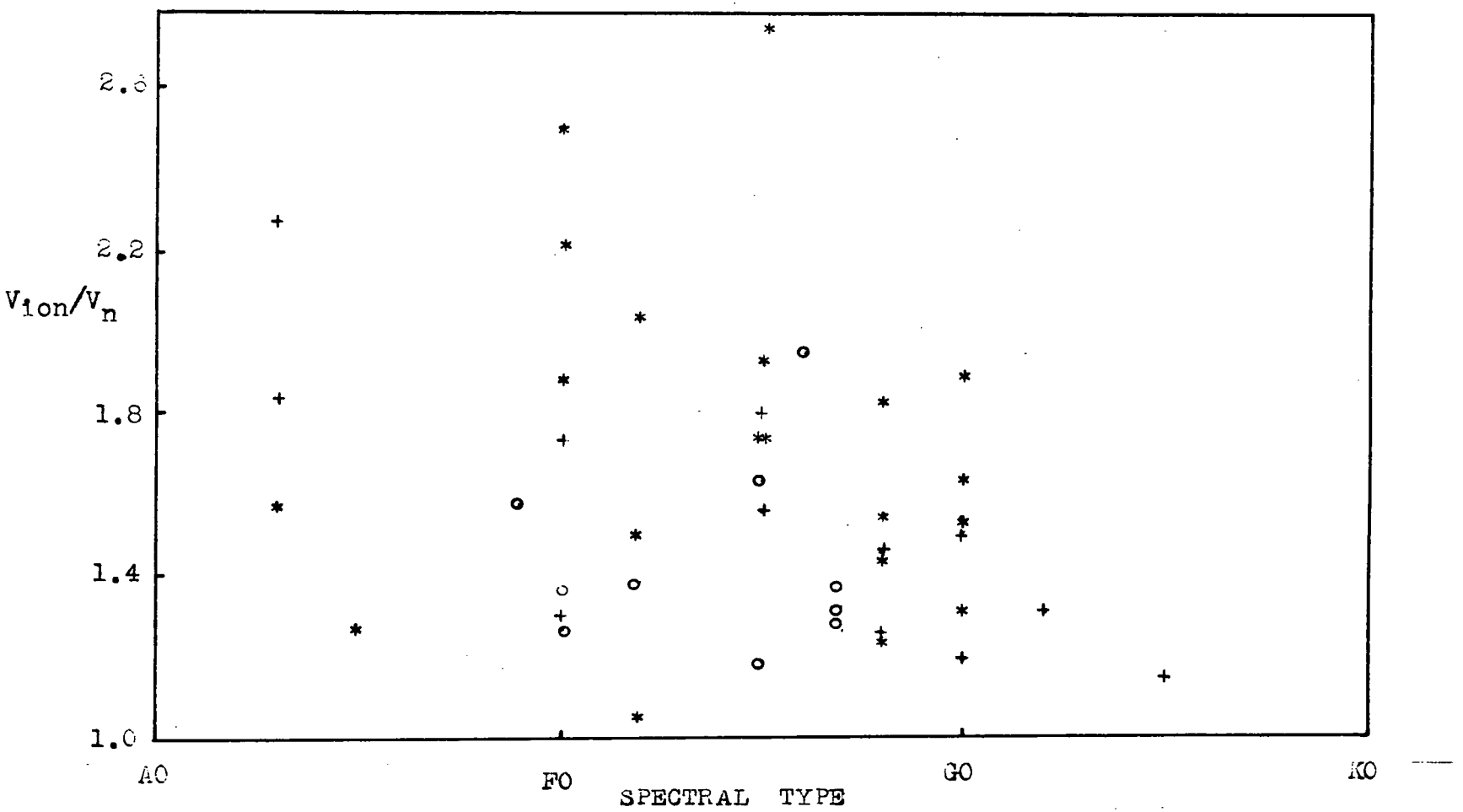

Figure 4.3 The ratio of the observed microturbulence for the ionized and neutral atoms as a function of spectral type and luminosity class.
* = Ia, + = Iab, o = Ib and II.

Rosendhal (1970b), Chaffee's argument is taken one step further by assuming that the position of the minimum is correlated with the depth of the outer convective zone, which moves towards the surface with increasing temperature and decreasing gravity. If we also assume that the shape of the profile of the velocity field remains approximately the same along the spectral sequence, then in the later spectral types we would observe regions above the velocity minimum in which the velocity increases outwards, which is consistent with the observations in the F-type stars. In the A-type supergiants, the velocity minimum should be closer to the surface than in the F-type supergiants. The reduced value of V_{ion}/V_n found for the A(2-3)Ia stars, compared with that found for the A(2-3)Iab stars, is consistent with this prediction. In the A(2-3)Iab stars, both the Fe I and Fe II lines are formed in the region above the velocity minimum, but in the Ia stars, because of their lower gravity, the minimum is shallower and the Fe II lines are formed above, and the Fe I lines below the minimum, accounting for the lower value of V_{ion}/V_n observed in the A(2-3)Ia stars.

This picture is not consistent with the drop in V_{ion} and V_n observed for the F5 stars, because this observation requires that the minimum occurs in the line-forming regions at F5. However, the minimum at F5 may be due to the change in the wavelength range from which the lines analysed were taken. The observed decrease in the ratio with decreasing temperature at a fixed gravity for the stars later than F0 is to be expected because the N(Fe I)/N(Fe II) ratio is higher, and causes the relative depth of formation of the lines of each ion to approach each other with decreasing temperature.

(e) Comments on the Determination of Microturbulent Velocities and Abundances using Model Atmospheres

To investigate the above-mentioned effects further, both detailed model atmosphere calculations of mean depths of line formation, and a further study of microturbulent velocities in A-type supergiants are required. Osmer (1972) indicated that by using his model for a F5Ia star, a microturbulent velocity of about 5 to 10 times the curve of growth value, or an overabundance of a factor of approximately 6 for iron, was required to reproduce the observed equivalent widths for the iron lines (both neutral and ionized), indicating that the models for the most luminous supergiants are not sufficiently realistic. Osmer points out that some, if not all, of this effect is due to the departure from NLTE in the lines.

Parsons (1967) has used a fairly basic model atmosphere to determine the elemental abundances in α Per (F5Ib), and apparently did not encounter the same problems as Osmer. Thus, it appears as though the less luminous supergiants can be dealt with satisfactorily with the currently available models. However Smith (1973), who studied microturbulence in main-sequence A stars, has pointed out that similar problems exist in these stars. He found that it is very difficult to determine the absolute scale of the microturbulence due to the uncertainty in the NLTE departures, the atomic parameters (oscillator strengths and damping constants), the effect of temperature stratification and the apparent dispersion-dependent errors in the equivalent-width scale.

It should be noted that a further difficulty arises when one tries to study the depth dependence of the microturbulence.

Rosendhal (1970b) has noted that the depth of formation of the Fe I lines is strongly dependent on the temperature distribution within the model atmosphere which, as shown by Carbon and Gingerich (1969), depends on the method of incorporating the line blanketing corrections.

The routines to calculate absorption line profiles and mean depths of line formation are under development at this present time, with the view to studying the depth dependence and absolute value of the microturbulence in the less luminous supergiants. Detailed analysis of the most luminous stars will have to wait until:

(1) more realistic model atmospheres that take into account some, if not all, of the dynamical effects are calculated, and

(2) more accurate high-dispersion equivalent-width and line-profile data is available.

4.4 The Abundances of the Elements

(a) Atmospheric Parameters of the 'Reversing Layer'

Having determined the (T_{eff}, log g) appropriate for each program star, this information can be used to estimate the temperature of the reversing layer, θ_{rev}. The effective temperature is the temperature of a layer with a mean optical depth $\tau \simeq 0.8$, but the lines are formed closer to the surface $\tau \simeq 0.15$, where the temperature is cooler. Using the model atmospheres available (Section 3.2), it is found that within the range of interest that $\theta_{rev} \simeq \theta_{eff} + 0.06$. The values of θ_{rev} finally adopted were the values given by the above equation weighted by up to 0.02, depending on the excitation temperatures observed.

The relative number densities of the neutral and singly-ionized

atoms of the one element can be determined from the horizontal shifts required to make the observed and theoretical curves coincide. Assuming the ionization temperature (θ_{ion}) to be equal to θ_{rev}, the electron pressure (Pe) can be determined from Saha's ionization equation using the observed relative number densities of the neutral and singly-ionized atoms. The values of log Pe determined in this manner from each element whose neutral and ionized lines were present were mostly within approximately 0.2 dex of the mean value. The values of θ_{rev} and log Pe were all reasonably consistent with the temperatures and electron pressures at a depth at $\tau \simeq 0.15$ in the appropriate model atmospheres. The finally adopted values of θ_{rev} and log Pe are given in Table 4.1.

(b) The Results

Abundances of between 18 and 32 different species, depending on the dispersion of the spectra, have been determined in each star. Having determined values of θ_{rev} and Pe, and by assuming these two parameters also control the continuous opacity, the continuous opacity can be calculated and the absolute number density of the species determined. The results of these abundance determinations are given in Table 4.3. The probable error associated with each determination depends on many parameters, and the notes to Table 4.3 give sufficient data to determine the probable error in any relative abundances. The uncertainty in the absolute abundances are very difficult to estimate. For a well-determined element such as iron, the uncertainty should not exceed 0.2 dex in the stars studied at high dispersion and 0.4 dex in the stars studied at low dispersion.

Table 4.3

Abundance Data for the Program Stars

Species	No. of Lines	Stage of Ionization			Abundance		
		I	II	III	Total	Normalized	Star - Solar
			α Lep				
H					23.6	12.0	
C I	3	20.3	*20.0*		20.4	8.8	0.2
Mg I	6	16.0	*18.7*	*15.0*	18.6	7.0	-0.3
Mg II	2		18.4				
Al I	2	13.6	*16.6*	*10.7*	16.6	5.0	-1.3
Si I	1	16.7	*18.6*				
Si II	3		19.1	*13.9*	19.0	7.4	-0.1
Ca I	14	13.9	*17.6*	*16.4*	17.6	6.0	-0.3
Ca II	2		17.6				
Sc II	12		14.8	*13.1*	14.8	3.2	0.2
Ti I	7	12.7	*16.0*				
Ti II	56		16.3	*14.0*	16.2	4.6	0.1
V I	4	12.3	*15.4*				
V II	23		15.4	*12.5*	15.4	3.8	-0.3
Cr I	21	13.7	*17.0*				
Cr II	31		16.8	*13.1*	16.9	5.3	0.1
Mn I	19	13.8	*16.5*	*12.7*	16.5	4.9	0.0
Mn II	3		16.5				
Fe I	153	15.7	*18.1*	*13.6*	18.1	6.5	-0.1
Fe II	33		18.1				
Co I	5	13.4	*15.6*	*10.9*	15.6	4.0	-0.6

Table 4.3 (cont.)

Species	No. of Lines	Stage of Ionization			Abundance		
		I	II	III	Total	Normalized	Star - Solar
			α Lep (cont.)				
Ni I	15	14.7	*16.8*	*11.1*	16.8	5.2	-0.5
Ni II	3		16.9				
Zn I	2	14.1	*15.5*	*9.7*	15.5	3.9	0.4
Sr II	2		14.1	*14.0*	14.4	2.8	-0.1
Y II	12		13.6	*12.2*	13.6	2.0	0.4
Zr II	14		14.4	*12.3*	14.4	2.8	0.2
Ba II	2		13.0	*13.4*	13.5	1.9	0.0
La II	1		13.2	*12.4*	13.3	1.7	-0.3
Ce II	19		12.9	*11.4*	12.9	1.3	-0.7
Eu II	2		11.6	*11.0*	11.7	0.1	-0.9
			α Car				
H					23.6	12.0	
C I	4	20.5	*20.1*		20.6	8.9	0.3
Na I	4	13.8	*17.9*		17.9	6.3	0.1
Mg I	8	15.6	*18.4*	*15.0*	18.4	6.8	-0.5
Mg II	2		18.4				
Al I	2	13.8	*16.9*	*11.2*	16.9	5.3	-1.0
Si I	1	16.6	*18.6*				
Si II	3		18.9	*14.0*	18.8	7.2	-0.3
Ca I	16	13.9	*17.8*	*16.7*	17.8	6.2	-0.1
Ca II	8		17.7	*16.6*			
Sc II	14		14.7	*13.1*	14.7	3.1	0.1

Table 4.3 (cont.)

Species	No. of Lines	Stage of Ionization			Abundance		
		I	II	III	Total	Normalized	Star - Solar
			α Car (cont.)				
Ti I	16	12.7	*16.1*				
Ti II	65		16.1	*14.0*	16.1	4.5	0.0
V I	4	12.1	*15.3*				
V II	27		15.3	*12.5*	15.3	3.7	-0.4
Cr I	27	13.7	*17.1*				
Cr II	33		17.0	*13.4*	17.0	5.4	0.2
Mn I	21	13.6	*16.4*	*12.7*	16.4	4.8	-0.1
Mn II	3		16.5				
Fe I	283	15.6	*18.1*				
Fe II	37		18.1	*13.8*	18.1	6.5	-0.1
Co I	5	13.3	*15.6*	*11.0*	15.6	4.0	-0.6
Ni I	44	14.5	*16.7*	*11.2*	16.7	5.1	-0.6
Ni II	3		16.7				
Zn I	3	14.5	*16.0*	*10.3*	16.0	4.4	0.9
Sr II	3		14.1	*14.1*	14.4	2.8	-0.1
Y II	18		13.8	*12.5*	13.8	2.2	0.6
Zr II	16		14.3	*12.3*	14.3	2.7	0.1
Ba II	4		13.1	*13.6*	13.7	2.1	0.2
La II	4		13.1	*12.4*	13.2	1.6	-0.4
Ce II	22		12.9	*11.5*	12.9	1.3	-0.7
Eu II	2		11.0	*10.5*	11.2	-0.4	-1.4
Gd II	2		10.9	*9.8*	10.9	-0.7	-1.8

Table 4.3 (cont.)

Species	No. of Lines	Stage of Ionization			Abundance		
		I	II	III	Total	Normalized	Star - Solar
			δ CMa				
H					23.6	12.0	
C I	3	21.3	*20.1*		21.4	9.8	1.2
Mg I	6	16.8	*19.2*	*14.0*	19.0	7.4	0.1
Mg II	2		18.5				
Al I	2	13.6	*16.5*	*8.7*	16.5	4.9	-1.4
Si I	1	17.4	*18.9*				
Si II	3		18.9	*12.2*	18.9	7.3	-0.2
Ca I	13	13.8	*17.4*	*15.1*	17.4	5.8	-0.5
Ca II	2		17.5				
Sc II	10		14.8	*12.0*	14.8	3.2	0.2
Ti I	4	12.9	*16.0*				
Ti II	44		16.4	*12.9*	16.3	4.7	0.2
V I	3	12.3	*15.2*				
V II	16		15.6	*11.3*	15.5	3.9	-0.2
Cr I	19	14.0	*17.2*				
Cr II	25		17.2	*11.8*	17.2	5.6	0.4
Mn I	20	14.0	*16.5*	*11.1*	16.5	4.9	0.0
Fe I	109	16.1	*18.2*	*12.1*	18.2	6.6	0.0
Fe II	29		18.2				
Co I	4	14.0	*15.9*	*9.7*	15.9	4.3	-0.3
Ni I	12	14.9	*16.8*	*9.3*	16.9	5.3	-0.4
Ni II	3		17.0				
Zn I	3	14.8	*15.7*	*8.0*	15.7	4.1	0.6

Table 4.3 (cont.)

Species	No. of Lines	Stage of Ionization			Abundance		
		I	II	III	Total	Normalized	Star - Solar
			δ CMa (cont.)				
Sr II	2		14.8	*13.8*	14.8	3.2	0.3
Y II	2		13.6	*11.1*	13.6	2.0	0.4
Zr II	9		14.6	*11.3*	14.6	3.0	0.4
Ba II	3		13.8	*13.3*	13.9	2.3	0.6
La II	3		13.9	*12.2*	13.9	2.3	0.3
Ce II	15		13.4	*10.8*	13.4	1.8	-0.2
			i Car				
H					23.6	12.0	
C I	3	20.1	*19.8*		20.2	8.6	0.0
Mg I	6	15.6	*18.5*	*15.2*	18.5	6.9	-0.2
Mg II	2		18.5				
Al I	2	13.6	*16.8*	*11.2*	16.8	5.2	-1.1
Si I	1	16.2	*18.3*				
Si II	3		18.5	*13.7*	18.4	6.8	-0.7
Ca I	14	13.5	*17.4*	*16.4*	17.4	5.8	-0.5
Ca II	2		17.6				
Sc II	12		14.5	*13.0*	14.5	2.9	-0.1
Ti I	9	12.4	*15.9*				
Ti II	52		15.9	*13.9*	15.9	4.3	-0.2
V I	4	12.3	*15.5*				
V II	25		15.2	*12.5*	15.2	3.6	-0.5

Table 4.3 (cont.)

Species	No. of Lines	Stage of Ionization			Abundance		
		I	II	III	Total	Normalized	Star - Solar
			i Car (cont.)				
Cr I	22	13.3	*16.8*				
Cr II	32		16.8	*13.7*	16.8	5.2	0.0
Mn I	21	13.4	*16.3*				
Mn II	3		16.4	*12.8*	16.4	4.8	-0.1
Fe I	192	15.5	*18.1*				
Fe II	36		18.2	*14.0*	18.1	6.5	-0.1
Co I	6	13.1	*15.5*	*11.0*	15.5	3.9	-0.7
Ni I	24	14.4	*16.7*	*11.3*	16.6	5.0	-0.7
Ni II	3		16.4				
Zn I	2	13.9	*15.5*	*9.9*	15.5	3.9	0.4
Sr II	3		14.0	*14.1*	14.4	2.8	-0.1
Y II	12		13.2	*12.0*	13.2	1.6	0.0
Zr II	15		14.2	*12.3*	14.2	2.6	0.0
Ba II	4		13.0	*13.6*	13.7	2.1	0.2
La II	3		13.0	*12.4*	13.1	1.5	-0.5
Ce II	20		12.4	*11.2*	12.4	0.8	-1.2
Eu II	2		11.0	*10.6*	11.1	-0.5	-1.5
Gd II	2		10.4	*9.4*	10.4	-1.2	-2.3
			i Sco				
H					23.6	12.0	
C I	3	20.3	*19.8*		20.4	8.8	0.2
Mg I	9	16.0	*18.8*	*15.0*	18.6	7.0	-0.3
Mg II	2		18.0				
Al I	2	13.8	*16.9*	*10.9*	16.9	5.3	-1.0

Table 4.3 (cont.)

Species	No. of Lines	Stage of Ionization			Abundance		
		I	II	III	Total	Normalized	Star - Solar
			i Sco (cont.)				
Si I	1	16.8	*18.7*				
Si II	3		18.5	*13.3*	18.5	6.9	-0.6
Ca I	11	13.7	*17.5*	*16.4*	17.6	6.0	-0.3
Ca II	2		18.1				
Sc II	12		14.7	*13.0*	14.7	3.1	0.1
Ti I	5	12.4	*15.8*				
Ti II	41		16.1	*13.8*	16.0	4.4	-0.1
V II	15		15.3	*12.3*	15.3	3.7	-0.4
Cr I	14	13.4	*16.8*				
Cr II	20		17.1	*13.2*	17.0	5.4	0.2
Mn I	10	13.3	*16.1*	*12.2*	16.1	4.5	-0.4
Fe I	107	15.6	*18.1*	*15.6*	18.1	6.5	-0.1
Fe II	27		18.1				
Co I	3	13.1	*15.4*	*10.5*	15.4	3.8	-0.8
Ni I	12	14.6	*16.8*	*11.0*	16.7	5.1	-0.6
Ni II	3		16.5				
Zn I	2	14.6	*16.1*	*10.8*	16.1	4.5	1.0
Sr II	2		14.9	*14.8*	15.1	3.5	0.7
Y II	9		13.8	*12.4*	13.8	2.2	0.6
Zr II	9		14.6	*12.4*	14.6	3.0	0.4
Ba II	2		12.8	*13.2*	13.3	1.7	-0.3
La II	4		13.1	*12.4*	13.2	1.6	-0.4
Eu II	2		10.9	*10.4*	11.0	-0.6	-1.6

Table 4.3 (cont.)

Species	No. of Lines	Stage of Ionization			Abundance		
		I	II	III	Total	Normalized	Star - Solar
			π Sag				
H					23.6	12.0	
C I	3	20.6	*19.5*		20.6	9.0	0.4
Mg I	10	16.3	*18.4*	*14.1*	18.4	6.8	-0.5
Mg II	2		18.4				
Al I	2	14.7	*17.1*	*10.4*	17.1	5.5	-0.8
Si I	1	17.4	*18.6*				
Si II	3		18.6	*12.8*	18.6	7.0	-0.5
Ca I	8	14.6	*17.7*	*15.8*	17.7	6.1	-0.2
Ca II	2		17.6				
Sc II	10		14.6	*12.2*	14.6	3.0	0.0
Ti I	6	13.4	*16.1*				
Ti II	41		16.0	*13.1*	16.0	4.4	-0.1
V II	7		15.3	*11.7*	15.3	3.7	-0.4
Cr I	11	14.1	*16.8*	*12.4*	16.9	5.3	0.1
Cr II	22		17.0				
Mn I	9	14.6	*16.7*	*12.1*	16.7	5.1	0.2
Fe I	79	16.4	*18.2*	*12.9*	18.2	6.6	0.0
Fe II	26		18.2				
Co I	4	13.9	*15.5*	*11.0*	15.5	3.9	-0.7
Ni I	10	15.5	*17.0*	*10.6*	17.0	5.4	-0.3
Ni II	3		16.9				
Sr II	2		14.7	*13.9*	14.7	3.1	0.2
Y II	5		13.8	*11.7*	13.8	2.2	0.7
Zr II	5		14.3	*11.5*	14.3	2.7	0.1
Ba II	2		13.3	*13.1*	13.5	1.9	0.0

Table 4.3 (cont.)

Species	No. of lines	Stage of Ionization			Abundance		
		I	II	III	Total	Normalized	Star - Solar
			b Vel				
H					23.6	12.0	
Mg I	4	15.4	*18.4*	*15.1*	18.3	6.7	-0.6
Mg II	2		18.1				
Al I	2	13.5	*16.8*	*11.1*	16.8	5.2	-1.1
Si II	3		18.8	*13.9*	18.8	7.2	-0.3
Ca I	8	13.3	*17.3*	*16.3*	17.3	5.7	-0.6
Ca II	2		17.2				
Sc II	8		14.6	*13.1*	14.6	3.0	0.0
Ti II	38		16.1	*14.1*	16.1	4.5	0.0
V II	11		15.3	*12.6*	15.3	3.7	-0.4
Cr I	5	13.1	*16.8*	*13.1*	17.0	5.4	0.2
Cr II	22		17.1				
Mn I	5	13.5	*16.5*	*12.9*	16.5	4.9	0.0
Fe I	35	15.4	*18.1*	*13.8*	18.1	6.5	-0.1
Fe II	25		18.1				
Ni II	2		16.6	*11.2*	16.6	5.0	-0.7
Sr II	2		14.0	*14.1*	14.4	2.8	-0.1
Y II	4		13.8	*12.4*	13.8	2.2	0.6
Zr II	6		14.2	*12.3*	14.2	2.6	0.0
Ba II	1		12.6	*13.2*	13.3	1.7	-0.2

Table 4.3 (cont.)

Species	No. of Lines	Stage of Ionization			Abundance		
		I	II	III	Total	Normalized	Star - Solar
			ν Car				
H					23.6	12.0	
Mg I	4	15.6	*18.5*	*14.9*	18.5	6.9	-0.4
Mg II	2		18.5				
Al I	2	13.4	*16.4*	*10.5*	16.4	4.8	-1.5
Si I	1	16.8	*18.9*				
Si II	3		18.9	*13.8*	18.9	7.3	-0.2
Ca I	8	13.9	*17.8*	*16.5*	17.9	6.3	0.0
Ca II	2		18.0				
Sc II	10		14.9	*13.1*	14.9	3.3	0.3
Ti II	37		16.0	*14.0*	16.0	4.4	-0.1
V II	10		15.3	*12.3*	15.3	3.7	-0.4
Cr I	6	13.7	*17.2*				
Cr II	22		17.2	*13.3*	17.2	5.6	0.4
Mn I	6	13.3	*16.2*	*12.3*	16.2	4.6	-0.3
Fe I	38	15.4	*18.0*				
Fe II	24		18.1	*13.7*	18.1	6.5	-0.1
Ni II	2		16.9	*11.2*	16.9	5.3	-0.4
Sr II	2		13.8	*13.6*	14.0	2.4	-0.5
Y II	4		13.9	*12.4*	13.9	2.3	0.7
Zr II	5		14.3	*12.1*	14.3	2.7	0.0
Ba II	1		12.2	*12.0*	12.4	0.8	-1.1
La II	1		13.1	*12.2*	13.1	1.5	-0.5

Table 4.3 (cont.)

Species	No. of Lines	Stage of Ionization			Abundance		
		I	II	III	Total	Normalized	Star - Solar
			195 Car				
H					23.6	12.0	
Mg I	1	15.1	*18.7*	*16.0*	18.5	6.9	-0.4
Mg II	2		18.3				
Al I	2	13.3	*17.2*	*12.3*	17.2	5.6	-0.7
Si II	3		18.8	*16.0*	18.8	7.2	-0.3
Ca I	8	13.2	*17.8*	*17.5*	18.0	6.4	0.1
Ca II	2		16.6				
Sc II	8		14.5	*13.7*	14.5	2.9	-0.1
Ti II	37		15.7	*14.4*	15.7	4.1	-0.4
V II	9		15.2	*13.2*	15.2	3.6	-0.1
Cr I	2	13.0	*17.1*				
Cr II	17		17.1	*14.3*	17.1	5.5	0.3
Mn I	4	12.5	*16.1*	*13.2*	16.1	4.5	-0.4
Fe I	31	14.9	*18.2*	*14.7*	18.2	6.6	0.0
Fe II	25		18.3	*14.8*			
Ni II	2		16.4	*11.6*	16.4	4.8	-0.9
Sr II	2		13.2	*14.0*	14.0	2.4	-0.5
Zr II	4		13.8	*12.6*	13.8	2.2	-0.4
Ba II	1		12.1	*13.4*	13.4	1.8	-0.1

Table 4.3 (cont.)

Species	No. of Lines	Stage of Ionization			Abundance		
		I	II	III	Total	Normalized	Star - Solar
			HD 97534				
H					23.6	12.0	
Mg I	1	15.2	*18.8*				
Mg II	2		18.4	*15.6*	18.6	7.0	-0.3
Al I	2	13.1	*16.9*	*11.8*	16.9	5.3	-1.0
Si II	3		18.9	*16.2*	18.9	7.3	-0.2
Ca I	8	13.5	*17.9*	*17.7*	18.0	6.4	0.1
Ca II	2		16.7				
Sc II	9		14.5	*13.6*	14.5	2.9	-0.1
Ti II	39		15.7	*14.3*	15.7	4.1	-0.4
V II	8		14.9	*12.8*	14.9	3.3	-0.4
Cr I	2	13.0	*17.1*				
Cr II	17		17.0	*14.1*	17.0	5.4	0.2
Mn I	4	12.6	*16.1*	*13.1*	16.1	4.5	-0.4
Fe I	34	14.8	*18.0*				
Fe II	25		18.1	*14.5*	18.1	6.5	-0.1
Ni II	2		16.4	*11.6*	16.4	4.8	-0.9
Sr II	2		13.0	*13.7*	13.8	2.2	-0.7
Zr II	5		13.8	*12.5*	13.8	2.2	-0.4
Ba II	1		11.6	*12.8*	12.8	1.2	-0.7
La II	1		13.2	*13.3*	13.6	2.0	0.0

Table 4.3 (cont.)

Species	No. of Lines	Stage of Ionization			Abundance		
		I	II	III	Total	Normalized	Star - Solar
			θ Sco				
H					23.6	12.0	
Na I	4	14.3	*18.2*		18.2	6.6	0.4
Mg I	8	16.8	*19.3*	*15.9*	19.3	7.7	0.4
Mg II	2		19.5				
Al I	2	14.7	*17.5*	*11.6*	17.5	5.9	-0.4
Si I	1	18.3	*19.9*	*14.8*			
Si II	3		19.5	*14.3*	19.5	7.9	0.4
Ca I	2	14.8	*18.3*	*17.0*	18.2	6.6	0.2
Ca II	2		18.1				
Sc II	7		14.8	*13.0*	14.8	3.2	0.2
Ti II	18		16.1	*13.9*	16.1	4.5	0.0
V II	4		15.4	*12.4*	15.4	3.8	-0.3
Cr II	9		16.8	*12.9*	16.8	5.2	0.0
Fe I	38	15.9	*18.1*	*13.4*	18.1	6.5	-0.1
Fe II	15		18.1				
Ni II	2		16.5	*10.7*	16.5	4.9	-0.8
Sr II	1		14.1	*13.8*	14.3	2.7	-0.2
Y II	5		14.0	*12.5*	14.0	2.4	0.8
Zr II	3		14.1	*11.9*	14.1	2.5	-0.1
Ba II	1		12.5	*12.8*	13.0	1.4	-0.3
La II	1		13.5	*12.6*	13.5	1.9	-0.1

Notes to Table 4.3

(1) Column 2 gives the number of different lines used. For the stars photographed at high dispersion (α Lep, α Car, δ CMa, ι Car, i Sco and π Sag), many of the lines have been measured on two or more plates and the average equivalent width, weighted for plate quality, has been used in the abundance determination.

(2) The abundances are given on a logarithmic scale, i.e., the number in columns 3 to 7 refer to the logarithm of the number density of the respective species.

(3) The numbers in italics in columns 4 and 5 have been determined using the Saha ionization equation and the θ_{ion} and log Pe values listed in Table 4.1.

(4) The normalized abundances are given on the scale of log N(H) = 12.00, where N(H) is the number density of hydrogen.

(5) The suggested solar abundances as given by Aller (1968) have been used to calculate the differences between the stellar and solar abundances (column 8).

(6) The uncertainties quoted below reflect the uncertainties indicated by the scatter of the points about the theoretical curve along the abscissa (i.e., abundance axis). These errors reflect errors in the equivalent width measurements and the internal errors in the oscillator strengths. They do not include systematic errors that may be introduced through errors in the calculation of the continuous opacity or the absolute scale of the oscillator strengths used.

High-Dispersion Stars

No. of lines analysed	> 50	20 - 50	8 - 20	< 8
Uncertainty in log $N(X)$	0.1	0.15	0.2	0.4*

Low-Dispersion Stars

No. of lines analysed	> 30	15 - 30	8 - 15	< 8
Uncertainty in log $N(X)$	0.15	0.2	0.3	0.4*

* In this case it is extremely difficult to estimate the error, as the apparent abundance may be strongly dependent on the particular line analysed.

(7) Although θ Sco was observed at high dispersion, its abundances are known with less certainty than those of the low-dispersion stars because of its high rotational velocity.

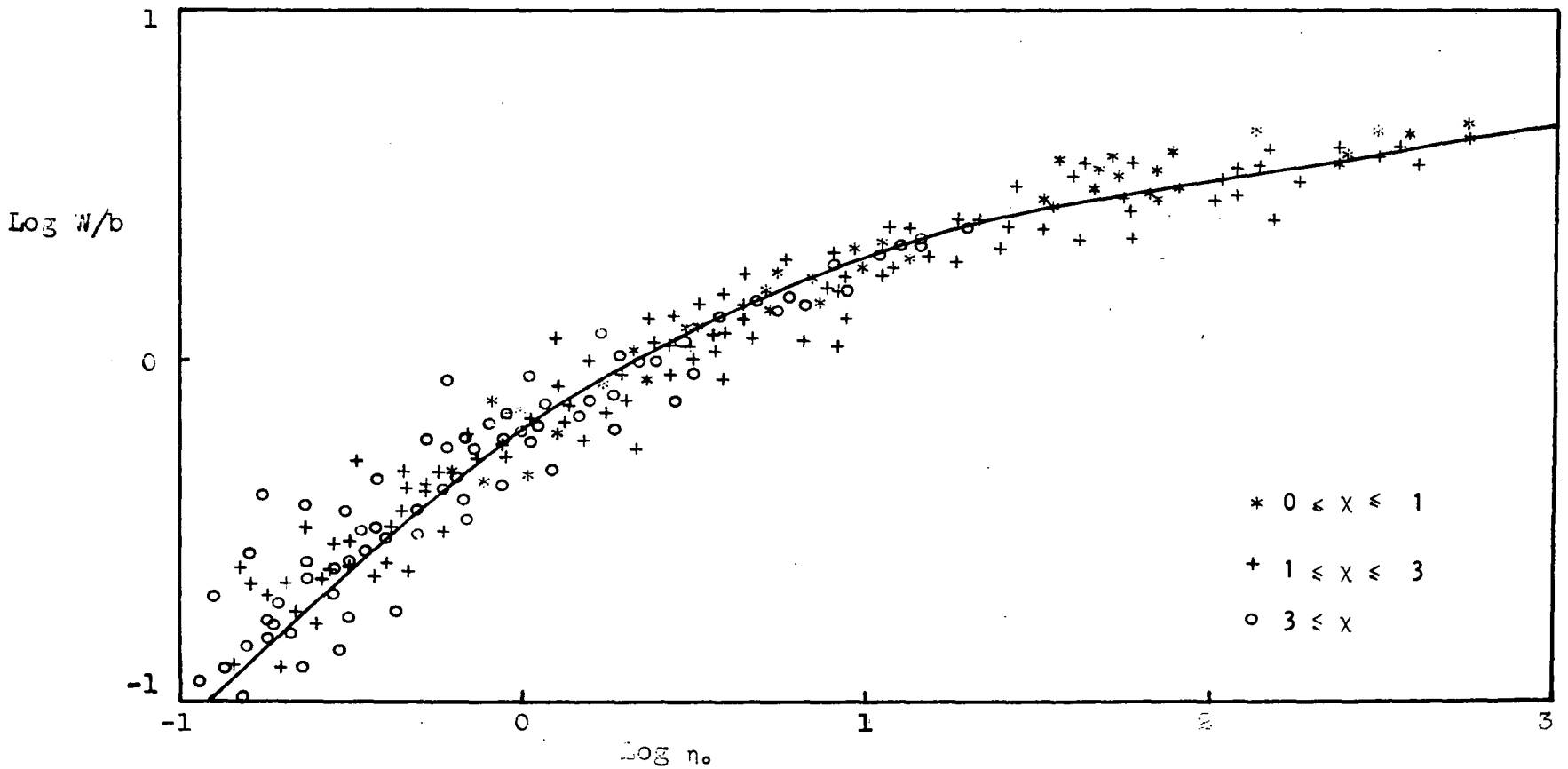

Figure 4.4a Curve of growth for Fe I in α Car. The solid curve is Wruble's curve of growth for the Milne-Eddington model with $B_0/B_1 = 2/3$ and log a = -3.0.

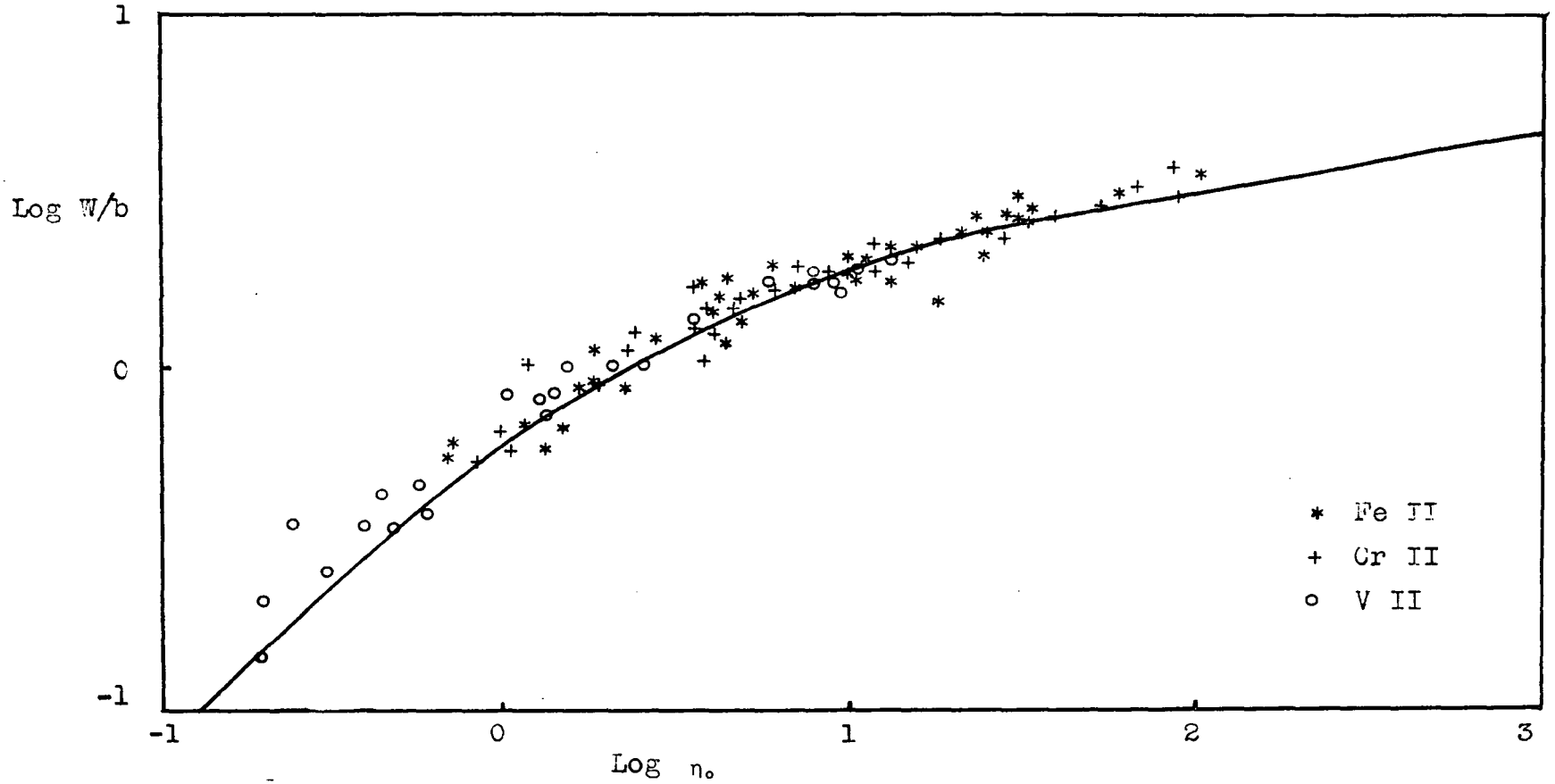

Figure 4.4b Curve of growth for Fe II, Cr II and V II in α Car.

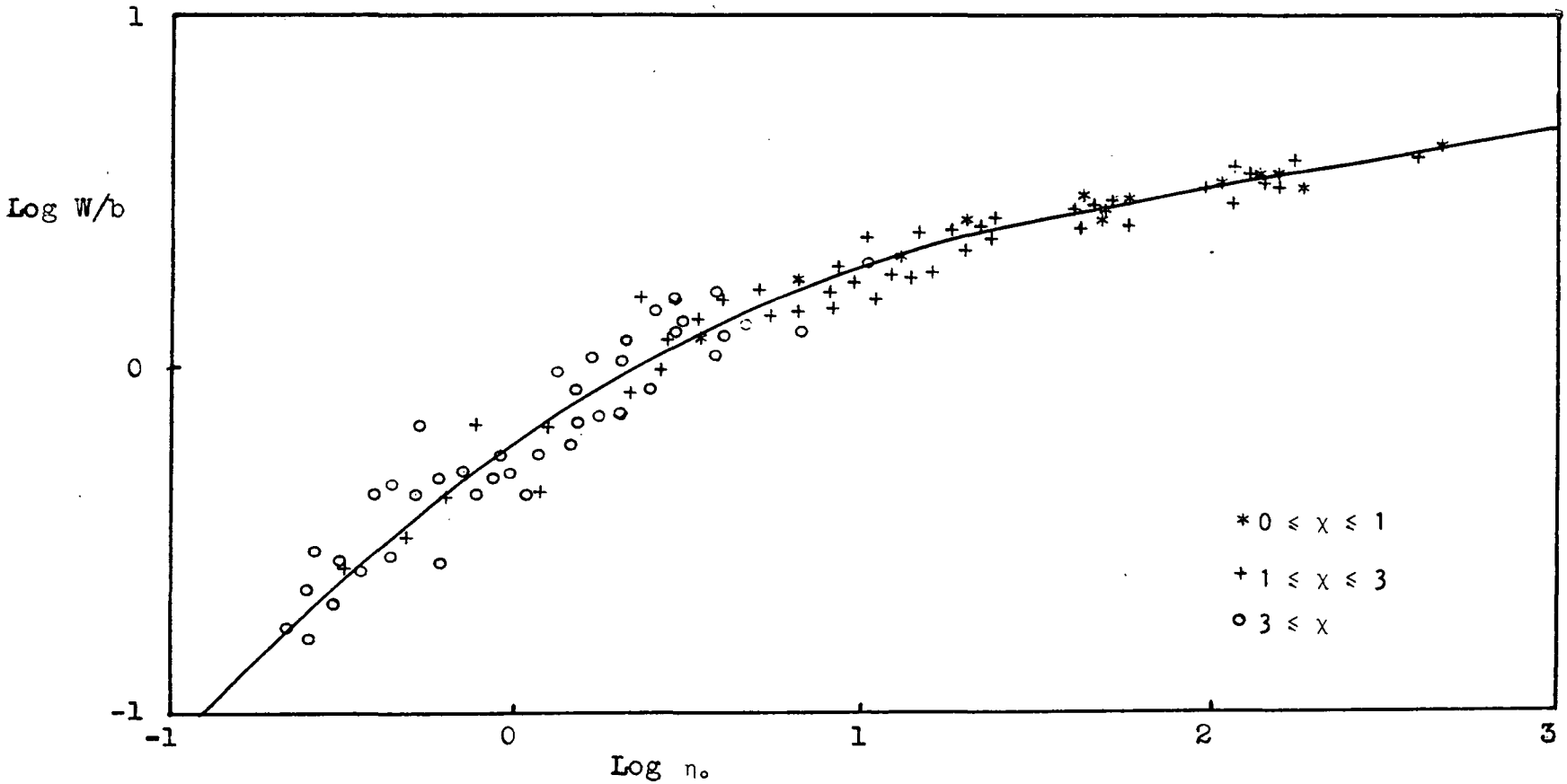

Figure 4.4c Curve of growth for Fe I in i Sco.

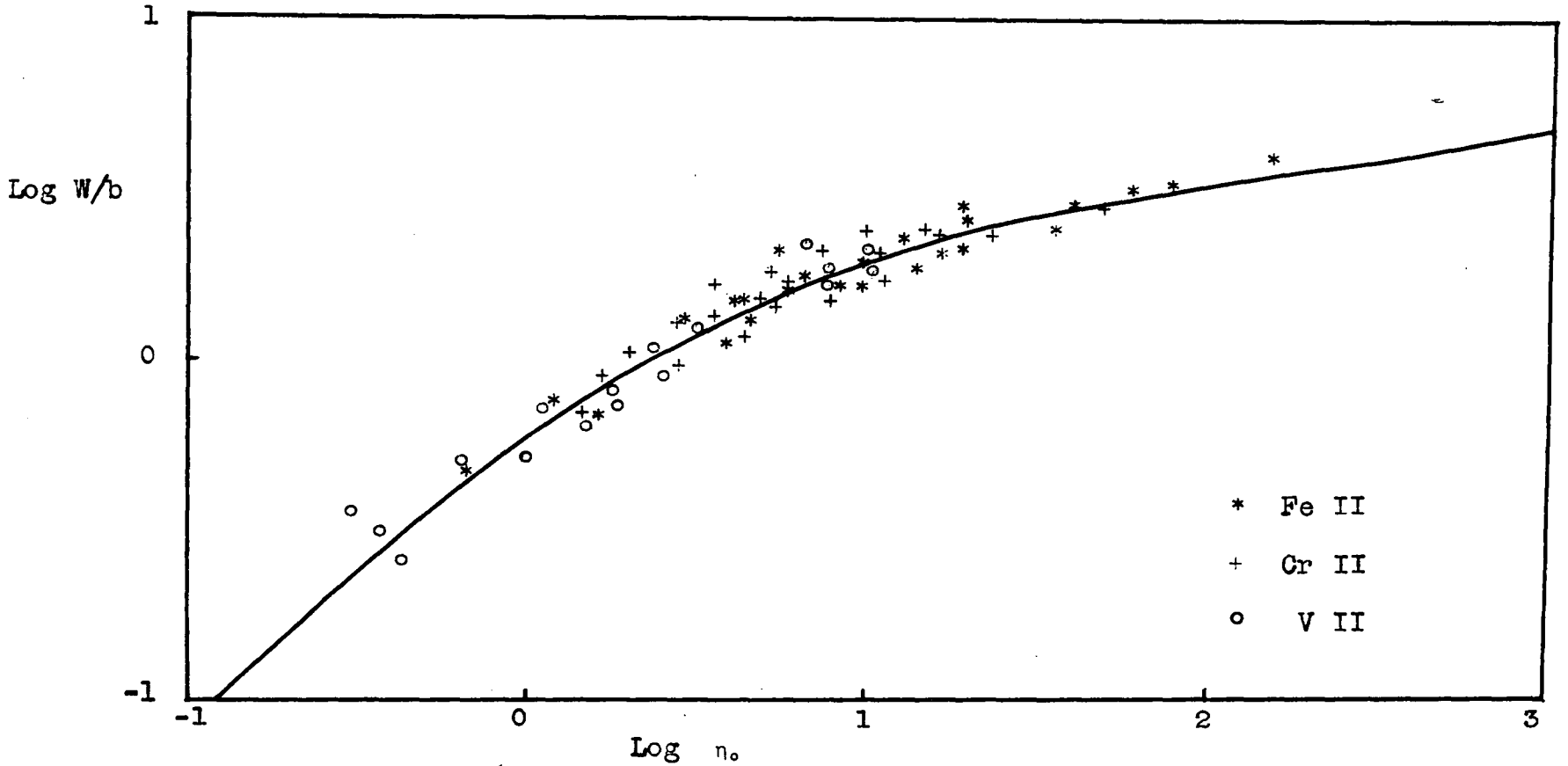

Figure 4.4d Curve of growth for Fe II, Cr II and V II in i Sco.

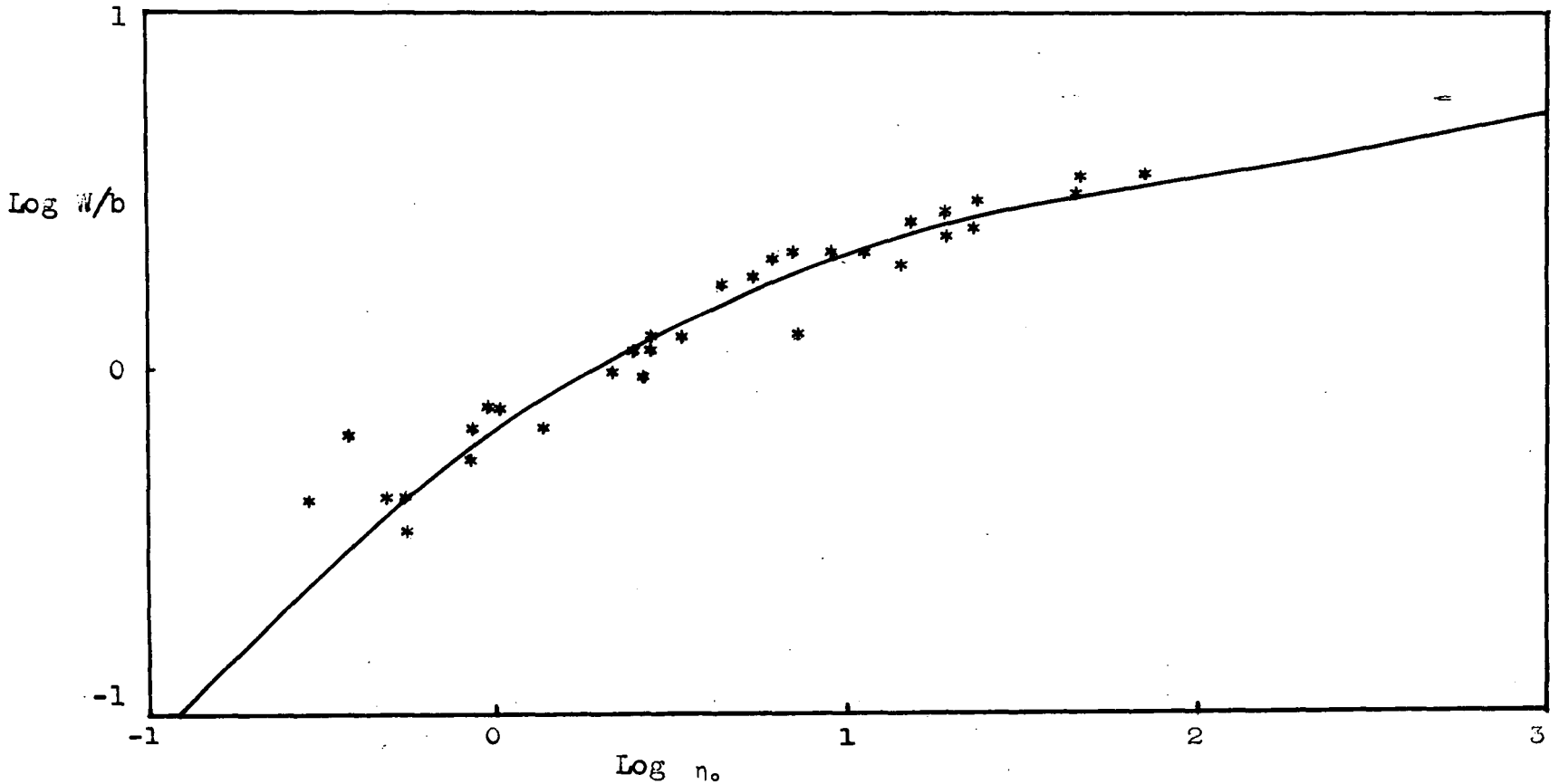

Figure 4.4e Curve of growth for Fe I in HD 97534.

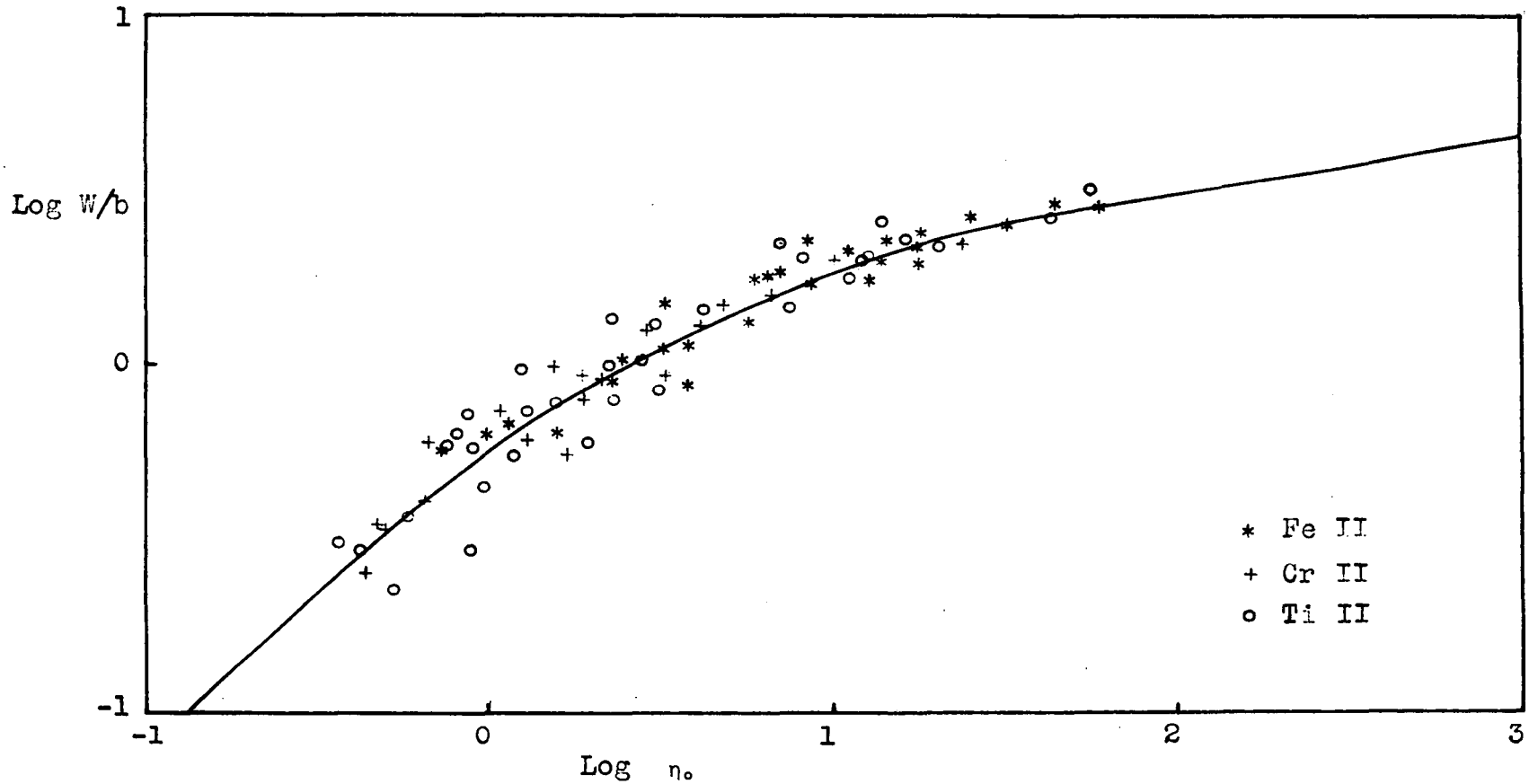

Figure 4.4f Curve of growth for Fe II, Cr II and Ti II in HD 97534.

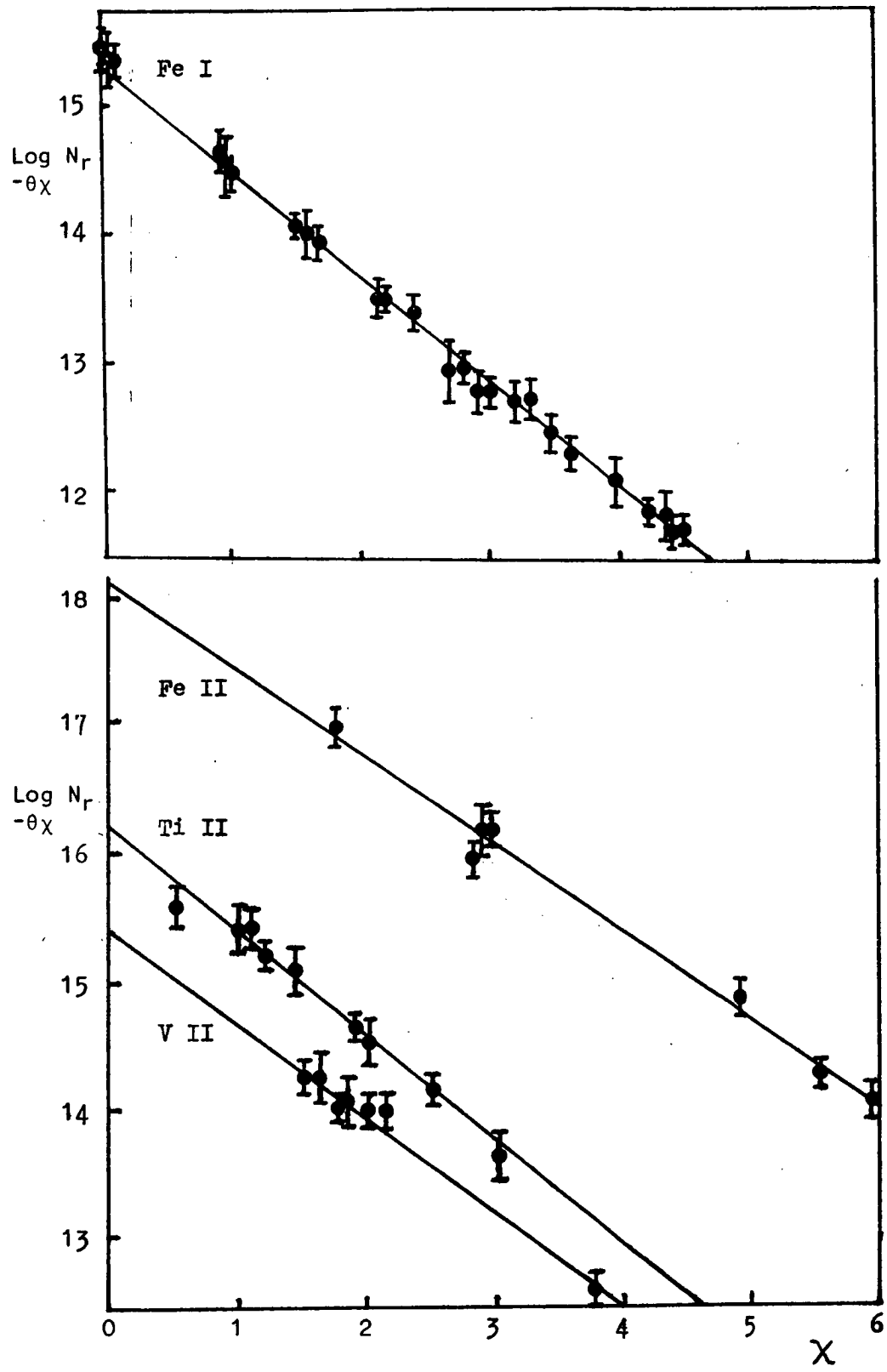

Figures 4.5(a) & (b) $\log N_r - \theta\chi$ as a function of excitation potential (χ) for Fe I, and V II, Ti II and Fe II in α Car.

The main difficulty with the stars studied at low dispersion is the crowding of the lines, making it difficult to place the continuum, and many of the lines that were useful at high dispersion are now strongly blended and unusable. Also some species, namely Ni I, Ti I, Y II and Ce II, that were represented by up to 20 measurable lines at high dispersion, have no measurable lines at low dispersion because their lines are very weak and are not discernable above the plate noise at the lower dispersion.

Figures 4.4(a-f) show the observed curves of growth for Fe I and composite curves for the well-represented singly ionized species in α Car, i Sco and HD 97534. Figures 4.5(a) and (b) show the plots of $\log N_{rs} - \theta\chi$ against χ for Fe I and the singly-ionized species for which θ_{exc}II was measurable in α Car.

(c) Discussion of Individual Elements

In the following subsections, carbon through to gadolinium, we discuss the lines used, the accuracy of, and particular problems associated with, the determination of the abundance of each element. Several terms which will be used in the following discussion are now defined:

(1) By low-dispersion stars we mean the stars observed at 9 $\mathring{A}\ mm^{-1}$ (b Vel, α Car, 19 Car and HD 97534) and θ Sco, which was observed at 2.1 $\mathring{A}\ mm^{-1}$, but because of its high rotational velocity, the effective resolution of the stellar spectrum was worse than on the 9 $\mathring{A}\ mm^{-1}$ plates.

(2) High-dispersion stars refer to the stars observed at 2.1 $\mathring{A}\ mm^{-1}$, with the exception of θ Sco, i.e., α Lep, α Car, δ CMa, i Car, i Sco and π Sag.

(3) By rms scatter is meant the root mean square scatter about the theoretical curve of the observed points along the abcissa (i.e., abundance axis).

(4) By underabundance and overabundance we are referring to the apparent stellar abundances compared with the suggested solar abundances given by Aller (1968).

Carbon

Carbon was represented by three weak lines, λλ4770, 4772 and 4776 which were measurable in all the high-dispersion stars; none of these lines were measurable in the low-dispersion stars. The derived abundance depends strongly on θ_{exc}I because of the high excitation potential of these lines. The observed carbon abundance in all stars, with the exception of δ CMa, was in the range log N(C) = 8.8 ± 0,2, which is within the experimental error of the solar abundance of log N(C) = 8.6. The observed apparent overabundance in δ CMa (+ 1.0 dex with respect to the mean of the observed abundances in the other program stars) indicates that δ CMa is significantly overabundant in carbon.

Sodium

The sodium abundance can be determined from the D lines, but the derived abundance depends strongly on the damping constant chosen. Plates covering the appropriate wavelength range were only available for θ Sco. The D lines and two weaker lines, λ5683 and λ5688, were measured in θ Sco; these two pairs of lines gave an abundance of log N(Na) = 6.6 ± 0.1, which indicates an apparent overabundance of 0.4 dex. There are four very weak sodium lines in the blue region

of the spectrum, but these were only measurable with sufficient accuracy to justify analysis in α Car. The observed apparent abundance in α Car was log N(Na) = 6.3 ± 0.2, which is essentially the solar abundance.

Magnesium

Lines of both Mg I and Mg II were present and measurable in all the program stars. The usable lines of Mg I in the high-dispersion stars showed very little scatter about the mean curve of growth, and gave an abundance with an internal standard deviation of typically 0.24 dex. Two lines of Mg II were present, λ4481.13 and λ4481.34, but on the majority of stars only their combined equivalent width could be measured.

In α Car and i Car, the two narrow-lined stars, these two lines were partially resolved and their individual equivalent widths could be measured. The equivalent widths were adjusted to take into account the effective lowering of the continuum due to the presence of the other line, making use of the curves published by Moore, Minnaert and Houtgast (1966).

In the cases where the two lines were not resolved, the two methods used to determine the Mg II abundance were:

(i) use the observed equivalent width of the blend and the sum of the oscillator strengths, or

(ii) use the observed ratio of the equivalent widths in α Car and i Car to split the equivalent width of the blend, and correct the resultant equivalent widths for the apparent depression of the continuum.

The two methods gave essentially the same abundance, and the mean of the

two values was adopted. In all stars the magnesium abundance derived from both Mg I and Mg II was in agreement to within the anticipated errors.

All the program stars showed an apparent underabundance in the range 0.4 ± 0.2 dex, with the exceptions of θ Sco, which showed an apparent overabundance of 0.4 dex, and δ CMa, which showed a normal abundance.

Apparent underabundances in magnesium of 0.2 and 0.3 dex with respect to the sun have been found in α Cygni and HD 33579 respectively (two A-type supergiants) by Przybylski (1968), who used the same theoretical curve of growth as that used here.

Aluminium

The observed aluminium abundance in the program stars is down by 1.1 ± 0.4 dex compared with the suggested solar value of log N(Al) = 6.3. The only two lines of aluminium that are available for analysis are the two resonance lines λ3962 and λ3944, which occur in the wings of H_7 and the calcium H and K lines. Low aluminium abundances have been previously observed in A and F giants and supergiants when curve of growth methods have been employed (Table 4.4), and only the resonance lines used. The depression of the continuum by the wings of H_7 and the calcium H and K lines will significantly affect the observed equivalent widths of the aluminium lines used. Corrections have been applied using the same method as that described above for the Mg II lines.

On the basis of the present data, it is impossible to say with any certainty whether the observed underabundance in the luminous A and F stars is real or not. Either an abundance analysis based on the

model atmosphere approach or an analysis based on lines other than the resonance lines is necessary to resolve this point.

Table 4.4

Observed Aluminium Abundances in Luminous A and F Stars

Star	Sp. Type	Abundance $[Al]^{*}_{\odot}$	Reference
41 Cyg	F2Ib	-0.8	Kipper (1967)
ν Her	F2II-III	-0.4	"
HD 33579	A5Ia	-0.9	Przybylski (1968)

Note

$[Al]^{*}_{\odot} = [\log N(Al)]_{*} - [\log N(Al)]_{\odot}$ where * refers to the star and $\odot$ to the sun.

Silicon

In the stars studied at high dispersion, lines of both neutral and singly-ionized silicon were measurable, but at low dispersion only the lines of ionized silicon could be measured. The single line of Si I λ3905 was used and the lines of Si II used were λλ3856, 3863, 4128 and 4131.

The abundance derived from neutral and ionized silicon were not in close agreement (up to 0.4 dex discrepancy), but this is to be anticipated because of the small number of lines available. The program stars appear to be underabundant by 0.3 ± 0.2 dex with respect to the suggested solar abundance. θ Sco is the only exception, and it shows an apparent overabundance of 0.4 dex.

Calcium

Neutral calcium is represented by sufficient lines in all stars, with the exception of θ Sco, to allow the determination of the relative calcium abundance to a high degree of certainty, i.e., ± 0.2 dex for the high resolution and ± 0.3 dex for the low resolution stars. The calcium abundance derived from the H and K lines is strongly dependent on the value of the damping constant adopted, but in most cases it shows good agreement with that derived from the neutral lines. However, in the two most luminous stars, 195 Car and HD 97534, the abundance derived from the Ca I and the Ca II lines showed a 1.0 dex discrepancy, the Ca II lines showing the lower abundance. Przybylski found similar significant discrepancies between the calcium abundances derived from the lines of neutral and singly-ionized atoms in the A-type Ia supergiants HD 33579 and α Cyg.

The program stars, in general, appear to be underabundant by 0.3 ± 0.2 dex in calcium. θ Sco, for which the calcium abundance determination is of low certainty, shows an overabundance of 0.3 dex. Other workers have found similar underabundances of calcium in the luminous F stars. Thus it would appear that these stars show an apparent 0.3 ± 0.2 dex underabundance in calcium.

Scandium

There are eight or more measurable lines of Sc II in all the program stars, however, there were no suitable Sc I lines in the wavelength range covered. In the high-dispersion stars the points showed little scatter from the curve of growth; the rms scatter was 0.14 dex. However, in the low-resolution stars, particularly HD 97534 and 195 Car,

the scatter about the curve of growth was very large, with a rms scatter of 0.6 dex. The equivalent widths of the Sc II lines in these two stars were checked, but this result could not be improved upon. The observed abundances ranged from an underabundance of 0.1 dex for 195 Car and HD 97534 to an overabundance of 0.3 dex for ν Car, giving a mean overabundance of 0.1 ± 0.2 dex. The scandium abundance has been measured in a number of luminous A and F stars previously and the results are summarised in Table 4.5. There is such a large range in the observed scandium abundances that it is impossible to obtain any conclusive results about the normality of the scandium abundance in the program stars.

Table 4.5

Observed Scandium Abundances in Luminous A and F Stars

Star	Sp	Abundance $[Sc/Fe]_{\odot}^{*}$	Reference
ϕ Cas	F0Ia	-0.3	Searle, Sargent and Jugaku (1963)
89 Her	F2Ia	-0.8	"
HD 161796	F3Ib	-0.6	"
α Per	F5Ib	-0.7	"
35 Cyg	F5Ib	-0.3	Preston (1961)
γ Cyg	F8Ib	-0.3	"
HD 33579	A5Ia	0.0	Przybylski (1968)
ν Her	F2II-III	0.4	Kipper (1967)
41 Cyg	F2Ib	0.0	"

Note

$[Sc/Fe]_{\odot}^{*} = [\log N(Sc) - \log N(Fe)]_{*} - [\log N(Sc) - \log N(Fe)]_{\odot}$ where * refers to the star and $\odot$ to the sun.

Titanium

Lines of both neutral and singly-ionized titanium were observed and measurable in the stars studied at high dispersion. In the stars studied at low dispersion only the lines of Ti II were measurable. The Ti II curves of growth showed a large amount of scatter, particularly in the more luminous stars.

The abundances derived from both stages of ionization were in reasonable agreement, with the exception of δ CMa, but in this star only four doubtful Ti I lines were available. The program stars, with the exception of HD 97534 and 195 Car, appear to have normal titanium abundances within the anticipated errors. HD 97534 and 195 Car both showed an underabundance of 0.4 dex, which is considered significant. The titanium abundances observed by other workers show as large a variation as the observed scandium abundances (Table 4.5).

Vanadium

Lines of singly-ionized vanadium were measurable in all stars, but lines of neutral vanadium were measurable in only several of the stars studied at high dispersion. Only in δ CMa was there a significant difference (0.4 dex) between the abundance indicated by the lines of neutral and singly-ionized atoms. However, only three lines of V I were analysed in this star. The observed abundances were all in the range -0.4 ± 0.1 dex with respect to the suggested solar abundance. The stars studied by other workers all show a similar underabundance (0.4 ± 0.2 dex) in vanadium.

Chromium

Lines of neutral and singly-ionized atoms of chromium were observed in all stars except θ Sco, where only the strongest lines of singly-ionized chromium were measurable. The agreement between the observed abundances from both species was good in all stars and the mean chromium overabundance was 0.2 ± 0.1 dex, with the exception of δ CMa, which showed a 0.4 dex overabundance. Przybylski (1968) observed an overabundance of 0.3 dex in the stars he studied, whereas Kipper (1967) and Searle, Sargent and Jugaku (1963) observed an underabundance of 0.4 dex in the stars they studied. Preston (1961) observed a normal chromium abundance in the stars he studied.

Manganese

There were only three of the program stars, α Lep, α Car and i Car, in which lines of singly-ionized manganese could be measured. Lines of neutral manganese were measurable in all the stars except θ Sco, for which a manganese abundance could not be determined. The agreement between the abundances derived from the lines of neutral and the singly-ionized atoms was good. The observed manganese abundances varied from an apparent overabundance of 0.2 dex for π Sag to a 0.4 dex underabundance in i Sco, HD 97534 and 195 Car. The manganese abundances observed by other workers for the other luminous F-type stars analysed show a similar spread.

Iron

In the stars studied at high dispersion there were between 79 (π Sag) and 283 (α Car) usable Fe I lines and about 30 usable Fe II lines.

For the stars studied at low dispersion, there were in excess of 25 usable lines of Fe I and Fe II, with the exception of θ Sco, where there were only 15 usable lines of Fe II. The abundances derived from the neutral and singly-ionized lines are in close agreement because of the method used for determining the electron pressure, where the ionization of iron was given higher weight due to the relatively high number of lines used. The observed iron abundances are all within 0.1 dex of the solar value* and the range of observed abundances is also 0.1 dex. The absolute iron abundances derived by other workers for the high-luminosity A and F stars are also in close agreement with the suggested solar value.

Cobalt

Only in the high-dispersion stars were there a small number of usable neutral cobalt lines. The observed cobalt abundances indicated an underabundance of 0.7 ± 0.1 dex with respect to the suggested solar abundance. It should be noted that since these abundances were determined from neutral lines only, they are not particularly reliable because they are subject to possible errors in θ_{ion} and the electron pressure. Kipper (1967) determined the cobalt abundance in ν Her and 41 Cyg and found ν Her to have a normal cobalt abundance, and 41 Cyg a 0.3 dex underabundance.

---

* Many recent studies have criticized the often used oscillator-strength scale of Corliss and Bozman (1962) upon which the Corliss and Warner (1964) scale is based for Fe I lines. Corliss and Tech (1968) have slightly modified this scale for the higher level lines, and their values have been used in this study. The overwhelming majority of recent studies suggest that the Corliss and Warner values are too large by an amount which depends on the upper excitation potential. Some agreement has been reached (see, e.g., Wolnik, Berthel, and Wares 1970) that the solar photospheric iron abundance lies somewhere in the range of log N(Fe) = 7.3 to 7.6 (where log N(H) = 12.0).

Nickel

Suitable lines of both neutral and singly-ionized nickel were found in the stars studied at high dispersion (three nickel Ni II lines and up to 44 Ni I lines). Only the three lines of singly-ionized nickel were measurable in the stars studied at low dispersion. The abundances indicated by the lines of neutral and singly-ionized atoms agreed to within the anticipated error. All the program stars appear to be underabundant in nickel, the underabundance ranging from 0.3 dex in π Sag to 0.9 dex in HD 97534 and 195 Car, and having a mean value of 0.6 ± 0.2 dex. Searle, et al. found nickel to have a mean underabundance of 0.8 ± 0.2 dex in the stars they studied, Przybylski found an underabundance of 0.8 dex in HD 33579 and Kipper found essentially normal nickel abundances in the two stars he studied.

Zinc

Three lines of neutral zinc, λλ4680, 4722 and 4810, were measured in α Car and δ CMa; two of these were measurable in α Lep, i Car and i Sco. The abundances derived from each line in a particular star were in very close agreement in all cases. Zinc shows an apparent overabundance in all the program stars for which a zinc abundance was determined, the overabundance ranging from 0.4 dex for α Lep and i Car to 1.0 dex for i Sco.

Strontium

The only lines of strontium that were suitable for analysis were the two resonance lines, λ4708 and λ4216 and the line λ4162; not all these lines were measurable in all the stars.

The observed strontium abundance varied between an overabundance of 0.7 dex for i Sco and an underabundance of 0.7 dex for HD 97534, with the majority of stars showing a slightly low strontium abundance (-0.2 dex). A similarly wide range of strontium abundances have been observed by the above mentioned workers.

Yttrium

Lines of singly ionized yttrium were measurable in all the stars studied at high dispersion; ν Car and θ Sco were the only two stars studied at low dispersion for which the yttrium abundance could be determined. The 18 lines observed in α Car showed a large scatter (rms scatter = 0.4 dex) about the mean curve of growth, indicating that in the stars where fewer lines were observed the derived yttrium abundance could show large deviations from the intrinsic abundance. yttrium appears to be overabundant in the program stars. The observed abundances range from normal for i Car to a 0.8 dex overabundance for θ Sco. The mean observed overabundance was 0.5 ± 0.3 dex compared with the suggested solar value. Similar overabundances have been observed in the stars studied by Kipper (1967) and Preston (1961). Przybylski (1968) found an underabundance of 1.0 dex in the supergiant HD 33579.

Zirconium

The zirconium abundance has been determined for all the program stars from lines of singly-ionized atoms. More than 10 lines were used in the stars studied at high dispersion, but only about half this number were usable in the stars studied at low dispersion. The scatter of the points about the mean curve of growth was small

(rms scatter = 0.18 dex) and therefore, the abundances derived even when only a few lines are available should be reliable. The apparent zirconium abundance ranges from an overabundance of 0.6 dex for δ CMa to an underabundance of 0.4 dex for HD 97534 and 195 Car. The remaining 8 program stars show a mean overabundance of 0.1 ± 0.1 dex. The observed zirconium abundance in the luminous A and F stars studied previously show a large range, and generally indicate an underabundance in this element of about 0.5 dex.

Barium

Up to four lines, the two resonance lines λ4554 and λ4934 and the two weak lines λ4130 and λ4166, of singly-ionized barium were observed in the program stars. In the low-dispersion stars only the resonance line λ4554 was usable. In general, the resonance lines showed a 0.3 dex lower abundance than the other lines, so the barium abundances derived for the stars studied at low dispersion are only tentative. The observed barium abundances vary from an apparent overabundance of 0.6 dex for δ CMa to an underabundance of 1.1 dex in ν Car. The mean observed underabundance was 0.2 ± 0.4 dex. The other luminous A and F stars previously analysed show similar large variations in the observed barium abundance, indicating a mean underabundance of 0.3 ± 0.3 dex.

Lanthanum

Only lines of singly-ionized lanthanum were observed. Four lines were measurable in α Car and i Sco, three in δ CMa and i Car and one in α Lep, ν Car, HD 97534 and θ Sco. Thus the derived abundances are not very reliable. All the stars in which the lanthanum abundance was determined, except δ CMa, showed an underabundance of 0.3 ± 0.2 dex;

δ CMa showed an overabundance of 0.3 dex. The stars studied by Preston (1961), Kipper (1967) and Searle, Sargent and Jugaku (1963) all showed essentially normal or slight underabundances in lanthanum, with a mean observed underabundance of 0.3 ± 0.2 dex.

Cerium

The cerium abundance has been derived for four stars, α Lep, α Car, δ CMa and i Car, from the lines of singly-ionized atoms. The abundance has been derived from 15 or more lines of relatively low excitation potential (< 1.0 eV), so the derived abundances should be reliable. Cerium was found to be significantly underabundant (0.8 ± 0.2 dex) in α Lep, α Car and i Car, while δ CMa showed a 0.2 dex underabundance. The other luminous A and F stars analysed show a mean apparent underabundance of 0.5 ± 0.3 dex.

Europium

The two resonance lines, λ3820 and λ4130, of singly-ionized europium were used to derive the europium abundance in α Lep, α Car, i Car and i Sco. The two lines gave essentially the same abundance (0.05 dex discrepancy) in all cases except i Sco, where there was a 0.2 dex discrepancy. Europium appears to be significantly underabundant (1.4 ± 0.2 dex) in all four stars, but the reliability of this result is uncertain because only resonance lines were used for the abundance determination. A mean underabundance of 0.5 ± 0.1 dex was observed in φ Cas, 89 Her and HD 161796 by Searle, et al.; Preston found essentially normal abundances for europium in 35 Cyg and γ Cyg.

Gadolinium

The gadolinium abundance in α Car and i Car was determined from the λ3768 and λ4130 lines of singly-ionized gadolinium. The abundances indicated by each line were in close agreement in each star and indicate an underabundance of 1.8 dex for α Car and 2.3 dex for i Car. Kipper (1967) found an essentially normal gadolinium abundance in 41 Cyg, using the same absolute oscillator strengths.

(d) Discussion of Observed Stellar Abundances

α Lep, α Car, b Vel, i Car, ν Car, i Sco and π Sag all exhibit essentially the same abundances. Since the abundances observed for ν Car and b Vel are the same as those observed for the five stars studied at high dispersion, it appears that the observed abundances are dispersion independent. The less luminous supergiants and giants studied all show essentially the same abundances. Thus, the derived abundances appear to be independent of luminosity and spectral type over the ranges approximately $-2.5 < M_V < -7.0$ and A9 to F2. The small rms scatter about the mean for the majority of elements studied indicate that the relative values of the abundances have been determined to an accuracy of 0.15 dex or better. This means that even small abundance variations can be detected with some certainty.

In the following discussion the mean of the observed abundances for these seven stars will be taken to represent the abundances in 'normal' luminous early F-type stars. The mean abundances and the rms scatter are given in Table 4.6, as well as the differences between the mean abundance and the suggested solar abundances (Aller 1968).

Table 4.6

Abundance Intercomparisons

Element	Abundance							
	Solar	± σ	Mean	± R.M.S. Scatter	$[x]_{\theta}^{mean}$	$[x]_{mean}^{\delta\ CMa}$	$[x]_{mean}^{195,HD^4}$	$[x]_{mean}^{\theta\ Sco}$
H	12.00		12.00					
C[1]	8.55	0.15	8.88	0.13	+0.33	+0.9		
Mg	7.26	0.2	6.89	0.13	-0.37	+0.5	+0.00	+0.8
Al	6.33	0.15	5.36	0.25	-1.03	-0.03	+0.20	+0.6
Si	7.50	0.10	7.09	0.20	-0.41	+0.2	+0.15	+0.8
Ca	6.36	0.05	5.95	0.16	-0.41	-0.1	+0.5	+0.6
Sc	3.02	0.02	3.06	0.13	+0.04	+0.1	-0.15	+0.2
Ti	4.55	0.2	4.40	0.14	-0.15	+0.3	-0.30	+0.1
V	4.08	0.2	3.70	0.06	-0.38	+0.2	-0.25	+0.1
Cr	5.22	0.15	5.39	0.12	+0.17	+0.02	+0.05	-0.2
Mn	4.88	0.2	4.76	0.20	-0.12	+0.1	-0.25	
Fe	6.58	0.10	6.53	0.04	-0.05	+0.05	+0.00	+0.0

Table 4.6 (cont.)

Element	Abundance							
	Solar	± σ	Mean	± R.M.S. Scatter	$[x]_{\theta}^{mean}$	$[x]_{mean}^{\delta\ CMa}$	$[x]_{mean}^{195,HD}$ [4]	$[x]_{mean}^{\theta\ Sco}$
Co [1]	4.62	0.2	3.90	0.08	-0.72	+0.04		
Ni	5.67	0.2	5.10	0.12	-0.57	+0.2	-0.30	-0.2
Zn [1]	3.50	0.2	4.19	0.32	+0.69	-0.1		
Sr	2.90	0.2	2.80	0.25	-0.10	+0.4	-0.50	-0.1
Y [1]	1.62	0.2	2.20	0.08	+0.58	-0.2		+0.2
Zr	2.65	0.2	2.65	0.20	+0.00	+0.4	-0.45	-0.1
Ba [2]	1.70	0.2	1.70	0.18	+0.00	+0.6	-0.20	-0.3
La	2.03	0.4	1.60	0.08	-0.43	+0.7	+0.40	-0.3
Ce [3]	1.98	0.4	1.21	0.22	-0.77	+0.6		
Eu	0.96	0.4	-0.30	0.27	-1.26			

Notes to Table 4.6

1 Only the stars studied at high dispersion were used to form the mean.

2 ν Car was not used because it showed a large deviation (-1.1 dex).

3 Only α Lep, α Car and i Car were used to form the mean.

4 195, HD refers to the average abundance of 195 Car and HD 97534.

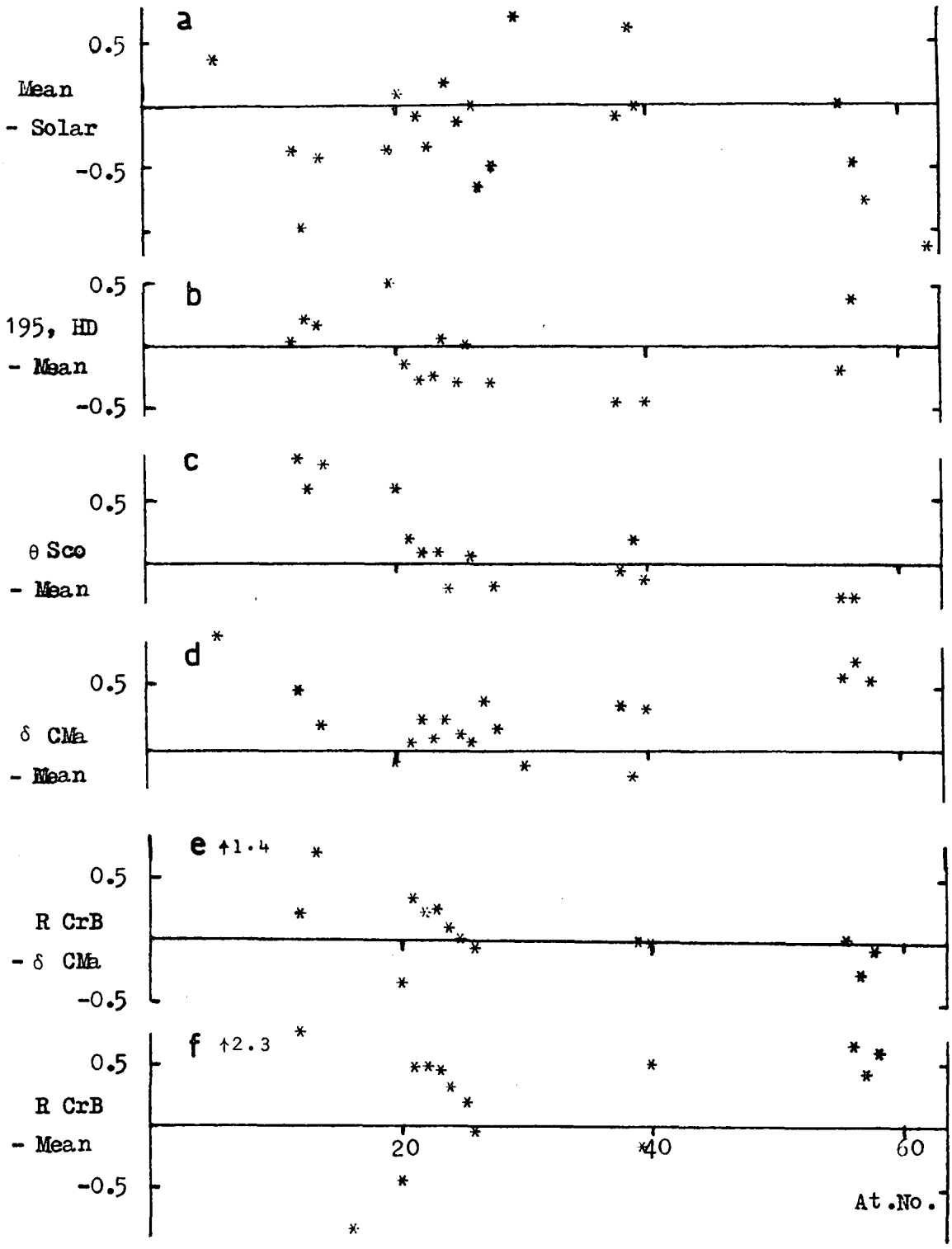

Figure 4.6(a-f) Comparison between the mean observed abundances of the 'normal' stars and those observed for the sun, θ Sco, δ CMa, R CrB and the average observed abundances of HD 97534 and 195 Car (195, HD). The abundance differences between δ CMa and R CrB are also shown.

These differences are also shown in Figure 4.6(a). The 'normal' stars appear to show a significant underabundance in more than half of the elements for which an abundance determination was possible, with a mean underabundance of 0.2 dex. The only elements which show a significant overabundance are carbon, zinc and yttrium. These abundance deviations may represent real abundance variations or they may reflect systematic errors introduced through the particular curve of growth or lines used.

In Table 4.6 a comparison is made between the abundances observed in the 'normal' stars and δ CMa, θ Sco, and the mean abundances observed for 195 Car and HD 97534. The abundance differences for these stars are shown in Figure 4.6(b-d).

(i) δ CMa

On examination of Figure 4.6(d), it is obvious that δ CMa shows significant overabundances in the elements of high and low atomic weight with respect to the mean abundances of the 'normal' stars. The iron group elements show essentially normal abundances, with the exception of titanium, which may be slightly overabundant (≃0.3 dex). These discrepancies may be real or may be due to systematic effects introduced by the method of abundance determination. They do suggest, however, that it would be worthwhile to investigate the abundances in a group of stars of spectral type F8Ia or similar to determine if δ CMa is typical or not of these stars.

The striking feature of the observed abundances in δ CMa is the large apparent overabundance of carbon, 1.2 dex with respect to the solar value and 0.9 dex with respect to the 'normal' program stars. This abundance has been determined using three unblended C I lines of

high excitation potential (7.5eV), so errors in θ_{exc} I may have affected the result. A 0.1 error in θ_{exc} I would cause a 0.4 dex change in the C/Fe ratio but, since all the stars have been analysed in the same manner, any systematic error in the determination of the excitation temperature should approximately cancel. As C I lines were used, the derived abundance is also affected by errors in the ionization temperature and electron pressure, but the agreement between the abundances indicated by neutral and singly-ionized atoms in δ CMa (Table 4.3) indicate that θ_{ion} and log Pe are at least consistent with the observations. The three lines used to determine the carbon abundance in δ CMa occur in a region of the spectrum where line crowding is not a problem and accurate placement of the continuum is possible.

Searle (1961), who used δ CMa as a 'normal' comparison star for the analysis of the supergiant variable R Coronae Borealis, has measured the equivalent widths of eight carbon lines. His equivalent widths for the three lines used here are slightly larger (≃ 0.07 dex) than those observed in this investigation, and would therefore suggest a slightly higher abundance. The other five C I lines measured by Searle were very strongly blended or occurred in a region where the placement of the continuum was dubious. The results published by Searle suggest that these lines would indicate an even higher carbon abundance in δ CMa than the three lines that were used. Comparison of the abundance trends in δ CMa and those found for the two R Coronae Borealis stars R CrB and RY Sag (Danziger 1965) shows that the same trends as observed in the R CrB stars are present in δ CMa (Figures 4.6(d) and (e)).

(ii) 195 Car, HD 97534

The abundance data for 195 Car and HD 97534 (Table 4.3) shows that these two stars have almost identical abundances, with the exception of barium, where there is a 0.6 dex discrepancy. Comparison of the mean abundances of 195 Car and HD 97534 and the mean abundances of the 'normal' stars (Figure 4.6(b)) show that for most elements these two stars have the 'normal' abundances, but there appears to be significant departures for calcium, titanium, vanadium, nickel, strontium, zirconium and lanthanum. However, these discrepancies are all less than 0.5 dex and probably reflect systematic errors due to the method of abundance analysis used and the small number of lines available for the abundance determinations. These two stars are an order of magnitude more luminous than the other program stars, with significantly higher temperatures, lower gravities and electron and gas pressures. Therefore, the assumptions on which the analyses are based are more unrealistic than in the other program stars, with the possible exception of δ CMa. Because of the low continuous opacity and high microturbulent velocities, the absorption lines in these stars are intrinsically very strong. This, coupled with their moderate macro-turbulence (or rotational velocity) and the low dispersion used, makes analysis of these two stars particularly difficult because the placement of the continuum is doubtful and the number of usable lines is quite small, being less than five for most species. Further investigation of the spectra of these two stars at a dispersion of about 4 $\mathring{A}\ mm^{-1}$ in the wavelength range 3800$\mathring{A}$ - 6700$\mathring{A}$ is warranted. Unfortunately, this is outside the capability of the 40cm telescope-spectrograph system currently available.

(iii) θ Sco

θ Sco shows significant abundance anomalies (Table 4.6 and Figure 4.6(c)) and appears to be overabundant in the elements of low atomic weight, essentially normal in the iron group elements and marginally underabundant in the elements of higher atomic weight. Once again, the abundance determinations are of low accuracy because of difficulty in placing the continuum and the small number of lines that were usable. However, in this case the accuracy of the abundance determinations cannot be easily improved upon because the spectral range 3800Å - 6700Å was covered, and the limitation is the high rotational velocity of this star (90 km sec^{-1}). It should be noted in passing that the observed atomic number dependence of the abundance deviations in θ Sco is the opposite to that shown by metallic-lined stars of similar spectral type, HD 174704 (F5Ib) and τ UMa (Preston, 1961).

5.5 Abundance Comparisons with other Interesting Supergiant Stars

(a) Introduction

Having determined the abundances in a self-consistent manner for such a large number of similar stars, we can use the mean of the observed abundances and their rms scatter to see if other interesting stars show significant abundance deviations. Some care must be exercised when comparing abundance determinations of different workers because different theoretical curves of growth or absolute oscillator strengths may have been used. Another problem which must be overcome are the systematic errors due to an incorrect determination of the continuous opacity (M.E. approx.) or the number of hydrogen atoms above the photosphere (S.S. approx.). It is considered that the most

satisfactory approach to attempt to overcome these problems is to compare the differences between the ratio of the elemental abundance, $N(X)$, with that of iron, $N(Fe)$, in the star and the sun, where the solar and stellar abundances have been determined for each star using the same absolute oscillator strengths, or the relative abundances determined by a differential curve of growth technique. To express the relative abundances, we define

$$\left[\frac{X}{Fe}\right]_{b-\odot}^{a-\odot} = \left\{ \log\left[\frac{N(X)}{N(Fe)}\right]_a - \log\left[\frac{N(X)}{N(Fe)}\right]_\odot \right\}_{f_1} - \left\{ \log\left[\frac{N(X)}{N(Fe)}\right]_b - \log\left[\frac{N(X)}{N(Fe)}\right]_\odot \right\}_{f_2} ,$$

where a and b represent the two stars and f_1 and f_2 represent the different scales of oscillator strengths. The disadvantage of this technique is that the errors associated with the abundance determinations in the sun enter into the expression twice. This makes the uncertainty associated with the results of a comparison made in this manner very large, and only large abundance variations can be detected using this technique.

In the following subsections we will compare the observed abundances in the Large Magellanic Cloud supergiant HD 33579, the two high latitude supergiants 89 Her and HD 161796, and the supergiant variable R CrB with those observed for the 'normal' program stars.

(b) HD 33579

The intermediate A-type supergiant HD 33579 has been compared with α Cygni (A2Ia) by Przybylski (1968); they were found to have essentially the same abundances. Comparison of the observed

abundances for HD 33579 with the mean observed abundances for the 'normal' program stars (Table 4.7) shows that HD 33579 is slightly over-abundant ($\simeq$ 0.3 dex) in most elements with respect to these stars, indicating HD 33579 exhibits essentially solar abundances. A similar conclusion was drawn by Przybylski (1968). Silicon is the only element which shows a significant overabundance of +1.5 dex. The observed abundances should be reliable since six lines were used in HD 33579 and three of four of these were used in the program stars whose abundances were averaged to calculate the mean silicon abundance. Some of the overabundance (0.2 dex) may be due to the slight differences in the oscillator strengths used. The method of analysis employed by Przybylski is the same as that used here. Thus the overabundance of silicon in HD 33579 is probably real.

(c) 89 Her and HD 161796

Two more F-type Ia supergiant stars of particular interest are 89 Her (F2Ia) and HD 161796 (F3Ib). These two stars occur at high galactic latitudes, approximately 1.0 kpc and 1.7 kpc above the galactic plane (Searle, Sargent and Jugaku 1963) and it is of interest to determine whether they have the same chemical composition as the super-giants closer to the galactic plane. Searle et al. made a comparison between these two high latitude supergiants and the two supergiants ϕ Cas and α Per in the galactic plane. They came to the conclusion that the four stars had the same chemical composition to within the estimated errors. Comparison of the abundances derived for these two stars and the mean abundances derived from the 'normal' program stars (Table 4.7) shows there are abundance differences of up to $\pm$ 0.8 dex.

Table 4.7

Abundance Intercomparisons between the 'Normal' Stars and HD 33579, α Per, φ Cas, 89 Her and HD 161796.

Element	$\left[\frac{X}{Fe}\right]^{*-\odot}_{mean-\odot}$						
	HD 33579	± σ	α Per	φ Cas	89 Her	HD 161796	± σ^1
Mg	+0.2	0.8					
Al	+0.3	1.0					
Si	+1.5	0.6					
Ca	+1.1	0.9					
Sc	+0.0	0.4	-0.7	-0.3	-0.8	-0.6	0.5
Ti	-0.1	0.5	-0.3	-0.1	-0.4	-0.3	0.4
V	+0.0	0.6	-0.4	-0.3	-0.2	-0.1	0.6
Cr	+0.4	0.5	-0.6	-0.6	-0.5	-0.6	0.5
Mn	+1.0	0.9					
Ni	+0.0	0.6	-0.1	-0.5	-0.2	-0.3	0.5
Sr	+0.4	0.9					
Zr	-0.2	0.6	-0.6	-0.5	-0.7	-0.9	0.7
Ba	-0.2	0.8					
La			+0.1	+0.6	0.0	-0.2	0.8
Ce				+0.6	+0.4	+1.1	0.8
Eu			+1.0	+0.6	+0.8	+0.7	0.8

Note to Table 4.7

1 σ refers to the standard deviation for α Per, ϕ Cas, 89 Her, and HD 161796. The values adopted for one standard deviation have been estimated from the uncertainty in the solar and published stellar abundances and the rms scatter observed in the program stars used to form the mean. The adopted standard deviations are very liberal and should only be considered as upper values.

However, the low latitude supergiants, ϕ Cas and α Per, show similar trends when analysed in a similar manner (i.e., by a differential curve of growth technique with respect to the sun). Parsons (1967), who analysed α Per by a model atmosphere technique, found this star to have solar abundances within the usual factor of two or three. This suggests that the observed abundance discrepancies are most likely due to the combined systematic errors in the two methods employed for the abundance determinations, rather than differences in the intrinsic abundances. To resolve this point, the equivalent width data for 89 Her and HD 161796 (Abt 1960) has been re-analysed using the same techniques as used for the analysis of the program stars.

The atmospheric parameters derived in this investigation are given in Table 4.8, as well as those derived by Searle et al. Agreement between the two sets of parameters is good. The microturbulent velocities derived here are approximately 10% larger and the temperature adopted for the reversing layer slightly cooler than those found by Searle et al. As was emphasized by Abt, the strong zero volt lines of Fe I lie systematically above the other lines; this effect, present in all supergiants, is especially marked in 89 Her. These lines were not included in the analysis. As noted by Searle et al., the lines of Fe I were scattered rather widely about the mean curve (rms scatter $\simeq$ 0.18 dex). The lines of Fe II and Cr I defined a good curve with little scatter (rms scatter $\simeq$ 0.10 and 0.13 respectively). Searle et al. noted that Ti II defined a good curve with little scatter in both stars, but in this analysis the Ti II lines showed a large scatter (rms scatter $\simeq$ 0.25) in both stars.

Table 4.8

Comparison of Atmospheric Parameters determined for 89 Her and HD 161796

This Investigation

Star \ Parameter	Sp. Type	V_n (km sec^{-1})	V_{ion} (km sec^{-1})	θ_{exc} I	θ_{exc} II[1]	log Pe	θ_{rev}[2]
89 Her	F2Ia	10	12	0.91	0.76	0.4	(0.83)
HD 161796	F3Ib	11	12	0.93	0.77	0.6	(0.85)

Searle, Sargent and Jugaku (1963)

Star \ Parameter	Sp. Type	V_n (km sec^{-1})	V_{ion} (km sec^{-1})	θ_{exc} I	θ_{exc} II	log Pe	θ_{rev}
89 Her	F2Ia	9.1	9.1	0.80	0.80	0.4	0.75
HD 161796	F3Ib	10.7	10.7	0.80	0.80	0.6	0.73

Notes to Table 4.8

1 θ_{exc} II was derived from the Ti II lines alone because this was the only species in which there was a sufficient spread of excitation temperatures represented for the determination of θ_{exc} II.

2 Brackets indicate estimated values. In the case of 89 Her, for which Osmer (1970) suggests the atmospheric parameters $T_{eff} = 6750^{o}K$ and log g = 0.3 are appropriate, the temperature at $\tau = 0.15$ in this model atmosphere was adopted as the temperature appropriate to the reversing layer. The temperature for HD 161796 was derived by scaling θ_{rev} for 89 Her the amount indicated by the differences in the observed excitation temperatures.

The derived absolute abundances for 89 Her and HD 161796 are given in Table 4.9(a and b). Table 4.10 gives the results of a comparison made between these two stars, the mean abundances of the 'normal' program stars, and also the mean abundances observed for 19 Cam and HD 97534.

Examination of Tables 4.7 and 4.10 clearly shows that the deviation in the derived abundances of 89 Her and HD 161796 from the 'normal' program stars and the average abundance of 19 Cam and HD 97534 are significantly reduced when the two high latitude supergiants are analysed in the same manner as the program stars. The abundances derived for 89 Her and HD 161796 show that these stars show no significant abundance deviations from the 'normal' F-type supergiants. HD 161796, which has a luminosity class similar to the 'normal' F-type stars, shows a closer resemblance to the 'normal' stars than the two high luminosity stars, 19 Cam and HD 97534. On the other hand, 89 Her, which is similar in luminosity to 19 Cam and HD 97534, shows a marginally closer resemblance to these two stars than to the 'normal' stars. The above results indicate that the apparent differences between the abundances for 89 Her and HD 161796 as found by Searle et al. and the 'normal' F-type supergiants were due to systematic errors introduced through the use of different techniques for the analyses, rather than intrinsic abundance anomalies.

(d) R Coronae Borealis

Searle (1961), who carried out a differential curve of growth analysis of R CrB with respect to δ CMa, found R CrB to be slightly over-abundant ($\simeq$ 0.2 dex) with respect to δ CMa. In this investigation,

Table 4.9

Abundance Results for 89 Her and HD 161796

Species	No. of Lines	Stage of Ionization		Abundance		R.M.S. Scatter
		I	II	Normalized	Star-Solar	
			89 Her			
H				12.00		
Sc II	6		14.2	2.6	-0.4	0.21
Ti II	18		15.7	4.1	-0.4	0.26
Cr II	8		17.1	5.5	0.3	0.14
V II	2		15.4	3.8	-0.3	
Fe I	43	15.6	*18.1*			0.18
Fe II	13		18.1	6.5	-0.1	0.10
Ni II	2		16.7	5.1	-0.6	
Zr II	1		14.3	2.7	0.0	
La II	1		12.8	1.2	-0.8	
Ce II	1		12.7	1.1	-0.9	
Eu II	1		11.4	-0.2	-1.1	
			HD 161796			
Sc II	4		14.4	2.8	-0.2	0.31
Ti II	18		15.9	4.3	-0.2	0.25
Cr II	8		17.3	5.7	0.5	0.12
V II	2		15.6	4.0	-0.1	
Fe I	38	15.6	*18.1*			0.17
Fe II	13		18.1	6.5	-0.1	0.09
Ni II	1		16.9	5.3	-0.4	
Zr II	1		14.1	2.5	-0.2	
La II	1		12.6	1.0	-1.0	
Ce II	1		13.6	2.0	0.0	
Eu II	1		11.3	-0.3	-1.2	

Table 4.10

Abundance Intercomparisons

Element	$\left[\frac{X}{Fe}\right]_{mean}^{89\ Her}$	± σ	$\left[\frac{X}{Fe}\right]_{mean}^{HD\ 161796}$	± σ	$\left[\frac{X}{Fe}\right]_{195,HD}^{89\ Her}$	± σ	$\left[\frac{X}{Fe}\right]_{195,HD}^{HD\ 161796}$	± σ
Sc	-0.4	0.3	-0.2	0.3	-0.3	0.4	-0.1	0.4
Ti	-0.2	0.2	0.0	0.2	+0.1	0.3	+0.3	0.3
V	+0.1	0.4	+0.3	0.4	+0.3	0.5	+0.5	0.5
Cr	+0.2	0.2	+0.4	0.2	+0.1	0.3	+0.3	0.3
Ni	+0.0	0.4	+0.2	0.4	+0.3	0.5	+0.5	0.5
Zr	+0.1	0.4	-0.1	0.4	+0.5	0.5	+0.3	0.5
La	-0.3	0.4	-0.5	0.4	-0.7	0.5	-0.9	0.5
Ce	-0.1	0.4	+0.8	0.4				
Eu	+0.2	0.4	+0.1	0.4				

Note that $\left[\frac{X}{Fe}\right]_{a}^{b}$ has its usual meaning; in the case of $\left[\frac{X}{Fe}\right]_{195,HD}^{b}$, 195,HD represents the average abundance of 195 Car and HD 97534.

δ CMa has been found to show an apparent overabundance of 0.3 dex with respect to the sun, indicating R CrB shows an apparent 0.5 dex mean overabundance with respect to the sun.

The abundance of R CrB, corrected for the apparent abundances in δ CMa, are given in Table 4.11 and shown in Figure 4.6(f).

Table 4.11

Abundances for R CrB

Element	C	Mg	Ca	Sc	Ti	V	Cr
$[X]_{\odot}^{R\ CrB}$	2.6	0.3	-0.9	0.6	0.4	0	0.5

Element	Mn	Fe	Y	Zr	Ba	La	Ce
$[X]_{\odot}^{R\ CrB}$	0.0	-0.1	0.4	0.4	0.6	0.0	-0.2

Note $[X]_{\odot}^{R\ CrB}$ has its usual meaning.

The significant abundance anomalies in R CrB are an apparent 400 times overabundance of carbon, and an 8 times underabundance in calcium with respect to the suggested solar abundances of Aller (1968).

4.6 Summary

Significant new trends were found in the microturbulence of the F I stars, which may indicate that the equivalent width of O I λ7774 line is not temperature insensitive over the range F0 to G0 in the supergiants.

A simple extension of Chaffee's model (1970) for the depth dependence of the microturbulence along the main sequence satisfactorily explains all but one of the observed temperature and luminosity

dependent variations in the microturbulence. The trend not explained is the drop in the observed microturbulence at F5 in the Ia stars, but this may be due to the change in spectral lines used to determine the microturbulence.

The results of the curve of growth abundance analysis of the program stars indicate:

(1) All the program stars, except δ CMa and θ Sco, have essentially the same abundances and these indicate a slight apparent underabundance in more than half of the elements studied. It is not possible to say whether these underabundances are intrinsic or due to the method of analysis adopted. The rms scatter of the observed abundances about the mean values indicate that the relative abundances have been determined to an accuracy of ±0.15 dex in the majority of cases. The slightly different abundances found for 195 Car, HD 97534, 89 Her and the 'normal' stars suggest that the observed apparent abundances may be temperature and gravity dependent in the most luminous late A and early F stars.

(2) The abundances derived using the curve of growth analysis are independent of luminosity and spectral type over the ranges $-2.5 > M_V > -7.0$ and A9 to F2.

(3) It was found that δ CMa exhibits similar abundance anomalies to the R Coronae Borealis stars R CrB and RY Sag. As R CrB was analysed with respect to δ CMA by Searle (1961), the abundances indicated by Searle for R CrB need significant corrections. There appears to be a 400 times overabundance of carbon in R CrB.

(4) The stars HD 33579, 89 Her and HD 161796 all have essentially solar abundances. The only large apparent deviation is the 1.5 dex overabundance of silicon in HD 33579.

The differences in the abundances indicated for 89 Her and HD 161796 by the differential curve of growth analysis of Searle, Sargent and Jugaku (1963) and one performed here using the Wrubel curve of growth show the need for extreme care when comparing abundance data obtained using different methods.

The small scatter in the curves of growth for the stars studied at high dispersion (with the exception of θ Sco) indicate that the equivalent width data is of sufficiently high quality to warrant a detailed model atmosphere analysis to determine the microturbulent velocities and elemental abundances in these stars.

CONCLUSION

Here the various conclusions reached in the course of this investigation are summarised and the directions in which future observational and theoretical work on the luminous early F-type stars might proceed are briefly outlined, (with special reference to the 40cm telescope-spectrograph system).

The results of the present study on this group of stars are as follows:

(1) Large discrepancies were observed between the gravities indicated by the Balmer jump and H_γ line profiles in the most luminous F0 to F2 Ia supergiants with log g < 0.8. These discrepancies were also observed, but to a lesser extent, in the F0 to F2 Ia supergiants with log g in the range 0.8 < log g < 1.2.

(2) Macroturbulent motions are insignificant in the line-forming regions of the F-type supergiant stars with log g ≃ 1.6, as shown by the fine-line stars α Car and i Car, but there is some evidence for the presence of macroturbulent motions of approximately 16 km sec^{-1} in the most luminous Ia supergiants.

(3) Gravities indicated by the models using the H_γ line profiles are less than those indicated by calculations based on the cluster members. The differences in gravities can be reduced by including a macro-turbulent pressure term in the equation of hydrostatic equilibrium.

(4) The rotational velocity of θ Sco suggests that the early F Ib supergiants tend to conserve angular momentum during their evolution off the main sequence and that they must rotate as rigid bodies for some, if not all, of this phase of their evolution.

(5) A significant hitherto unobserved trend was found in the Fe II microturbulent velocity of the Ia supergiants. It was previously thought that the Fe II microturbulent velocity in the Ia stars increased through the spectral range F0 to G0, but the results presented in this dissertation show that it follows the same trends as the Fe I microturbulent velocity and the microturbulence trends observed in the main-sequence stars. Similar trends were also found in the combined results of the Iab supergiants and type II giants. The Iab supergiants observed show that the microturbulence in these stars decreases through the spectral range A0 to F0.

(6) An extension of Chaffee's model for the depth dependence of the microturbulence explains all the trends in the microturbulence, except the dip at F5 shown by the Ia and Ib supergiants and the class II giants.

(7) The abundances of the program stars are essentially solar, with the exception of θ Sco and δ CMa. The carbon abundances in δ CMa is ten times that observed in the sun and barium, lanthanum and cerium also show significant overabundances ($\geq$ 0.6 dex) in δ CMa. The luminous F-type stars show an apparent slight overall underabundance in the elements, but these abundance variations are probably due to the method of analysis used rather than intrinsic abundance differences between these stars and the sun.

(8) Abundances derived using the Wruble curve of growth appear to be temperature independent in the range A9 to F3 and gravity independent in the range of spectral classes II to Ia (excluding the most luminous Ia stars). There is some evidence to suggest that the abundances are luminosity dependent in the most luminous late A and early F Ia stars.

(9) Comparisons drawn between HD 33579, 89 Her, HD 161796 and the 'normal' stars give the following results:

(a) HD 33579 is found to have solar abundances to within the usual factor of two or three.

(b) When analysed in a similar manner to the program stars, 89 Her and HD 161796 appear to have essentially the same abundances as the 'normal' program stars, HD 161796 showing the best agreement. The abundances of 89 Her are in marginally closer agreement with the abundances found for the two high luminosity stars 195 Car and HD 97534.

Projects which could be undertaken with the 40cm telescope-spectrograph system without the need for further instrumentation include:

(1) the acquisition of the spectrum of α Car and possibly α Lep and i Sco over an extended wavelength range from approximately 3300Å to 7500Å (or redder) at 1.4, 2.1 or 4 Å mm^{-1}, depending on the wavelength. These plates could be taken with a small entrance slit (25μ projected on the plate) to give a resolution sufficiently high to allow line profiles to be determined.

(2) a further investigation into the O I λ7774 line as a luminosity indicator. All the equipment (grating, grating drive and photomultiplier (ITT FW118)) is available to enable the setting up of a system similar to that used by Osmer (1970) for the measurement of the strength of this line. The 40cm telescope may not be large enough to allow observation of a sufficient number of stars and it may be necessary to wait until the 100cm telescope is operational before this project is viable.

(3) the determination of the turbulence variations in any of the program stars, a point well worth investigation.

(4) further observation of the two late A- or early F-type Ia supergiants studied here. This is of particular interest because of the high

microturbulent velocities observed, and the possibility of mass loss. A set of plates in the range 3800Å to 5000Å at approximately 4 Å mm^{-1} would allow a more accurate determination of microturbulent velocities and abundances. It may be just possible with the 40cm telescope to take some red plates to investigate whether mass loss from these stars is taking place or not - another worthwhile investigation.

(5) a study of the colour- and total flux-variation of the program stars. It has been reported by Auman (1969) that the temperature above the ionization zone in a typical F-type supergiant could vary by as much as $2000^{\circ}K$. This variation should show up in the stellar flux and colours. It would be a simple matter to observe two colours and the total flux to measure these variations and investigate the time scale over which the variations take place.

From the theoretical point of view, it would be of interest to perform a model atmosphere analysis on the equivalent width data presented for the high-dispersion stars, with the exception of θ Sco. The small amount of scatter about the mean curve of growth indicates that the equivalent data is of sufficient quality to warrant such an analysis. The appropriate (T_{eff}, log g) values have been determined here. For the most luminous early F-type supergiants, the possible reasons for the large discrepancy between the gravity indicated by the Balmer jump and the gravity calculated for the cluster members using evolutionary models could be investigated. The pressure - inversion zone in the F-type supergiants, and the possible connection with the microturbulent velocities and the narrowing of the hydrogen lines is also well worth further investigation.

BIBLIOGRAPHY

Abt, H.A. (1957a), *Ap.J.*, **126**, 138.

———, (1957b), *Ap.J.*, **126**, 503.

———, (1958), *Ap.J.*, **127**, 658.

———, (1960), *Ap.J.*, **131**, 99.

Albers, H. (1969), *Ap.J.*, **156**, L37.

Allen, C.W. (1963), *Astrophysical Quantities* (2nd ed.; London: Athlone Press).

Aller, L.H. (1960), *Stellar Atmospheres*, ed. J.L. Greenstein (Chicago: University of Chicago Press), p. 156.

———, (1963), *Atmospheres of the Sun and Stars* (New York: Ronald Press).

———, (1968), *Proc. A.S.A.*, **1**, 133.

Aller, L.H., Faulkner, D.J., and Norton, R.H. (1966), *Ap.J.*, **144**, 1073.

Auman, J.R. (1969), *Theory and Observations of Normal Stellar Atmospheres*, ed. O. Gingerich (Cambridge, Mass.: M.I.T. Press), p. 131.

Bell, R.A., and Rogers, A.W. (1965), *M.N.R.A.S.*, **129**, 127.

Bidelman, W.P., and McKellar, A. (1957), *Pub. A.S.P.*, **69**, 31.

Blaauw, A. (1963), *Basic Astronomical Data*, ed. K.A. Strand (Chicago: University of Chicago Press), p. 383.

Blanco, V.M., Demers, S., Douglass, G.G., and Fitzgerald, M.P. (1968), *U.S.Naval Obs.*, Publ. 21.

Böhm-Vitense, E. (1956), *Pub. A.S.P.*, **68**, 57.

———, (1973), *Ap.J.*, **181**, 379.

Bonsack, W.K. (1959), *Ap.J.*, **130**, 843.

Bonsack, W.K., and Culver, R.B. (1966), *Ap.J.*, **145**, 767.

Bosworth, P.K. (1971), Unpublished Hons. Thesis, University of Tasmania.

Broadfoot, A.L. (1966), *Applied Optics*, **5**, 1259.

Carbon, D.F., and Gingerich, O. (1969), *Theory and Observations of Normal Stellar Atmospheres*, ed. O. Gingerich (Cambridge, Mass.: M.I.T. Press), p. 377.

Castley, J.C. (1969), Unpublished Hons. Thesis, University of Tasmania.

Cayrel, R., and Cayrel de Strobel, G. (1966), *Ann. Rev. Astr. and Ap.*, 4, 1.

Chaffee, F.H. (1970), *Astron. and Ap.*, 4, 291.

Chandrasekhar, S. (1961), *Hydrodynamic and Hydromagnetic Stability* (Oxford: Clarendon Press), Chap. 10.

Corliss, C.H. (1965), *N.B.S. Journal of Research*, 69A, 87.

Corliss, C.H., and Bozmann, W.R. (1962), *NBS Monog.*, No. 53.

Corliss, C.H., and Tech, J.L. (1968), *NBS Monog.*, No. 108.

Corliss, C.H., and Warner, B. (1964), *Ap.J. Suppl.*, No. 8, 395.

Crawford, D.L. (1970), *Stellar Rotation*. ed. A. Slettebak (D. Reidel Pub.Co.: Dordrecht Holland), p. 204.

Crawford, D.L., Barnes, J.V., Faure, B.Q., and Golson, J.C. (1966), *A.J.*, 71, 709.

Crawford, D.J., Barnes, J.V., and Golson, J.C. (1970), *A.J.*, 75, 624.

Danziger, I.J. (1965), *M.N.R.A.S.*, 130, 199.

Davis, S.P. (1970), *Diffraction Grating Spectrographs* (Holt, Rinehart and Winston, Inc.) p. 53.

Difley, J.A. (1968), *A.J.*, 73, 762.

Dunham, T. (1956), *Vistas in Astronomy*, 2, ed. A. Beer (Oxford: Pergamon Press), 1223.

Edmonds, F.N., Schlüter, H., and Wells, D.C. (1967), *Mem.R.A.S.*, 71, 271.

Fernie, F.D. (1963), *Obs.*, 83, 33.

Gillett, F.C., Hyland, A.R., and Stein, W.A. (1970), *Ap.J.*, 162, L21.

Golberg, L. (1958), *Ap.J.*, 127, 308.

Greenstein, J.L. (1942), *Ap.J.*, 95, 161.

———, (1948), *ibid*, 107, 151.

Griem, H.R. (1967), *Ap.J.*, 147, 1092.

Griffin, R., and Griffin, R. (1967), *M.N.R.A.S.*, 137, 253.

Hanbury-Brown, R., Davis, J., Allen, L.R., and Rome, J.M. (1967), *M.N.R.A.S.*, **137**, 393.

Hayes, D.S. (1970), *Ap.J.*, **159**, 165.

Hoag, A.A., and Miller, W.C. (1969), *Appl. Optics*, **8**, 2417.

Huang, S.S. (1953), *Ap.J.*, **118**, 285.

Huang, S.S., and Struve, O. (1955), *Ap.J.*, **121**, 84.

Humphreys, R.M., Strecker, D.W., and Ney, E.P. (1971), *Ap.J.*, **167**, L35.

Iben, I. (1966), *Ap.J.*, **143**, 505.

Johnson, H.L. (1966), *Ann. Rev. Astr. and Ap.*, **4**, 193.

Johnson, H.L., Mitchell, R.I., Iriarte, B., and Wiśniewski, W.Z. (1966) *Comm. Lunar and Plan. Lab.*, No. **63**.

Johnson, H.L., and Morgan, W.W. (1953), *Ap.J.*, **117**, 313.

Kalkofen, W. (1968), *Ap.J.*, **151**, 317.

Keenan, P.C., and Hynek, J.A. (1950), *Ap.J.*, **111**, 1.

Kipper, T.A. (1967), *Astrophys.*, **3**, 185.

Kondo, Y., Henize, K.G., and Kotila, C.L. (1970), *Ap.J.*, **159**, 927.

Kraft, R.P., and Wruble, M.H. (1965), *Ap.J.*, **142**, 703.

Kron, G.E. (1958), *P.A.S.P.*, **70**, 561.

Kron, G.E., White, H.S., and Gascoigne, S.C.B. (1953), *Ap.J.*, **118**, 502.

Krueger, T.K., Aller, L.H., Ross, J., and Czyzak, S.J. (1968), *Ap.J.*, **152**, 765.

Kurucz, R.L. (1969), *Theory and Observation of Normal Stellar Atmospheres*, ed. O. Gingerich (Cambridge, Mass.: M.I.T. Press), p. 375.

———, (1969a), *Ap.J.*, **156**, 235.

Lambert, D.L. (1968), *M.N.R.A.S.*, **138**, 143.

Lambert, D.L., and Warner, B. (1968a), *M.N.R.A.S.*, **138**, 181.

———, (1968b), *ibid*, 213.

———, (1968c), *ibid*, **139**, 35.

———, (1968d), *ibid*, **140**, 197.

Lindeman, E., and Hauck, B. (1973), *Astron. and Ap. Suppl.*, **11**, 119.

Lloyd Evans, T. (1969), *M.N.R.A.S.*, **146**, 101.

Matsushima, S. (1969), *Ap.J.*, **158**, 1137.

Merrill, P. (1934), *Ap.J.*, **79**, 183.

Michie, N.A. (1970), *Aust. Elec. Eng.*, May 1970, 29.

Mihalas, D. (1969), *Ap.J.*, **156**, L155.

Miller, W.C. (1964), *Pub. A.S.P.*, **76**, 328.

Mitchell, R.I. (1960), *Ap.J.*, **132**, 68.

Moore, C.E., Minnaert, M.G.J., and Houtgast, J. (1966), *Second Revision of Rowland's Preliminary Table of the Solar Spectrum Wavelengths, NBS Mono.* No. **61**.

Oke, J.B. (1964), *Ap.J.*, **140**, 689.

Oke, J.B., and Schild, R.E. (1970), *Ap.J.*, **161**, 1015.

Olson, E.C. (1968), *Ap.J.*, **153**, 187.

Osmer, P.S. (1970), Unpublished Ph.D. Thesis, (Calif. Inst. of Tech.)

———, (1972), *Ap.J. Suppl.* No. **206**, 247.

Parsons, S.B. (1964), *Ap.J.*, **140**, 853.

———, (1967), *ibid*, **150**, 263.

———, (1969), *Ap.J. Suppl.* No. **159**, 127.

———, (1970), *Ap.J.*, **159**, 951.

———, (1971), *ibid*, **164**, 355.

Parsons, S.B., and Peytremann, E. (1973), *Ap.J.*, **180**, 71.

Pesch, P. (1959), *Ap.J.*, **130**, 764.

Porteus, D.R. (1973), Private Communication.

Preston, G.W. (1961), *Ap.J.*, **134**, 797.

Przybylski, A. (1968), *M.N.R.A.S.*, **139**, 313.

Rosendhal, J.D. (1970a), *Ap.J.*, **159**, 107.

———, (1970b), *ibid*, **160**, 627.

Rosendhal, J.D., and Wegner, G. (1970), *Ap.J.*, **162**, 547.

Sargent, W.L.W. (1961), *Ap.J.*, **134**, 142.

Sargent, W.L.W., and Osmer, P.S. (1968), *Mass Loss from Stars*, ed. M. Hack (Dordrecht, Holland: D. Reidel Publn. Co.), p. 57.

Schatzman, E. (1962), *Ann. d'ap.*, **25**, 18.

Searle, L. (1961), *Ap.J.*, **133**, 531.

Searle, L., Sargent, W.L.W., and Jugaku, J. (1963), *Ap.J.*, **137**, 268.

Smith, M.A. (1973), *Ap.J.*, **182**, 159.

Stebbins, J., and Kron, G.E. (1964), *Ap.J.*, **139**, 424.

Stecher, T.P. (1969), *A.J.*, **74**, 98.

Stothers, R. (1966), *Ap.J.*, **143**, 91.

Strom, S.E. (1969), *Theory and Observation of Normal Stellar Atmospheres*, ed. O. Gingerich (Cambridge, Mass.: M.I.T. Press), p. 99.

Strom, S.E., and Peterson, D.M. (1968), *Ap.J.*, **152**, 859.

Strömgren, B. (1966), *Ann. Rev. Astr. and Ap.*, **4**, 433.

Strömgren, B., and Perry, C. (1965), (unpublished).

Struve, O., and Elvey, C.T. (1934), *Ap.J.*, **79**, 409.

Uesugi, A., and Fukuda, I. (1970), *Mem. of the Faculty of Sc., Koyoto Uni., Series of Phys. Ap. Geophys. and Chem.*, **33**, Art. 5.

Underhill, A.B. (1949), *M.N.R.A.S.*, **109**, 562.

Unno. W. (1959a), *Ap.J.*, **129**, 375.

———, (1959b), *ibid*, 388,

Unsöld, A. (1955), *Physik der Sternatmosphären* (Berlin: Springer-Verlag).

Wackerling, L.R. (1970), *Mem. R.A.S.*, **73**, 153.

Waterworth, M.D. (1966), Unpublished Ph.D. Thesis (Imperial College: London).

Warner, B. (1967), *Mem. R.A.S.*, **70**, 165.

———, (1968), *M.N.R.A.S.*, **138**, 229.

Whiteoak, J.B. (1966), *Ap.J.*, **144**, 305.

Wiese, W.L., Smith, M.W., and Glennon, B.M. (1966), *NSRDS-NBS*, No. 4.

———, (1969), *ibid*, No. 22.

Willstrop, R.V. (1960), *M.N.R.A.S.*, **121**, 17.

Wolf, S.C., Kuhi, L.V., and Hayes, D. (1968), *Ap.J.*, **152**, 871.

Wolnik, S.J., Berthel, R.O., and Wares, G.W. (1970), *Ap.J.*, **162**, 1037.

Wrubel, M.H. (1949), *Ap.J.*, **109**, 66.

———, (1954), *ibid*, **119**, 51.

———, (1960), quoted by L.H. Aller in *Stellar Atmospheres*, ed. J.L. Greenstein (Chicago: University of Chicago Press), p. 198.

Appendix 1

INSTRUMENTATION OF THE 40cm TELESCOPE

A1.1 Introduction

A 40cm telescope is generally considered too small to warrant the expense of fitting it with a Coudé spectrograph. This is in fact the case in the northern Hemisphere, where most of the endeavour in stellar spectroscopy has been concentrated. However, the southern sky, where the majority of stars are concentrated, has been largely neglected in comparison, and even some of the brightest stars have not been analysed in detail at high dispersion. There is therefore a large number of analyses that can be carried out using a small telescope and Coudé spectrograph, such as the instrumentation at the University of Tasmania's Observatory.

The 40cm telescope has been previously described (Castley (1969)) and hence will not be described in detail here, apart from reporting that the declination axis has since been fitted with a stepping motor drive (6 steps per second of arc), which has ten speeds ranging from 5 sec of arc per minute for guiding to 1 degree per minute for setting.

In this chapter a few basic details of the observing site are dealt with, and the results of a clear night survey conducted over a 3½ year period ending September 1973 are presented. The design principles and details of the Coudé spectrograph are then given. In Sections A1.2 to A1.11 details of the associated equipment (wavelength and photometric calibration apparatus, the slit-viewing optics and autoguider, the spectrum widener, the exposure meter, the

pre-flashing unit, the photographic plate processing facilities and the low-resolution scanner) are given, together with other relevant data, such as approximate exposure times.

A1.2 Some Statistics about the Observing Site

The University of Tasmania's Astronomical Observatory is situated on Canopus Hill (890 feet), about 20 minutes by car from the University. The site is shielded from the direct lights of Hobart by the intervening hills, but the background sky brightness corresponds to a 19th magnitude star per square second of arc (white light).

Over the 3½ year period, ending September 1973, a clear night survey has been conducted and this shows that, on the average, one can expect 7 clear nights per month (this includes half nights). Fluctuations about this mean are very large; October, November and December normally have less than 7, and February and March more than 7 clear nights per month. Two examples of the large fluctuations will be cited here: In the period October 10th 1971 to November 15th 1971 there was only one clear night, and in February 1972 there were 16 clear nights. Clear nights normally come in groups, 3 or 4 at a time.

The seeing is rarely better than 1.5 seconds of arc and typically in the range 2 to 3 seconds of arc. On one still summer's night the image of α Car (m_v) = (-0.8) passed straight through a 60μ entrance slit (1 sec. of arc $\simeq$ 62μ), leaving only a slight halo on the slit jaws, indicating the seeing was better than 1 sec. of arc.

A1.3 The Spectrograph

The optical principles employed in a Coudé Spectrograph have been previously described in some detail by Dunham (1956), and only a brief résumé will be given here. Basically, the optical components of the spectrograph are:

(1) An adjustable slit (5-1000μ), situated at the Coudé focus of the telescope.

(2) A collimating mirror, situated with the adjustable slit in its focal plane.

(3) The grating, situated in the beam of parallel light produced by the collimator mirror.

(4) A camera mirror, situated such that its centre of curvature lies on or near the centre of the grating, to bring the collimated beam from the grating to focus.

(5) A means of recording the resultant intensity distribution of light: photographic plate or photo-electric scanner.

The focal length of the collimator mirror is specified by the focal ratio of the beam from the telescope and the length of the rulings on the grating; in our case the telescope beam is f/31 and the rulings 12cm in length, indicating a collimator of focal length 31 x 12 = 372cm is required. Actually the collimator turned out to have a focal length of approximately 365 cm. The two camera mirrors currently being used were loaned by the Fund for Astrophysical Research Inc., New York, and have focal lengths of 120cm and 180cm and a diameter of 75cm. The collimator and cameras are spherical mirrors and thus, to minimise the aberrations of the system, they are used as close to on-axis as practically possible.

There are two gratings currently available: a replica supplied by the CSIRO, Melbourne, which has a ruled area of 11cm x 15cm (600 lines mm^{-1}), blazed at 5500Å in the first order, and a replica, supplied by Bausch and Lomb, with a ruled area 13cm x 16cm (1200 lines mm^{-1}), blazed at 1μ in the first order.

The spectrograph is housed in an insulated room 3.4m x 7m x 3m on the northern side of the dome. It is normal practice to support all the optics associated with the spectrograph from a single large frame, which is supported on three isolated mounts. Due to the cost involved at the time of construction, this has not been possible, but no resultant degradation in image quality has been observed. The optics at the slit head are all supported from a 1.2cm thick steel plate, which was built into the southern wall of the building. The remaining optics, with the exception of the 180cm camera, are supported on a 2m x 3m steel frame, approximately 1.3m above floor level. The collimator mirror is supported on a stand, which can be moved on two rails parallel to the light beam from the slit to allow focusing. Both gratings have their own stands, which also move on rails so that they can be easily interchanged. The plate holders, photomultiplier (for the low-dispersion scanner) and the image tube mount each have their own stands, or share stands in such a way that they can easily be interchanged and repositioned accurately so that focus is maintained. Because of its weight, the 120cm focal length camera is supported on a steel trolley, the rails for which are arranged so that this mirror can be moved behind the collimator when not in use. The 180cm camera is supported on its own frame behind the main frame.

The trolley for the 120cm camera is constructed so that the mirror can be rotated to direct the beam along a path about 1m from the grating where provision has been made to mount a pressure controlled Fabry-Perot interferometer and associated equipment. The slit can be replaced with a turret containing 8 circular apertures, ranging in size from 5 secs of arc to 2 mins of arc when projected on the sky, for use with the Fabry-Perot system.

Each camera has its own plate holder for 25cm x 5cm or 25cm x 10cm photographic plates, with the ledges that support the plates machined to the same radius as the focal length of the camera. The method finally adopted for machining the ledges proved to be simple and very effective. Firstly, two templates were made with the appropriate radius of curvature, one convex and the other concave. The 1.2cm aluminium frame for the two plate holders was bent so that the concave template fitted exactly. The ledges were then machined flat and when the frame was released it returned to its original form (flat), and the ledges had the appropriate curvature. The curvature could be checked with the convex template and minor adjustments made with a scraper. Corrections were made until the fitting was better than .08mm, as this is essential for the 120cm camera. Glass plates 1mm thick were bent to the required radius for either camera without breakage.

The layout of the components for the spectrograph is shown in Figure A1.1, and the layout of the components at the slit head is shown in Figure A1.2.

The telescope Coudé mirrors and the spectrograph entrance slit, collimator, and gratings were aligned by mounting a laser on the roof of the spectrograph room, and directing the beam into the telescope

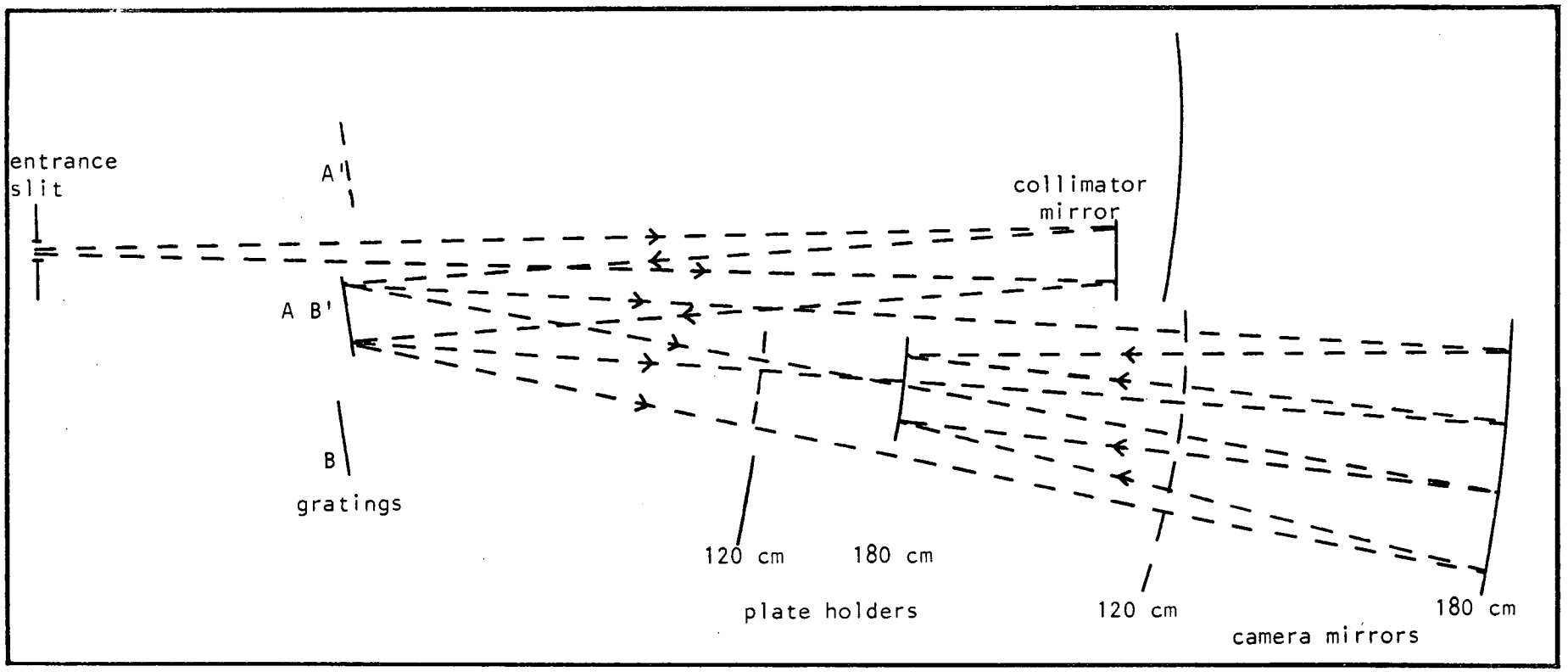

Figure A1.1 Diagram of the spectrograph with grating A and 180 cm camera mirror in use. The dashed lines show the position of the components when grating B and 120 cm camera mirror is in use.

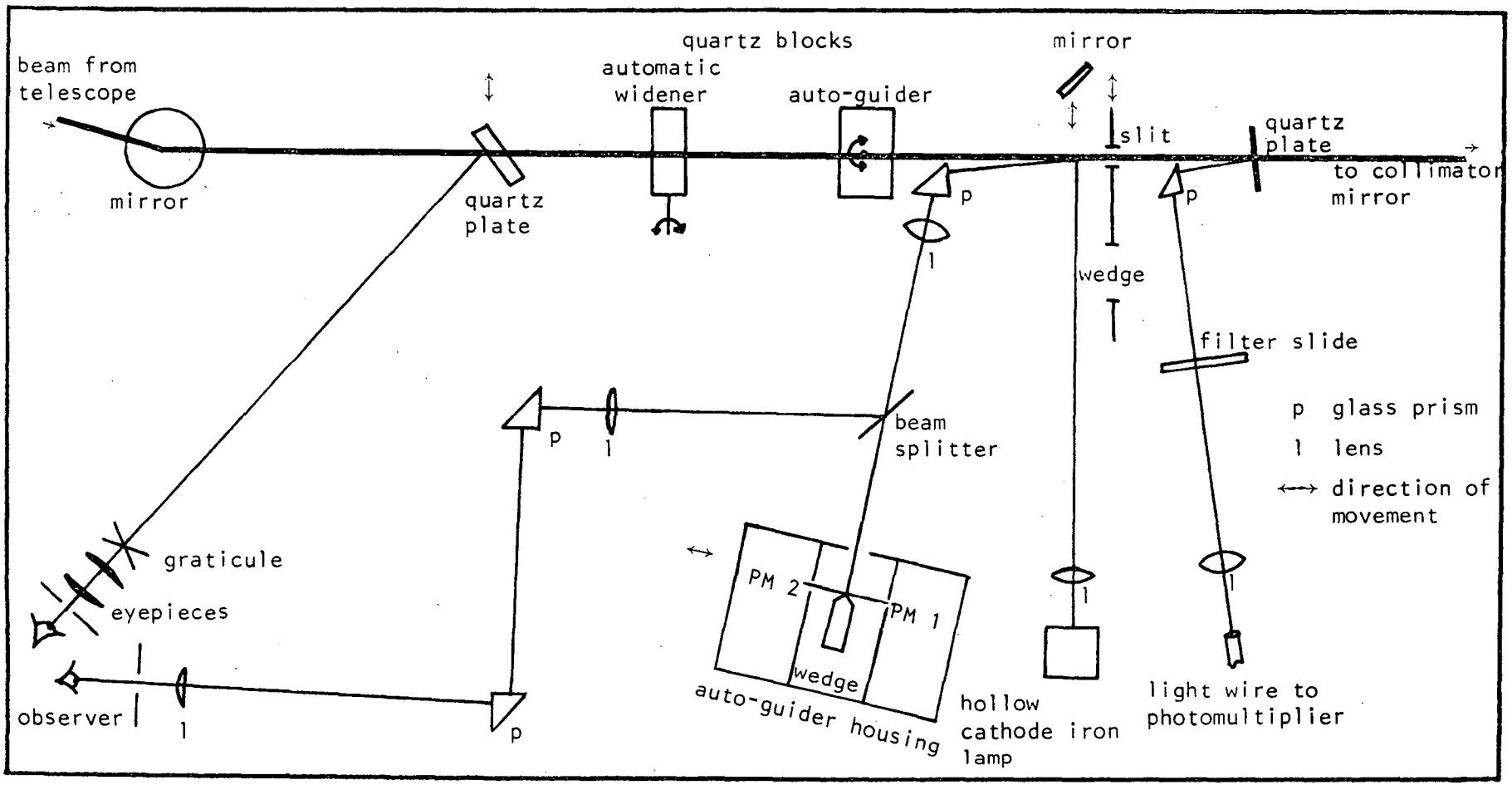

Figure A1.2 Schematic diagram of layout of components at the slit head.

down the optical axis defined by the primary. This had previously been set to coincide with the mechanical axis of the tube. Each mirror in turn was adjusted so that the beam striking the next did so centrally, and the slit position adjusted so that the light struck the appropriate area. The alignment of the telescope mirrors was checked by observing bright stars and checking each mirror for vignetting. The alignment was found to be satisfactory using this technique. The final check, of course, is whether the telescope will track accurately or not. After setting the telescope's mechanical axis to point at the South Pole and setting the right ascension drive at the correct speed, the telescope tracked quite satisfactorily for Coudé work.

Having set the slit, collimator mirror and gratings, the axis of the spectrograph has been over-determined and alignment can be carried out using the procedures outlined in "Diffraction Grating Spectrographs" by Davis (1970). The only criticism of these procedures is the method given for setting up the plate holder; a much more satisfactory method was found to be as follows: using a strong source (e.g. Hg discharge lamp) in front of the slit, set the grating such that the zeroth order comes to focus in the centre of the plate holder. A piece of aluminised glass is placed in the plate holder,and the axes of the plate holder adjusted until the image of the slit appears on itself.

Quite a simple technique was also developed for focusing the plate holders, using a bright source and the zeroth order of the grating. A powerful microscope (200x), supported on a magnetic base, is positioned so that it looks at the image of the zeroth order in the centre of the plate holder, and is focused on a piece of

ground glass, 0.5mm thick, in the plate holder. The ground glass is then removed, without disturbing the microscope, and the plate holder mount supporting the microscope moved until the zero order image is accurately in focus in the microscope. The focus is then checked in a similar manner at each end of the plate holder, and the plate holder rotated slightly if necessary. The focus determined in this way could not be improved upon by taking a series of exposures, separated by 0.05mm in distance in the line of sight to the camera mirror. It was found that there is a focal tolerance of approximately 0.2mm for the 180cm camera and 0.1mm for the 120cm camera.

Initially there was a 10cm diameter aperture between the dome and the spectrograph room through which the various beams could pass, but on windy nights it was found that there was a considerable draught passing through this hole. The turbulence produced by this was significantly reducing the resolution of the spectrograph. To prevent this a 4mm quartz plate was fastened over this hole at a small angle, approximately 3°, to the light path. The light reflected from this plate, approximately 8%, was used for the exposure meter (see Section A1.7.).

After this modification the observed resolution was controlled by the entrance slit width chosen and appeared to be independent of exposure time or weather conditions. Long term stability is sufficient to allow exposures stopped by cloud on one night to be finished on the next, but this may not always be possible. One one occasion, when an exposure was stopped half way due to cloud, there was not another clear night for 8 days, during which there were

extremes of summer weather conditions. The exposure was completed on the next clear night and, on development, the plate showed two spectra displaced by about 0.07mm in the direction of the dispersion.

A1.4 Wavelength Calibration

Wavelength calibration was provided by means of a neon-filled hollow cathode iron lamp which, in the visible, produces the neon spectrum. Unfortunately, because the usable length of the entrance slit was only 16mm, there was not sufficient room to allow a wavelength comparison spectrum to be placed both above and below the stellar spectrum. Light from the central portion of the hollow cathode is condensed and imaged (f/31 beam) onto the slit jaws, evenly illuminating approximately 6mm of the slit, giving reference lines 3mm and 2mm long on the plates taken with the 180cm and 120cm cameras respectively. A list of approximate exposure times is given in Table A1.1.

A1.5 Photometric Calibration

There has been considerable discussion as to whether photometric calibration should be provided on each plate, or simply on a piece of plate from the same batch, using the same instrument as that used for the stellar exposure, or another instrument. Because of the ease with which photometric calibration spectra can be placed on each plate, and the lack of evidence to suggest that any other method is to be preferred, apparatus to provide wedge slit photometric calibration spectra on each plate has been constructed.

Owing to space considerations at the slit head, the spectrograph could not be fitted with an elaborate photometric

Table A1.1

Exposure times for the wavelength and photometric calibration spectra

Plate type		IIa-0	I03a-0	IIa-E&D	I03a-F	IIa-0
Dispersion (Å mm^{-1})		9	9	9	9	2.4
Exposure Time (seconds)	Wavelength	25	12	10	5	80
	Photometric	50	25	10	20	80

Plate type		I03a-0	Ia-0	IIa-E&D	I03a-F	IIa-0
Dispersion (Å mm^{-1})		2.4	2.4	2.4	2.4	1.4
Exposure Time (seconds)	Wavelength	60	40	60	40	100
	Photometric	60	40	70	100	360

Notes

(1) For pre-flashed plates reduce all times by 30%.

(2) Wavelength calibration exposure times are for a 140μ entrance slit and a 28 ma cathode current.

(3) The times for other dispersions and entrance slit widths can be estimated by noting that the exposure time is inversely proportional to both the dispersion and the entrance slit width for the wavelength calibration spectra, and inversely proportional to the dispersion alone for the photometric calibration spectra.

calibration system (Dunham (1956)) in which the spectral distribution of the light could be adjusted to match the efficiency of the spectrograph-photographic plate system. However, the spectral distribution of the light from the system constructed proved to be quite adequate for the wavelength region of interest in the present investigation, from 3800Å to 6000Å. Once again, due to space considerations, a photometric calibration spectra could only be placed on one side of the stellar spectrum.

An evenly illuminated plate of ground glass, 1mm thick and 40mm in diameter, was used as the immediate source of illumination. Light from this plate is then imaged, via a lens and two mirrors, onto another piece of ground glass and the wedge, both of which are in the focal plane of the spectrograph. Suitable baffling in the spectrograph room prevents unwanted scattered light affecting the photographic plate. The aperture of the grating is the aperture stop of the system, therefore ensuring that the same fraction of light from each section of the wedge passes through the spectrograph. The wedge can be replaced by a rectangular aperture to check the uniformity of illumination on the wedge.

The physical size of the slit and the steel mounting plate necessitated the mounting of the wedge and the slit on a movable slide so that the slit could be moved out of, and the wedge into, position. Therefore it is not possible to expose both the stellar spectrum and photometric calibration spectrum at the same time. No provision has been made for the alteration of exposure times. A list of approximate exposure times is given in Table A1.1.

AI.6 Rocking Quartz Block for Widening Spectra

The stellar image at the Coudé focus of the 40cm telescope is approximately 150μ in diameter if the seeing is 2 seconds of arc (Bosworth (1971)), which will produce a spectrum 75μ wide on the photographic plate of the 180cm camera. This is much too narrow to allow accurate microphotometry. The currently accepted lower limit for accurate microphotometry is approximately 0.5mm, and to achieve this an artificial means of widening the spectrum must be provided. This can be done in two ways: the observer manually moving the star up and down the slit jaws with the slow-motion controls, or by mechanical means.

The latter method is preferable because, at the Coudé focus, the rotation of the coordinate system for guiding makes it difficult to cause the image to travel up and down the slit without executing a somewhat irregular path, except on rare occasions when one of the guiding axes is parallel or nearly parallel to the slit jaws.

> "The gain in flux and the uniform automatic action of a mechanical widener more than offsets the losses due to reflections",

Dunham (1956). This was confirmed in the early stages of operation of the spectrograph when manual widening was employed. Spectra with uniform density at right angles to the dispersion were very rarely obtained.

The normal method employed to widen the spectrum is to place a quartz block in the beam before the slit, and rock this backwards and forwards in such a manner that the stellar image spends an equal amount of time at each point on the slit. Normally the quartz block

is driven from a cam and a series of adjustable levers to control the distance moved by the star on the slit. The advent of integrated circuits and stepping motors has made the design, construction and use of the automatic widener much simpler. In the following paragraphs a brief description of the theoretical considerations is given, followed by a brief description of the automatic widener used on the 40cm telescope.

The lateral displacement, Δd, of a beam by a plane parallel block of quartz of refractive index μ and thickness t is given by Waterworth (1966) as

$$\Delta d = t \sin I \left\{ 1 - \frac{\cos I}{\sqrt{\mu^2 - \sin^2 I}} \right\} ,$$

where I is the angle of incidence. Calculations show this expression is linear to within 4% for $|I| < 25^{\circ}$ (i.e. $\Delta d \propto I$ for $|I| < 25^{\circ}$). Therefore a plate, travelling with uniform angular velocity within these limits, will cause the deflected beam to move with uniform velocity. Another consideration is the reflective losses from the quartz plate, which increase with increasing angle of incidence. To reduce these losses to a minimum, the angle of incidence was kept to within $\pm 20^{\circ}$.

The plane-parallel quartz block, 20mm thick situated 20cm in front of the slit, is driven at uniform velocity, via a 250:1 reduction gear box, by a small Phillips stepping motor. This motor is stepped a preset number of steps and then reversed. The number of steps determines the excursion of the star on the slit and is controlled from a single rotary switch. There are eight different widening settings separated by a factor of approximately 1.3,

ranging from 0.7mm to 6mm on the entrance slit. In the advent of more or less widening being required, this can easily be achieved by changing the thickness of the quartz block.

The widener is provided with a handset containing a switch for starting and stopping, and two press buttons to allow initial setting up. For convenience, the widener starts and stops at the same position in its cycle each time. Scans across the widened spectrum show that the density across the spectrum is uniform, except at the extreme edges, where seeing effects cause a slight reduction in density.

A1.7 The Slit-Viewing Optics and Autoguider

The Coudé focus of the telescope has been equipped with two eye pieces, one with a relatively large field of view (4' of arc), and another which enables viewing of the stellar image on the slit jaws. There is a small movable quartz plate which can be manually moved into the Coudé beam to reflect some of the light (about 20%) to the wide-angle eyepiece. This eyepiece is used to find the star initially and set the star on the slit. There is an adjustable cross-graticule in the eyepiece which is set so that its centre corresponds to the appropriate position on the jaws of the slit. Having set the star on the slit, the quartz plate is removed from the beam to maintain maximum efficiency.

The second eyepiece shares the light reflected from the slit jaws with the autoguider. The slit jaws, which are polished stainless steel, are inclined at a small angle (approximately 2^{o}) to the Coudé beam. The light reflected from the jaws is turned through

90° by a small prism*, after which it passes through a lens, producing a 4x magnified image. The beam is split just after passing this lens by a semi-reflecting mirror, placed at 45° to the beam so that half the light falls on the image dissector in the autoguider, and the other half passes through a series of prisms and lenses to the observer's eye.

The basic principles and design of the autoguider have been described by Bosworth (1971), but since that time, because of the lack of sensitivity and the need for automatic guiding in one dimension only, the design has been radically changed. The relatively short focal length of the telescope means that the movement of the stellar image up and down the slit jaws due to the seeing is small (< 0.3mm) compared with the displacement necessary to widen the spectra sufficiently, approximately 2mm. Thus there is no need for automatic guiding in the direction parallel to the slit. The control circuitry of the autoguider has been converted from the analogue, DC motor system of Bosworth to a digital system employing a stepping motor. A block diagram of the autoguider is given in Figure AI.3.

This system is designed so that, having once set the sensitivity controls, no more adjustments are necessary. The autoguider can be used on a star of any brightness, down to its limit of fourth magnitude, without adjustment. One of the disadvantages of a small telescope, from the autoguider's point of view, is that a large proportion of the starlight passes through the entrance slit,

---

* Glass prisms, rather than mirrors, have been used where possible because they are maintenance free and, in this application, ultraviolet transmission is not important.

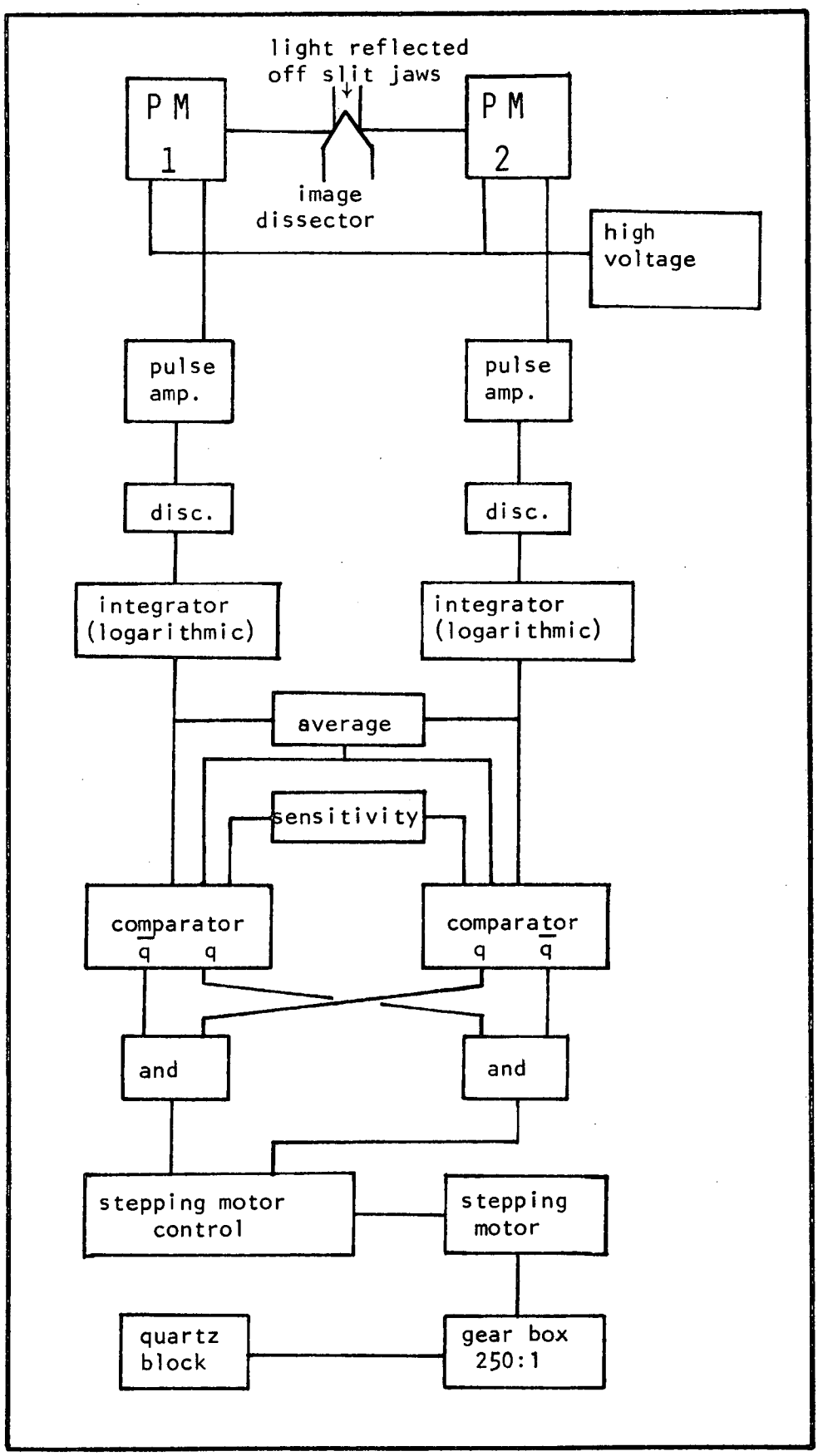

Figure A1.3 Block diagram of autoguider electronics.

except in cases of very poor seeing. There is very little light for the autoguider to work on, and in the case when the star is accurately centred and the seeing good, none. This necessitates the very careful balancing of both halves of the system and the sensitivity control settings. The low brightness limit of the autoguider could be increased to fifth magnitude by replacing the semi-transparent mirror with a remote-controlled mirror so that all the light reflected from the slit jaws passes into the autoguider or to the observer.

Due to the fact that the axes of the telescope rotate on the slit, manual guiding is difficult, particularly when the star is far from the meridian and changes in atmospheric refraction necessitate corrections in both co-ordinates at frequent intervals. For manual guiding of stars fainter than the autoguider limit, the autoguider has been provided with a handset which gives the observer direct control of the stepping motor. This has the advantage that the movement of the star is always at right angles to the length of the slit and removes the uncertainty in which way the star will go if a particular button is depressed.

Reflective losses from the quartz plate become significant if the angle of incidence exceeds approximately $\pm 20^{o}$. Two small micro-switches have been fitted that turn on small lamps when the angle of incidence exceeds this limit, telling the observer that the telescope needs a minor pointing correction via the slow-motion controls. Typically the time between adjustments of this type is between 15 and 90 minutes, depending on the seeing conditions and the region of the sky at which the telescope is pointing. Reflective losses from

the quartz plate are far outweighed by the faster response time of the autoguider over that of the observer, and exposure times fell by approximately 30% when the autoguider was brought into routine service.

A1.8 The Exposure Meter

It was mentioned previously that a quartz plate had to be fitted in the aperture between the dome and the spectrograph room to prevent turbulence in the light path. Purposely, this plate was fitted after the entrance slit and inclined at a small angle to the beam so that light reflected by it ($\simeq$ 8%) could be used for the exposure meter. The light reflected from the plate is turned through 90° by a small prism, after which it passes through a remotely-controlled filter slide and is focused onto a light wire, which carries the light to the photocathode of a photomultiplier 1.2m away. Provision has been made for cooling the photomultiplier, but this is not necessary for stars brighter than fifth magnitude.

Pulses from the photomultiplier are amplified, discriminated, and counted by two counters, one displaying the count for each 10 second interval, the other displaying the total number of counts, giving the observer a measure of the instantaneous and integrated flux through the slit. The filter slide has five positions, placing either U,B,V, a red filter or no filter at all in the beam. Typical integrated counts required for correct exposure are given Table A1.2.

Table A1.2

Integrated count from star for correct exposure

Plate Type	IIa-0	I03a-0	IIa-0	IIa-0	I03a-0	Ia-0	IIa-0
Centre wavelength	4300	4300	3800	4200 4500	4800	4200	4800
Dispersion ($\AA\ mm^{-1}$)	9	9	2.1	2.1	2.1	2.1	2.1
Counts	$1.5_{10}4$	$1.0_{10}4$	$1.0_{10}5$	$7.5_{10}4$	$5.0_{10}4$	$3.5_{10}4$	$9.0_{10}4$

These numbers should only be used to make an initial estimate because the count needed depends on so many unknown variables that the exposure meter needs calibrating for each observing run.

A1.9 The Pre-Flashing Unit

There are many methods that can be employed to increase the sensitivity of photographic emulsions. A good review of the subject is given by Hoag and Miller (1969). The two methods suitable for emulsions of O-sensitizing that are to be used here are baking and pre-flashing. For the type of work reported here, Miller (1964) indicates baking is to be preferred over pre-flashing, from the photographic point of view. However, plates require up to two days for baking and once baked do not maintain their increased sensitivity for more than several days, even under deep freeze conditions. Thus one must be fairly sure of having a clear night between two and six days after commencement of baking, or else the plates will be wasted.

Pre-flashing, on the other hand, requires about one minute before the plate is to be used and, from the point of view of

economics, is to be preferred. An additional advantage, although one involving only convenience, is the speed and facility with which pre-flashing can be applied. Baking requires special, carefully regulated ovens, whereas pre-flashing can be applied with the simplest equipment.

Speed gains of between two and four have been reported for baking by Hoag and Miller (1969), and from two to six for pre-flashing (Miller (1964)), depending on the amount of pre-exposure and the exposure time. A speed gain of approximately two to three is to be expected with the IIa-0 and I03a-0 plates using a two second pre-flash, which produces a pre-exposure fog density of 0.3. Pre-flashing has the additional advantages of removing the initial hump in the density-intensity curve, increasing the linear section of this curve, and improving the accuracy to which the cores of the strongest lines can be determined. For the above-mentioned reasons, pre-flashing has been used as the plate sensitising method in the work reported here.

The pre-flashing unit is of very simple construction; a small (5W) arc lamp was used as the light source, in front of which were mounted a ground glass screen and an air shutter. These were all mounted as a single unit and this was attached to the ceiling in the back of the spectrograph room. The ceiling and walls of the room are flat black, thus eliminating unwanted reflections. The plate to be pre-flashed was placed in a shallow, flat black container and pre-flashed to give a background fog density of approximately 0.3. The intensity of the illumination is altered by placing different aperture stops over the ground glass screen.

The pre-exposure fog was tested for uniformity and the fog proved to be adequately uniform, except for the first and last 12mm of the plate, where the density decreases slowly towards the edge of the plate. A similar non-uniformity in these regions is observed in the background fog of unflashed plates and it is thought to be due to the method of supporting the plates, and possibly the method of agitation during development. This is of little consequence since these sections of the plates are not normally used. Stellar exposure times for a pre-flashed plate fell to approximately 60% of that required for a plate that was not pre-flashed for the same continuum density above fog (exposures in the range 100-180 minutes).

A1.10 Photographic Plate Processing Facilities

A photographic plate cutter, processing tanks and agitator for the developing tank were constructed in the Physics Department workshop to sketches, photographs and, in the case of the processing tanks, engineering drawings, kindly supplied by Mr. J. McKinlay of the Mt. Stromlo and Siding Spring Observatory, Canberra. The developing process followed was the same as that normally used, 6 minutes in D19 at 20^{o}C, stop bath, two fixers, clearing agent, water rinse and distilled water wash. The details of the process and recipes for the solutions were also kindly supplied by Mr. J. McKinlay.

The dark room was maintained at 20^{o}C by means of a "Proportional Power Controller" (Michie (1970)), which was capable of supplying up to 1000W. This was sufficient in the summer, but in the winter an additional heater (500W continuous) was required. There is no provision for cooling the dark room, except by circulating cool outside air via the Expelair fans. It was found that the solutions

maintained the same temperature as the room air, providing the lids were kept on the processing tanks when not in use. The lids can be removed for up to 15 minutes without the solutions undergoing a significant change in temperature.

A1.11 The Low-Resolution Scanner

Because of its size, the 40cm telescope is not capable of supporting a Cassegrain Scanner, so the Coudé spectrograph has been constructed so that it can double as a low-resolution scanner. The efficiency of this system compared with that of a Cassegrain Scanner is slightly reduced because of the increased number of reflections needed to get the light to Coudé focus.

As mentioned previously, the Coudé spectrograph is to be used as a pre-monochromator for the pressure-controlled Fabry-Perot. To make wavelength selection easier, one of the grating stands has been fitted with a stepping motor drive capable of setting the observed wavelength in the focal plane of the camera to approximately 0.1Å at 5000Å, using the CSIRO grating.

A central controller, based on an ex-PMG Uni-selector, was constructed; this controlled the position of the grating, via the stepping motor drive, such that each of the Oke (1964) standard wavelengths between 3390Å and 5840Å was centred on the entrance slot (50Å wide) for the photomultiplier. The wavelengths are scanned, in order, from 3390Å up to 5840Å and then back again. Provision has been made to stop the cycle anywhere and reset to start, preset the number of counts to be collected or the time spent at each wavelength, and preset the time for which the integration time and

counts are displayed (this must exceed 3 seconds to allow time for the wavelength change).

The stellar flux through the slit is also recorded at each wavelength, via the exposure meter system, to allow corrections to be made for changes in flux through the slit due to guiding errors or changes in atmospheric transparency. At present the results (two counts and the integration time) must be recorded manually at each wavelength, but an interface between the timer, scalers, and a high speed punch (1000ch sec^{-1}) is under construction. Wavelengths are indicated by an up-down counter, which can also be used to set any desired wavelength on the entrance slit of the recording photomultiplier. A block diagram of the system is shown in Figure A1.4.

An EMI 6094B photomultiplier was used as the detector in the focal plane of the camera mirror (this tube was already on hand). This is an end-on viewing tube with a 10mm diameter photocathode (S-11 response). The dark current in the tube is typically 800 counts per second at room temperature and drops to between 1 and 2 counts per second at $-45^{\circ}C$.

Initial trial scans of α Car ($m_v = -0.8$) in December 1972 indicate that in the ultraviolet (50Å band-pass centred on 3390Å) the typical count rate is 10,000 counts sec^{-1}. Since some of the program stars (Section 2.2) are more than 5 magnitudes fainter than α Car, count rates down to 50 counts per sec. are anticipated, so the photomultiplier has to be cooled.

A photomultiplier cooling system based on the design of Broadfoot (1966) was ordered but, owing to delays, this was not available for the 1972-73 summer observing season. This meant that the continuous energy distribution of the majority of the program stars

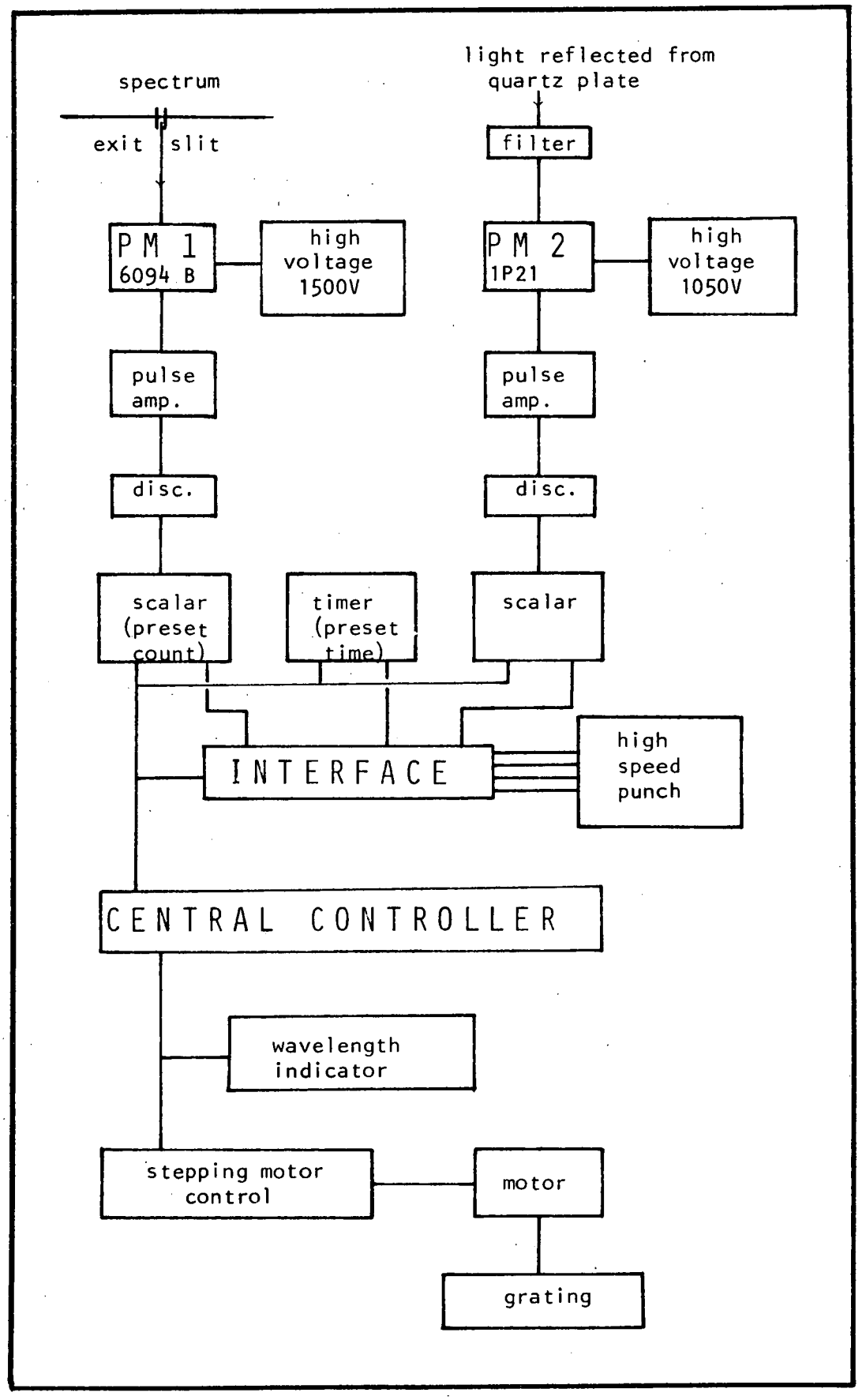

Figure A1.4 Block diagram of low-resolution scanner.

could not be determined in the time available, hence this instrument was not proceeded with any further.

A reduction program has been written for the PDP-8F computer to perform the data averaging, calculate the extinction coefficients and calculate the continuous energy distribution, plus the uncertainty in the results. This program is based on the program currently used for the reduction of the scanner data at the Mt. Stromlo Observatory, Canberra. A copy of this program was kindly loaned by Dr. R.D. Watson.

Appendix II

PHOTOMETRY DATA

(a) *ubvy* and Hβ photometry data* taken from Crawford, Barnes and Golson (1970), Strömgren and Perry (1965), and Crawford, Barnes, Faure and Golson (1966).

Star	HR	*b-y*	*c1*	*m1*	β
Ø Cas	382	0.492	1.473	0.008	2.664
α Per	1017	0.304	1.076	0.194	2.677
α Lep	1865	0.139	1.504	0.148	2.730
α Car	2326	0.110	1.512	0.128	2.732
δ CMa	2693	0.375	0.929	0.322	2.661
b Vel	3445	0.512	1.399	0.033	2.609
i Car	3699	0.123	1.542	0.130	2.755
ν Car	3890	0.193	1.400	0.116	2.724
195 Car	4110	0.402	1.189	-0.021	2.567
HD 97534	4352	0.420	1.188	-0.014	2.572
θ Sco	6553	0.234	1.010	0.189	2.670
i Sco	6615	0.337	1.459	0.107	2.676
89 Her	6685	0.230	1.361	0.130	2.645
π Sag	7264	0.227	1.082	0.161	2.702

* The *ubvy* and Hβ photometry data has now been brought together in a single publication by Lindemann and Hauck (1973).

(b) UBVRI photometry, UBV system of Johnson and Morgan (1953), combined with the RI system of Kron, White and Gascoigne (1953), data taken from Johnson, Mitchell, Iriarte and Wisniewski (1966) and the UBV data taken from Blanco, Demers, Douglass, and Fitzgerald (1968).

Star	HR	V	U-V	B-V	V-R	V-I
Ø Cas	382	4.99	1.17	0.68	0.64	1.20
α Per	1017	1.79	0.87	0.48	0.45	0.78
α Lep	1865	2.57	0.45	0.20	0.22	0.43
α Car	2326	-0.75	0.19	0.15	0.24	0.44
δ CMa	2693	1.80	1.18	0.68	-	-
b Vel	3445	3.83	0.98	0.70	0.63	1.23
i Car	3699	2.25	0.34	0.18	-	-
ν Car	3890	2.97	0.40	0.27	-	-
195 Car	4110	4.65	0.56	0.51	-	-
HD 97534	4352	4.60	0.60	0.55	-	-
θ Sco	6553	1.81	0.62	0.40	0.35	0.55
i Sco	6615	3.03	0.77	0.51	-	-
π Sag	7264	2.88	0.58	0.34	0.34	0.58

(c) UBVGRI photometry of Stebbins, Whitford and Kron taken from Kron (1958). The values of $E_{(P-V)}$ have been determined by Kron. Note that $E_{(P-V)} = E_{(B-V)}/1.78$.

Star	HR	U	V	B	G	R	I	$E_{(P-V)}$
Ø Cas	382	0.56	-0.03	0.08	0.00	-0.08	-0.33	0.43
α Per	1017	0.10	-0.27	-0.11	-0.02	0.13	0.22	0.11
α Lep	1865	-0.18	-0.58	-0.26	-0.01	0.28	0.48	0.09
δ CMa	2693	0.46	0.00	-0.03	0.00	0.00	0.08	0.02

Appendix III

HYDROGEN BALMER AND CALCIUM K LINE DATA

(i) Hydrogen Gamma Line Profiles

Star \ Δλ	0.0	0.5	1	2	4	6	8	12	16	20	25	N
α Lep	.12	.19	.30	.39	.56	.68	.77	.90	.96	.97	.985	2
α Car	.05	.20	.34	.47	.61	.72	.80	.88	.93	.96	.977	3
δ CMa	.06	.19	.43	.66	.86	.94	.97	.99	1.0	-		2
i Car	.13	.24	.33	.46	.64	.76	.83	.91	.95	.97	.985	2
ν Car	.17	.26	.37	.54	.76	.83	.88	.94	.98	.99	1.0	1
θ Sco[2]	.20	.23	.34	.57	.72	.80	.84	.94	.96	-	1.0	2
i Sco	.06	.18	.33	.59	.75	.82	.88	.95	.98	.99	1.0	3
π Sag	.15	.26	.38	.57	.72	.79	.85	.92	.95	.98	.995	1

(ii) Hydrogen Delta Line Profiles

Star \ Δλ	0.0	0.5	1	2	4	6	8	12	16	20	25	N
α Lep	.11	.22	.30	.42	.60	.72	.82	.94	.98	.99	1.0	2
α Car	.04	.23	.33	.48	.71	.85	.90	.96	.975	.985	.994	3
δ CMa[1,2]	.10	.33	.45	.57	.84	-	.94	-	1.0			1
b Vel[2]	.18	.30	.51	.71	.86	.92	.95	.99	1.0			1
i Car	.16	.28	.35	.44	.63	.78	.82	.90	.93	.97	.99	2
ν Car	.17	.26	.38	.56	.74	.83	.89	.94	.97	.99	1.0	1
195 Car[1,2]	.06	.20	.44	.70	.91	.98	1.0					1
HD 97534[b2]	.09	.16	.39	.69	.90	.98	1.0					1
θ Sco[2]	.24	.28	.39	.54	.69	.78	.84	.91	.95	.97	.99	2
i Sco	.04	.08	.22	.56	.75	.86	.91	.97	.99	1.0		2
π Sag	.14	.30	.45	.58	.70	.78	.84	.91	.95	.98	.995	1

(iii) H_8 Line Profiles

Star \ Δλ	0.0	0.5	1	2	4	6	8	12	16	20	N
α Lep	.15	.18	.35	.46	.64	.77	.86	.95	.99	1.0	2
α Car	.03	.12	.23	.36	.57	.69	.77	.91	.95	.98	3
δ CMa[1,2]	.09	.96	.58	-	.93	-	1.0				1
b Vel[2]	.20	.33	.54	.75	.88	.95	.98	1.0			1
i Car[2]	.16	.21	.32	.44	.64	.78	.86	.97	.99	1.0	2
ν Car	.12	.14	.22	.43	.70	.84	.93	.98	.99	1.0	1
195 Car[2]	.14	.25	.37	.69	.90	.96	.99	1.0			1
HD 97534[2]	.15	.15	.40	.69	.86	.98	1.0				1
θ Sco[2]	.19	.22	.27	.40	.59	.73	.85	.97	.99	1.0	2
i Sco[2]	.07	.13	.26	.47	.71	.84	.94	.98	.99	1.0	1
π Sag	.10	.25	.40	.50	.67	.78	.87	.94	.98	1.0	1

Notes.

1. Low accuracy because of large metal lines in the wings, (see text).

2. Low accuracy because of difficulty in placing the continuum, (Table 2.3).

N Refers to the number of plates averaged to give the profiles.

(iv) Balmer line Equivalent Widths

Star \ line	H_β	H_γ	H_δ	H_8	H_9	H_{10}	H_{11}	H_{12}	H_{13}	H_{14}	H_{15}
α Lep	8.4	9.7	8.4	8.2	8.6	7.9	5.9	5.2	3.9	2.5	1.7
α Car	11.5	10.0	9.8	9.8	8.9	7.5	6.0	3.7	2.9	2.2	2.0
δ CMa	6.5	4.3	4.8	3.2	3.1	-	-	-	-	-	-
b Vel	2.8	3.5	3.4	4.0	4.6	3.5	2.9	3.4	3.1	2.3	2.2
i Car	9.0	9.3	9.8	8.1	7.7	6.1	5.5	4.6	3.9	3.0	2.6
ν Car	7.0	7.4	7.6	6.6	6.0	5.5	4.6	3.6	2.7	2.2	1.6
195 Car	-	3.1	3.4	3.3	3.3	3.1	2.9	2.9	3.0	2.7	2.7
HD 97534	-	3.3	4.0	3.7	4.2	4.0	3.9	3.6	3.1	2.5	2.7
θ Sco	7.9	7.9	7.6	7.9	7.3	6.4	4.0	3.9	2.5	1.7	1.9
i Sco	-	6.6	6.4	6.6	6.4	5.9	6.1	5.8	4.7	3.4	2.6
π Sag	7.4	7.1	7.2	7.5	7.2	6.0	5.5	4.9	3.1	3.6	2.3

(v) Calcium K line profiles

Star \ Δλ	0.0	0.5	1	2	4	6	8	12	16	20	W	N
α Lep	.04	.05	.09	.24	.59	.81	.93	.98	1.0		7.5	2
α Car	.025	.04	.08	.29	.68	.86	.92	.98	1.0		7.2	3
δ CMa[1,2]	.04	.04	.05	.07	.15	.26	.40	.70	.81	.90	18.0	2
b Vel[2]	.07	.09	.15	.36	.70	.82	.90	.98	1.0		6.7	1
i Car	.03	.04	.09	.37	.78	.91	.96	.99	1.0		6.2	2
ν Car	.07	.10	.21	.48	.80	.93	.98	1.0			5.1	1
195 Car[1,2]	.07	.09	.23	.63	.85	.94	.98	1.0			4.3	1
HD 97534[1,2]	.05	.07	.24	.61	.85	.93	.97	1.0			4.3	1
θ Sco[2]	.04	.05	.07	.15	.35	.64	.83	.98	1.0		10.5	1
i Sco	.03	.04	.06	.12	.37	.67	.81	.95	1.0		10.7	2
π Sag	.03	.04	.07	.18	.45	.70	.81	.90	.98	1.0	10.8	1

Notes.

1. Low accuracy because of large metal lines in wings

2. Low accuracy because of difficulty in placing the continuum (Table 2.3)

N Refers to the number of plates averaged to give the profile.

Appendix IV

METAL LINE STRENGTHS

This Appendix contains the list of equivalent widths of all the unblended lines identifiable in the tracings of the Coudé plates that were obtained for the program stars. The number of plates averaged to give the mean equivalent widths tabulated in the operation is typically 2 or 3, and sometimes 4 for the stars studied at 1.4 and 2.1 $\mathring{A}\ mm^{-1}$ dispersion (i.e. α Lep, α Car, δ CMa, i Car, i Sco, θ Sco and π Sag). The equivalent widths of the stars studied at low dispersion (i.e. b Vel, ν Car, 195 Car and HD 97534) were taken from only one plate in each case.

In the Appendix the lines in all cases are grouped according to element, with lower atomic weights preceeding. The lines of the singly-ionized species are given for the high-dispersion stars, then the neutral lines of these stars, followed in a similar manner by the lines for the low-dispersion stars. Within each species, the lines are ordered in groups of increasing excitation potential, and within the groups of excitation potential, in order of increasing wavelength.

The tables contain the wavelength of the lines, the lower excitation potential, the value of log gf used in the abundance analysis and the measured equivalent widths in the form $-\log W/\lambda$. The sources of the log gf values are given at the end of the Appendix.

TABLE A4

ELEMENT MG II

EP	LAM	-LOG(GF)	ALEP	ACAR	DCMA	ICAR	ISCO	PI SAG
8.86	4481.13	-0.58	4.15	4.25	4.18	4.13	4.10	4.32
8.86	4481.34	-0.75	4.07	4.17	4.10	4.01	4.03	4.24

ELEMENT SI II

6.86	3856.03	0.66	4.03	4.20	3.89	4.29	3.74	4.23
6.86	3862.59	0.92	4.11	4.34	3.98	4.37	3.84	4.35
9.84	4128.10	-0.60		4.40	4.04	4.58		
9.84	4130.86	-0.77	4.20	4.38	3.99	4.35	4.32	4.62

ELEMENT CA II

0.00	3933.68	-0.14	2.72	2.69	2.34	2.82	2.56	2.56
0.00	3968.40	0.16	2.74	2.79	2.42	2.86	2.46	2.44
3.14	3706.04	0.46		3.82		3.95		
3.14	3736.92	0.16		4.02		4.00		
7.51	5001.47	0.53		4.81				
7.51	5021.15	1.23		5.38				
7.51	5307.23	0.88		5.25				
8.44	5339.21	0.05		4.89				

ELEMENT SC II

0.31	3923.50	2.22	5.12	5.34		5.48	4.73	
0.31	4246.84	-0.19	4.03	4.16	3.70	4.17	3.64	4.21
0.61	4294.78	1.27	4.40	4.68	4.11	4.76	4.16	4.70
0.61	4305.71	1.20	4.20	4.59	3.86	4.55	3.95	
0.61	4314.09	0.10	3.95	4.24		4.17	3.79	4.25
0.61	4325.00	0.37	4.00	4.25	3.71	4.32	3.79	4.33
0.61	4354.62	1.50	4.46	4.79	3.92	4.83	4.28	4.86
0.61	4374.47	0.45	4.03	4.27	3.80	4.34	3.86	4.24
0.61	4400.40	0.72	4.17	4.36	3.75	4.31	3.89	4.34
0.61	4415.56	0.84	4.21	4.44	3.83	4.39	3.89	
0.61	4420.67	2.32	5.14	5.42	5.21	5.42	4.73	5.34
0.61	4431.36	2.13	4.77	5.12	4.23	4.90	4.57	5.35
1.36	5031.02	0.38		4.42				
1.45	5239.82	0.50		4.42				

ELEMENT TI II

0.57	3685.20	-0.25	3.91	4.10		4.04		
0.57	3761.32	-0.14	3.88			4.10		
0.57	3774.65	2.08	4.34	4.67		4.63		
0.57	3814.59	1.54	4.07	4.28		4.38		
0.57	3981.99	1.72	4.24	4.42	3.86	4.53	3.86	
0.57	3987.61	1.01		4.59	4.09		4.00	4.71
0.57	4012.39	1.58	4.03	4.30	3.81	4.35	3.78	4.35
0.61	3759.30	-0.30	3.82	4.01		3.99		
0.61	3813.39	1.66	4.13	4.33		4.40		
0.61	4025.13	1.95	4.12	4.37	3.91	4.40	4.00	4.29
0.61	4056.19	2.46	4.35	4.80	4.09	4.72	4.29	4.71
1.08	4184.31	1.56	4.31	4.46	3.88	4.61	3.97	4.43
1.08	4294.14	0.90	4.01	4.15		4.27	3.73	4.19
1.08	4337.93	0.86	4.02	4.32	3.78	4.22	3.87	4.17
1.08	4344.29	1.73	4.21	4.46	3.94	4.38	4.07	4.24

TABLE A4 (CONT) ELEMENT I 111

EP	LAM	-LOG(GF)	ALEP	ACAR	DCMA	ICAR	ISCO	PI SAG
1.08	4344.29	1.73	4.21	4.46	3.94	4.38	4.07	4.24
1.08	4395.04	0.50	3.91	4.17	3.75	4.14	3.71	4.18
1.08	4443.81	0.68	4.05	4.18		4.19	3.73	4.25
1.08	4450.49	1.41	4.21	4.26	3.87	4.33	3.89	
1.08	4469.15	1.84		4.63		4.66		
1.08	4493.53	1.92	4.31	4.77	4.03	4.74	4.35	4.87
1.13	3900.54	0.13	3.94	4.07	3.64	4.18	3.69	4.06
1.13	3913.47	0.24	3.96	4.07	3.67	4.24	3.71	4.12
1.13	4341.37	1.76		4.65				
1.13	4444.56	1.86	4.27	4.43	3.99	4.51		4.50
1.13	4468.50	0.65			3.72	4.22	3.75	4.15
1.13	4501.28	0.79	4.11	4.21	3.71	4.17	3.78	4.19
1.13	4545.14	1.61	4.50	4.59	3.97	4.65	4.11	4.62
1.16	4290.23	0.84	3.99	4.10	3.77	4.23	3.79	
1.16	4300.05	0.55	3.93	4.02	3.76	4.21	3.66	4.14
1.16	4301.93	1.08	4.01	4.16	3.79	4.32	3.79	4.24
1.16	4312.88	1.05	4.01	4.18	3.79	4.29	3.77	4.28
1.16	4417.72	1.18	4.09	4.33	3.80	4.27	3.85	4.27
1.16	4464.46	1.66	4.16	4.30	3.87	4.39	3.96	4.35
1.16	4470.86	1.80	4.30	4.45	3.95	4.47	4.08	4.43
1.22	4391.93	2.03	4.36	4.66		4.69		
1.22	4394.07	1.47	4.19	4.31	3.90	4.43	3.95	4.57
1.22	4395.85	1.53	4.20	4.47	3.94	4.48	3.95	4.57
1.22	4399.78	1.06	4.17	4.31	3.87	4.28	3.87	
1.22	4409.25	2.07	4.34	4.78	4.10	4.80		
1.22	4409.53	2.07	4.34	4.78	4.04	4.80		
1.22	4418.34	1.67	4.23	4.60	3.90	4.43	4.04	4.43
1.22	4524.69	2.06		4.88		4.87		
1.22	4544.02	2.08	4.54	4.76	4.06	4.63	4.21	4.62
1.22	4563.77	0.86	4.04	4.18	3.73	4.13	3.77	4.16
1.22	4568.33	1.93	4.36	4.78	4.11	4.80	4.32	4.90
1.22	4589.95	1.61	4.24	4.31	3.83	4.29	3.95	4.36
1.57	3741.65	-0.03	3.98			4.15		
1.57	3776.06	0.84	4.20	4.50		4.41		
1.57	4529.49	1.52	4.36	4.48	4.05	4.45		4.45
1.57	4571.98	0.31		4.11	3.69		3.71	4.12
1.57	5188.70	0.82		4.24				
1.57	5226.54	0.97		4.24				
1.57	5336.79	1.35		4.43				
1.89	4028.34	0.65	4.13	4.34	3.82	4.35	3.83	4.26
1.89	4053.82	0.80		4.40		4.33		4.23
1.89	5129.16	0.93		4.38				
2.05	4316.80	1.07	4.26	4.50	4.01	4.61	3.98	4.66
2.05	4330.25	1.58	4.34	4.60	4.15	4.56		
2.05	4350.84	1.32	4.26	4.53	4.00	4.61	4.18	4.43
2.05	4374.82	1.04	4.23	4.46		4.56	4.04	4.43
2.05	4421.94	1.14	4.34	4.62	4.00	4.56		
2.05	4779.98	1.00	4.27	4.54	3.92	4.63		
2.05	4805.10	0.76	4.19	4.38	3.91	4.45		4.34
2.60	4174.08	0.84	4.37	4.55		4.69	4.19	
2.60	4367.68	0.39	4.13	4.43		4.49		
2.60	4386.85	0.46	4.16	4.34	3.88	4.44	4.07	4.57
3.11	4488.33	-0.01	4.30	4.43	3.89	4.46	4.06	4.48

TABLE A4 (CONT)

ELEMENT V2

EP	LAM	-LOG(GF)	ALEP	ACAR	DCMA	ICAR	ISCO	PI SAG
1.40	3850.40	2.01	4.81	5.03		5.05		
1.40	3866.72	1.24	4.28	4.74		4.87		
1.40	3896.14	1.11	4.27	4.52	3.92	4.66	4.07	
1.40	3916.41	0.80		4.51			3.98	
1.40	3929.72	1.37	4.64	4.80		4.82	4.42	
1.40	4002.93	1.28	4.58	4.69	4.06	4.66	4.32	
1.48	3903.26	0.86	4.22	4.40		4.62		
1.48	3951.96	0.52	4.25	4.46	3.91	4.42	3.87	4.37
1.48	3997.11	1.03	4.37	4.53		4.49	4.06	
1.48	4036.77	1.42	4.52	4.81	4.14	4.86	4.38	4.79
1.68	3715.47	-0.11	4.12	4.11		4.34		
1.68	3718.15	0.92	4.49	4.90		4.93		
1.68	4178.38	1.66	4.56	5.05		5.04		
1.68	4202.35	1.23	4.45	4.77		4.74		
1.68	4234.22	2.11	5.02	5.35	4.42	5.35		
1.79	3884.84	0.98	4.39	4.83	4.13	4.99	4.32	
1.79	3899.14	0.37	4.29	4.45	3.93	4.55	3.96	4.51
1.79	4005.65	0.22	4.16	4.43	3.87	4.40	3.91	4.35
1.79	4008.17	1.61	4.84	5.16	4.36	5.11	4.82	5.00
1.79	4023.38	0.36	4.31	4.48	3.83	4.53	3.95	4.42
1.79	4039.57	1.60	5.06	5.19	4.42	5.26		
1.79	4051.05	1.26		5.29	4.13	5.29	4.49	
2.04	4183.46	0.77	4.40	4.63	4.04	4.68	4.08	4.59
2.04	4225.21	1.07	4.60	4.85	4.15			
2.27	4564.57	1.15			4.31			
2.27	4600.20	1.36	4.78	5.13	4.46	5.11	4.69	
3.75	3985.79	0.33		5.56		5.65		

ELEMENT CR11

3.10	3715.18	1.02	4.14	4.35		4.37		
3.10	3738.36	1.14	4.14	4.40		4.37		
3.10	3754.56	1.44	4.27	4.48		4.40		
3.10	4051.92	2.10	4.39	4.65	4.08	4.61		
3.10	4111.00	1.86	4.27	4.58	3.91	4.50	4.01	4.48
3.10	4113.22	2.58	4.68	4.89	4.27	4.98	4.25	
3.10	4170.64	2.34		5.22		5.17	4.26	
3.10	4217.06	2.38		5.11	4.38	5.26		
3.87	4242.38	1.02	4.20	4.29	3.82	4.47	3.90	4.41
3.87	4246.42	3.05		5.37		5.55		
3.87	4252.63	1.85	4.51	4.53	4.08	4.74	4.06	4.63
3.87	4261.93	1.21	4.18	4.34	3.94	4.43	3.87	4.46
3.87	4269.29	2.06	4.52	4.79	4.16	4.84	4.11	4.60
3.87	4275.56	1.34	4.30	4.40	4.05	4.57	3.93	4.57
3.87	4284.23	1.64	4.40	4.61	3.95	4.65	4.15	4.55
3.87	4812.35	1.39	4.52	4.64	4.24	4.78		
3.87	4824.14	1.01	4.26	4.34	3.92	4.41	3.88	4.05
3.87	4836.24	1.89	4.49	4.57	4.12	4.66	4.17	4.43
3.87	4848.25	1.13	4.30	4.38	3.92	4.43	3.95	4.14
3.87	4856.19	2.06	4.59	4.86		4.89		4.50
3.87	4864.32	1.46	4.53	4.52	4.06	4.60	4.04	4.31
3.87	4876.40	1.56	4.48	4.51	4.09	4.61		4.29
3.87	4876.48	1.94	4.69	4.69	4.29	4.81		4.48
4.07	4554.99	1.44	4.32	4.46	4.06	4.45	4.01	4.47

TABLE A4 (CONT) ELEMENT CR11

EP	LAM	-LOG(GF)	ALEP	ACAR	DCMA	ICAR	ISCO	PI SAG
4.07	4558.65	0.31	4.10	4.22	3.83	4.15	3.83	4.20
4.07	4588.20	0.65	4.27	4.29	3.90	4.27	3.90	4.33
4.07	4592.06	1.37	4.52	4.44	3.96	4.45	4.08	4.38
4.07	4616.63	1.51	4.32	4.49	4.02	4.49	4.10	4.36
4.07	4618.79	0.98	4.35	4.33	3.97	4.33	4.03	4.27
4.07	4634.04	1.19	4.31	4.36	3.94	4.35	4.02	4.44
4.07	5237.32	0.15		4.30				
4.07	5334.87	0.62		4.47				
5.32	4145.76	1.14	4.77	4.59	4.07	4.79		4.71
5.32	4224.86	1.27		4.89				
6.48	4049.00	-1.80				5.18		

ELEMENT MN II

1.81	4174.32	3.32	4.74	4.95		4.97		
1.81	4205.39	3.26	4.59	4.75		4.73		
5.40	4326.62	0.90	4.79	5.26		5.19		

ELEMENT FE11

1.67	3938.30	3.40	4.25	4.45		4.34	3.81	4.27
2.28	3746.57	2.99	4.42					
2.56	3824.93	2.28	4.27	4.50				
2.56	4128.74	2.86	4.33	4.60	4.01	4.53	3.95	4.46
2.56	4178.86	2.00	4.02	4.16	3.72	4.29	3.72	4.17
2.56	4233.17	1.43	4.06	4.23	3.78	4.17	3.55	4.15
2.56	4648.95	2.94						4.53
2.70	3974.17	2.58	4.52					
2.70	4273.33	2.27	4.17	4.44	3.93	4.43		
2.70	4296.58	2.36	4.09	4.38	3.79	4.37	3.88	4.31
2.70	4303.18	2.00	4.05	4.33	3.79	4.30	3.80	4.31
2.70	4413.59	3.20	4.46	4.85	4.08	4.80		
2.78	4369.41	2.90	4.17	4.57	4.04	4.46		
2.78	4385.39	2.02	4.03	4.26	3.83	4.27	3.85	4.22
2.78	4416.83	2.09	4.12	4.80	3.78	4.25	3.85	4.31
2.78	4489.18	2.23	4.19	4.32	3.81	4.33	3.94	4.32
2.83	4472.93	2.67	4.28	4.49	3.90	4.47		
2.83	4491.41	2.09	4.20	4.31	3.90	4.31	3.94	4.36
2.83	4508.29	1.76	4.10	4.24	3.88	4.20	3.83	4.30
2.83	4515.34	1.91	4.06	4.22	3.86	4.22	3.89	4.23
2.83	4520.23	1.87	4.14	4.29	3.81	4.23	3.86	4.27
2.83	4522.64	1.51	4.04	4.16	3.73	4.14	3.78	4.13
2.83	4541.52	2.29	4.25	4.34	3.92	4.33	3.95	4.37
2.83	4555.89	1.79	4.05	4.21	3.91	4.14	3.78	4.14
2.83	4576.34	2.22	4.29	4.34	3.91	4.30	3.92	
2.83	4582.83	2.44	4.29	4.41	3.85	4.38	3.97	4.41
2.83	4583.84	1.25	4.01	4.11	3.78	4.07	3.71	4.12
2.83	4620.52	2.63	4.31	4.43	4.06	4.38	4.01	4.38
2.83	4629.34	1.78	4.14	4.20	3.85	4.15	3.87	4.20
2.83	4663.71	3.02	4.56	4.69	4.49	4.57	4.27	4.61

TABLE A4 (CONT) ELEMENT FE11

EP	TAM -LOG(GF)		AFEP	ACAR	DCMA	ICAR	ISCO	PT SAG
2.83	4666.75	2.50	4.30	4.34	4.04	4.33	4.10	4.35
2.83	4731.47	2.28	4.29	4.38	3.98	4.62	3.95	4.31
2.89	4923.93	0.70		4.15	3.68	4.12		
4.73	3755.57	1.89	4.60	4.91		4.88		
4.73	3781.52	2.20	4.52	4.86		5.02		
4.73	3827.08	1.80	4.33	4.58		4.64	3.91	
5.57	3906.03	1.39		4.81		4.77	4.16	
5.91	3938.97	1.39	4.70	4.90		4.90	4.40	4.82
5.91	4635.31	0.95	4.54	4.71	4.36	4.67	4.27	4.71
7.87	4631.90	0.88		5.82				
7.87	4652.28	0.50		5.71				
				ELEMENT NI II				
3.10	3769.46	0.03		4.44			3.88	
4.03	4015.48	1.25	4.38	4.77	4.23	4.66	4.40	4.80
4.03	4244.81	2.03	4.92	5.11	4.44	5.31	4.93	5.33
4.03	4362.10	1.43	4.53	4.77	4.36	4.98	4.48	4.93
				ELEMENT SR II				
0.00	4077.72	0.58	3.79	4.11	3.51	4.11	3.53	3.93
0.00	4215.54	0.70	4.02	4.15	3.67	4.17	3.62	3.98
2.94	4161.78	0.50		4.89		5.04		
				ELEMENT Y11				
0.02	3710.29	-0.59	4.08	4.33		4.30		
0.10	3747.55	0.86	4.49	4.87		4.88		
0.10	3788.70	-0.10	4.18	4.43		4.52	3.81	
0.10	3818.34	0.71	4.50	4.74		4.82	3.97	
0.10	3950.36	0.44	4.39	4.61	4.01	4.61	3.92	4.52
0.10	4358.72	0.53	4.41		4.04			
0.13	3774.33	-0.36	4.15	4.44		4.39	3.76	
0.18	4309.63	0.98	4.49	4.67	3.94	4.73	4.08	4.52
0.41	4374.94	0.27	4.34	4.46		4.56	3.90	
1.00	4854.87	0.27	4.46	4.95	3.97	4.93	4.07	4.75
1.00	4883.69	-0.17	4.32	4.45	3.88	4.48	3.98	4.29
1.00	4900.12	-0.01	4.35	4.51	3.87	4.68	4.04	4.43
1.00	5087.43	0.17		4.56				
1.00	5119.12	1.31		5.28				
1.00	5123.22	0.88		5.11				
1.00	5200.42	0.63		4.94				
1.00	5205.73	0.28		4.72				
1.00	5509.91	0.82		5.26				
1.74	5473.39	0.75		5.42				
1.84	5402.78	1.21		4.98				
				ELEMENT EU II				
0.00	3819.69	-0.02	4.58	5.10		5.18	4.74	4.77
0.00	4129.72	0.31	4.74	5.34		5.27	4.92	4.92
				ELEMENT GD II				
0.60	3768.39	-0.25		5.67		5.58		
0.60	4130.37	-0.10		5.77		5.62		

TABLE A4 (CONT)

EP	LAM	-LOG(GF)	ALEP	ACAR	DCMA	ICAR	ISCO	PI	SAG
				ELEMENT ZR II					
0.53	3766.82	0.76	4.45	4.85		4.67			
0.53	3817.58	0.88	4.41	4.63		4.74			
0.53	3915.94	0.89	4.52	4.66			4.01		
0.53	3999.00	0.50	4.29	4.54	3.95	4.57			
0.53	4211.90	1.21	4.56	4.81	4.09	4.82	4.16	4.74	
0.71	3991.12	0.30	4.32	4.66	3.97	4.59			
0.71	4050.33	0.96	4.46	5.04	4.12	4.95	4.16		
0.71	4156.24	0.85	4.58	4.50	3.99	4.76	4.09		
0.71	4161.21	0.71	4.50	4.46		4.69			
0.71	4208.99	0.54	4.48	4.58	3.94	4.70	4.06	4.62	
0.71	4496.97	1.13		4.95	4.24	4.95	4.35	4.75	
0.80	4034.09	1.58	4.77	5.19	4.43	5.40	4.70		
0.80	4149.20	0.13	4.18	4.54	3.81	4.42	3.88	4.30	
0.96	4613.92	1.30		5.28		5.66		5.06	
1.49	4443.00	0.49	4.69	4.90		4.90			
1.76	4251.61	0.72	4.97	5.26	4.37	5.48	4.67		
				ELEMENT BA II					
0.00	4554.04	-0.19	4.17	4.28	3.72	4.24	3.92	4.18	
0.00	4934.03	0.13		4.36		4.33			
2.72	4130.66	-0.56		4.88	4.14	4.88	4.77		
2.72	4165.99	0.39	4.88	5.30	4.42	5.26	4.92	4.84	
				ELEMENT LA II					
0.17	3995.75	0.58	4.74	5.12	4.06	5.12	4.57		
0.17	4333.76	0.60		5.15	4.03	5.03	4.68		
0.32	4123.23	0.40		4.84	3.91		4.38		
0.40	3988.53	0.26		4.99		5.03	4.45		
				ELEMENT CE II					
0.11	4429.29	-0.07		5.74					
0.32	3940.36	0.43		5.52		5.69			
0.32	3960.92	0.43	4.86	5.18	4.39	5.39			
0.32	3999.24	-0.09	4.89	5.37		5.10			
0.32	4120.83	0.74	5.14	5.84	4.50	6.01			
0.32	4486.91	0.62	5.65	5.95	4.48	5.95			
0.48	4562.37	0.07	5.15	5.36	4.31	5.62			
0.52	3848.61	0.08	4.89	5.63		5.51			
0.52	4014.93	0.23	5.56	5.70	4.43	5.60			
0.52	4042.59	0.22		5.65	4.31	5.65			
0.52	4073.49	-0.05	4.83	4.91		5.46			
0.52	4364.66	0.35	5.24	5.69	4.39	5.94			
0.52	4628.16	0.14	4.87	5.22	4.31				
0.61	4214.04	0.58	5.72	6.15	4.62	5.78			
0.70	4068.84	-0.36	4.83	5.91	4.43	5.91			
0.70	4193.11	0.10	5.02	5.04	4.38	5.78			
0.70	4349.80	0.40	5.34	5.68	4.54	6.04			
0.70	4382.18	0.17	5.16	5.44	4.34	5.80			
0.86	3942.75	-0.64	4.90	5.12		5.29			
0.86	3993.11	0.10	5.20	5.56					
0.86	4186.62	-0.67	4.56	4.92	4.02	5.28			
0.93	3993.83	-0.21	5.00	5.65		5.65			
0.93	4497.86	0.49		5.75					
0.93	4560.28	0.15	5.13	5.55	4.55	6.18			

TABLE A4 (CONT)

EP	LAM	-LOG(GF)	ALEP	ACAR	DCMA	ICAR	ISCO	PI SAG
				ELEMENT C I				
7.49	4770.00	2.28	5.38	5.11	4.83	5.20	4.98	4.90
7.49	4771.71	1.70	4.64	4.71	4.26	4.78	4.50	4.38
7.49	4775.86	2.20	5.05	4.95	4.60	5.36	4.78	4.69
7.68	5380.32	1.82		4.69				
				ELEMENT NA I				
2.10	4494.20	1.82		5.81				
2.10	4497.68	1.52		5.75				
2.10	4668.57	1.25		5.44				
2.10	4982.83	0.91		5.10				
				ELEMENT MG I				
0.00	4571.10	5.40	5.10	5.58	4.40	5.48	4.88	
2.71	3829.36	0.21	4.00	4.19	3.62	4.15	3.74	3.93
2.71	3832.31	0.33	4.04	4.20	3.68	4.13	3.82	4.00
2.71	3838.30	0.33	4.06	4.16	3.63	4.11	3.81	4.04
2.71	5172.69	0.38		4.17				
2.71	5183.62	0.16		4.18				
4.34	3986.76	1.91		4.54				4.52
4.34	4703.00	0.58	4.31	4.40	4.07	4.64	4.29	4.28
4.34	4730.03	2.04	5.20	5.44	4.77	5.72	5.20	4.98
				ELEMENT AL I				
0.00	3944.02	-0.62	4.20	4.29	4.02	4.32	3.91	4.04
0.00	3961.11	-0.32	4.24	4.31	3.86	4.27	3.85	4.15
				ELEMENT SI I				
1.91	3905.53	0.67	4.04	4.16	3.69	4.25	3.75	3.97
				ELEMENT CA1				
0.00	4226.74	-0.24	4.09	4.13	3.69	4.23	3.75	3.98
1.88	4283.01	0.26	4.54	4.63	4.10	4.80	4.40	4.52
1.88	4289.37	0.30	4.41	4.65	4.10	4.87		
1.88	4298.99	0.41		4.72		4.90		
1.88	4302.54	-0.27	4.31	4.42		4.60		
1.88	4318.66	0.21	4.51	4.61	4.12	4.81	4.33	4.50
1.88	4425.44	0.56	4.59	4.87	4.23	4.77	4.57	4.57
1.88	4434.97	0.26	4.55	4.63	4.09	4.65	4.43	4.48
1.88	4435.69	0.69	4.61	4.85	4.35	4.80	4.69	4.64
1.88	4454.79	-0.25	4.28	4.39	4.00	4.46	4.22	4.25
1.88	4455.89	0.51	4.67	4.75	4.22	4.80	4.65	4.49
2.52	4578.56	0.56	4.88	5.32	4.58	5.36		5.18
2.52	4585.87	0.19	4.68	5.05	4.40	5.06	4.88	4.76
2.71	4355.09	0.43	4.94	5.30	4.60	5.49	5.04	
2.71	4526.93	0.43		5.35	4.58	5.19	5.11	4.96
2.93	4685.27	0.88	5.31					
2.93	5512.98	0.29		5.28				

TABLE A4 (CONT) ELEMENT I 1

EP	LAM	-LOG(GF)	ALEP	ACAR	DCMA	ICAR	ISCO	PI SAG
0.00	3741.06	0.10	4.79	5.34		5.40		
0.00	3989.77	-0.01	4.54	4.78	4.20	4.78	4.70	4.49
0.05	3752.86	-0.11		5.11		5.07		
0.05	3998.64	-0.16	4.89	5.00	4.30	5.02		
0.05	4681.92	0.99		5.77				
0.05	5210.39	0.90		5.49				
0.84	4298.68	-0.22		5.63				
0.84	4301.10	-0.54	4.93	5.29		5.35	5.03	4.68
0.84	4512.74	0.25		5.42				
0.84	4533.25	-0.64	4.81	5.29	4.24	5.02	4.96	4.62
0.84	4534.78	-0.41	5.18	5.24	4.40	5.51		5.18
0.84	4535.57	-0.22	5.05	5.36	4.40	5.36	5.26	4.88
0.84	4552.46	0.17		5.38				
0.84	4981.74	-0.57		5.14				
0.84	4999.51	-0.38		5.21				
1.73	4617.28	-0.71		5.71	4.89	5.97	5.27	5.36
				ELEMENT V I				
0.00	3844.45	0.97	5.11			5.98		
0.00	4030.76	0.48					4.09	
0.00	4033.07	0.64					4.20	
0.00	4034.49	0.88					4.26	
0.30	4111.79	-0.45	4.46	5.47	4.44	5.20		
0.30	4379.24	-0.48	5.04	5.39	4.41	5.80		5.56
0.30	4389.99	-0.05	5.34	6.04	4.77	5.69		
2.11	4018.10	-0.35					4.56	
2.13	4296.08	-0.57	5.33	5.52		5.93		5.24
2.28	4754.04	-0.13					4.90	
2.28	4783.42	-0.11					4.88	
2.64	4055.55	-0.47					5.06	
2.90	4451.59	-0.69					4.61	
2.90	4766.42	-0.45					4.98	
3.07	4061.73	-0.92					5.01	
3.07	4458.25	-0.40					5.35	
				ELEMENT CR1				
0.00	4254.35	0.27	4.12	4.41	3.90	4.42	3.94	4.28
0.00	4274.81	0.39	4.20	4.46	4.02	4.49	3.99	4.34
0.00	4289.73	0.58	4.17	4.60		4.59	4.04	
0.98	3921.05	0.69		4.92		5.09	4.55	4.89
0.98	4371.29	0.90	4.60					
0.98	4545.96	0.97	5.11	5.43	4.56	5.40	5.18	
0.98	4600.75	1.02		5.62	4.62	5.49		
0.98	4613.36	1.37	4.97	5.23	4.66	5.55	5.06	
0.98	4616.13	0.95		5.23	4.66	5.39	4.97	
0.98	4626.18	1.00	4.82	5.16	4.55	5.52	4.82	5.19
0.98	4651.29	0.97		5.39	4.65	5.71	5.27	5.22
0.98	4652.17	0.79	4.80	5.15	4.47	5.16	4.97	5.01
0.98	5204.51	0.19		4.57				
0.98	5206.04	-0.01		4.50				
0.98	5208.43	-0.12		4.56				
0.98	5298.28	1.07		5.17				

TABLE 44 (CONT) ELEMENT CR1

EP	LAM	-LOG(GF)	ALFP	ACAR	DCMA	ICAR	ISCO	RI	SAG
0.98	5345.81	0.98		5.02					
1.03	3941.50	0.82		5.27		5.45	4.75		
1.03	4646.17	0.49	4.72	4.93	4.34	5.01	4.76	4.61	
2.54	3963.69	-1.34	4.81			4.85		4.77	
2.71	3849.01	-0.54		5.24		5.28			
3.01	4379.77	-1.36						4.75	
3.01	4693.95	-0.01	5.37		5.01	5.63			
3.09	4500.30	-0.24	4.81			5.02			
3.09	4511.90	-0.37	5.40		4.70	5.70	5.05		
3.09	4540.71	-0.78	5.06	5.30	4.66	5.62			
3.09	4756.12	-0.87	5.21	5.47	4.72	5.90			
3.19	4708.02	-0.70		5.50					
3.19	4718.42	-0.82	5.42	5.33	4.74	5.59			
3.19	4708.02	-0.70	5.35		4.72	5.97			
3.55	4764.29	-0.38				5.28			
3.87	4001.45	-1.05	5.30	5.82		5.56			
3.87	4039.10	-1.13	5.31	5.61	4.83	5.70			
3.87	4280.40	-0.79	5.15	5.68	4.93	5.68			
3.98	4192.10	-0.46	5.32			5.16	4.84		
4.18	4752.10	-0.88		5.77	5.25				

ELEMENT MN1

0.00	4030.76	0.48	4.26	4.39	3.91	4.38		4.13
0.00	4033.07	0.64	4.35	4.56	3.95	4.53		4.23
0.00	4034.49	0.88	4.43	4.63	4.00	4.63		4.21
2.11	3809.58	-0.34	4.62					
2.11	4018.10	-0.35	4.68	4.99	4.17	5.00		
2.28	4754.04	-0.13	4.89	5.07	4.38	5.28		4.56
2.28	4783.42	-0.11	4.69	4.90	4.34	5.11		4.36
2.28	4823.51	-0.15	4.84	4.91	4.27	5.10		
2.64	4035.55	-0.47	4.61	5.13	4.37	5.29		4.70
2.90	4235.14	-0.47	4.97	5.48		5.67		
2.90	4235.29	-0.58		5.33	4.37	5.48		
2.90	4265.93	-0.37		5.73				
2.90	4281.10	-0.31	4.91	5.49	4.38	5.49		5.03
2.90	4451.59	-0.69	4.61	4.81	4.35	4.83		4.72
2.90	4498.90	-0.21	5.10	5.35	4.93	5.51		
2.90	4709.72	0.05	5.42	5.67	4.74	5.77		5.08
2.90	4739.11	0.12		5.98	4.83			
2.90	4761.52	-0.03	5.28	5.50	4.68	5.83		
2.90	4762.37	-0.60	4.64	4.77	4.38	4.89		
2.90	4765.86	-0.25		5.30	4.64	5.50		4.72
2.90	4766.42	-0.45	4.90	5.10	4.38	5.25		4.64
3.07	4061.73	-0.92	4.71	5.21	4.31	5.18		
3.07	4458.25	-0.40	5.22	5.33		5.50		
3.13	4026.44	-0.27	5.06	5.60	4.76	5.53		

TABLE A4 (CONT) ELEMENT FE1

EP	LAM	-LOG(GF)	ALEP	ACAR	DCMA	ICAR	ISCO	PI	SAG
0.00	3719.95	0.32		4.17		4.16			
0.00	3859.92	0.57	4.00	4.15	3.67	4.25	3.77	3.92	
0.00	4216.19	2.98	4.69	4.83		4.93			
0.00	4375.94	2.57	4.41	4.72	3.96	4.83	4.53	4.55	
0.05	3705.58	1.10	4.21			4.25			
0.05	3856.38	1.15	4.10	4.20	3.71	4.31	3.81	4.07	
0.05	3886.29	0.90	4.12	4.16	3.74	4.35	3.89		
0.05	3922.92	1.44	4.12	4.29	3.86	4.33			
0.05	4199.99	4.21		5.58	4.83	5.48			
0.05	4389.25	3.90		5.94	4.64				
0.05	4427.32	2.51	4.57	4.73	3.96	4.66			
0.09	3745.57	0.63	4.12	4.24		4.21			
0.09	3899.72	1.32	4.19	4.27	3.78	4.40	3.94	4.12	
0.09	3930.31	1.31	4.25	4.23		4.31			
0.11	3895.67	1.44	4.13	4.24		4.34	3.94		
0.11	3920.27	1.49	4.19	4.33	3.74	4.42	3.89	4.15	
0.91	3820.44	-0.41	4.07	4.12		4.25			
0.91	3825.89	-0.24	4.09	4.15		4.26		4.00	
0.91	3887.06	0.81		4.36		4.54	3.99		
0.91	4174.92	2.34	4.55	5.24	4.00	5.04	4.92	4.72	
0.91	4994.14	2.90		5.22					
0.91	5012.07	2.41		4.90					
0.91	5127.37	2.91		5.23					
0.91	5269.55	1.35		4.47					
0.91	5328.05	1.46		4.82					
0.91	5397.14	1.88		4.73					
0.96	3709.26	0.30	4.23	4.29		4.26			
0.96	3727.63	0.30	4.05	4.36		4.29			
0.96	3758.25	-0.31	4.04	4.26		4.23			
0.96	3799.56	0.47	4.26						
0.96	3834.23	-0.01	4.11	4.17		4.22			
0.96	5083.34	2.74		4.99					
0.96	5501.48	2.66		4.98					
1.00	3767.20	0.02				4.27			
1.00	3787.89	0.47	4.11	4.32		4.37			
1.00	3790.10	1.18	4.23	4.50		4.61			
1.00	3795.01	0.38	4.19	4.32		4.36			
1.00	3840.45	0.20	4.12	4.28		4.27	3.81	4.08	
1.00	3849.98	0.44	4.12	4.28		4.34		4.11	
1.00	3850.83	1.22	4.20	4.40		4.53	4.04	4.22	
1.00	3865.53	0.57	4.10	4.23	3.76	4.28	3.89	4.18	
1.00	5434.53	1.97		4.74					
1.00	5506.79	2.44		5.04					
1.48	3815.85	-0.60	4.12	4.22		4.29			
1.48	4032.64	1.79		4.92					
1.48	4045.83	-0.68	3.94	4.17	3.61	4.27	3.79	3.92	
1.48	4147.68	1.48	4.64	4.64	4.00	4.96	4.50	4.47	
1.48	4202.04	0.25	4.20	4.30		4.40			
1.48	4271.77	-0.20	4.06	4.25	3.82	4.28	3.81		
1.48	4383.56	-0.35	4.02	4.12	3.68	4.21	3.83	4.13	
1.48	4602.95	1.46	4.59	4.76		4.84	4.52	4.58	
1.48	4733.59	2.38	5.18	5.28	4.45				
1.48	5171.61	1.28		4.58					
1.56	3827.83	-0.55	4.11	4.19		4.24		3.97	

TABLE A4 (CONT) ELEMENT FE1

EP	LAM	-LOG(GF)	ALEP	ACAR	DCMA	ICAR	ISCO	PI SAG
1.56	4005.25	0.07	4.16	4.35		4.34	3.90	4.20
1.56	4063.60	-0.44	4.07	4.28	3.59	4.25	3.85	4.05
1.56	4143.88	0.07	4.20	4.32	3.89	4.35	3.96	
1.56	4337.05	1.15	4.48	4.83	3.97	4.64		
1.56	4404.76	-0.25	4.10	4.32	3.77	4.31	3.94	
1.56	5194.95	1.63		4.81				
1.56	5328.54	1.50		4.64				
1.56	5332.90	2.36		5.09				
1.61	3841.06	-0.47	4.00	4.43		4.32	3.80	4.08
1.61	4071.75	-0.42		4.19	3.72	4.30	3.87	4.17
1.61	4132.07	0.16		4.27	3.74	4.37	3.93	4.22
1.61	4325.78	-0.24	4.05	4.13	3.75	4.21	3.90	4.09
1.61	4602.01	2.50		5.55	4.53	5.49		
1.61	5216.28	1.65		4.80				
1.61	5341.03	1.59		4.75				
2.18	3753.62	0.07	4.46	4.73		4.65		
2.18	3852.58	-0.57	4.37	4.60	3.89	4.68	4.14	4.22
2.18	3949.96	0.48	4.56	4.59		4.76		
2.18	4233.61	-0.09		4.51	3.83	4.63		
2.18	4282.41	0.26	4.35	4.36	3.85	4.52	4.15	4.42
2.22	3760.54	0.47	4.50	4.86		4.88		
2.22	3781.19	1.40	4.84	5.06		5.37		
2.22	3807.54	0.33		4.52		4.70		
2.22	3977.75	0.28	4.40	4.53	4.00	4.60	4.16	4.38
2.22	4352.74	0.56	4.38	4.57	3.95	4.74	4.38	
2.22	4408.43	0.95	4.62	4.95	4.03	4.93		
2.22	4430.62	1.02	4.73	4.90	4.20	4.83		
2.22	4442.35	0.50	4.49	4.88	3.94			
2.22	4447.73	0.48	4.50	4.67	3.97	4.72	4.52	4.50
2.22	4494.57	0.35	4.38	4.52	3.95	4.59	4.25	
2.22	5049.83	1.00		4.73				
2.22	5079.23	1.45		5.03				
2.22	5198.72	1.50		5.10				
2.22	5250.65	1.52		5.04				
2.42	3845.47	0.56	4.35	4.58		4.58		
2.42	3859.22	-0.06	4.29	4.51	3.96	4.64	4.07	
2.42	3885.52	0.36	4.63	4.68		4.93	4.33	
2.42	4187.05	-0.17	4.30	4.42	3.89	4.60	4.14	4.23
2.42	4187.81	-0.13	4.24	4.36	3.94	4.48	4.08	4.23
2.42	4235.95	-0.31	4.28	4.31		4.55	3.96	
2.42	4260.49	-0.63	4.15	4.22	3.87	4.40	3.93	4.09
2.42	4271.16	-0.25	4.29	4.47	3.90	4.48	3.96	
2.47	3794.35	0.19	4.47	4.72		4.75		
2.47	4191.44	-0.06	4.23	4.42	3.83	4.58	4.15	4.28
2.47	4222.22	0.35	4.40	4.49	4.00	4.80		4.41
2.47	4250.13	-0.25	4.32	4.40	3.91	4.57	4.01	4.25
2.59	3867.93	1.09			4.41		4.97	
2.59	4067.28	0.52	4.61	4.87		4.83		
2.69	3864.37	0.40	4.65	4.76	4.13	4.96	4.36	
2.69	3952.62	0.26	4.50	4.65	3.91	4.60	4.34	4.42
2.69	3998.05	-0.05	4.48	4.56		4.62	4.24	
2.76	3907.94	0.30	4.50	4.81	4.07	4.92	4.51	4.68
2.76	3995.99	0.67	4.82	4.95		5.08		
2.76	4007.28	0.45	4.59	4.90	4.28	4.99	4.70	

TABLE A4 (CONT) ELEMENT FE1

EP	LAM	-LOG(GF)	ALEP	ACAR	DCMA	ICAR	ISCO	PI SAG
2.76	4021.87	-0.12	4.41	4.49	3.95	4.66	4.30	4.43
2.76	4206.97	0.87	4.91	4.96	4.40	5.29	4.63	
2.85	3808.73	0.30	4.54	4.61		4.84		
2.85	3809.05	0.93	5.06	5.10		5.68		
2.85	3925.65	0.22	4.67	4.79		4.93		
2.85	3942.45	0.22	4.55	4.86		4.90	4.45	4.29
2.85	4032.46	1.25		5.13				
2.85	4062.45	-0.05	4.50	4.88	3.86	4.81	4.49	4.66
2.85	4107.49	-0.07	4.44	4.61	3.96	4.68	4.36	4.74
2.85	4132.91	0.09	4.63	4.63	4.01	4.88	4.44	
2.85	4134.69	-0.18	4.44	4.49	3.91	4.67	4.19	4.35
2.85	4156.81	-0.12	4.34	4.54	3.86	4.67	4.26	4.39
2.85	4175.64	-0.09	4.37	4.65	3.95	4.81		
2.85	4181.76	-0.45		4.52	3.89	4.52		
2.85	4184.90	0.06	4.51	4.68	4.06	4.86		4.59
2.85	4213.65	0.56	4.85	4.97	4.32	5.16	4.62	4.77
2.85	4443.20	0.22		4.74		4.85		
2.85	4454.39	0.51		4.85		5.00		
2.85	4466.53	-0.18	4.42	4.55		4.66	4.33	4.42
2.85	4741.53	1.17		5.40	4.68			
2.85	4871.32	-0.11	4.40	4.49	3.99	4.54	4.26	4.26
2.85	4872.14	0.05	4.53	4.64	4.06	4.60	4.35	4.35
2.85	4890.76	0.09	4.35	4.52	3.95	4.60	4.29	4.21
2.85	4891.50	-0.17	4.34	4.46	3.94	4.56	4.21	4.14
2.85	4919.00	-0.02		4.57	3.94	4.62	4.21	4.09
2.85	4920.51	-0.30		4.43	3.91	4.47	4.09	4.05
2.85	4938.82	0.62		4.95		5.22		
2.85	4985.55	1.03		5.25				
2.85	5006.12	0.33		4.62				
2.99	3701.09	-1.15				4.46		
2.99	3701.95	-1.15		4.15				
2.99	3707.04	-0.75	4.39	4.40		4.68		
2.99	4000.46	0.69		5.10		5.03		4.81
2.99	4120.21	0.38	4.73	4.92		5.08		4.73
2.99	4348.95	1.38		5.79				
2.99	4647.44	0.47	4.74	4.90	4.30	4.93		4.63
2.99	4691.42	0.59		5.07	4.33	5.47		4.58
2.99	5192.35	-0.18		4.47				
3.05	3744.11	-0.35	4.40	4.90		4.83		
3.05	3766.66	0.31	4.67	4.89		4.88		
3.05	3839.26	-0.53	4.53	4.69		4.69		
3.05	3867.22	-0.31	4.44	4.66	3.98	4.77	4.21	4.41
3.05	3955.96	0.55	4.86	5.18		5.17		
3.05	3990.38	0.62		5.15		5.26		
3.05	3994.12	0.59	4.89	5.19	4.31	4.97	4.93	
3.05	4074.79	0.12	4.67	4.87	4.06	4.98	4.57	4.63
3.05	4143.42	-0.65	4.20	4.50	3.89	4.56	4.14	
3.05	4182.39	0.35	4.67	5.02		5.12	4.42	
3.05	4199.11	-0.84	4.30	4.37	3.89	4.53	4.00	4.19
3.05	4248.23	0.51	4.82	5.07	4.29	5.11	4.70	
3.05	4267.83	0.31		5.07	4.40			
3.05	4298.04	0.55	4.78	4.98	4.29	5.40	4.76	
3.05	4387.90	0.62		4.97	4.36	5.28	4.74	
3.05	4390.97	0.62		4.59				

TABLE A4 (CONT) ELEMENT FE1

EP	LAM	-LOG(GF)	ALEP	ACAR	DCMA	ICAR	ISCO	PI SAG
3.05	4740.34	1.69		5.30				
3.05	5266.56	-0.09		4.52				
3.05	5281.80	0.25		4.79				
3.25	3740.24	-0.45	4.48	4.88		4.96		
3.25	3765.55	-1.31	4.25	4.53		4.32		
3.25	3821.19	-1.09	4.33	4.54		4.60		
3.25	3846.81	-0.79	4.29	4.54		4.55	4.15	4.35
3.25	3941.28	0.35	4.82	4.97		5.03		
3.25	3947.02	0.18	4.69	4.99	4.30	4.92		
3.25	3948.11	-0.20	4.55	4.68		4.83	4.45	
3.25	3948.78	-0.55		4.58		4.64		
3.25	3951.17	-0.46	4.57	4.63		4.72	4.48	
3.25	3955.36	0.32	4.72					
3.25	3956.46	-0.61	4.35	4.58		4.56		
3.25	3963.45	1.33		5.26				
3.25	4016.42	0.57	4.89	5.46		5.52		
3.25	4018.27	0.55	4.62	4.96		5.04	4.60	
3.25	4031.97	0.14		5.00		5.16		
3.25	4067.98	-0.35	4.40	4.59	4.03	4.77	4.35	4.53
3.25	4070.78	-0.04	4.48	4.80	3.95	4.67	4.41	4.63
3.25	4073.77	0.02		4.85	4.01	4.97	4.57	4.72
3.25	4076.64	-0.28	4.50	4.68		4.61		
3.25	4285.45	0.36	4.79	4.82	4.40	5.11	4.79	4.79
3.25	4327.92	0.83	4.94	5.68	4.62	5.52	5.16	
3.25	4377.79	1.34		5.44		5.80	4.94	
3.25	4442.36	0.50		4.88				
3.25	4613.21	0.86		5.46				
3.25	4625.05	0.62	5.11	4.99	4.34	5.02	4.76	4.76
3.25	4637.51	0.56	5.05	5.06	4.36	5.08	4.76	
3.25	4707.28	0.23		5.02	4.21	5.17		
3.25	4736.78	0.02	4.58	4.69	4.10	4.82	4.40	4.50
3.25	5215.19	0.17		4.87				
3.25	5217.40	0.37		4.96				
3.25	5263.31	0.19		4.79				
3.25	5283.63	-0.20		4.60				
3.25	5302.31	0.04		4.69				
3.25	5339.94	0.11		4.84				
3.33	3804.01	0.24	4.69	5.10		5.24		
3.33	3805.35	-1.21	4.33	4.50		4.48		
3.33	3810.76	-0.10	4.52	4.77		4.90		
3.33	3985.39	0.28	4.91	5.00	4.37	5.12	4.70	4.84
3.33	3986.18	0.00	4.82	4.88	4.23	4.99	4.60	
3.33	4084.50	-0.24		4.74	4.13	4.78	4.44	
3.33	4195.34	-0.27	4.48	4.55	3.97	4.68		4.45
3.33	4227.44	-1.01	4.14	4.26	3.89	4.38	4.02	4.24
3.33	4966.09	0.30		4.88				
3.40	4072.51	0.32	4.66	4.83		4.76	4.50	4.76
3.40	4137.00	-0.32	4.66	4.63	4.13	4.83	4.29	
3.40	4157.79	-0.34		4.66		4.85	4.30	4.50
3.40	4158.79	0.01				5.06		
3.40	4168.62	1.07		5.42		5.44		
3.40	4168.95	0.73	5.08	5.11		5.62	4.77	
3.40	4176.58	-0.18	4.62	4.73	4.07	4.84	4.32	4.52
3.40	4196.21	-0.07	4.62	4.77		5.03	4.30	4.62

TABLE A4 (CONT) ELEMENT FE1

EP	LAM	-LOG(GF)	ALEP	ACAR	DCMA	ICAR	ISCO	PI SAG
3.40	4200.93	0.08	4.69	5.04	4.30	5.04		4.74
3.40	4217.56	-0.27	4.58	4.64	4.19	4.90	4.23	
3.40	4238.82	-0.60	4.45	4.52	4.15	4.66	4.11	4.53
3.40	4247.43	-0.57	4.45	4.48		4.73		
3.40	4907.74	1.31		5.65				
3.40	4910.02	0.93		5.26				
3.40	4946.39	0.74		5.18				
3.40	4950.11	1.07		5.30				
3.40	5002.80	1.03		5.24				
3.55	3846.42	-0.54		4.86		4.90	4.35	
3.55	3960.28	0.24		5.20		5.45	5.00	
3.55	4118.55	-1.16		4.57	3.87	4.54		
3.55	4246.09	0.17	4.90	4.94	4.24	5.35		
3.55	4309.04	0.00	4.67	5.05	4.32	5.27		
3.55	4382.76	-0.01	4.80	5.10		5.44		
3.55	4388.41	-0.20	4.57	4.85	4.34	4.93	4.60	4.78
3.55	4525.14	-0.17		4.69				
3.55	4547.85	-0.01	5.00	5.26		5.24		
3.55	4560.10	1.07		5.76				
3.55	4638.02	0.24		4.99	4.41		4.76	4.79
3.55	4678.85	-0.15		4.81	4.26		4.65	4.56
3.55	5365.41	0.36		4.91				
3.65	4433.23	-0.05		5.17	4.38	5.10		
3.65	4469.38	-0.37		4.65		4.85		
3.65	4484.22	-0.23	4.72	4.94	4.11	4.99	4.87	4.62
3.65	4485.68	0.21		5.20		5.40		4.87
3.65	4643.47	0.46	5.06	5.19	4.59	5.18	5.06	5.01
3.65	4669.17	0.42	5.13	5.24		5.27		
3.65	4673.17	0.40		5.39		5.47		
3.65	4673.28	0.90		5.47			5.19	
3.65	4700.16	0.85		5.44			5.19	
3.65	4704.95	0.55	5.29	5.39	4.77	5.72		5.07
3.65	4728.55	0.37	5.40	5.08	4.44	5.40	4.98	
3.65	5242.50	0.19		4.91				
3.88	4392.59	0.63		6.04		6.04		
3.88	4885.43	0.67		5.33				
3.88	5001.87	-0.42		4.70				
3.88	5005.72	-0.33		4.75				
3.96	4985.26	0.06		5.28				
3.96	5014.95	-0.32		4.94				
3.96	5022.24	-0.06		5.03				
4.07	4735.85	0.05		5.47	4.65	5.68		
4.15	4800.65	0.26		5.68				
4.15	4910.33	0.27		5.23				
4.15	4967.90	0.21		5.08				
4.15	4988.95	0.11		5.36				
4.15	5027.13	-0.11		5.10				
4.15	5133.70	-0.89		4.53				
4.15	5137.39	-0.48		4.81				
4.15	5162.28	-0.76		4.66				
4.15	5391.46	0.08		5.27				
4.15	5473.90	0.03		5.14				
4.22	4188.74	-0.37		4.81	4.24	4.96	4.81	
4.22	4933.34	0.11		5.14				

TABLE A4 (CONT) ELEMENT FE1

EP	LAM	-LOG(GF)	ALEP	ACAR	DCMA	ICAR	ISCO	PI	SAG
4.22	5027.76	0.33		5.62					
4.22	5074.75	-0.54		4.86					
4.22	5126.20	0.10		5.37					
4.22	5165.41	-0.33		4.95					
4.22	5195.48	-0.62		5.04					
4.31	5078.98	-0.41		4.90					
4.31	5090.78	-0.22		4.96					
4.31	5109.66	0.06		5.18					
4.31	5121.65	-0.07		5.06					
4.31	5383.38	-1.17		4.57					
4.31	5424.08	-1.18		4.60					
4.42	5364.88	-0.91		4.64					
4.42	5367.48	-0.99		4.71					
4.42	5369.97	-1.07		4.61					
4.42	5389.48	-0.38		5.00					
4.42	5398.29	-0.27		5.26					
4.42	5400.51	-0.58		5.02					
4.42	5415.21	-1.20		4.61					
4.42	5445.05	-0.67		4.81					
4.42	5463.28	-0.63		4.92					
4.47	5462.97	-0.48		4.97					
				ELEMENT CO I					
0.10	3979.52	2.36	4.90		4.60	5.26	4.62		
0.43	3873.13	0.31	4.57	4.85		5.00			
0.43	4020.90	1.58	5.30		4.56	5.83	5.13	5.30	
0.92	3845.47	-0.21	4.57	4.83		5.01		4.68	
0.92	3995.31	-0.16	4.77	5.01	4.19	4.91	4.72	4.48	
0.92	4121.33	0.03	4.84	5.05	4.19	5.27	4.92	4.77	
1.05	3997.91	0.51	5.30	5.56		5.40			
				ELEMENT ZN I					
4.01	4680.14	-0.92	5.33	5.44	4.58		5.19		
4.01	4722.16	-0.45	5.02	5.17	4.66	5.53			
4.01	4810.54	-0.24		4.97	4.83	5.15	4.71		

TABLE A4 (CONT) ELEMENT NI1

EP	LAM	-LOG(GF)	ALEP	ACAR	DCMA	ICAR	ISCO	PI SAG
0.42	3775.58	0.91	4.35	4.40		4.63		
0.42	3807.15	0.79	4.36	4.58		4.56		
0.42	3831.70	1.61	4.56	4.91		4.96	4.41	4.58
0.42	3858.30	0.56	4.29	4.41	3.91	4.47	3.85	4.19
1.68	4331.65	1.37	5.03	5.41	4.60	5.46		
1.83	5476.92	0.58		4.75				
3.19	4401.53	-0.86	4.60	4.98	4.34	5.00	4.56	
3.40	4389.87	0.75			4.69			
3.40	4470.49	-0.59	4.87	5.29		5.27		
3.40	4648.66	-0.80		5.16		4.99		4.59
3.40	4714.42	-0.90	4.63	5.02	4.28	5.09	4.50	4.54
3.40	4786.54	-0.50	4.83	5.02	4.38	5.08	4.64	4.73
3.48	4605.00	-0.73		5.32			4.82	
3.48	4715.76	-0.62		5.33				
3.48	4756.52	-0.39	4.99	5.26	4.53	5.42	4.77	4.85
3.54	3844.24	-0.21	4.96					
3.54	4829.02	-0.30	4.94	5.32	4.58	5.21		4.69
3.54	4831.18	-0.35	4.89	5.21	4.63	5.24	4.87	4.86
3.54	4855.42	-0.55	4.78	5.22		5.21		4.69
3.54	4866.27	-0.47	5.13	5.29	4.61			
3.54	4904.41	-0.45		5.21	4.56	5.26		4.66
3.54	5017.58	-0.59		5.22				
3.61	3908.93	-0.44		5.31		5.16		
3.61	3984.15	-0.29		5.45		5.28		
3.61	4686.22	-0.32		5.44			5.37	
3.61	4806.99	-0.19		5.38		5.40	4.92	
3.61	4980.18	-0.56		5.22				
3.61	4998.23	0.06		5.52				
3.61	5000.35	-0.18		5.42				
3.61	5035.37	-0.80		4.92				
3.61	5080.53	-0.91		5.14				
3.61	5081.12	-0.88		5.07				
3.70	4017.47	-0.18		5.35		5.35	5.00	
3.70	4703.82	-0.11		5.50				
3.70	5099.94	-0.39		5.23				
3.70	5146.48	-0.49		5.41				
3.74	5084.10	-0.46		5.16				
3.83	3912.29	-0.34		5.59	4.55	5.29		
3.83	3962.09	-0.09		5.64		5.69		
3.83	4295.89	-0.01		5.73		5.59	5.16	
3.83	5038.59	-0.02		5.80				
3.83	5115.40	-0.52		5.23				
3.90	4027.67	0.20		5.76		5.83		
3.90	5155.77	-0.54		5.30				
4.10	4236.38	-0.12		5.45		5.67		
4.10	4732.47	-0.09		5.90				

TABLE A4 (CONT)

ELEMENT MG II

EP	LAM	-LOG(GF)	BVEL	VCAR	HD97534	195CAR	TH SCO
8.86	4481.13	-0.58	4.14	4.27	3.92	4.11	3.95
8.86	4481.34	-0.75	4.06	4.17	3.84	4.03	3.87

ELEMENT SI II

6.86	3856.03	0.66	3.82	4.11	3.79	3.90	
6.86	3862.59	0.92	3.91	4.27	3.83	3.83	3.93
9.84	4130.86	-0.77	4.32	4.66	4.32	4.44	

ELEMENT CA II

0.00	3933.68	-0.14	2.75	2.95	2.96	2.97	2.63
0.00	3968.40	0.16	2.82	3.00	2.96	3.00	2.60

ELEMENT SC II

0.31	4246.84	-0.19	3.85	4.10	3.92	3.79	
0.61	4305.71	1.20	4.36	4.42	4.59	4.54	4.06
0.61	4314.09	0.10	3.86	4.43	4.33	4.46	4.52
0.61	4325.00	0.37	3.79	4.20	3.95	4.16	4.16
0.61	4354.62	1.50	4.51	4.53	4.90	4.61	4.52
0.61	4374.47	0.45	4.05	4.22	4.19	4.24	4.52
0.61	4400.40	0.72	4.02	4.38	4.08	4.04	
0.61	4415.56	0.84		4.39			
0.61	4420.67	2.32		5.17	4.95	4.65	
0.61	4431.36	2.13	4.56	4.77	4.61		
1.36	4670.41	0.51					4.37
1.36	5031.02	0.38					4.16
1.36	5239.82	0.50					4.44

ELEMENT I I11

0.57	3981.99	1.72	4.06	4.42	4.26	4.06	
0.57	3987.61	1.01	4.13	4.65	4.56	4.44	4.60
0.57	4012.39	1.58	3.96	4.26	3.99	3.87	4.28
0.61	4056.19	2.46	4.53	4.77	4.93	4.57	
1.08	4184.31	1.56	4.32	4.62	4.48	4.37	
1.08	4294.14	0.90	3.84	4.16	3.88	3.83	
1.08	4337.93	0.86	3.82	4.34	3.90	3.94	
1.08	4344.29	1.73	4.19	4.36	4.30	4.34	
1.08	4395.04	0.50	3.86	4.17	3.86	3.92	
1.08	4443.61	0.68	3.74	4.10	3.88	3.90	4.05
1.08	4450.49	1.41	3.95	4.35	4.01	4.17	4.27
1.08	4493.53	1.92	4.55	4.71	4.43	4.44	
1.13	3900.54	0.07	3.63	4.11	3.69	3.69	3.84
1.13	3913.47	0.17	3.55	4.07	3.75	3.84	4.03
1.13	4444.56	1.86	4.35	4.40	4.44	4.17	4.41
1.13	4468.50	0.65	3.89	4.25	3.87	3.97	3.95
1.13	4501.28	0.79	3.81	4.19	3.86	3.95	3.98

TABLE A4 (CONT)

EP	LAM	-LOG(GF)	BVEL	VCAR	HD97534	195CAR	TH SCO
			ELEMENT TI11				
1.13	4545.14	1.61	4.43	4.99	4.68	4.53	
1.16	4290.23	0.84	3.91	4.17	3.95	3.85	3.93
1.16	4300.05	0.55	3.88	4.11	3.83	3.79	3.98
1.16	4301.93	1.08	3.79	4.34	3.95	3.93	4.06
1.16	4312.88	1.05	3.86	4.43	3.94	3.96	4.16
1.16	4330.71	-0.00	4.43	4.73	4.38		
1.16	4464.46	1.66	4.13	4.35	4.20	4.33	
1.16	4470.86	1.80	4.26	4.47	4.32	4.24	
1.22	4399.76	1.06	4.00	4.38	4.08	4.04	
1.22	4544.02	2.08	4.50	4.99	4.72	4.75	4.58
1.22	4563.77	0.86	3.86	4.29	3.84	3.96	4.07
1.22	4568.33	1.93	4.49	5.12	4.62	4.56	
1.22	4589.95	1.61	4.05	4.41	4.06	4.04	4.40
1.57	4529.49	1.52	4.28	4.54	4.36	4.37	
1.57	4571.98	0.31	3.87	4.16	3.77	3.91	3.98
1.89	4028.34	0.65	3.96	4.43	4.01	3.90	4.34
1.89	4053.82	0.80	4.02	4.25	4.16	4.06	
2.05	4316.80	1.07	4.27		4.44	4.38	
2.05	4330.25	1.58	4.43		4.73	4.28	
2.05	4421.94	1.14	4.27	4.60	4.53	4.47	
2.05	4805.10	0.76					4.25
2.60	4386.85	0.46	4.28	4.50	4.30	4.30	
3.11	4488.33	-0.01	4.20	4.47	4.20		
			ELEMENT V2				
1.40	3866.72	1.24	4.29				
1.40	3896.14	1.11	4.27	4.64	4.27	4.25	
1.40	3916.41	0.80					4.46
1.40	4002.93	1.28					4.59
1.48	3951.96	0.52	4.15	4.44	4.34	4.12	
1.48	4036.77	1.42	4.65	4.87	4.91	4.55	
1.79	3884.84	0.98	4.51	4.89	4.59	4.33	
1.79	3899.14	0.37	4.05	4.51	4.16	3.99	4.21
1.79	4005.65	0.22	4.00	4.40	4.35	4.06	4.20
1.79	4008.17	1.61	4.82	5.13	5.13	4.82	
1.79	4023.38	0.36	4.06	4.60	4.26	4.29	
1.79	4051.05	1.26	4.61	5.01			
2.27	4600.20	1.36	4.82	4.96			
			ELEMENT CR11				
3.10	4051.92	2.10	4.16	4.52	4.41	4.15	
3.10	4111.00	1.86	4.04	4.53	4.30	4.13	4.36
3.10	4113.22	2.58	4.35	4.73	4.84	4.52	
3.87	4242.38	1.02	4.10	4.39	3.96	3.94	4.51
3.87	4252.63	1.85	4.33	4.46	4.29	4.18	
3.87	4261.93	1.21		4.43	4.04	4.14	4.49

TABLE A4 (CONT) ELEMENT CR11

EP	LAM	-LOG(GF)	BVEL	VCAR	HD97534	195CAR	TH SCO
3.87	4269.29	2.06	4.38	4.73	4.55	4.47	4.93
3.87	4275.56	1.34	4.15	4.45	4.19	4.29	4.54
3.87	4284.23	1.64	4.31	4.48	4.40	4.22	
3.87	4812.35	1.39	4.55	4.57			
3.87	4824.14	1.01	3.98	4.24			
3.87	4836.24	1.89	4.39	4.60			
3.87	4848.25	1.13	3.99	4.29			4.21
3.87	4864.32	1.46	4.18	4.57			
4.07	4554.99	1.44	4.20	4.68	4.19	4.19	
4.07	4558.65	0.31	4.00	4.26	3.84	3.77	4.19
4.07	4588.20	0.65	4.00	4.43	3.87	3.85	
4.07	4592.06	1.37	4.32	4.62	4.18	4.06	
4.07	4616.63	1.51	4.34	4.66	4.16	4.12	4.55
4.07	4618.79	0.98	4.11	4.29	3.97	3.92	
4.07	4634.04	1.19	4.23	4.42	4.04	4.19	4.49
5.32	4145.76	1.14	4.54	4.62	4.63	4.54	
			ELEMENT FE11				
1.67	3938.30	3.40	4.08	4.29	4.00	3.95	
2.56	4178.86	2.00	3.78	4.26	3.84	3.88	
2.70	3974.17	2.58	4.08		4.22	4.00	
2.70	4273.33	2.27		4.52			
2.70	4296.58	2.36	4.00	4.34	3.93	4.00	
2.70	4303.18	2.00	4.03	4.22	3.87	3.82	
2.78	4369.41	2.90	4.39	4.56	4.36	4.21	
2.78	4385.39	2.02	3.94	4.23	3.85	3.82	
2.78	4489.18	2.23	4.05	4.39	3.91	3.95	3.92
2.83	4472.93	2.67	4.30	4.47	4.21	4.43	
2.83	4491.41	2.09	4.06	4.39	3.81	4.07	
2.83	4508.29	1.76	3.98	4.22	3.83	3.86	4.10
2.83	4515.34	1.91	3.99	4.23	3.94	3.79	4.12
2.83	4520.23	1.87	3.97	4.33	3.83	3.86	4.23
2.83	4522.64	1.51	3.86	4.12	3.78	3.72	4.05
2.83	4541.52	2.29	4.09	4.47	4.05	4.03	4.25
2.83	4555.89	1.79	3.87	4.18	3.86	3.78	
2.83	4576.34	2.22	4.04	4.36	3.92	3.85	4.27
2.83	4582.83	2.44	4.07	4.46	4.12	4.01	4.28
2.83	4583.84	1.25	3.77	4.08	3.73	3.68	3.93
2.83	4620.52	2.63	4.28	4.53	4.13	4.11	
2.83	4629.34	1.78	3.93	4.36	3.82	3.79	4.06
2.83	4663.71	3.02	4.61		4.36	4.21	4.31
2.83	4666.75	2.50	4.11	4.52	4.12	3.97	4.15
2.83	4731.47	2.28	4.21	4.53	4.01	4.02	
5.91	4635.31	0.95	4.52	4.89	4.39	4.41	4.22

TABLE A4 (CONT) ELEMENT NI II

EP	LAM	-LOG(GF)	BVEL	VCAR	HD97534	195CAR	TH SCO
4.03	4015.48	0.58	4.17	4.71	4.60	4.60	
4.03	4333.76	0.60					5.03
4.03	4362.10	1.43	4.63	4.83	4.60	4.59	4.69
			ELEMENT SR II				
0.00	4077.72	0.58	3.71	4.10	3.94	3.86	
0.00	4215.54	0.70	3.85	4.16	4.09	3.98	4.02
			ELEMENT Y II				
0.10	3950.36	0.44					4.12
0.13	3982.59	0.79	4.18	4.60			
1.00	4854.87	0.26	4.32	4.78			4.39
1.00	4883.69	-0.17	4.13	4.48			4.09
1.00	4900.12	-0.10	4.19	4.49			4.39
1.00	5087.43	0.17					4.52
			ELEMENT ZR II				
0.53	3999.00	0.50	4.30	4.60			
0.53	4211.90	1.21	4.58		4.83	4.85	
0.71	3991.12	0.30	4.25	4.60	4.76	4.49	4.52
0.71	4208.99	0.54	4.35	4.67	4.75	4.58	4.78
0.71	4496.97	1.13	4.68	5.11	4.68		
0.80	4149.20	0.13	4.16	4.52	4.36	4.30	4.38
			ELEMENT BA II				
0.00	4554.04	-0.19	4.18	4.61	4.56	4.19	4.34
			ELEMENT LA II				
0.17	4333.76	0.60		5.16	4.69		4.71

TABLE A4 (CONT)

EP	LAM	-LOG(GF)	BVEL	VCAR	HD97534	195CAR	TH SCO
			ELEMENT NA I				
0.00	5889.97	-0.11					3.92
0.00	5895.94	0.19					3.98
2.10	5682.60	0.71					4.61
2.10	5688.20	0.40					4.53
			ELEMENT MG I				
2.71	3829.36	0.21	3.97	4.28		3.88	3.90
2.71	3832.31	0.33	4.30	4.50	3.95	3.86	3.81
2.71	3838.30	0.33	4.28	4.58	3.87	3.88	3.89
2.71	5167.33	0.86					3.94
2.71	5172.69	0.38					3.84
2.71	5183.62	0.16					3.87
			ELEMENT AL I				
0.00	3944.02	0.62	4.21	4.54	4.34	4.17	4.08
0.00	3961.11	0.32	4.13	4.35	4.19	4.14	4.10
			ELEMENT SI I				
1.91	3905.53	0.67	3.80	4.15	3.88	3.75	3.75
			ELEMENT CA I				
0.00	4226.74	-0.24	4.20	4.40	4.21	4.40	3.96
1.88	4283.01	0.26	4.89	4.93	4.73	4.69	
1.88	4318.66	-0.22	5.13	4.53	4.54	4.98	
1.88	4425.44	0.56	5.00	4.97	5.02	5.10	
1.88	4434.97	0.26	4.57	4.42	4.61	4.87	
1.88	4435.69	0.69	5.00	4.84	4.71	5.08	
1.88	4454.79	-0.25	4.38	4.28	4.27	4.58	
1.88	4455.89	0.51	4.94	4.89	4.69	5.10	
2.93	5857.46	-0.17					4.32
			ELEMENT MN I				
0.00	4254.35	0.27	4.25	4.45	4.28	4.30	
0.00	4274.81	0.39	4.85	4.63	4.73	4.43	
0.98	4371.29	0.90		5.34			
0.98	4652.17	0.79		5.19			
1.03	3941.50	0.82	5.45				
1.03	4646.17	0.49		5.01			
2.54	3963.69	-1.34	4.78	4.90			

TABLE A4 (CONT) ELEMENT FE1

EP	LAM	-LOG(GF)	HVEL	VCAR	HD97534	195CAR	TH SCO
0.00	3859.92	0.57	3.94	4.14	4.11	3.93	3.93
0.00	4375.94	2.57			4.90	5.04	
0.05	3922.92	1.44	4.27	4.34	4.35	4.30	4.40
0.05	4427.32	2.51				4.99	
0.09	3930.31	1.31	4.25	4.45	4.29	4.27	
0.11	3895.67	1.44					4.29
0.11	3920.27	1.49	4.24	4.42	4.38	4.34	4.12
0.91	5397.14	1.88					4.33
1.00	3840.45	0.20	4.11		4.20	4.12	4.19
1.00	3865.53	0.57	4.19	4.37	4.19	3.99	4.14
1.00	5434.53	1.97					4.50
1.48	4045.83	-0.68	3.92	4.20	4.08	4.00	4.03
1.48	4271.77	-0.20	4.12	4.31	4.33	4.17	4.13
1.48	4383.56	-0.35	4.09		4.25	4.11	4.04
1.48	4602.95	1.46					4.52
1.56	4005.25	0.07					4.06
1.56	4053.60	-0.44	3.92	4.24	4.10	4.02	4.01
1.56	4143.88	0.07	4.32	4.50	4.54		4.32
1.56	4404.76	-0.25	4.17	4.32	4.34	4.06	4.33
1.61	3841.06	-0.47	4.11	4.26	4.24	4.12	
1.61	4071.75	-0.42	3.90	4.35	4.18	4.07	4.05
1.61	4132.07	0.16					4.10
2.18	3852.58	-0.57	3.98	4.32	4.28	4.11	
2.18	4282.41	0.26	4.52	4.63	4.82		4.43
2.22	4447.73	0.48	4.84	5.05	4.80		4.42
2.22	4494.57	0.35					4.40
2.42	4187.05	-0.17		4.92			4.42
2.42	4187.81	-0.13		4.54			4.45
2.42	4235.95	-0.31	4.25	4.51	4.55	4.45	4.30
2.42	4260.49	-0.63	4.12	4.35	4.29	4.44	4.28
2.42	4271.16	-0.25	4.33	4.48	4.55	4.48	
2.47	4191.44	-0.06		4.58			4.37
2.47	4222.22	0.35	4.58	4.88	4.85	4.72	
2.47	4250.13	-0.25	4.32	4.58	4.57	4.48	
2.76	4021.87	-0.12					4.30
2.85	4062.45	-0.05	4.65	4.76	4.85	4.73	4.61
2.85	4107.49	-0.07	4.77	4.87	4.76	4.90	
2.85	4134.69	-0.18	4.73	4.67			
2.85	4181.76	-0.45		4.54			
2.85	4466.53	-0.18			4.70		
2.85	4871.32	-0.11	4.51	4.78			4.29
2.85	4872.14	0.05	4.65	4.91			
2.85	4890.76	0.09	4.54	4.69			
2.85	4891.50	-0.17	4.39	4.72			
2.85	4919.00	-0.02					4.39
2.85	4920.51	-0.30					4.15
3.05	4074.79	0.12				4.83	
3.05	4143.42	-0.65	4.50	4.66	4.62	4.54	
3.25	4070.78	-0.04	4.68	4.89	4.78		
3.25	5283.63	-0.20					4.42
3.25	5302.31	0.04					4.42
3.33	4227.44	-1.01	4.20	4.46	4.51	4.33	
3.33	4966.09	0.30					4.65
3.40	4137.00	-0.32	4.78	4.94	4.92	4.70	

TABLE A4 (CONT) ELEMENT FE1

EP	LAM	-LOG(GF)	BVEL	VCAR	HD97534	195CAR	TH SCO
3.40	4217.56	-0.27	4.90	5.00	4.93	4.83	
3.40	4238.82	-0.60	4.51	4.67	4.70	4.64	
3.55	4118.55	-1.16			4.66	4.54	
3.55	4388.41	-0.20		5.04	5.00		
3.55	4638.02	0.24					4.74
4.15	4967.90	0.21					4.92
4.31	5383.38	-1.17					4.50
4.42	5367.48	-0.99					4.43

Sources of f-values

Species	Source of f-value
C I	Lambert (1968)
C I*	Wiese, Smith and Glennon (1966)
Na I, Al I	Lambert and Warner (1968a)
Mg I, Ca I, Ba II, Sr II	Lambert and Warner (1968d)
Mg II*, Si II*, Ca II*	Wiese, Smith and Glennon (1969)
Si I	Lambert and Warner (1968c)
Sc II	Warner (1968)
Ti II, V II, Cr II Mn II, Fe II, Ni II	Warner (1967)
Ti I, V I, Cr I*, Mn I, Co I, Ni I, Zn I, Zr II, La II, Ce II, Eu II, Gd II	Corliss and Bozman (1962)
Fe I*	Corliss and Tech (1968)
Y II	Krueger, Aller, Ross and Czyzak (1968)

Note that * indicates f-values used in this investigation are from sources other than those used for the determination of the suggested solar abundances, Aller (1968).

Appendix V

CENTRAL DEPTHS AND EQUIVALENT WIDTHS OF SELECTED LINES IN α CAR

λ	element	W (mÅ)	$\frac{W}{\lambda} \times 10^6$	$\frac{R_o}{R_c}$	λ	element	W (mÅ)	$\frac{W}{\lambda} \times 10^6$	$\frac{R_o}{R_c}$
3845.2	Fe I	91	24	0.54	3906.0	Fe II	60	15	0.45
3845.5	Co I	28	7	0.37	3907.5	Sc II	15	3.8	0.15
3846.4	Fe I	45	12	0.36	3911.0	Fe I	27	6.9	0.26
3846.8	Fe I	34	35	0.66	3911.4	Mn I	20	5.1	0.19
3849.36	Cr I	122	32	0.61	3913.6	Ti II	249	64	0.89
3850.0	Fe I	160	41	0.72	3915.9	Zn II	70	17.9	0.43
3856.3	Fe I	182	47	0.78	3916.7	Fe I	70	17.9	0.43
3857.7	Cr I	9	2.4	0.9	3920.3	Fe I	203	51.7	0.82
3858.3	Ni I	146	38	0.69	3920.6	Fe I	21	5.3	0.22
3859.9	Fe I	203	53	0.82	3922.9	Fe II	203	51.7	0.82
3864.0	Fe II	54	14	0.40	3925.2	Fe II	17	4.3	0.17
3865.5	Fe I	221	57	0.85	3944.0	Al I	206	52	0.78
3900.54	Ti II	235	60	0.86	3947.5	Fe I	63	16	0.41

λ	element	W (mÅ)	$\frac{W}{\lambda} \times 10^6$	$\frac{R_o}{R_c}$	λ	element	W (mÅ)	$\frac{W}{\lambda} \times 10^6$	$\frac{R_o}{R_c}$
3948.1	Fe I	83	21	0.49	4008.2	V II	22	5.5	0.21
3951.2	Fe I	92	23	0.53	4012.3	Ti II	232	58	0.86
3952.0	V II	16	41	0.72	4014.5	Sc II	161	40	0.72
3961.5	Al I	184	46	0.77	4021.9	Fe I	13	32	0.60
3963.1	Fe I	55	14	0.41	4023.3	V II	154	38	0.71
3994.1	Fe I	26	6.5	0.23	4025.13	Ti II	200	50	0.82
3995.3	Co I	45	11	0.35	4027.7	Ti II	221	55	0.84
3995.7	La II	36	9.0	0.29	4030.8	Mn II	190	47	0.78
4000.5	Fe I	38	9.5	0.31	4034.1	Zr II	22	5.4	0.18
4001.7	Fe I	39	9.7	0.31	4034.5	Mn I	139	34	0.67
4002.3	Fe I	48	12	0.36	4039.6	Zr II	24	6.0	0.21
4002.9	V II	110	27	0.64	4045.8	Fe I	260	64	0.91
4006.3	Fe I	40	10	0.31	4063.6	Fe I	254	62	0.87
4007.3	Fe I	48	12	0.38					